3D Bioprinted Cartilaginous Templates as Developmentally Inspired Implants for Large Bone Defect Regeneration

Trinity College Dublin
Coláiste na Tríonóide, Baile Átha Cliath
The University of Dublin

A thesis submitted to the University of Dublin in partial fulfilment of the requirements for the degree of

Doctor in Philosophy

Pierluca Pitacco

May 2022

Supervisor:

Prof. Daniel J. Kelly

Declaration

I declare that this thesis has not been submitted as an exercise for a degree at this or any other university and it is entirely my own work.

I agree to deposit this thesis in the University's open access institutional repository or allow the Library to do so on my behalf, subject to Irish Copyright Legislation and Trinity College Library conditions of use and acknowledgement.

Pierluca Pitacco

28/12/2021

Summary

Although bone has an inherent capacity for self-repair, bone defects above a critical size cannot heal on their own and their repair represents a significant clinical challenge. The current clinical gold standard treatment for such defects is autografting; however, there are a number of drawbacks associated with this approach. This has led to an increased interest in the field of bone tissue engineering (BTE), which aims to combine engineering technology and the principles of biological science to develop strategies for the repair and regeneration of lost or damaged bone tissue.

Nowadays, there is increasing interest in the field of BTE in mimicking natural tissue developmental processes as a means of directing regeneration *in vivo*. Developmentally inspired BTE strategies that try to recapitulate the endochondral ossification (EO) pathway have shown promise for repairing critically sized defects in pre-clinical studies. Although recapitulating EO offers a promising route to bone regeneration, translating such developmentally inspired TE approaches to a clinical setting requires a number of key challenges to be addressed. These challenges can potentially be addressed using emerging 3D bioprinting strategies. 3D bioprinting technologies enable precise control of the construct fabrication process, allowing the spatial patterning of cells, bioactive factors and biomaterials in 3D space. In addition to these challenges, there are numerous practical, logistical and regulatory considerations associated with the use of live cells and tissues. This has motivated increased interest in the decellularisation of *in vitro* engineered tissues as a means of producing extracellular matrix (ECM) based *off-the-shelf* implants for *in vivo* tissue engineering and regenerative medicine applications. Such o*ff-the-shelf* implants represent a potential alternative, easier to commercialise and translate into the clinic, since they are easily transported and stored, are available ready-to-use and may face less onerous regulations to be clinically approved.

The overall goal of this thesis is to 3D bioprint mechanically reinforced cartilaginous templates as developmentally inspired implants for large bone defect regeneration. The specific aims to realise this goal are: (i) to assess whether fibrin hydrogels can support chondrogenesis of hMSCs and progression along an endochondral pathway *in vitro*, (ii) to investigate how the fibrinogen content within fibrin based bioinks influences chondrogenesis of encapsulated hMSCs and to mechanically reinforce 3D bioprinted cartilaginous templates with a 3D printed polymer network, (iii) to 3D bioprint reinforced

cartilage and hypertrophic cartilage templates and assess their capacity to support large bone defect healing *in vivo* in a rat femoral defect model, and (iv) to assess the capacity of decellularised cartilage and hypertrophic cartilage templates to promote bone regeneration *in vivo*. In chapter 3 of this thesis it is demonstrated that fibrin hydrogels can support hMSCs chondrogenesis and progression along an endochondral pathway *in vitro*. Over time in culture, embedded MSCs secreted an ECM rich in sGAG and collagen. It was also demonstrated that micro-channels included in the design of these constructs to facilitate nutrient transport *in vitro* and potentially vascularisation *in vivo*, remained patent throughout the culture period. Chapter 4 describes a biofabrication method that uses fibrin-based bioinks to bioprint reinforced hMSCs-laden constructs, which are consequently cultured to produce cartilaginous templates. It was decided to use 3D bioprinting to produce these templates because the complex moulding techniques used in chapter 3 could have limited the future development of grafts with patient-specific geometries. It was observed that the fibrinogen content within such fibrin-based bioinks influences chondrogenesis of the encapsulated hMSCs, and that it is possible to mechanically reinforce these 3D bioprinted cartilaginous templates with a 3D printed polymer network. In chapter 5 different *in vitro* culture conditions are used to engineer *chondrogenic* and *early hypertrophic* cartilaginous cartilage templates. It was observed that chondrogenic priming of such hMSC laden constructs was required to support robust vascularisation and graft mineralisation *in vivo* following their subcutaneous implantation into nude mice. In addition, following their implantation into rat femoral bone defects, these primed constructs were rapidly remodelled into bone *in vivo*, with *early hypertrophic* constructs supporting higher levels of vascularisation and bone formation compared to the *chondrogenic* constructs. Finally, chapter 6 of this thesis presents a process to decellularise the engineered cartilaginous grafts from chapter 5 to produce *off-the-shelf* hypertrophic cartilage grafts, which are shown to support osteogenesis of hMSCs *in vitro*. The capacity of such decellularised constructs to direct bone repair *in vivo* is also assessed, showing that decellularisation diminished the bone forming capacity of the engineered grafts, and the resulting grafts possessed inferior osteoinductivity compared to control collagen sponges soak loaded with BMP-2.

Overall, the results of this thesis demonstrate that 3D bioprinting is a viable approach to scale-up the engineering of developmentally inspired templates for BTE, and support the continued development of such 3D bioprinted cartilage templates as a new class of regenerative implant for large bone defects.

Acknowledgments

First of all, I would like to sincerely thank you, Danny, for all your support and supervision during all these years, and for having given me this great opportunity. I can't express here all my gratitude. Gráinne, thank you for being the first one there who believed in me and allowed me to join the TCBE family; you have been an incredible guide. Andy, you paved the road for my PhD: the big opportunity you gave me to work on your project played a fundamental role in the choice of starting my PhD, so thanks a lot. A big thank as well to both Dave and Fiona, my senior postdocs during all these years; I really appreciate your daily help and support, and your availability when needed. Pedro, you have been an incredible reference point to me since day one, thanks so much for everything. Dinorath, thanks so much for your so pure friendship, inside and outside the lab; *te quiero mucho*.

My beloved *bit-cheeses*, I can't find the words to say how grateful I am to have met you and to have shared with you so many special memories. You all have been my rock during the toughest days, and gave me the best laughs; your friendships and our group profoundly shaped my PhD into the incredible experience it has been. To Mathieu, the best lock-down companion possible, I can't thank you enough for everything. To the Lime Street crew, I am so pleased I could shared with you these past years; you definitely made my journey funnier, happier and less stressed. Now I can say that being part of our "bubble" during the pandemic is the only thing that saved me from going mad. Can't thank you enough for all the great time and amazing memories together. Giovanni, I am so grateful our paths crossed, and even if it was for less than a year, I felt like having a second brother; I really value all the things we shared. A very big thank goes to all my friends back in Trieste, who always managed to make me feel close to them, as if I never left, and for always making time for me whenever I was able to come back; your support has been incredible and I will never forget it. Lollo, Niki, Richi, Damian, Pappa, Maxi, Cava, Meuri, Redo, Roccia, *ve vojo ben*. A special thank you from the bottom of my heart to Yazmín for being such a huge support and being at my side during the toughest years, and to her family for the last crazy writing months; I won't forget. Yaz, thank you so much for everything you have done daily, and for having introduced me to a new, wonderful and special world, yours; I feel so lucky, *te amo*. Last but not least, I would like to thank my mum, dad and brother: without you believing in me, I would not be here today. Thank you so much for everything, your help, your patience, your sacrifices and your love.

List of Abbreviations

3D	three-dimensional
AC	articular cartilage
ALP	alkaline phosphatase
ASC	adipose stem cells
BMP	bone morphogenetic protein
BMSC	bone marrow stem cell
BTE	bone tissue engineering
CAR	chimeric antigen receptor
CDM	chondrogenic differentiation medium
Col	collagen
Col-nHA	collagen type I – nano hydroxyapatite
CC	chondrocyte
DAPI	4’,6-diamidino-2-phenylindole
DI H_20	deionised water
DNA	deoxyribonucleic acid
DIW	direct ink writing
DBM	demineralised bone matrix
DCB	decellularised bone matrix
ECM	extracellular matrix
EDTA	ethylenediaminetetraacetic acid
EGTA	ethylene glycol tetraacetic acid
EO	endochondral ossification

EPC	endothelial progenitor cells
EV	extracellular vesicle
FBS	fetal bovine serum
FDA	Food and Drug Administration
FDM	fused deposition modelling
FGF	fibroblastic growth factor
FRESH	freeform reversible embedding of suspended hydrogels
GAM	gene activated matrix
GelMA	gelatin methacrylamide
GP	growth plate
HA	hyaluronic acid
hgDMEM	high glucose dulbecco's modified eagle's medium
HSC	hematopoietic stem cells
IHH	indian hedgehog
IPN	interpenetrating polymer network
ITR	inverted terminal repeats
LIFT	laser-induced forward transfer
Lig	ligament
LN_2	liquid nitrogen
MMP	matrix metalloproteinases
MSC	mesenchymal stem cell
NIH	National Institutes of Health
OA	osteoarthritis
OSM	osteogenic differentiation medium

PTHrP	parathyroid hormone-related protein
PBS	phosphate-buffered saline
PCL	polycaprolactone
PEEK	polyetheretherketone
PLG	poly lactide-co-glycolide
PLGA	poly(lactic-co-glycolic) acid
POC	primary ossification centre
PSeD	poly sebacoyl diglyceride
rAAV	recombinant adeno-associated virus
RFP	red fluorescent protein
ROI	region of interest
RNA	ribonucleic acid
RT	room temperature
SAXS	small angle X-ray scattering
SEM	scanning electron microscopy
SDS	sodium dodecyl sulfate
sGAG	sulfated glycosaminoglycans
SLA	stereolithography
SLS	selective laser sintering
SOC	secondary ossification centre
SOX-9	SRY-Box 9
SVF	stromal vascular fraction
TCP	tissue culture plastic
TE	tissue engineering

TGF-β	transforming growth factor-β
VEGF	vascular endothelial growth factor
VOI	volume of interest
XPAN	expansion media
μCT	micro-computed tomography

Table of Contents

Chapter 1: Introduction

1.1 The clinical problem of large bone defect healing

Although bone has an inherent capacity for self-repair, this can be exceeded following trauma or disease, with negative impacts on patients and society worldwide. In fact, it is estimated that about 1,500,000 long bone fractures occur every year in the Unites States alone [1], with more than 500,000 bone grafting procedures to treat non-union or large defects performed annually in the United Sates [2], while more than 2 million are performed worldwide [3, 4]. To effectively treat critically sized defects, an external intervention is required. The current clinical gold standard treatment for such defects is the use of an autologous bone graft, where a patient's own bone is harvested and relocated to the defect site. Despite positive clinical outcomes, the use of autografts is limited by the scarcity of suitable and harvestable autologous bone and associated donor site morbidity [5, 6]. Such challenges have led to an increased interest in the field of bone tissue engineering (BTE), which aims to combine engineering technology and the principles of biological science to develop strategies for the repair and regeneration of lost or damaged tissue [7, 8]. BTE focuses on using specific combinations of different cell types, biomaterials and biomolecules in order to engineer bone grafts which, upon implantation *in vivo*, can transform into living bone tissue [9].

1.2 Developmentally inspired tissue engineering strategies for large bone defect healing

The majority of our bones develop through the process of endochondral ossification (EO), which involves the production by chondrocytes of a hyaline cartilage template that over time is replaced by mineralised bone tissue. EO begins with the condensation of mesenchymal stem cells (MSCs), which differentiate along a chondrogenic lineage [10, 11]. The resulting chondrocytes (CCs), under the control of the indian hedgehog (IHH)/parathyroid hormone-related protein (PTHrP) negative-feedback loop, undergo a coordinated sequence of proliferation and hypertrophy, providing a growing template for bone formation [12]. CCs then secrete type X collagen, angiogenic factors such as vascular

endothelial growth factor (VEGF) and the enzyme alkaline phosphatase (ALP), leading to cartilage calcification [13]. These hypertrophic chondrocytes also secrete matrix metalloproteinases (MMPs), which degrade the surrounding matrix template, allowing the invasion of other cells and blood vessels [14]. Incoming osteoprogenitor cells differentiate into trabecular bone-forming osteoblasts, while hematopoietic and endothelial cells establish the bone marrow [15]. Osteoprogenitors differentiate into osteoblasts, which subsequently deposit the periosteal bone collar, a predecessor of cortical bones, forming the primary ossification centre (POC) [16]; from there, osteoblasts start to lay down new woven bone. Over time, following a similar process, a secondary ossification centre (SOC) is formed at both ends of long bones. In the central diaphyseal region between the primary and secondary ossification centres, a cartilaginous layer, known as the growth plate, persists. This growth plate is responsible for continued longitudinal bone growth until it is entirely replaced by bone.

There is increasing interest in the field of tissue engineering in mimicking such developmental processes as a means of directing regeneration *in vivo*, a concept sometimes referred to as "developmental engineering" [17]. Developmentally inspired BTE strategies that try to recapitulate the EO pathway have shown promise for repairing critically sized defects. It has been demonstrated that cartilaginous templates, generated using adult MSCs, become vascularised and form bone following implantation *in vivo* [18, 19]. Moreover, pre-clinical studies have demonstrated that hypertrophic cartilage templates, engineering using bone marrow MSCs, can successfully regenerate large bone defects in rats [20-22].

Although recapitulating EO offers a promising route to bone regeneration, translating such developmentally inspired TE approaches to a clinical setting requires a number of key challenges to be addressed. These include scaling-up the engineering of such cartilaginous templates to match the size and geometry of critically sized defects in humans. It is well known that nutrient transfer limitations can arise in such larger engineered grafts, resulting in the formation of core regions devoid of cells and matrix [19]. Problems can also arise when larger constructs are implanted *in vivo*, whereby core regions of avascular cartilage often persist and are not converted into bone [23, 24]. Another challenge is ensuring that the *in vitro* engineered tissues are provided with the necessary mechanical support to perform their function in the adult body. Typically engineered cartilaginous templates possess relatively poor mechanical properties, which represents an issue in load bearing defects. This problem can potentially be addressed by the addition of a secondary reinforcing

material [25]. In many clinical scenarios it is also important that the engineered graft accurately mimics the specific patient anatomy. To achieve this very fine control over construct fabrication is required, ideally using patient specific imaging (e.g. computed tomography (CT) data) to inform the tissue engineering process. This would open up the possibility of tissue engineering anatomically accurate templates for bone regeneration. Finally, it is important to note that to date, the majority of such EO pre-clinical studies have been undertaken using engineered grafts generated from animal cells; prior to clinical translation in man it will be necessary to confirm that such approaches are also efficacious using human MSCs. This thesis aims to engineer, using hMSCs, mechanically reinforced cartilage and hypertrophic cartilage templates and to assess their capacity to support large bone defect healing *in vivo* in a rat femoral defect model.

1.3 Decellularised engineered tissues as *off-the-shelf* grafts for regenerative medicine

While TE strategies that recapitulate the developmental processes such as EO offer a promising route to bone regeneration, clinical translation and commercialisation of any cell-based therapy is complex and challenging. There are numerous practical, logistical and regulatory considerations associated with the use of live cells and tissues that hinder their direct translation to a clinical setting [26]. These challenges have motivated increased interest in the decellularisation of *in vitro* engineered tissues as a means of producing extracellular matrix (ECM) based *off-the-shelf* implants for *in vivo* tissue engineering and regenerative medicine applications [27]. Such o*ff-the-shelf* implants represent a potential alternative to viable cellular constructs since they are easier to commercialise and translate into the clinic, they are easily transported and stored, are available ready-to-use and may face less onerous regulations to be clinically approved. A notable example of such an *off-the-shelf* product derived from *in vitro* engineered ECM is the Humacyte© vascular graft, which is currently in clinical use [28, 29]. This bioengineered human acellular vessel is generated by seeding human smooth muscle cells into a tubular biodegradable mesh scaffold, which is then cultured for 8 weeks within a bioreactor system before being decellularised. The relative success of this concept suggests that it could be applied to other clinical targets such as large bone defect healing. This possibility will be investigated as last aim of this thesis.

1.4 3D bioprinting as a tool for bone tissue engineering

Many of the aforementioned challenges associated with existing developmentally inspired EO TE strategies (such as scalability, cartilaginous templates intrinsic low mechanical properties, patient-specific geometry) can potentially be addressed using emerging 3D bioprinting strategies. 3D bioprinting technologies enable precise control of the construct fabrication process, allowing the spatial patterning of cells, bioactive factors and biomaterials in 3D space [30-33]. As such, they enable tight control of the internal and external architectures of scaffolds and engineered constructs [34, 35]. In this way it is possible to engineer tissue architectures conducive to nutrient transport and waste removal and/or that support vascularisation upon implantation *in vivo* [36, 37]. Moreover, it is possible to introduce reinforcing scaffolding materials into the biofabrication process, thereby address the issue of providing sufficient mechanical properties to softer TE constructs. 3D printed polymeric frames have been extensively used to reinforce soft hydrogels, bioinks and engineered tissues in order to allow them to better withstand challenging physiological loads typically encountered *in vivo* [38-43]. Finally, another advantage of bioprinting technology is that it can be integrated with patient specific computed tomography (CT) data, making it possible to create anatomically accurate templates for BTE, which is especially important when attempting to repair complex clinical fractures.

Although 3D bioprinting techniques offer tremendous potential in the field of tissue engineering, realising its potential for the development of hypertrophic cartilage templates for endochondral bone tissue engineering requires the identification of a suitable bioink. Such a hydrogel ink must be printable, support chondrogenesis of MSCs *in vitro* and degrade *in vivo* to enable vascularisation and conversion of the cartilage graft into bone. Previous studies have demonstrated that hydrogel persistence *in vivo* can delay the conversion of engineered cartilage templates into bone [21, 44], hindering proper bone regeneration and so challenging the development of hydrogel bioinks for developmentally inspired bioprinting strategies. In order to create 3D bioprinted cartilaginous templates for use in large bone defect regeneration, this thesis will seek to identify a promising bioink and to assess its ability to support hMSCs chondrogenesis and progression along an endochondral

pathway *in vitro*, and then its capacity to support the conversion of an engineered cartilage template into bone *in vivo*.

1.5 Objective of the thesis

A large number of approaches, involving different regenerative pathways, fabrication techniques, materials, cells and biomolecules are currently being explored for large bone defect regeneration, suggesting that the ideal graft to restore such defects has yet to be identified. The overall goal of this thesis is to 3D bioprint mechanically reinforced cartilaginous templates as developmentally inspired implants for large bone defect regeneration. The following specific aims are proposed to realize this goal:

Specific aim 1: **To assess whether fibrin hydrogels can support chondrogenesis of hMSCs and progression along an endochondral pathway *in vitro*.**

Fibrin is a natural biopolymer that possesses many biological properties needed for successful biomaterial-based tissue regeneration, including excellent *in vivo* biocompatibility and biodegradation properties. Furthermore, it has previously been used as a bioink for the bioprinting of osseous implants [30]. The first aim of this thesis to assess whether fibrin hydrogel constructs can support chondrogenesis of hMSCs and progression along an endochondral pathway *in vitro*. The architecture of these engineered tissue will also be modified to improve nutrient transport *in vitro* (Chapter 3).

Specific aim 2: **To investigate how the fibrinogen content within fibrin based bioinks influences chondrogenesis of encapsulated hMSCs and to mechanically reinforce 3D bioprinted cartilaginous templates with a 3D printed polymer network.**

Hydrogel concentration plays an important role in the definition of biomaterials properties. Here two fibrinogen concentrations will be compared to investigate how fibrinogen content within fibrin based bioinks influences chondrogenesis of hMSCs. A potential limitation of such engineered cartilage templates is their relatively poor mechanical properties, which may limit their use in a load bearing environment. To address this concern,

this thesis will use a 3D printed polycaprolactone (PCL) frame to mechanically reinforce the bioprinted cartilage templates (Chapter 4).

Specific aim 3: **To 3D bioprint reinforced cartilage and hypertrophic cartilage templates and assess their capacity to support large bone defect healing *in vivo* in a rat femoral defect model.**

Using the fibrin-based bioink, this thesis will next 3D bioprint mechanically reinforced, hMSC laden constructs that will be differentially primed to engineer either a *chondrogenic* or an *early hypertrophic* template. A mice subcutaneous implantation model will be used to confirm that such *chondrogenic* templates can support vascularisation and endochondral bone formation *in vivo*. A critically sized rat femoral defect model will then be used to assess the capacity of both the bioprinted *chondrogenic* and the *early hypertrophic* templates to support bone regeneration compared to a gold standard of collagen scaffold based BMP-2 delivery (Chapter 5).

Specific aim 4: **To assess the capacity of decellularised cartilage and hypertrophic cartilage templates to promote bone regeneration *in vivo***

Here different decellularisation methods will be applied to tissue engineered templates to reduce construct DNA levels whilst retaining the extracellular matrix (ECM) components secreted in culture. To produce *off-the-shelf* implants for large bone defect healing, bioprinted cartilaginous templates with different phenotypes (*chondrogenic*, *early hypertrophic* and *late hypertrophic*) will be decellularised and freeze-dried. These decellularised cartilage templates will be then assessed for their osteogenic potential *in vitro* by reseeding them with hMSCs and culturing them in minimal osteogenic media. Finally, the critically sized rat femoral defect model will again be used to investigate the capacity of such decellularised grafts to promote bone regeneration *in vivo* (Chapter 6).

Chapter 2: Literature Review

2.1 Bone physiology and biology

2.1.1 Bone formation and development

Bone can develop following two distinct processes, intramembranous or endochondral ossification (EO). Most parts of the craniofacial complex, the scapula and clavicula, are formed through intramembranous ossification [45], while the rest of the bones of the skeleton are formed by endochondral ossification [46].

Intramembranous ossification (Fig. 2.1A) starts with the formation of the blastema, a condensation of mesenchymal cells which initiate the production of a type I collagen matrix and secretion of other molecules [47], establishing in this way an ossification centre [10, 11]. In the centre of the blastema, cells begin to differentiate into osteoblasts, which start to secrete osteoid, the organic portion of the bone matrix. Over time, through the accumulation of calcium phosphate in the form of hydroxyapatite, osteoid calcifies, leading to bone formation [48].

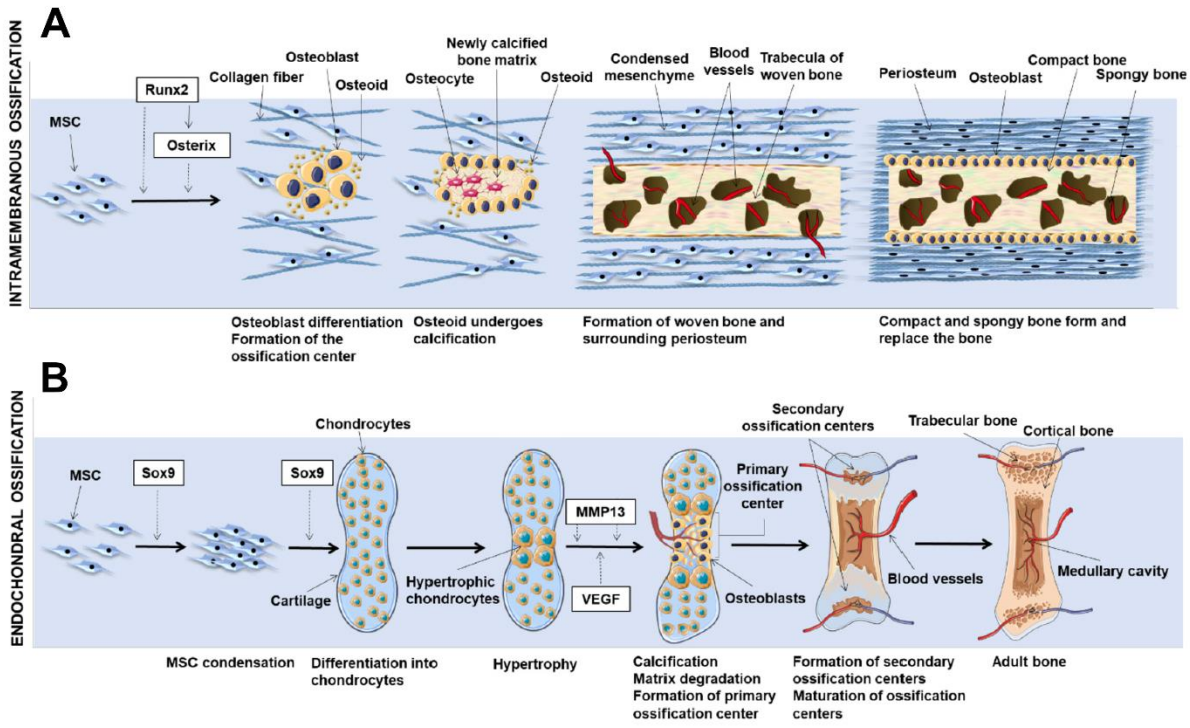

Figure 2.1: Schematic representation of (A) intramembranous and (B) endochondral ossification. Adapted from [49].

Endochondral ossification involves the production by chondrocytes of a hyaline cartilage template, which over time is replaced by mineralised bone tissue (Fig. 2.1B). EO begins with the adhesion of mesenchymal cells (MSCs) into clusters or condensations [10, 11]; these MSCs are differentiated into chondroblasts by the transcription factor SOX-9. At the centre of the condensation, chondroblasts begin to synthetize intercellular matrix, which starts to engulf some cells, leading to their differentiation into chondrocytes (CCs) [46]. Chondrocytes proliferate and secrete a cartilaginous matrix rich in type II collagen, aggrecan and other proteoglycans [50], contributing to the growth of the bone precursor. While matrix deposition spreads from the centre to the margin of the original condensation, the CCs encapsulated in the matrix at the centre of the template stop proliferating and undergo hypertrophy. Subsequently, CCs secrete type X collagen, angiogenic factors such as vascular endothelial growth factor (VEGF), and the enzyme alkaline phosphatase (ALP), leading to cartilage calcification [13]. When chondrocytes undergo hypertrophy, they enlarge in size and so the volume occupied by the cells increase consequently [51, 52]. To compensate for this decrease in free volume, hypertrophic chondrocytes secrete matrix metalloproteinases (MMPs), which degrade the surrounding matrix template, allowing the

invasion of other cells and blood vessels [14]. MMPs not only drive the degradation of the ECM to allow cell migration and vessels infiltration, but they participate as well in the alteration of the ECM microenvironment (altering in this way cell behaviour), in the modulation of biologically active molecules, in the regulation of other proteases activity and in the control of cell attachment, proliferation, differentiation, and apoptosis [53-55]. As already pointed out, the remodelling of the matrix by MMPs activity is essential to the invasion of blood vessels, which deliver osteoblast progenitors, osteoclasts, blood vessel endothelial cells and hematopoietic cells into the hypertrophic cartilage [56]. Incoming osteoprogenitor cells differentiate into trabecular bone-forming osteoblasts initiating the mineralisation of the cartilaginous matrix, while hematopoietic and endothelial cells establish the bone marrow [15]. This process initiates at the circumference of the diaphysis of long bones, where hypertrophic CCs direct osteoprogenitors in the perichondrium to differentiate into osteoblasts. They subsequently deposit the periosteal bone collar, a predecessor of cortical bones, around the cartilage anlage, forming the primary ossification centre (POC) [16]. The perichondrium is replaced by the periosteum, which provides the osteoblasts needed for the subperiosteal expansion of the bone collar. The creation and expansion of the bone collar increasingly reduce the nutrients supply to the initial cartilage template, which may contrite to its calcification [46]. Some of the chondrocytes are eliminated through either apoptosis or autophagy [57, 58], while others are believed to be able to transdifferentiate into osteoblasts and have an active role in endochondral ossification, promoting bone health [59]. The ability of chondrocytes to transdifferentiate into osteoblasts has been demonstrated *in vivo* [60-62], but the role and contribution of chondrocyte-to-osteoblast transdifferentiation during endochondral ossification is still not fully understood. The cartilage remnants are then partially resorbed by osteoclasts, while new woven bone is laid down by osteoblasts. Over time, following a similar process, a secondary ossification centre (SOC) is formed at both ends of the long bone in the epiphyses. In the central diaphyseal region between the primary and secondary ossification centres, a cartilaginous layer, known as the growth plate or epiphysis, persists. This growth plate is responsible for continued longitudinal bone growth until the epiphyseal plate is entirely replaced by bone, in the late teens and early twenties for humans, when growth finally ceases.

2.1.2 Bone structure and composition

Bone is a mineralised hard tissue with multiple functions; these include protection of various organs, providing structure and support for the body itself, as well as key roles in hematopoiesis, mineral metabolism and as an endocrine organ. Bone is a composite material consisting of mineral (~65%), organic matrix component (~25%), water (~10%) and lipids (~1%) [63]. The inorganic portion consists mainly of a nanocrystalline, highly substituted and lower crystallinity analogue of hydroxyapatite [$Ca_{10}(PO_4)_6(OH)_2$], as evidenced by TEM and small angle X-ray scattering (SAXS) [64-66]. On the other side, the organic phase of bone is composed primarily of type I collagen (~90%), noncollagenous proteins (~5%), and lipids (~2%) [46]. In general, the proteins in the bone ECM can be classified into two main groups, structural proteins (collagen and fibronectin) and proteins with specialised functions. As already pointed out, the most present protein in the bone matrix is type I collagen, which is a triple helical molecule formed by two identical amino-acid α1-chains and one structurally similar but genetically different α2-chain [67]. The collagen function is to provide a template for mineral deposition, grant elasticity to the tissue, stabilize the ECM, and bind other macromolecules. On the other hand, the proteins with specialised functions mainly play a role in the regulation of collagen fibril diameter and cell attachment, and act as signalling molecules, growth factors, or enzymes.

Bone can carry out its multiple diverse functions thanks to its hierarchical organisation on several structural levels, from the macro to the nanometric scale [68] (Fig. 2.2). Starting from the nanoscale level (Fig. 2.2A), the type I collagen and mineral form a composite material, in which the collagen provides resilience and ductility while the mineral gives stiffness and structure.

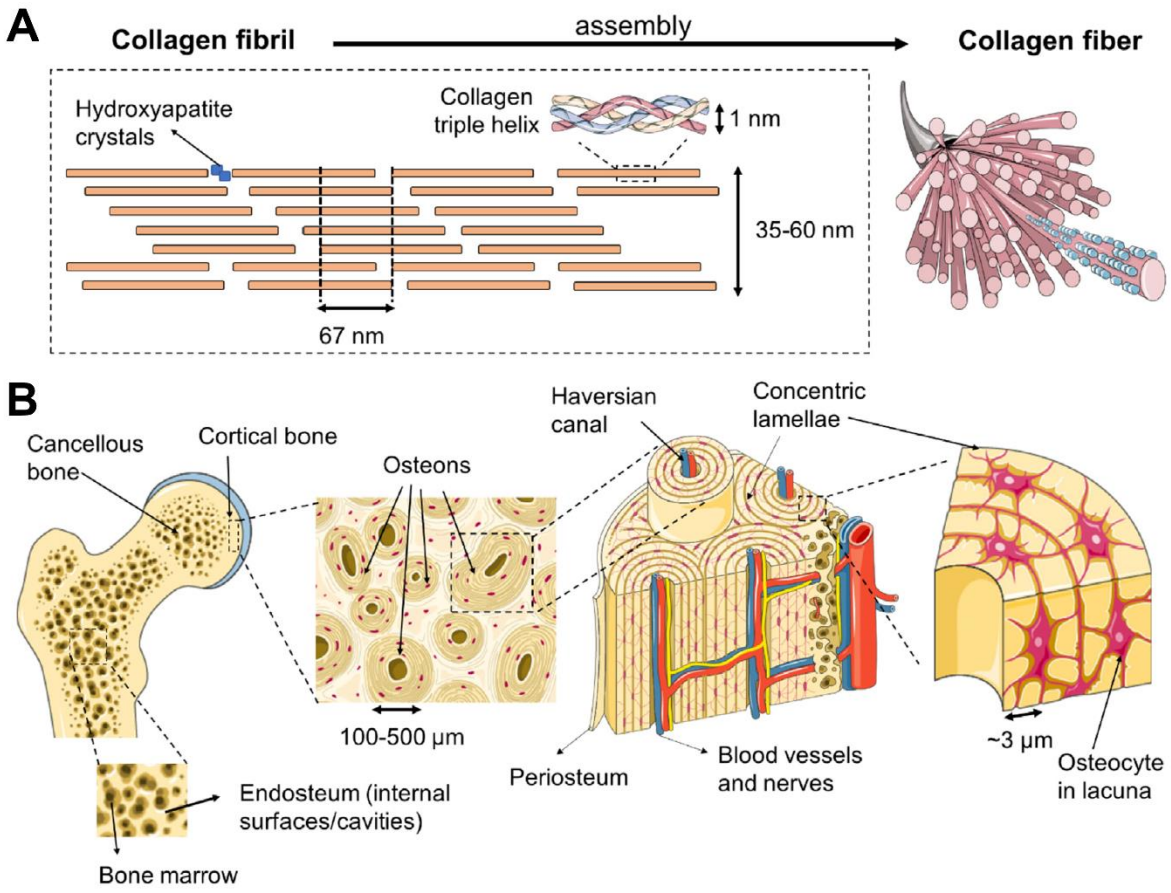

Figure 2.2: (A) Schematic representation of bone constituents at the nanoscale. (B) Macroscopic-to-microscopic schematic view of bone structure. The structure includes cancellous and cortical bone, osteon structure, and osteocyte network. Adapted from [49].

At a microscopic level, the individual collagen fibres and the interspersed mineral are organised in different ways in relation to bone specific functional needs, both mechanical and biological. Bone can be dense (cortical or compact bone) or quite porous (trabecular, cancellous or spongy bone) (Fig. 2.2B). Cortical bone is composed of structural units called osteons or secondary Haversian systems, consisting of multiple layers of concentric rings of calcified matrix that surround a central canal containing blood vessels, nerves and lymphatic vessels [69]. On the contrary, trabecular bone is an open cell porous network, meaning it is less dense then the cortical bone. This makes it weaker and more flexible. Finally, at the macroscopic level bone is composed of a dense cortical shell, encasing the trabecular bone, which is typically located at the ends of the long bones, near the joints and in the core of long bones and vertebrae, where it houses the marrow component (Fig. 2.2B).

There are three main bone cellular types: osteoblasts, osteocytes and osteoclasts. Osteoblasts are involved in bone formation, they synthesize the organic ECM called osteoid, which become mineralised through the accumulation of calcium phosphate. After active bone formation, osteoblasts can follow three possible paths: they either undergo apoptosis, become trapped in the mineralising bone matrix where they differentiate into osteocytes, or become "inactive" lining cells, continuing to exist on quiescent bone surfaces. The latter participate with osteocytes in the calcium exchange between the mineralised matrix and the bone marrow compartment, and can be reactivated when needed for local bone formation processes [70, 71]. As already mentioned, osteocytes are derived from osteoblast progenitors which become trapped in small spaces called lacunae during the process of matrix deposition. Osteocytes are the most abundant bone cell type, forming over the 90% of total cells, as compared to 4–6% of osteoblasts and 1–2% osteoclasts [72]. Osteocytes are regularly distributed throughout the mineralised matrix and connected to each other, to the cells on the bone surface and even to cells inside the bone marrow through dendrite-like extensions contained in fluid-filled micro-channels called canaliculi, which are present in all the bone matrix [73]. Using the canaliculi, they can communicate with each other and receive nutrients from blood supplies. Osteocytes have a central role in bone homeostasis since they act as mechanosensors, maintaining mineral concentrations in the bone matrix in response to mechanical loading and hormonal stimuli on bone. They regulate bone remodelling through communication with osteoblasts and osteoclasts [74], where old bone is resorbed by the osteoclasts and new bone is deposited by osteoblasts. Finally, osteoclasts are multinucleated giant cells responsible for bone resorption. Unlike osteoblasts, and consequently osteocytes, which are of mesenchymal origin, osteoclasts are of haematopoietic origin. To reabsorb bone osteoclasts use a two-step process, initiating with the dissolution of the mineralised matrix, followed by the enzymatic degradation of the organic matrix.

2.2 Bone tissue engineering

2.2.1 Fundamentals of bone tissue engineering

Although native bone has an inherent capacity for self-repair, bone disorders, that lead to significant alterations in appearance and function exceeding its regenerative ability

and remaining unhealed, can derive from multiple causes, including trauma, cancer or congenital diseases, and have a significant influence on patients and society worldwide. In fact, it is estimated that about 1,500,000 long bone fractures occur every year in the Unites States alone [1], that more than 500,000 bone grafting procedures to treat non-union or large defects are performed in the United Sates annually [2], and more than 2 million in the world [3, 4]. To effectively treat non-unions, an external intervention is required. A bone graft is the second most frequently transplanted tissue, coming right after blood transfusion [75, 76]. Currently, the clinical gold standard treatment for such defects is the use of an autologous bone graft, where a patient's own bone is harvested and relocated to the defect site. Autografts still represent the gold standard treatment option because of their immune-compatibility, osteoconductivity and the presence of autologous progenitor cells to enhance the repair process. However, despite some positive clinical outcomes, the use of autografts is affected by some important complications such as the scarcity of suitable and harvestable autologous bone and the severe associated donor site morbidity [5, 6].

Challenges associated with traditional bone grafts has led to an increased interest in the field of bone tissue engineering (BTE), which aims to combine engineering technology and the principles of biological science to develop strategies for the repair and regeneration of lost or damaged tissue [7, 8]. BTE focuses on using together combinations of several cell types, scaffolds, and growth factors in order to generate living bone tissues. By combining osteogenic cells, osteoinductive scaffolds, and external stimuli, experimental bone grafts resembling autologous grafts have been engineered [9]. BTE strategies usually fall into three main categories: (1) cell-based strategies; (2) growth-factor based strategies; and (3) matrix-based strategies [77]. However, in the vast majority of the experimental works, two or more of these strategies are used together towards a solution. Cell-based therapies for BTE include stem cell and gene modification [78]. Stem cell therapies may involve embryonic or adult stem cells with the potential to undergo specific differentiation. Possible stem cell sources for BTE are presented and discussed in paragraph 2.2.2. These progenitor cells are promising tools for regenerative therapy due to proliferation capabilities, preservation of bioactivity after freezing, and their high regenerative capacity [79]. However, these cells represent only less than 0.001% of the cellular content of bone marrow, and even less as age increases [80]. The limited quantity of MSCs there has led to the development of methods to isolate them from fresh bone marrow and expand them *in vitro*. It has been demonstrated that isolated MSCs can undergo *in vitro* expansion and proliferation, without losing osteogenic potential

[81]. Hence, these cells may be isolated from a patient, expanded in culture, and seeded onto a carrier or scaffold and implanted into the defect. Besides the direct use of stem cells, other cell-based therapies are focusing on the potential use of eukaryotic or stem cells after their genetic modification for tissue regeneration. Briefly, in such therapies, the cells are isolated and a vector is inserted into the cells; the vector contains a genetic code to upregulate specific cellular functions, which are targeted to improve tissue regeneration. Growth factors are critical molecules for tissue repair and regeneration, capable of stimulating a variety of cellular processes including cell proliferation, migration, differentiation and multicellular morphogenesis during development and tissue healing. This is why recombinant growth factors have raised a lot of hope for regenerative medicine applications and several products based on growth factors have been developed [82]. However, while using growth factors to promote tissue healing and regeneration has widely shown promising results in pre-clinical settings, their direct application and success in the clinic are limited to few cases; the most important of these is represented by BMP-2, which is here briefly reviewed in paragraph 2.2.3. Indeed, translation of growth factors based therapies present limitations, such as poor stability, short half-life, rapid diffusion from the delivery site, and low cost-effectiveness [83]. The attempt to overcome those limitations using supraphysiological doses has led in many cases to serious side-effects and poor effectiveness, which are mainly linked to sub-optimal delivery systems and lack of control over growth factors signalling. These issues prove the need to design new innovative strategies allowing the use of lower and localised doses of growth factors where delivery and signalling are tightly controlled. An example is the engineering and design of novel biomaterial-based delivery systems [84]. As already mentioned, besides the use of different cell types and growth factors, BTE has been focusing on biomaterial-based approaches [9]. Among different biomaterials, the use of the extracellular matrix as a biomaterial in tissue engineering has gained increasing recognition, not only because it can serve as supportive structural template [85, 86], but also as a reservoir of biological cues capable of instructing the regenerative processes [87]. This is why the ECM has been indicated as one of the best candidates for graft fabrication in the context of bone regeneration applications [88]. The use of ECM in BTE approaches will be discussed in more detail in the following paragraph.

All these strategies require interaction between osteogenic, osteoinductive, and osteoconductive elements. Osteogenic components include cells that support bone production such as osteoprogenitor cells or differentiated osteoblasts. Osteoinductive factors

include bioactive chemicals that induce recruitment, differentiation, and proliferation of the proper cell types. An osteoconductive element can be represented by a material that supports bone growth on itself. An osteoconductive scaffold may provide mechanical support, sites for cell attachment and vascular ingrowth, and a delivery vehicle for implanted growth factors and cells [89]. To be successful, a potential tissue-engineering strategy must fulfil several design requirements; these include (i) providing temporary mechanical support, (ii) acting as a substrate for osteoid deposition and growth, and (iii) possessing a porous architecture to allow for vascularisation and bone cell ingrowth. A successful graft needs as well to be biodegradable (able to degrade in a controlled manner to facilitate load transfer to developing bone and to allow bone growth into the defect area, degrade into non-toxic products that can be safely removed by the body, not causing a significant inflammatory response), be capable of sterilisation without loss of bioactivity, support cell attachment, provide biological and physical cues to stimulate cell proliferation, migration, and differentiation, support angiogenesis, illicit a pro-regenerative immune response, promote mineralisation and consequently bone formation [90].

2.2.2 Stem cell sources for BTE applications

In the literature, various types of stem cells have been proposed as a viable and easy source of progenitor cells for the engineering of implants for bone regeneration. Here mesenchymal, embryonic and induced pluripotent stem cells are briefly reviewed.

2.2.2.1 Mesenchymal stem cells (MSCs)

Mesenchymal stem/stromal cells (MSCs) are multipotent adult stem/stromal cells that exhibit differentiation potential towards different tissue lineages, including bone (osteoblasts), cartilage (chondrocytes), muscle (myocytes), and fat (adipocytes). It has also been shown that adult MSCs can support tissue regeneration after injury [91, 92], and therefore have been studied extensively for their therapeutic potential in fracture healing and bone regeneration. MSCs can be isolated from many different tissues including bone marrow, skeletal muscle, synovial membrane, and adipose tissue. There has consequently been substantial research regarding the osteogenic potential of MSCs obtained from different tissue sites.

Bone marrow-derived stem cells (BMSCs) are currently the most commonly used and researched source of adult MSC due to their relatively easy harvesting, high proliferative capacity, and established regenerative potential [93]. Various animal models of clinically significant bone defects have shown that a cell-based therapy with allogenic BMSCs grafts is effective in regenerating bone, providing evidence for their use as a viable alternative to autologous bone transplants [94]. Studies have found BMSCs to be more efficient at differentiating into osteoblasts compared to adipose-derived MSCs (ADSCs) [95]. Culture-expanded BMSCs have also been used in large cohort clinical trials showing no complications in long-term follow-up [96-98]. Overall, the current body of literature provides support for the viability and utility of BMSCs in the clinical setting of bone defects. However, limitations regarding BMSCs cell yields during harvest, especially in older patients [99], the requirement of expansion when used alone (not as part of BM aspirate concentrate), the proven reduced regenerative ability with extended expansions [100] and an increased patient morbidity and risk related to the increased number of surgical procedures all necessitate the need for further research into possible alternative MSCs harvest sites.

Another readily available source of MSCs under investigation is adipose tissue as it can be easily isolated from plastic surgery or biopsies. Although direct grafting of adipose derived stem cells (ADSCs) has not demonstrated much success in healing critical sized bone defects [101], there has been interest in applying osteoinductive factors to ADSCs in the hopes of enhancing osteogenesis. A study by Di Bella et al. demonstrated bone regeneration in rabbit critical-sized skull defects treated with autologous, osteogenically-induced ADSCs grafted onto fibronectin-coated polylactic acid biomaterials [102]. Another study demonstrated repair of a cranial bone defect in canine models using osteogenically-induced ADSCs grafted onto a coral biomaterial [103]. Interestingly, two clinical studies combining ADSCs with specialised biomaterials [104] or autologous bone grafting [105] indicated bone reconstruction *in vivo*. Collectively, these studies demonstrate novel methods of enhancing bone formation using ADSCs, providing promising evidence for the potential therapeutic role ADSCs could play in BTE.

2.2.2.2 Embryonic stem cells

Pluripotent human embryonic stem cells (hESCs), first derived in 1998 from human blastocysts [106], maintain the developmental potential for all three embryonic germ layers even after months of *in vitro* proliferation, thus demonstrating a potential source for tissue engineering-based therapies. Successful differentiation of hESCs into the osteogenic lineage has been demonstrated in numerous studies both *in vitro* and *in vivo* [107, 108]. After osteogenic induction, hESCs have been shown to possess molecular and structural features resembling bone tissue by the formation of mineralized bone nodules *in vitro* [109, 110]. Although several advantages have been discovered concerning their use, hESCs have several limitations that must be further investigated. Challenges concerning the complicated conditions required to culture hESCs, including the feasibility and viability of using feeder layers, the danger of unexpected differentiation, especially their link to teratoma formation [111] and immune reactions, as well as the surrounding ethical, religious and moral debate, all pose challenges to the role of hESCs as active participants of regenerative medicine-based clinical protocols [112, 113].

2.2.2.3 Induced pluripotent stem cells (iPSCs)

Induced pluripotent stem cells (iPSCs), first developed by Takahashi and Yamanaka in 2006, are derived and reprogrammed directly from adult somatic cells, and have the ability to give rise to every type of cell in the body and to propagate indefinitely. For this reason, iPSCs hold enormous potential for the entire field of regenerative medicine, as they possess a comparable pluripotency and differentiation potential as hESCs [114], yet avoid immune rejection since they are derived from the patient's own cells [115]. iPSCs generated through embryoid bodies have been shown to generate MSC-like cells *in vitro* that have the potential of further differentiating into osteoblasts [116], while also demonstrating osteogenic potential comparable to that of BMSCs *in vivo* [117]. Additionally, animal studies have demonstrated that MSC-like cells cultured from iPSCs have the capacity to form mature mineralised material that is histologically similar to bone [118]. Kang et al. demonstrated the first direct differentiation of human iPSCs (hiPSCs) into functional osteoblasts that subsequently participated in the healing of critical sized bone defects without the formation of a teratoma [119]. Although the area of iPSC research is still new, taken together, these findings indicate the exciting promise iPSCs hold for the future of osteogenic tissue

engineering. Nevertheless, further clinical investigation focusing not only on efficacy (e.g., osteogenic potential) but also safety (e.g., teratoma formation) becomes paramount before accepting iPSCs as a viable therapeutic option. Finally, iPSC-based therapy brings additional challenges such as the technical and logistical issues related with their generation. Tissue sourcing, manufacturing protocols, required expansion, systematic testing and quality control, validation, and storage constitute technical aspects that impact the costs associated the generation of these products, delaying their translation into potential clinical therapies.

Based on all the things just reviewed, in this work of thesis it was decided to use for all the studies bone marrow-derived MSCs. At the moment, they still represent the most commonly used and researched source, and as well the most directly translatable to the clinic.

2.2.3 Clinical application of bone morphogenetic proteins for bone healing

As mentioned previously, growth factors are critical molecules for tissue repair and regeneration, capable of stimulating a variety of fundamental cellular processes. Extensive studies focusing on the underlying molecular mechanisms that regulate the recruitment and differentiation of bone-related cells, and the activity of macromolecules responsible for the bone remodelling, have led to the identification of specific factors involved in the healing process like parathyroid hormone (PTH), hypoxia-inducible factor 1a (HIF-1a), factors modulating the Wnt signalling pathway, and bone morphogenetic proteins (BMPs) [120, 121]. Among these, perhaps the most promising growth factor candidates are the bone morphogenetic proteins (BMPs), which were originally identified by their capabilities to induce the formation of bone when implanted at ectopic sites [122, 123]. Although the molecular mechanisms underlying osteoblastic differentiation still need to be identified, BMPs are recognized as key factors in a variety of chondrogenic and skeletogenic functions during normal embryonic development, playing for example an important role in regulating osteoblast differentiation and subsequent bone formation [124-127]. Recombinant forms of BMPs, particularly BMP-2, BMP-4 and BMP-7, have been shown to possess the ability to heal critical-sized bone defects in rodents, dogs, sheep and non-human primates when combined with a variety of carriers [128].

Currently, there are two commercially available BMPs, recombinant human rhBMP-2 (INFUSE®, Medtronic Sofamor Danek, Memphis, TN, USA) and rhBMP-7 (or Osteogenic Protein-1, BMP-7) (Stryker, Kalamazoo, MI, USA). They have been tested in several preclinical studies showing their ability to induce bone regeneration [129-131], and evaluated in clinical trials to treat various bone disorders such as non-unions, open fractures, and osteonecrosis [132-137]. In addition to these two, other BMP-containing osteoinductive materials are currently being evaluated in animal and clinical studies [138]. The successful application of BMPs led, in July 2002, to the approval by the European Medicines Agency (EMA) of rhBMP-2 (InductOs®) for the treatment of single-level lumbar spine fusion and for acute tibial fractures in adults [139]. In November 2002, the American Food and Drug Administration (FDA) approved the use of rhBMP-2 (INFUSE® Bone Graft Device) for the treatment of open tibial fractures after stabilisation with intramedullary nail fixation [139]. rhBMP-7 received official approval by the EMA in 2004 as Osteogenic Protein-1 (OP-1® or Osigraft®) as part of an implant for the treatment of recalcitrant long bone non-unions [140]. Nevertheless, despite early promising results, some severe complications have been reported in clinical setting, such as ectopic bone formation, haematomas in soft tissues, and bone resorption around implants [141-143]. Thus, while BMPs seemed promising for bone regeneration, potential and limitations remains debated.

Another factor critical to the successful use of BMPs for bone regeneration is their delivery method. As most commercial available products combine BMPs with biomaterials, the composition, structure and biomechanical properties of such carriers are considered key aspects for the modulation of BMPs availability at the site of injury [144]. In fact, these molecules are relatively soluble, and if not maintained by an appropriate carrier, they can be cleared from the site and diffuse into adjacent undesirable tissues, promoting adverse reactions (such as ectopic bone formation) [145]. Several materials have been tested in pre-clinical settings, such as collagen, calcium phosphate ceramics, and synthetic polymers [146]. Despite the use of delivery devices, usually large doses of BMPs are required to achieve the desired osteogenic effects, which makes the procedure expensive and increases the risk of clinical complications related to their supra-physiological concentration [147]. Therefore, new solutions for BMPs delivery able to maintain a more sustained and effective release pattern still need to be explored. In this thesis, the efficacy of developmentally inspired engineered tissues will be compared to BMP-2 loaded collagen sponges that have been optimised for bone regeneration.

2.2.4 Developmentally inspired strategies for BTE

Recent studies have proposed that *in vitro* TE approaches should aim to simulate *in vivo* developmental processes, trying to imitate natural factors that regulate cell differentiation and matrix production, following the concept of "developmental engineering" [17]. As previously discussed, bone can develop following two distinct processes, intramembranous or endochondral ossification; for this reason, BTE developmentally inspired strategies can be divided into two main categories, depending on the native developmental process they try to recapitulate. Following the natural development of the majority of the bones, including long bones, recently BTE approaches are focusing on mimicking the EO, trying to achieve bone regeneration by remodelling *in vitro* engineered cartilaginous templates [19, 148-151]. It has been demonstrated by Scotti et al. that adult BMSCs can support an EO process that is characterised by striking resemblance to naturally occurring EO during limb skeletal development, including phases of MSC condensation, hypertrophic differentiation, formation of a bony collar, MMP-mediated matrix remodeling, vascularisation, osteoclast activity, bone formation and finally development of functional hematopoietic foci (Fig. 2.3) [149].

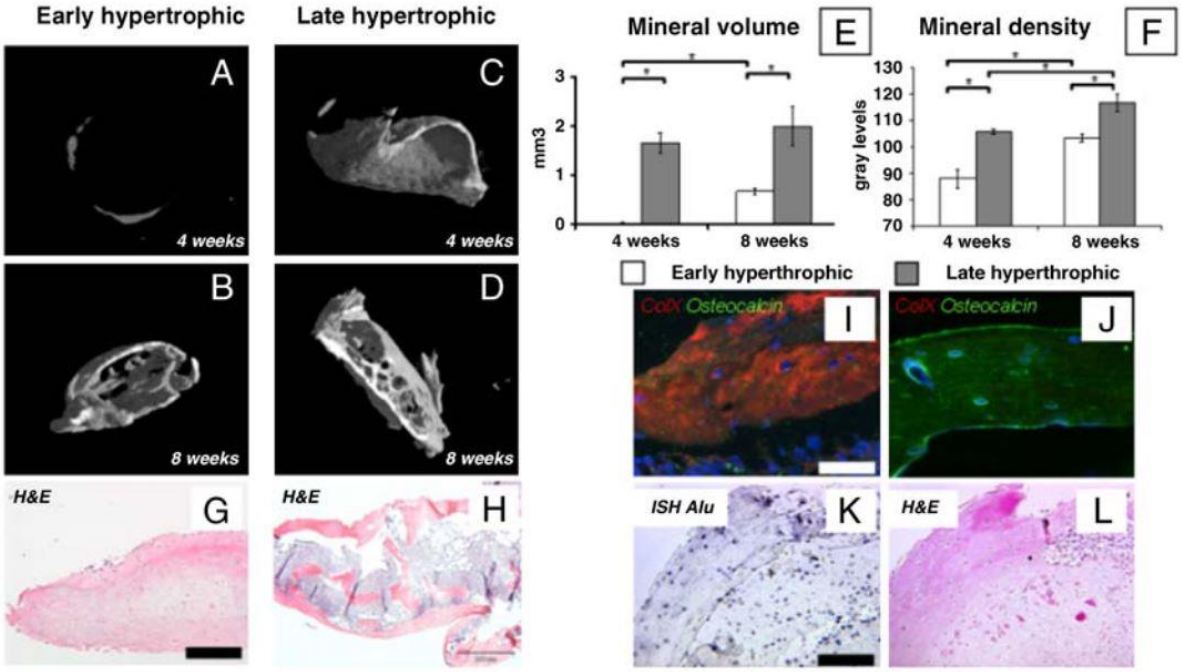

Figure 2.3: Morphometric analysis of the engineered bone tissue. (A–D) Three-dimensional μCT reconstructions and (E and F) quantitative histomorphometric data ($n = 4$) of mineral volume and density indicate higher bone quantity and more advanced maturation of late hypertrophic samples (* indicates significant differences; $p < 0.01$). (*G* and *H*) Trabecular-like structures were found both in the outer bony collar and in the inner core of late, but not early, hypertrophic samples. (Scale bar: 200 μm.) (*I* and *J*) Fluorescence characterisation for Col X (red) and osteocalcin (green) demonstrated the presence of mature lamellar bone only in late hypertrophic samples. (Scale bar: 50 μm.) (K and L) ISH to detect human *Alu* repeat sequences and hematoxylin/eosin staining of serial sections indicate that cells derived from the human adult MSC participated in the endochondral ossification process. (Scale bar: 100 μm) [149].

A follow up study by the same group reported it was possible to follow the endochondral approach to engineer whole bone organs at a size, structure, and degree of biological functionality comparable to that of native bones [19]. In this study, hBMSCs were seeded on type 1 collagen meshes and implanted subcutaneously in nude mice. After 12 of weeks of implantation, a functional bone organ containing a mature vascular network, and bone marrow spaces capable of hosting and maintaining hematopoietic stem cells (HSCs) had formed (Fig. 2.4).

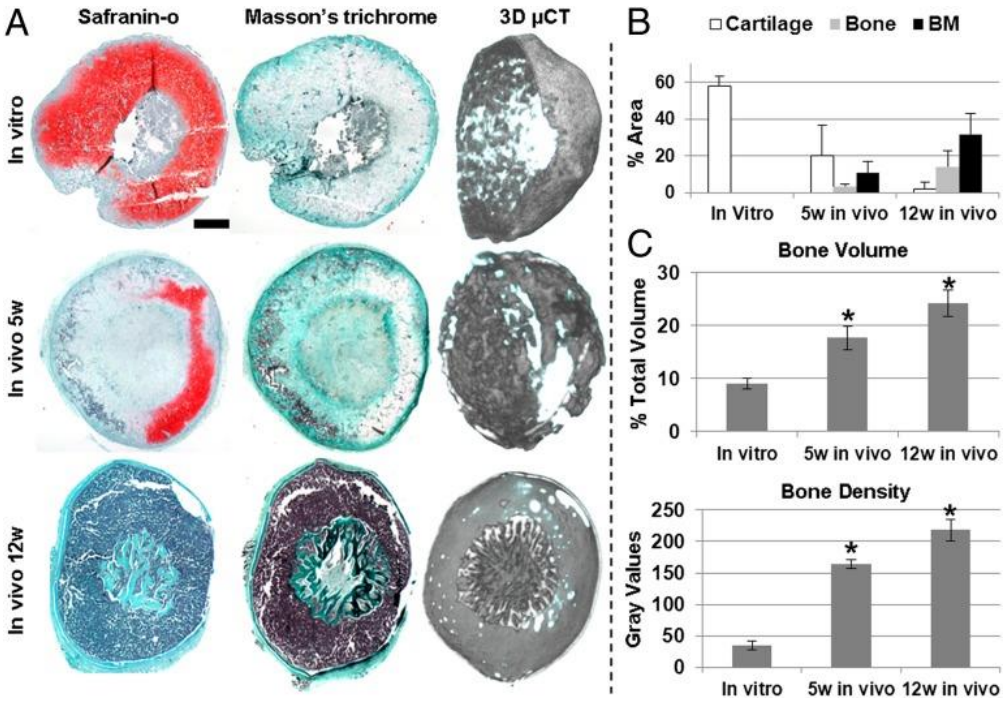

Figure 2.4: Demonstration of endochondral bone formation after implantation of engineered hypertrophic cartilage templates into subcutaneous pockets in nude mice. (A) Safranin-O and masson's

trichrome staining demonstrating conversion of the cartilage template (red in the saf-O) into bone (grey in the masson's trichrome) and 3D reconstructed µCT images of mineralisation after 5 and 12 weeks *in vivo*. (Scale bar, 1 mm.); (B) Quantitative histomorphometric data (n = 9) of cartilage, bone, and bone marrow. (C) Quantitative morphometric data (n = 4) of mineral volume and density ($p < 0.05$) [19].

In the last few years, a number of studies have demonstrated that it is possible to repair large bone defects in rodent models using such endochondral approaches [20-22, 44, 152, 153]. Chondrogenically differentiated BMSCs pellets were capable of inducing bone regeneration in orthotopic bone defects in rats by recapitulating EO [152] . In another study, Bernhard et al. developed tissue-engineered grafts using human adipose stem cells (ASC) [153]. These were differentiated into hypertrophic chondrocytes in decellularised bone scaffolds, which were then implanted into rat critical-size femoral defects. During the 12 weeks of implantation, these grafts showed rapid bone deposition and integration into the native skeleton, bridging the defects. Harada et al. reported the healing of rat large femoral bone defects, both 5mm and 15mm, following implantation of a chondrogenically primed poly(lactic-co-glycolic) acid (PLGA) scaffold [20]. In another study, chondrogenically primed (4 weeks in chondrogenic media followed by 3 weeks in hypertrophic media) rat bone marrow MSCs in alginate hydrogels successfully acted as templates to treat critically sized defects, promoting early bone formation [44]. Daly et al. produced, using GelMA as bioink, 3D printed hypertrophic cartilage grafts with an incorporated micro-channel network; these were proven to promote osteoclast/immune cell invasion and vascularisation, besides supporting controlled new bone formation [21]. Endochondral priming (3 weeks in chondrogenic media) was sufficient to induce vascularisation and subsequent mineralisation of hMSCs-seeded micro-fiber PCL scaffolds implanted in rat femoral large bone defects [22].

It is clear that recapitulating EO offers a promising route to bone regeneration. However, a number of challenges must be addressed before these approaches can be translated to a clinical setting. For example, to repair clinically size bone fractures, it will be necessary to engineer cartilaginous templates an order of magnitude larger than their rodent equivalents. Crucially, these templates must rapidly vascularise upon implantation *in vivo*. Strategies able to accelerate and direct vascularisation within hypertrophic cartilage templates will likely be required to successfully scale-up endochondral approaches to clinical dimensions. The clinical translation of the previously reported EO solutions is

hindered as well by practical, logistical and regulatory considerations due to the fact that they all consists of live cells and tissues. These challenges associated with the clinical translation of viable engineered tissues have motivated an increased research in the decellularisation of *in vitro* engineered tissues as a means of producing extracellular matrix (ECM) derived biomaterials and implants that are available *off-the-shelf* for tissue engineering and single-stage regenerative medicine procedures [27]. O*ff-the-shelf* implants represent an interesting alternative to viable constructs since they are easier to commercialise and translate into the clinic, as they are easily transported and stored, are available ready-to-use and they should face less onerous regulations to be clinically approved. The following sections will firstly introduce the ECM and its use as biomaterial for BTE. Different decellularisation methods will be reviewed, as will the use of decellularised ECMs in BTE.

2.2.5 Extracellular Matrix-based materials for BTE

As mentioned before, native bone tissue still represents the clinical gold standard for bone tissue regeneration. For this reason, several bone substitutes have been studied and developed to try to mimic native bone specific features to induce bone repair *in vivo* [154, 155]. Naturally, these osteoinductive features are related to the presence of osteogenic cell populations present in native bone, to biophysical parameters, such as structure (both macro and micro features) and mechanical properties, and to biochemical parameters, such as the presence of growths factors, minerals and cytokines [156]. Among these, biochemical factors provide pivotal instructive cues to drive the behaviour of cells, and native ECM represents a reservoir for those. The ECM is the noncellular component within all tissues and organs. It is a complex and essential entity consisting of water and a fibrillar network of glycoproteins, collagens, proteoglycans, polysaccharides and soluble factors deposited by the cells [157, 158]. The ECM provides a complex micro-environment that regulates cellular functions, such as adhesion, survival, migration, proliferation, differentiation, immune response, and wound healing, in addition to providing structural and physical stability to the tissue [159]. Each tissue in the body possesses a heterogeneous ECM with unique composition and topography [160, 161] that mediate cellular activities, in part by providing anchorage for cytokines and growth factors [162].

Native bone ECM acts as a reservoir of these cues, such as members of the transforming growth factor beta (TGF-β) family, including several bone morphogenetic

proteins (BMPs), angiogenic growth factors like the vascular endothelial growth factor (VEGF), and pro-inflammatory cytokines. All of these cues are presented in a complex and dynamic spatiotemporal manner, and are fundamental mediators of the different phases of bone formation and fracture-healing [163, 164]. It is therefore extremely challenging to mimic the complexity of the bone ECM using solely synthetic substitutes, and a lot of work has been done to improve the bioactivity of bone graft substitutes by adding discrete bone ECM components. Different ceramic particles (such as hydroxyapatite and tricalcium phosphate [165, 166]), selected growth factors [167] (such as TGF-βs [168], BMPs [169] and VEGF [170]), ECM proteins and peptides [171] (e.g. collagen type I [172], osteopontin and osteocalcin [173]) have all been incorporated into engineered bone grafts to enhance their bioactivity and bone regeneration. However, it remains challenging to recreate the native tissue in a reliable and effective way, because the aforementioned isolated components alone fail to mimic the molecular complexity and organised structure of the native bone tissue [174]. Moreover, optimal biological concentrations and release kinetics for most of the secreted factors and ECM molecules are still unknown, hindering the development of optimised solutions. This has motivated the development of bone graft substitutes using ECM derived biomaterials, obtained either from autologous, allogenic or xenogenic native tissues and organs [175, 176], or from the ECM secreted *in vitro* by cultured cells [160].

2.2.5.1 Native vs *in vitro* (cell-derived) engineered ECM

Over the past three decades, many tissue and organ ECMs have been used in pre-clinical research and clinical therapies. Some important examples include skin [177, 178], small intestinal submucosa (SIS) [179-181], pericardium [182-184], bladder wall [185-187], adipose tissue [188-190], vasculature [191, 192], neural tissue [193-195], trachea [196], skeletal muscle [197-199], tendon [200-202], ligament [203, 204] and bone [205-207]. Furthermore, several decellularised ECM products have been commercialised and approved by the Food and Drug Administration (FDA) for use in humans, and are currently used clinically, especially in soft tissue, bone, or cardiac applications. Examples of these products includes dermis tissue (AlloDerm® and Strattice™, LifeCell Corp.; TissueMend®, Stryker Corp.; GraftJacket®, Wright Medical Inc.; Conexa™, Tornier Inc., Allopatch®, Conmed), urinary bladder (MatriStem®, ACell Inc.), amniotic membrane (AmnioGraft®, Biotissue;

Aril™, Seed Biotech), pericardium (OrthAdapt® and Veritas®, Synovis Life Tech.; SJM™ Patch, St. Jude Medical), small intestine (Surgisis®, Cook Medical; CorMatrix® ECM, CorMatrix), demineralised bone matrix (DBM) (Puros® and InterGro®, Zimmer Biomet; BioSet™, Regeneration Tech.; DBX®, DePuy Synthes; Viagraf®, Smith & Nephew Inc.), heart valves (CryoValve®; CryoLife Inc.; Freestyle®, Medtronic Inc.). More complete overviews of the development and clinical applications of decellularised extracellular matrices from tissues and organs for tissue engineering and regenerative medicine can be found elsewhere [208, 209].

Tissue-derived ECMs have the advantage of maintaining the structures and compositions of the respective tissues and organs. However, they are characterised by limited availability (in case of autologous tissues), inherent heterogeneity, uncontrolled variability (that may arise from the age, health and gender of individual sources), potential host responses and pathogen transfer when allogenic and xenogeneic tissues and organs are used, uncontrollable degradation, and a limited ability for customisation beyond processing procedures and tissue source. In addition, for regenerative strategies that seek to mimic normal developmental process, for example endochondral ossification in the case of bone repair, it is clearly challenging to use native ECMs at different stages of tissue development [210]. On the other hand, ECM derived from *in vitro* cultured mammalian cells can provide an alternative to native tissue-derived ECM, targeting the aforementioned limitations. Similar to native tissue derived ECMs, such engineered ECMs are made up of a complex yet organised assembly of fibrillar proteins, growth factors, and matrix macromolecules, whose composition and organisation can be tuned depending on factors such as the cell type(s) and *in vitro* culture conditions.

This tunability can be achieved by modulating factors such as type(s) of cells used, dimensionality of culture (2D versus 3D), the use of bioreactors (e.g. perfusion, dynamic compression, hydrostatic pressure), media supplements and the possibility to genetically modify the source cells to overexpress or silence the expression of specific target molecules. Importantly, unlike native tissue-derived ECM, the availability of engineered ECM is theoretically unlimited, particularly if it can be produced using established cell lines. However, it is important to keep in mind that the cell type used is an essential parameter determining the ECM composition [211]. Interestingly, autologous ECM scaffolds could be prepared from autologous cells, which can be isolated from patients and subsequently expanded *in vitro*. The use of such autologous ECMs have the potential to avoid the

undesired host responses that may be induced by allogenic or xenogenic materials and address the limited availability of harvestable autologous native tissues [27]. Furthermore, if allogenic or xenogenic cells would be used, another benefit of producing ECM biomaterials from cultured cells is that they can be screened for pathogens and then maintained in a pathogen-free condition for ECM harvesting. Another key advantage of *in vitro* engineered ECM is that it is possible to generate constructs that mimic specific stages of tissue or organ development [212]. During development, stem cells differentiate and progress stepwise through different stages of maturation [213], a process that is accompanied by dynamic changes to the ECM [214, 215]. Again, by using specific cell types, culture conditions and biophysical stimuli, it is theoretically possible to design ECMs *in vitro* that mimic the dynamic matrix observed during different developmental stages [216]. Finally, using engineered ECM may enable easier and finer control on the design and production of 3D scaffolds with desired structural properties such as geometry and porosity, circumventing the possible limitation of poor cell penetration which can occur when repopulating decellularised native tissues.

Despite all these advantages, the generation of engineered ECM materials presents some limitations that need to be addressed [217]. Firstly, the amount of matrix material that can be collected from cell culture is generally small compared to what can be obtain from whole native tissues or organs, although strategies to scale-up the biomanufacturing of engineered tissues may address this concern. To engineer tissues with specific biochemical compositions, it may be necessary to use cells from younger donors and/or cells that have undergone limited monolayer expansion to avoid dedifferentiation. Engineered ECMs may possess poorer mechanical properties to their native equivalents, which in turn may negatively affect the mechanical functionality of the resulting graft. However, this problem has been addressed by combining engineered ECMs with synthetic materials with tuneable mechanical requirements. Moreover, donor-to-donor variability is generally associated with the use of primary cells, independently of the cell source, and this can limit the full exploitation of engineered ECM as biomaterials with standardised properties. This problem could be addressed by the use of immortalised cell lines as cell sources to produce the ECM [218]. Immortalised cell lines have been proven to be able to produce *in vitro* high quality matrix for at least 25 passages, increasing exponentially the amount of decellularised ECM that can be obtained from a single cell source [219]. Finally, another factor limiting the full potential of this technology, which is also associated with the use of native tissue derived

ECM, is the lack of an optimised decellularisation method. A more complete discussion on the decellularisation methods available and possible novel solutions are presented below.

2.3 ECM decellularisation

The decellularisation process is crucial for disrupting and removing cellular components from the ECM in order to prevent or minimise any negative inflammatory and immunological responses towards the biomaterial and decrease the risk of host rejection after *in vivo* implantation, especially in case of allogeneic and xenogeneic sources [220]. In fact, antigenic epitopes associated with allogeneic or xenogeneic cell membranes and intracellular components are usually recognised as foreign by the host and cause a destructive inflammatory response or immune-mediated rejection [221]. Decellularisation also typically represents the first step in the creation of *off-the-shelf* scaffolds from engineered ECM, whose structure and components can then be preserved after freeze-drying processing which allows for a cost-effective and easy storage and transport of such implants [222]. The main aim of decellularisation is to eliminate all cellular and nuclear materials while preserving the molecular composition, bioactivity and structural integrity of the matrix itself [216]. Thus, a good decellularisation requires a balance between preservation of bioactive cues in the ECM and removing potentially immunogenic components. To improve decellularisation outcomes, a variety of methods have been developed, which can be broadly divided into four categories: physical, chemical, enzymatic, and biological methods. The most effective and robust decellularisation protocols are usually a combination of more than one of the above methods. The quality of decellularisation can be partially assessed by how efficiently it removes cellular and genetic material, with the following criteria proposed in the literature: the obtained decellularised ECM must possess (1) less than 50 ng double-stranded DNA (dsDNA) per mg ECM dry weight, (2) less than 200 bp DNA fragment length, and (3) no visible nuclear material by 4’,6-diamidino-2-phenylindole (DAPI) or H&E staining [223]. Decellularisation techniques and the use of decellularised tissues, organs and engineered ECMs have been reviewed in depth elsewhere [85, 224-227], therefore they will only be discussed briefly here, with a focus instead on specific strategies that have been applied to decellularising engineered ECMs targeting bone defect healing.

2.3.1 Decellularisation methods

Physical methods (freeze-thawing, direct pressure, sonication, agitation, osmosis) can devitalise native or *in vitro* engineered tissue derived ECM by destroying cellular membranes, with consequent cell lysis [224], but do not necessarily remove all cellular components from the matrix. A very common physical method is repeated freeze-thawing cycles, used to form ice crystals inside the cells and lyse them. Physical methods have the advantage of minimally altering the ECM structure and mechanical properties. However, since these approaches result in incomplete removal of cellular debris, other methods may be necessary to obtain acellular tissues free of genetic material. Chemical approaches typically use alkaline or acidic reagents (calcium hydroxide, sodium sulphide, sodium hydroxide, ammonium hydroxide, peracetic acid, acetic acid and deoxycholic acid), hypotonic/hypertonic solutions, and/or detergents (Triton X-100, sodium dodecyl sulphate (SDS), CHAPS) to denature, solubilise and disrupt cellular components, membranes and DNA-protein interactions. Chemical reagents are very efficient in removing cellular components, including DNA; however, they can cause the loss of GAGs and damage the collagen, disrupting the ECM structure. For minimising the disruption of such important components, mild detergents, such as Triton X-100, are generally preferable to compounds such as SDS [228]. These milder detergents also retain greater ECM bioactivity [229]. Enzymatic decellularisation uses proteases (trypsin, dispase, collagenase) and nucleases (DNase, ribonuclease (RNase)). Trypsin is effective as a decellularising adjuvant but can cause damage to collagen networks with long exposure times. Nucleases (RNase and DNase solutions) are used to degrade any remnant of ribonucleic acid (RNA) or DNA, which can induce sterile inflammatory responses, and are often added to chemical treatments when decellularisation is not effective with detergents alone [230]. In general, enzymes can provide high specificity for removal of cell residues or undesirable ECM constituents. However, complete cell removal by enzymatic treatment alone is difficult and enzyme residues may impair recellularisation or evoke an adverse immune response [223]. Finally, biological methods include the use of chelating agents such as ethylenediaminetetraacetic acid (EDTA) and ethylene glycol tetraacetic acid (EGTA). By binding to metal ions and sequestering them, these agents helps in cell dissociation from ECM proteins [231, 232]. It is likely though, that chelating agents contribute as well to subtle disruptions in protein-protein interactions by the same mechanism [233]. Chelating agents alone are insufficient for complete cell removal, and they are therefore typically used in

combination with enzymes or detergents. All the aforementioned methods are efficient in decellularisation, but result, to different extents, in damage to the ECM material and do not guarantee the preservation of the structural, biochemical, or biomechanical features of the ECM itself.

With the objective of maintaining ECM bioactivity, a novel biological approach of devitalisation has been proposed, consisting in the specific activation of cell apoptosis [234]. To achieve this, an inducible genetic system [235] can be incorporated via retroviral transduction into cells to specifically induce their apoptosis on exposure to a clinical-grade chemical compound. This strategy offers the possibility to induce cell death and consequently achieve devitalisation, with, theoretically, minimal changes in the integrity of the ECM. During apoptosis, cells lose contact with the surrounding matrix while cellular constituents are kept strictly within the apoptotic bodies and cell membranes [236, 237]. This approach can be implemented with the application of a perfusion bioreactor system, which is helpful for removal of cellular fragments and debris. There are still a number of challenges that would need to be addressed to exclude presence of remaining living cells and limit undesirable effects, such as the retention of pro-inflammatory factors. However, decellularisation by intentional induction of cell death is an intriguing proposal that warrants further investigation.

Currently, there are no gold standard decellularisation methods for tissue- or cell-derived ECMs. The choice of specific decellularisation procedures generally depends on the ECM source and its properties, and as well on the characteristics of the resulting product that are sought. For example, an engineered ECM is usually less dense, and typically allows easier access for decellularising solutions. For this reason, milder solutions and shorter times are generally required in these cases, while harsher treatments are necessary for decellularising compact, native bone. An overview of the different combinations of methods used to realise biological scaffolds for orthopaedic tissue engineering from musculoskeletal tissues and *in vitro* engineered ECMs can be found here [220].

2.3.2 Decellularisation of *in vitro* engineered ECM for bone tissue engineering

A variety of cell types has been utilised to produce bone-like or osteoinductive ECMs, including human adipose-derived stem cells [238], BMSCs [239-244], amniotic fluid

stems [245], HUVEC [246], MSCs and HUVECs co-culture systems [211], dermal fibroblasts [247, 248], lung fibroblasts [249], nasal inferior turbinate tissue-derived mesenchymal stromal cells [250], embryonic stem cells [251], murine BMSCs [252], MC3T3-E1 [253-256], L929 fibroblasts [257], rat BMSCs [258, 259], primary rat osteoblasts [260, 261], and mesenchymal sword of Damocles (MSOD) [262]. Decellularised engineered ECMs have been investigated and used with promising results in several studies, mainly in three different forms/applications: (i) to produce biomimetic microenvironments for stem cell differentiation *in vitro*, (ii) to confer bioactivity to synthetic scaffolds through the deposition of matrix molecules on the scaffold surface, and (iii) to produce bulk biomaterials directly applicable in tissue regeneration.

2.3.2.1 Decellularised ECMs to investigate cell-ECM interactions

Decellularised cell-produced matrices have been used as substrates for cell culture to both investigate ECM-cell interactions and ECM regulation of cell differentiation, and to control *in vitro* cell functions and fate. *In vivo*, cells are always surrounded by their specific tissue ECM; for this reason, ECMs derived from different cell sources can be used to elucidate ECM-cell crosstalk and to study different ECM effects on cell functions, while trying to mimic a more realistic environment for cells during *in vitro* culture. For example, the ECM deposited *in vitro* by different cell types have been compared for their capacity to promote the osteogenic differentiation of bone marrow MSCs. Decellularised ECM sheets derived from bone marrow MSCs (BMSCs), MC3T3 osteoblasts, and L929 fibroblasts were reseeded with BMSCs to investigate their capacity to support osteogenesis [257]. The sheets obtained from BMSCs best supported the osteogenic differentiation of BMSCs, demonstrating the importance of the cell type when attempting to engineer osteoindutctive ECMs. Zhang et al. used ECM produced by human BMSCs (BM-ECM) *in vitro* as a platform to enhance the osteogenic potential and guide the differentiation of adipose stem cells (ASCs) into osteoblasts [240]. They demonstrated that BM-ECM provided a superior substrate for ASC expansion than tissue culture plastic (TCP), enhancing ASC proliferation, the expression of osteogenic markers (ALP, RUNX2, and OC) and their bone forming potential *in vivo*.

Engineered ECMs can also be used as substrate to support the maintenance of a specific cell phenotype during *ex vivo* expansion. Cell senescence and loss of phenotype

during culture is a major problem that limits the large-scale expansion and clinical use of cells such as MSCs. Sun et al. demonstrated how engineered ECM could be also used to prevent the negative effects of aging on MSCs [263]. They found that MSCs from aged animals can be rejuvenated and their defects in self-renewal and osteogenesis can be corrected by culturing them on an ECM generated by MSCs from young animals. In this way, the effectiveness of autologous MSC administration for therapeutic applications in adult patients could be optimised.

The majority of the studies investigating ECM-cell interactions have focused on static parameters; however, these parameters are dynamically altered *in vivo*, and it has been proven that during tissue development the ECM is dynamically remodelled through stepwise stages of maturation to regulate stem cell functions [264]. Hoshiba et al. developed a series of different biomimetic matrices mimicking ECM remodelling during the osteogenesis of MSCs (referred as "stepwise osteogenesis-mimicking matrices") to investigate how these differences effect cell fate [212]. Three types of matrix were prepared from culturing MSCs at different stages of osteogenesis: early stage (1 week in osteogenic medium), late stage (3 weeks in osteogenic medium) and stem cell matrix (1 week in medium without osteogenic induction factors). All the matrices supported the adhesion and proliferation of reseeded MSCs, but the different stages matrices showed different effects on cell fate, with the early stage matrix providing a more favourable microenvironment for osteogenesis. However, although these 2D stepwise osteogenesis-mimicking matrices may represent good *in vitro* models for analysing the roles of ECM in osteogenesis and provide a suitable microenvironment for the differentiation of stem cells for tissue regeneration purposes, they cannot closely mimic the *in vivo* 3D native microenvironments. To address this problem, the same group very recently developed stepwise osteogenesis-mimicking 3D PLGA-collagen-ECM hybrid meshes [265]. Three types of matrices were realised by culturing hMSCs in PLGA-collagen hybrid meshes and controlling their stages of the osteogenesis as in the previous study (stem cell stage, early stage and late stage), and they were used for hMSCs culturing and investigating their effects on the hMSCs functions (Fig. 2.5). The stepwise osteogenesis-mimicking hybrid meshes showed different ECM compositions, depending on their stage of osteogenesis, and their effects on the osteogenic differentiation of reseeded hMSCs varied. The osteogenic differentiation of hMSCs was increased by early stage scaffolds and moderately promoted by the late stage ones. On the other hand, stem cell stage scaffolds exhibited an inhibitory effect on hMSCs osteogenic differentiation.

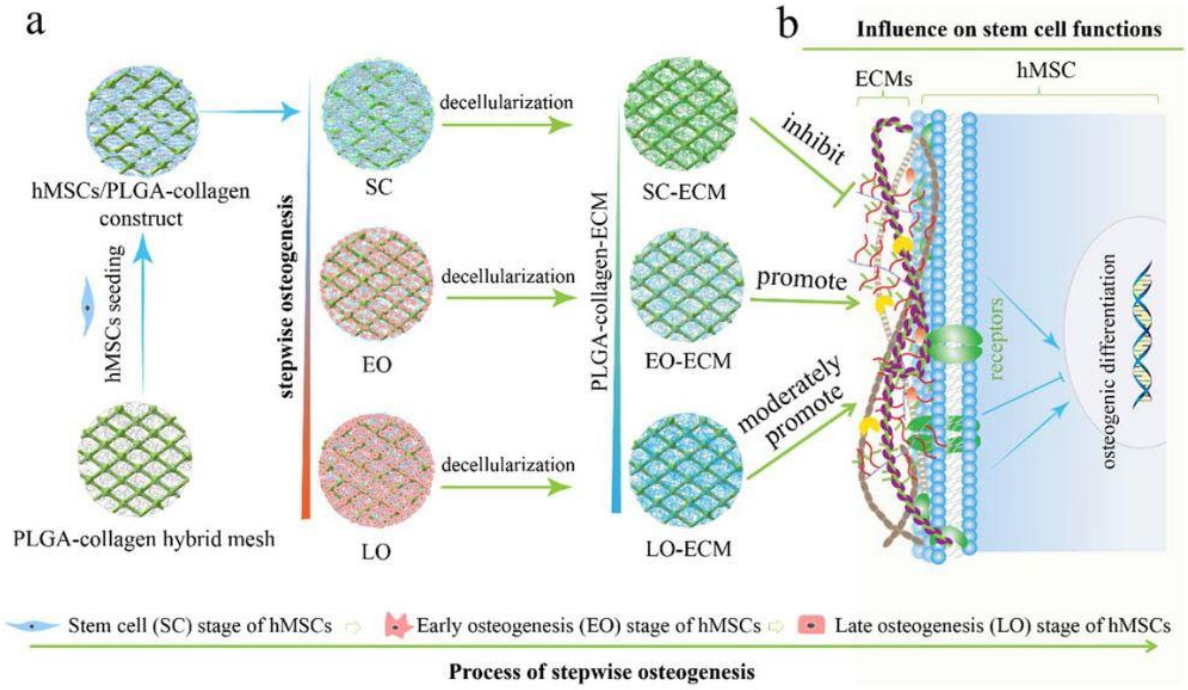

Figure 2.5: PLGA-collagen-ECM hybrid meshes mimicking stepwise osteogenesis. (A) Schematic illustration of the preparation of such meshes and (B) their influence on the proliferation and osteogenic differentiation of hMSCs (b) [265].

2.3.2.2 Decorating scaffold surfaces with engineered decellularised ECMs

Bone tissue engineering is strongly based on the realisation of 3D scaffolds to be implanted at the defect site to guide tissue regeneration. A well-engineered scaffold for regenerative medicine, which can be translated from the bench to the bedside, combines inspired design, technical innovation and precise know-how [266]. Different techniques, among which electrospinning and 3D printing can be found, have been used to fabricate scaffolds for BTE applications, offering advantages in controlling scaffold structural properties such as pore size, porosity and mechanical strength [267]. Nowadays, a large variety of materials are currently available for BTE purposes, which includes synthetic ceramics, polymers, metals and also biologically derived substrates [268]. Their ability to restore mechanical function has been successfully proven in a certain number of scenarios. However, the regeneration of host tissues driven by these materials remains challenging, because they usually lack the necessary bioactive sites and instructive cues, hampering cell attachment and differentiation capabilities [176]. To address this problem, engineered ECMs

can be deposited on the surface of 3D synthetic scaffolds to generate constructs with improved biological activities, capable of more closely mimicking the native tissue while possessing adequate structural and mechanical properties, which engineered matrices alone lack [216, 220]. The concept of enhancing the biological performance of the scaffolding material using cell-driven deposition of ECM is based firstly on a production phase which leads to ECM deposition at the surface of the scaffold, followed by a decellularisation process, which allows for subsequent storage of the modified scaffolds as *off-the-shelf* grafts. As opposed to their purified counterparts (discrete ECM components), cell-produced ornamented ECM offers a more complex environment composed of a multitude of factors at physiological concentrations [269]. 3D decellularised engineered ECM scaffolds for BTE have been obtained by the cell-derived ECM deposition on several organic and inorganic materials and their combinations. Examples includes poly-L-lactic acid (PLLA) [253], PLLA/gelatin [257], PCL [245, 270-273], hybrid PCL/PLGA [251], polyesterurethane (PEU) [242], poly sebacoyl diglyceride (PSeD) (Fig. 2.6) [238], biphasic calcium phosphate (BCP) [274], tricalcium phosphate beta (β-TCP) [246, 275], hydroxyapatite /β-TCP [243], hydroxyapatite [254, 261, 262, 276, 277], PCL/PLGA and PCL/PLGA/β-TCP [250], calcined bovine bone [255], titanium [258, 259, 278-281]. Besides enhancing the biological properties of the scaffolding material by culturing cells on their surface to deposit ECM and then decellularising it, as it was done in all the aforementioned studies, a recent alternative approach is to produce engineered ECM, decellularising it and then blending it with a polymer solution, which can then be used for electrospinning [211]. Using this approach, Junka & Yu fabricated electrospun PCL-decellularised ECM scaffolds characterised by a dual-layer structure, with embedded osteogenic and vascular cues derived from osteoblast and endothelial cells derived ECMs [282]. Finally, it has been shown as well that decellularised engineered coatings can be produced in 2D culture, successfully transferred to 3D substrates, for example on a poly lactide-co-glycolide (PLG) scaffold [283], or wrapped around a graphene oxide/collagen scaffold [284], and retain their capacity to modulate cell phenotype.

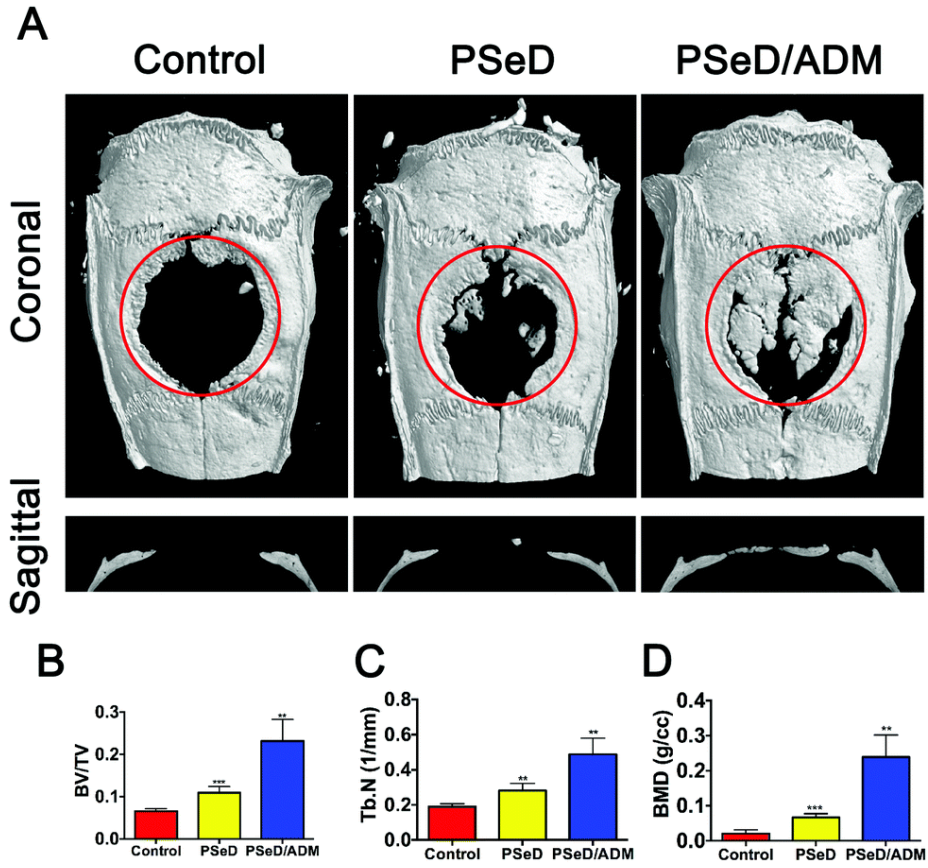

Figure 2.6: Adipose-derived matrix (ADM) enhanced the repair of critically sized rat calvarial defects. Micro-CT evaluation and morphometric analysis of calvarial bone repair for three groups: control (empty defect), PSeD (poly sebacoyl diglyceride mesh scaffold) and PSeD/ADM (PSeD mesh scaffold coated with ADM). (A) Representative coronal and sagittal images of calvarial bone defects 8 weeks post-implantation. Morphometric analysis of (B) bone volume/total volume (BV/TV), (C) trabecular number (Tb.N) and (D) bone mineral density (BMD). **p < 0.01, ***p < 0.001. [238].

2.3.2.3 Decellularised ECMs as bulk biomaterials

Decellularised engineered ECM has been also used to produce bulk biomaterials, which can be directly applied on their own in bone regeneration. Human dermal fibroblast have been used to produce decellularised ECM sheet for engineering a potential periosteum replacement [248]. It has been shown that these fibroblast-derived ECM sheets support *in vitro* MSCs growth and significantly influence MSCs osteogenic differentiation, driving an increased alkaline phosphatase activity, calcium deposition and bone-specific gene expression (Fig. 2.7). These ECM sheets were proven to bind significantly higher amounts of key growth factors (including ANG-1, TGF-β1, bFGF, and VEGF), as well as calcium phosphate on their surface, which contributed to high osteogenesis of the seeded MSCs.

These findings show the potential of these ECM sheet to be used as biomaterials in the engineering of a periosteum for critical sized bone regeneration applications. In another study, differentiating human BMSCs embedded in a 3D collagen/chitosan template were cultured to deposit embedded native ECM, which was then decellularised to create a 3D biomimetic scaffold for bone tissue engineering capable of triggering the differentiation of BMSCs toward an osteogenic lineage and promote nucleation of calcium phosphate polymorphs, forming a mineralised matrix [155]. This decellularised ECM scaffold was able, without the need for growth factors or differentiating agents, to induce differentiation of reseeded undifferentiated BMSCs by upregulation of several growth factors, transcription factors, ECM components, proteases, and receptors. Lu et al. developed a method to prepare different 3D engineered ECM scaffolds by culturing three cell types (human BMSCs, normal human articular chondrocytes, and normal human dermal fibroblasts) in a three-dimensional template (a knitted PLGA mesh), decellularising the obtained scaffold and finally selectively removing the template, leaving only the decellularised ECM scaffolds [285]. Autologous cells were also used to produce autologous ECM, which showed excellent biocompatibility when implanted in mice. The idea of using autologous cells is to produce autologous ECM capable of minimising undesirable host tissue responses.

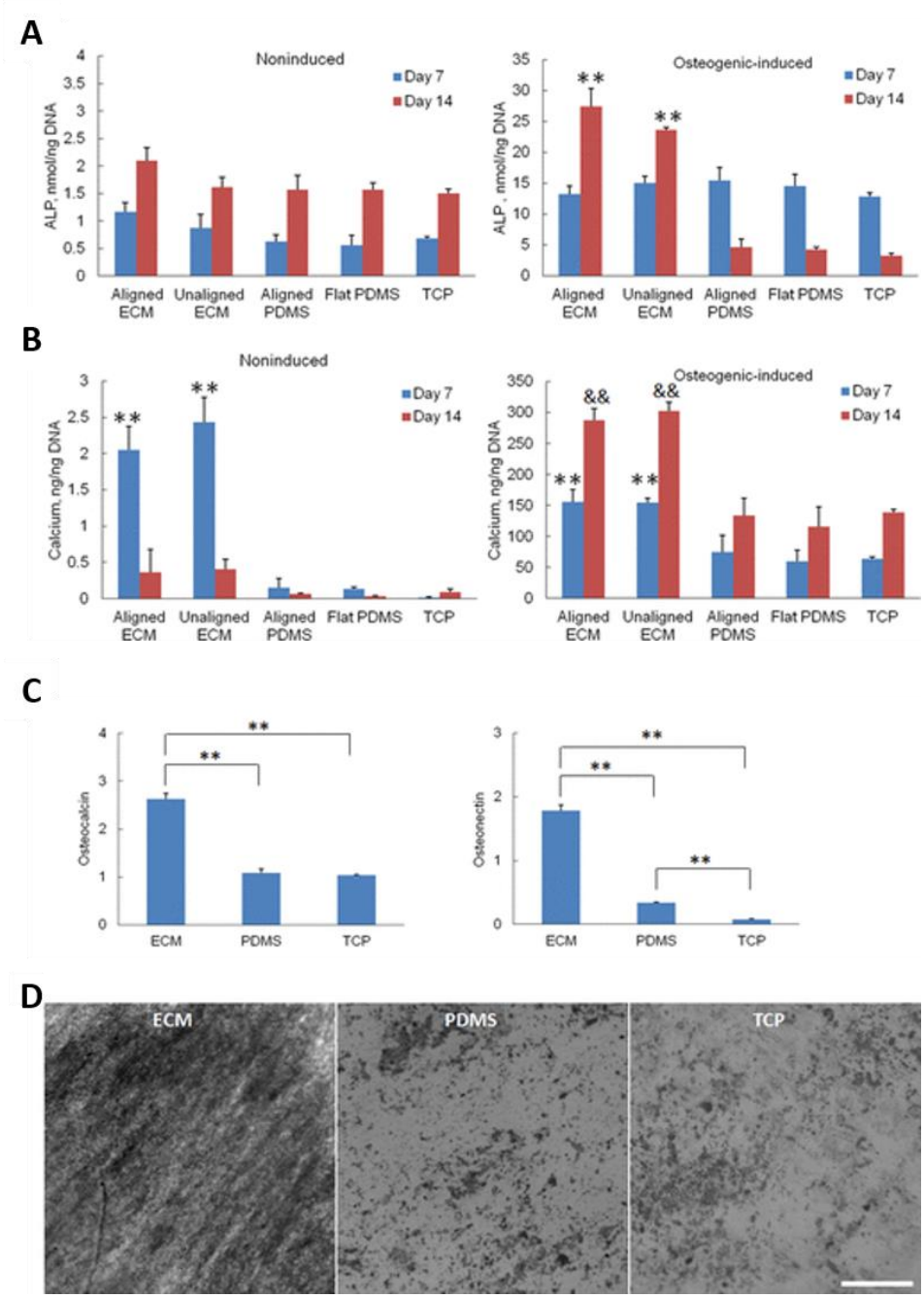

Figure 2.7: ECM sheet derived from human dermal fibroblast cells significantly increased alkaline phosphatase activity calcium deposition and bone-specific gene expression of seeded hMSCs, demonstrating their enhanced osteogenic potential and their ability to promote *in vitro* osteogenesis of hMSCs. The conventional cell culture substrates collagen I-coated polydimethylsiloxane (PDMS) and tissue culture plastic (TCP) were used as controls. ALP activity (A) and calcium deposition (B) from hMSCs in both noninduced and osteogenic-induced cultures on different substrates. ** $p < 0.01$ compared to PDMS and TCP on day 7; $^{\&\&}p < 0.01$ compared to PDMS and TCP on day 14. *ECM samples demonstrated the highest ALP activity and calcium deposition amount*. Gene expression (C) and Von Kossa staining (D) of osteogenic-induced hMSCs cultured on different substrates at day 14. **$p < 0.01$. Scale bar: 100 μm. *ECM samples showed significantly higher expression of osteogenesis-related genes and more mineralisation*. Adapted from [248].

2.3.2.4 Engineered decellularised cartilage templates for bone TE

Besides producing an ECM capable of directly driving MSCs osteogenic differentiation, engineered ECM could be designed to recapitulate the natural stages of bone tissue development and healing process. This could be done for example by creating a decellularised hypertrophic cartilage matrix, which, acting as a callus-like template, would be able to promote endogenous bone formation via endochondral ossification process. A number of studies have already demonstrated the capacity of living *in vitro* tissue engineered cartilaginous templates to undergo remodelling into bone tissue following endochondral ossification upon *in vivo* implantation [20, 149, 153, 286-290]. Applying the same concept, but decellularising the tissue engineered constructs prior to implantation, would help overcome a number of challenges that are intrinsic to these aforementioned living cell-based therapies, such as the need for autologous cells, the consequent high cost, complexity, due to the need for two surgical procedures, and all the associated regulatory hurdles [291]. To this end, Cunniffe et. al. developed porous decellularised tissue engineered hypertrophic cartilage (HT) scaffolds for large bone defect healing [292]. Human MSCs were cultured in transwell inserts and driven to hypertrophy with the addition of L-thyroxin and β-glycerophosphate to the media. After 6 weeks of culture, the hypertrophic cartilaginous ECMs were harvested, homogenised, decellularised, freeze-dried and cross-linked, prior to *in vivo* implantation in a subcutaneous nude mouse model and in critically sized rat femoral defect. The scaffolds were found to promote vascularisation and *de novo* mineral accumulation subcutaneously, and superior healing of critically sized bone defects in a rat femoral defect model (Fig. 2.8). Todorov et al. produced *off-the-shelf* allogenic hypertrophic cartilage grafts which could be used together with intraoperatively derived autologous cells (e.g. stromal vascular fraction (SVF) cells) [293]. Pellets of human MSCs were cultured for 3 weeks in chondrogenic medium, followed by 2 weeks in hypertrophic medium, and subsequently devitalised using freeze-thaw cycles. Grafts were obtained by mixing devitalised hypertrophic pellets with a suspension of SVF cells in fibrinogen and thrombin; they were then implanted ectopically in nude mice and orthotopically in a nude rat calvarial model. The grafts activated with SVF cells presented an enhanced capacity to form *de novo* bone tissue *in vivo*, being characterised by the remodeling of the pellets into trabecular bone organoids, their merging with each other and their bridging to host calvarium surrounding the defect.

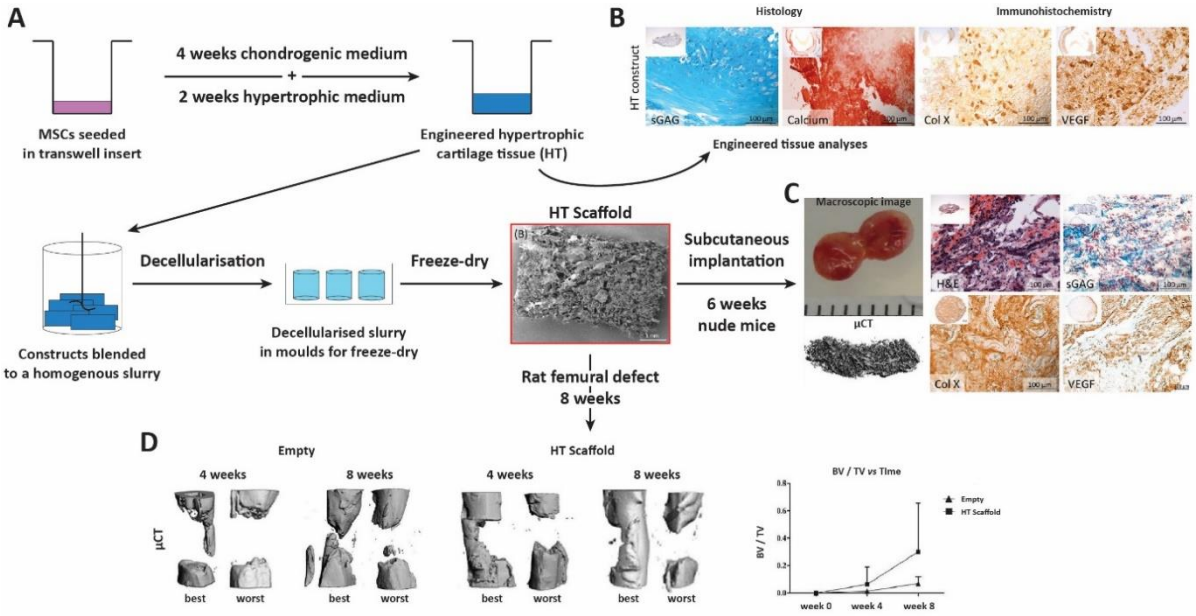

Figure 2.8: Realisation of porous decellularised tissue engineered hypertrophic cartilage (HT) as scaffold for large bone defect healing. (A) Construct realisation process; (B) histological and immunohistochemical analyses of the engineered hypertrophic cartilage tissue; (C) porous decellularised construct results after subcutaneous implantation; (D) bone regeneration in a femoral defect model (empty and decellularised hypertrophic cartilage scaffold (HT)). Adapted from [292]

In the same research group, Bourgine et al. induced chondrogenesis and subsequent hypertrophy of human MSCs to create engineered cartilaginous ECMs. These constructs were devitalised by the implementation of a death-inducible genetic system, capable of activating cell apoptosis [294]. The resulting hypertrophic cartilage templates were implanted subcutaneously in immune-deficient mice, and were found to efficiently remodel to form *de novo* bone tissue of host origin, including mature vasculature and bone marrow spaces (Fig. 2.9). More recently, Quang et al. cultured micro-aggregates of ATDC5 (~1000 cells per aggregate), a murine cell line with an intrinsic property to sequentially undergo hypertrophic chondrogenic differentiation, drove their *in vitro* hypertrophy, induced their mineralisation with beta-glycerophosphate, boosted their VEGF secretion using the hypoxia mimicking molecule phenanthroline, and subsequently devitalised/decellularised them to create what they referred to as micro tissue-engineered cartilage (MiTEC) [295]. Pre-clinical evaluation in orthotopic models of the MiTECs is need to assess their regenerative potential *in vivo*. Although only these few studies so far implemented the idea of decellularising

engineered *in vitro* engineered hypertrophic cartilage tissues, their results showed that there is a great potential in the use of such *off-the-shelf* implants capable of recruiting and instructing endogenous cells on the production of bone tissue following the native developmental pathway of endochondral ossification.

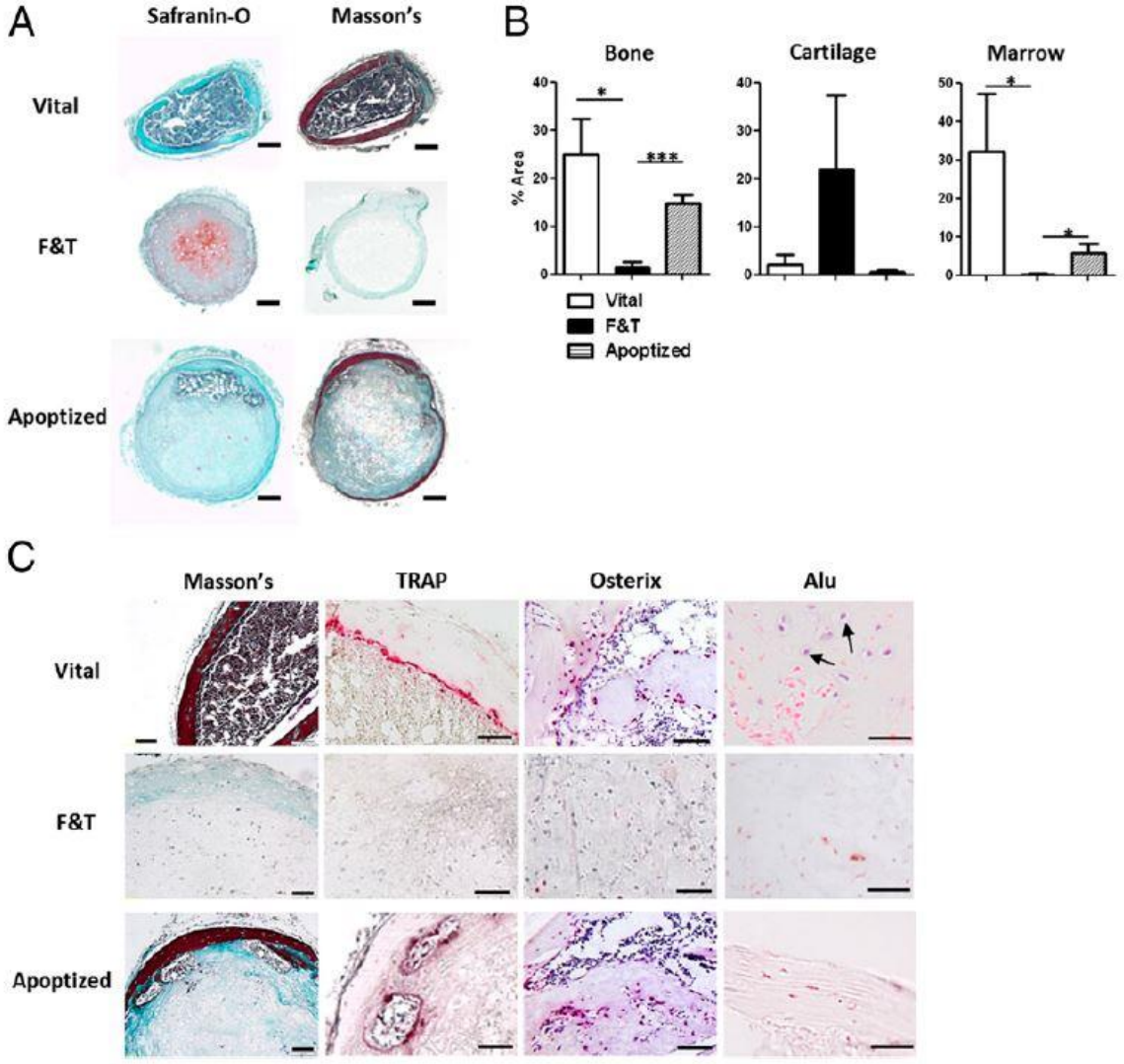

Figure 2.9: Endochondral bone formation assessment of implanted hypertrophic cartilage tissues. (A) Safranin-O and masson's trichrome staining of constructs retrieved 12 weeks after implantation. Vital constructs underwent a full remodeling into bone, whereas F&T samples resembled an immature collagenous matrix with abundant cartilage remnants. Apoptised samples displayed evidence of perichondral bone formation, embedding a hematopoietic compartment. (Scale bars, 200 μm.) (B) Histologic quantification of bone, cartilage, and marrow tissue areas in sections of explanted living and devitalised constructs. (C) Masson's Trichrome, tartrate-resistant alkaline phosphatase, osterix, and Alu staining were performed to, respectively, assess the presence of bone tissue, osteoclasts, osteoblasts, and human versus host cells. The

presence of host-derived osteoclasts and osteoblasts was detected only in Vital and Apoptised samples. Human cells were present only in Vital constructs (black arrows). (Scale bars, 100 μm.) [294].

All the examples presented in this paragraph show how engineered ECM possesses a great versatility and a huge potential in orthopaedic tissue regeneration applications. The beneficial effects of this class of biomaterials arise from its biophysical and biochemical properties: engineered ECM can enhance tissue regeneration acting as a biophysical template providing a suitable space for the adhesion and growth of *in vitro* seeded or *in vivo* migrated progenitor cells, but also by acting as a biochemical reservoir of cell-produced bioactive signalling molecules.

2.4 3D bioprinting for BTE

It has been already mentioned that each tissue has a different highly heterogenic ECM, with a unique 3D complex structure [160], from which arise its specific mechanical properties. It is clear that having control on the graft architecture is of fundamental importance. 3D printing, and biofabrication in general, represent a way to address this issue and acquire control over construct architecture and mechanical properties, allowing to engineer improved cell-derived matrices with specific geometry and structure, both at macro- (e.g., pore shape, geometry and size distribution) and micro-level (e.g., presence of microporosity, surface roughness and nanotopography), that mimic the native ECM environment, enhancing tissue regeneration.

2.4.1 3D printing technologies

In recent years, there has been increased interest in additive manufacturing strategies to produce constructs that more accurately mimic the native tissue environment. Architectural details that were previously unattainable or irreproducible can now be incorporated in an ordered way, and the composition of these constructs can be tuned spatially, further advancing the structural and chemical cues delivered to cells interacting with the scaffold [296].

3D printing is an additive manufacturing based technology for precise 3D construction, which, since its conception, has impacted several fields including engineering, manufacturing and medicine. It is a computer-aided manufacturing process which allows the patterning and assembling of living and non-living materials with a prescribed 3D organisation [297]. Among the currently employed 3D printing technologies like fused deposition modelling (FDM), direct ink writing (DIW), inkjet bioprinting, selective laser sintering (SLS), stereolithography (SLA) and laser-induced forward transfer (LIFT), the DIW and inkjet bioprinting are frequently preferred for 3D printing of live cells [298, 299]. The term 3D bioprinting is used to describe this precise layering of cells, biomaterials, and biologic factors with the goal of recapitulating and mimicking a biologic tissue [300]. Compared to traditional tissue engineering methods, 3D bioprinting allows for the precise spatial deposition of biomaterials and cells [301], resulting in a greater precision in the spatial relationship between the individual elements of the printed construct, and in the possibility to realise complex geometries and structures. For all these reasons, 3D bioprinting holds great promise for new regenerative medicine applications, pharmacokinetic or basic cell biology studies, and its development and application has been increasing constantly over the past few years [32, 302]. A schematic 3D bioprinting overview is presented in Fig. 2.10. As examples of the possible applications in TE, biofabrication has been recently adopted to engineer 3D constructs with the organisational features of different tissues, including skin [303], meniscus [304], aortic valves [305, 306], cartilage [307], bone [308], and blood vessels [309].

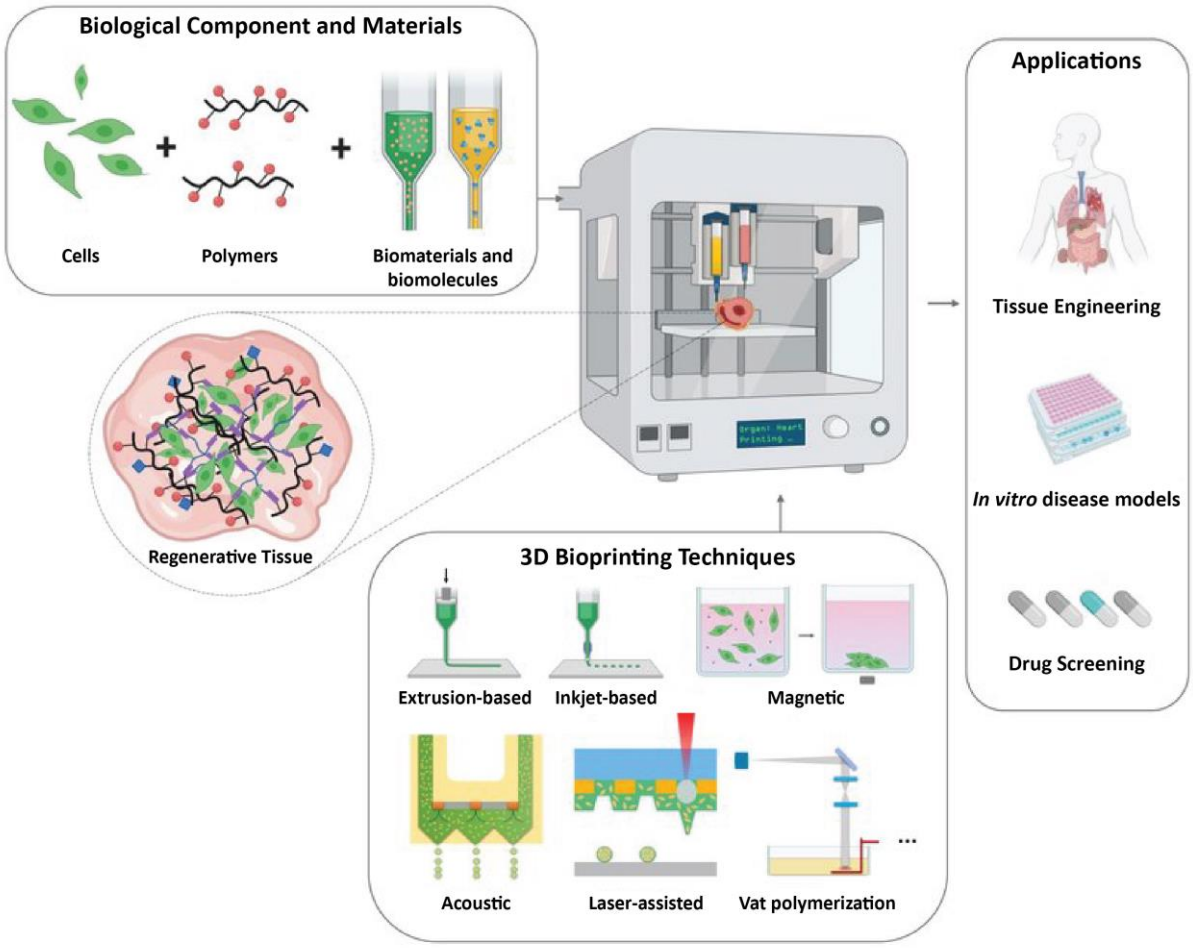

Figure 2.10: 3D bioprinting overview. Cells, polymers, biomaterials and biomolecules are used in combination to create 3D constructs through a number of different 3D bioprinting techniques (e.g. extrusion and inkjet-based, magnetic, acoustic, laser-assisted and vat polymerisation). The obtained constructs can be used directly or cultured to produce regenerative tissues, to then be applied as implants for tissue engineering applications, in *in vitro* disease models or in drug screening studies. Adapted from [310].

2.4.2 3D printing technologies applied to BTE

The use of 3D printing technologies for the design of bone tissue engineered constructs has been well documented over the years [311], however, the use of 3D bioprinting is still relatively new. Previous studies have investigated if a 3D bioprinted Matrigel porous scaffold containing co-culture of endothelial progenitor cells (EPCs) and multipotent stromal cells (MSCs), would lead to ectopic bone formation in nude mice [312]. Results showed that a bone-like tissue developed in the Matrigel scaffolds after 6 weeks of implantation. However, due to the low mechanical properties of Matrigel, load-bearing applications would require the addition of another reinforcing material. One way to address

this issue would be to design a bi-phasic scaffold. Previously a 3D bioprinted biphasic scaffold composed of a cell-laden hydrogel (alginate-methylcellulose blend) and a calcium phosphate cement (CPC) was investigated [313]. The CPC here has two functions: it is characterised by a resorbable hydroxyapatite structure, which mimics the mineral part of bone, and it exhibits suitable mechanical properties, which the hydrogel lacks. This study only looked at the *in vitro* cell viability of the constructs over 21 days so further investigation needs to be achieved to fully understand their benefits. In our group, we use 3D bioprinting to create hybrid constructs for bone TE using a combination of 3D printed PCL reinforced structures and bioprinted cell-laden hydrogels. Daly et al. developed a 3D bioprinted model of hypertrophic cartilage made from alginate bioink (functionalised with RGD-binding sites) mechanically reinforced with PCL fibres, mimicking the architecture of vertebral body [39]. After *in vitro* chondrogenic priming the biocomposite successfully transitioned into vascularised ectopic bone via the endochondral ossification process once implanted *in vivo*. Cunniffe et al. combined multi-tool biofabrication with non-viral gene delivery method to target ectopic bone formation [38]. Gene activated 3D printed constructs were established by co-printing MSCs-laden alginate and nHA-pDNA complexes (carrying BMP-2 and TGF-β3 plasmids) in-between reinforced PCL structures. The 3D bioprinted gene-activated constructs significantly increased vascularisation and mineralisation *in vivo* compared to cell-free controls. However, neither of these studies looked at bone formation in an orthotopic model.

2.4.3 Bioinks

A very important and usually limiting aspect of the use of 3D-bioprinting technologies is the selection of materials to be used in the formulation of bioinks [314]. Although major progress has been made with both natural and synthetic hydrogels in biofabrication [315], the formulation of suitable bioinks still presents some significant challenges. This is because bioinks needs to process certain physical and biological properties in order to be successful. Firstly, to print at high resolution, which is typically necessary for the fabrication of complex structures mimicking native tissues, bioinks need to possess specific physical properties, such as appropriate viscosity, shear-thinning behaviour, degradation rate and effective cross-linking during or after printing. Secondly, hydrogels used in bioink formulations need to be cell compatible cell instructive, since they

are loaded with live cells [316]. However, usually these physical and biological requirements tend to be contrasting and there is a lack of versatile materials able to meet all of them. A lot of research work is being done now to address this problem, since it has been recognised as a vital factor hindering further progress in this field [317-319]. The *biofabrication window* is a concept that describes the compromises that have traditionally been made to design bioinks [320], with researchers investigating and working between formulations that support high shape fidelity bioprinting (e.g. appropriate ink viscosity, shear thinning behaviour and yield stress) and those that are optimal for supporting cell proliferation, migration, growth, and differentiation (Fig.2.11).

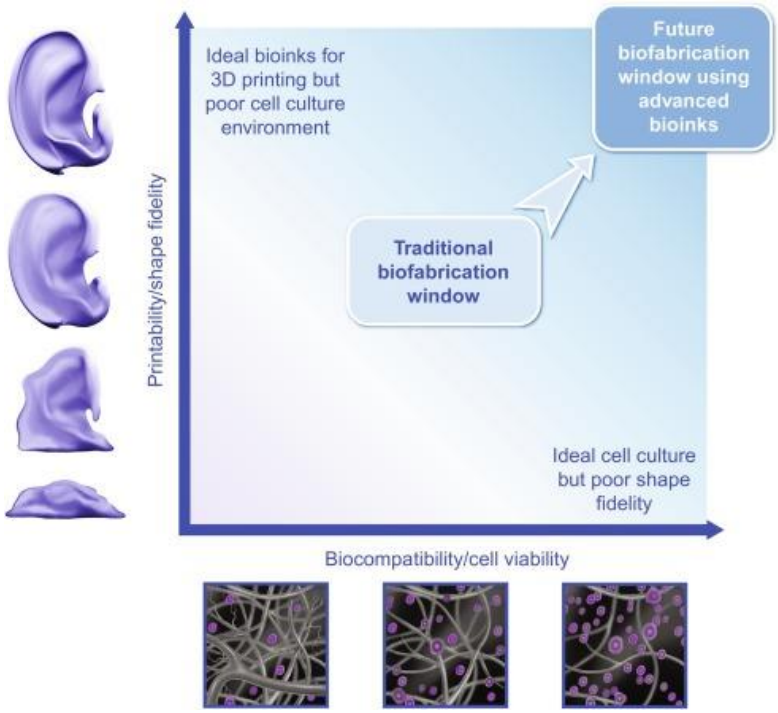

Figure 2.11: The biofabrication window. Improved bioprinted shape fidelity can be achieved with high polymer concentrations and/or crosslink densities; however, denser polymer networks can limit cell functions. Cells prefer lower polymer concentrations and/or crosslink densities which are difficult to bioprint. Advanced bioink strategies are being developed to create bioinks with high shape fidelity and excellent biocompatibility [321].

Shear thinning is the non-newtonian behaviour of fluids whose viscosity decreases when subjected to increased shear strain. Shear thinning results from a disruption to the weak physical self-assembling forces that can physically bind adjacent polymer chains.

These interactions are overcome during flow (under strain) but then reform when the strain is removed. This behaviour is exploited for bioink design and use. In fact, when shear strain is applied, during extrusion, the viscosity of the bioink will decrease initiating flow through the nozzle. After deposition of the bioink onto the platform, the shear strain is not applied anymore, thus the viscosity increases resulting in better material localisation and less filament spreading.

Many deposition-based biofabrication approaches have been used to realise 3D constructs for TE from hydrogels with cells and bioactive compounds [316, 318]. For the purpose of this review, the discussion will specifically focus on one of them: microextrusion. Microextrusion is one of the most widely used approaches in biofabrication and consists of bioink extrusion from a syringe barrel, usually disposable, through a nozzle, onto a building platform in the form of a filament. The extrusion can be pneumatic, piston or screw-driven. The main materials used are hydrogels, since they can be extruded while containing viable cells, growth factors and genetic material. The viscosity of the bioink must be sufficiently high to avoid tension driven droplet formation, to support extrusion of continuous filaments, and to allow construct shape retention after printing. Resolution that can be achieved with microextrusion is in the order of 200 μm, which is considerably lower compared to other methods, such as laser- or inkjet-based systems. Nevertheless, fabrication speed using microextrusion is consequently significantly higher [316].

In literature, a wide range of bioinks with suitable rheological behaviour can be found, which have been developed and used for 3D-bioprinting. Examples of materials compatible with such bioprinting technology are alginate [309, 322-325], GelMA [31, 35, 326], agarose [327-329], collagen [330-333], silk [334, 335], and hyaluronic acid [336-338]. For the purpose of our work, the next paragraph will focus on the use of fibrin in medicine and tissue engineering applications and the formulation of fibrin bioinks.

2.4.4 Fibrin in Tissue Engineering and 3D Bioprinting

Fibrin is a natural biopolymer involved in the coagulation cascade and results from the conversion of fibrinogen to cross-linked fibrin catalysed by thrombin. Gelation of fibrin occurs under physiological conditions without the need for modification of the basic components. When fibrinogen and the enzyme thrombin are combined, this causes the

cleavage of fibrinogen to fibrin, which then quickly assembles into a fibrin gel under physiological conditions. Fibrin and fibrinogen have critical roles in blood clotting, cellular and matrix interactions, inflammatory response, wound healing, and neoplasia [339]. For its properties, fibrin has been widely used in the clinic as a hemostatic agent in cardiac, liver, and spleen surgery. Importantly, it can be used in surgery for patients with hemophilia. Fibrin is used as well as a sealant and to reduce suture anastomosis in a variety of clinical applications [340]. A number of allogeneic fibrin sealants such as Tisseel®, Evicel™, and Crosseal™ have been approved by the Food and Drug Administration (FDA) for clinical use as hemostatic agents [341].

Naturally, fibrin provides a biocompatible structural scaffold, has adhesion capabilities, and possesses many of the important biological properties needed for successful tissue regeneration, such as excellent biocompatibility and biodegradation properties. Fibrin matrix is quickly remodelled and resorbed through natural fibrinolysis as cells deposit the tissue-specific extracellular matrix components during the regeneration of functional tissues. Moreover, it could be produced from the patient's own blood and used as an autologous scaffold; this would remove the potential risk of foreign body reaction or infection [342]. For all these reasons, fibrin represents an attractive biomaterial for tissue engineering applications [343], and it has been widely used in a variety of them, including adipose [344], cardiovascular [345-349], bone [350-352], cartilage [353-355], skin [356, 357], and nervous [358-360] tissue regeneration among many others. In addition, fibrin hydrogels have been used in applications for promoting angiogenesis [361-363]. The fibrin hydrogel as a potential scaffold has three major disadvantages/risks: the shrinkage of the gel that happens during the formation of flat sheets, low mechanical stiffness, and its rapid degradation, which might happen before the proper formation of tissue engineered structures [341, 349]. In order to improve its low mechanical properties, fibrin hydrogels can be combined with other scaffold materials to obtain constructs with desired mechanical strength. The most common material used for preparing composite scaffolds through biofabrication is polycaprolactone (PCL) [364, 365]. To prolong the stability of fibrin hydrogels and to tune their degradation rate, a number of strategies can be used. One approach is to optimize pH and the concentrations of fibrinogen and calcium ions (Ca^{2+}) [366]. Another strategy is to modify fibrin with a molecule such as polyethylene glycol, making the fibrin structure more stable [367]. Finally, protease inhibitors that are specific for plasmin and matrix metalloproteinases can be added to the *in vitro* culturing media [368], or alternatively, they

can be immobilised into the fibrin hydrogel [369, 370]. For decades, Aprotinin has been one of the most common protease inhibitor used in the clinic to reduce blood loss and blood transfusions [371]. However, the use of aprotinin is hindered by its lack of specificity since it inhibits a huge portion of the serine proteases present in blood [372]. A large clinical trial found no survival benefits of using aprotinin in surgery, and it has been withdrawn from general use. For this reason, a lot of efforts have been made to design plasmin inhibitors able to reduce bleeding after trauma and during surgery more specifically and effectively, and a number of inhibitors with higher potency and selectivity [373, 374] have emerged in the recent years. Nevertheless, aprotinin is still used in tissue engineering research to inhibit premature fibrin degradation, extending its mechanical integrity [375-378].

Although being characterised by excellent biological properties, fibrin does not meet the appropriate rheological properties required for the majority of the biofabrication processes, first of which viscosity. Being a relatively viscous material once polymerised, fibrin will associate with poor cell viabilities when used in filament-based deposition techniques. This is because in order to meet sufficient resolution standards small nozzles or high feeding speeds will be required, resulting in high shear and extensional forces [379]. To solve this problem, fibrinogen has been used instead. In contrast to fibrin, fibrinogen is characterised by low viscosity which sets a quite low limit on the complexity of the achievable constructs, which can easily collapse due to fibrinogen's low mechanical properties. For these reasons, fibrinogen has not been widely used for the printing of 3D structures. Bioprinting of fibrinogen has been achieved by addition of higher viscosity materials, usually referred to as "thickening agents", to create composite material constructs. Several groups addressed this problem by mixing fibrin with thickening components, able to provide the desired viscosity, like gelatin [380, 381], polyethylene glycol [382], hyaluronic acid [383] or gelatin and alginate together [384-388]. In these cases, researchers have usually relied heavily on the crosslinking of the other components (mainly alginate and gelatin) to produce 3D structures [389, 390]. Use of this additional crosslinking is not an absolute requirement, as fibrinogen itself can rapidly form a stable gel as already mentioned before. As such, the rationale for including the higher viscosity materials is typically to improve print fidelity and mechanical properties of the 3D structure. However, it is important to consider as well the biological effects that these included materials can have. This can be addressed by adding temporary thickening agents to the fibrinogen ink [30]. This approach involves mixing fibrinogen with a gelatin-based carrier gel containing

hyaluronic acid and glycerol, which possess an appropriate viscosity for 3D-printing. The novelty in this study is that post-printing the constructs are immersed in a thrombin bath, which causes the gelation of fibrin. However, all the other components of the bioink solution do not cross-link and can be washed away in a warm bath at 37 °C, leaving behind a fibrin only construct. They validated these bioinks by 3D printing human-scale tissue constructs (e.g. mandible bone, ear-shaped cartilage and skeletal muscle). Looking more in detail at the case of the mandible bone (Fig. 2.12), they used data from a CT scan of a human mandible defect to produce a CAD model of a defect shape, with dimensions of 3.6 cm × 3.0 cm × 1.6 cm (Fig. 2.12a). A text-based command motion program was used to determine the required dispensing paths of cell-laden hydrogel, PCL and and Pluronic F127 (Fig. 2.12b). PCL and the cell-laden hydrogel were printed layer by layer using Pluronic F127 as temporary support (Fig. 2.12c) and cross-linked in a thrombin bath. After being cultured in osteogenic media for 28 days (Fig. 2.12d), the construct was stained with alizarin red to investigate calcium deposition in the cell-laden hydrogel (Fig. 2.12e), which was confirmed [30].

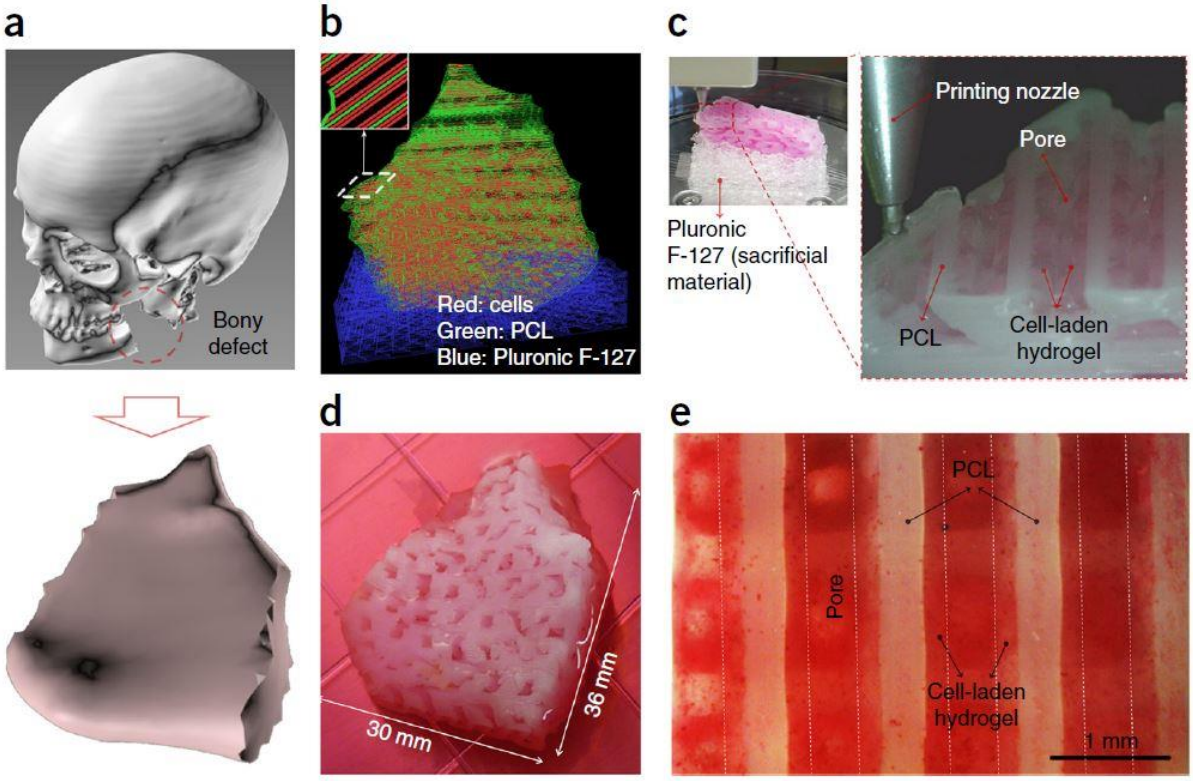

Figure 2.12: Mandible bone reconstruction. (a) 3D CAD model recognised a mandible bony defect from human CT image data. (b) 3D architecture of the mandible bone defect. Lines of green, blue and red colours indicate the dispensing paths of PCL, Pluronic F-127 and cell-laden hydrogel, respectively. (c) 3D printing

process. (d) Photograph of the 3D printed mandible bone defect construct, after 28 days of culture in osteogenic media. (e) Osteogenic differentiation was confirmed by alizarin red staining, indicating calcium deposition [30].

Along with these approaches, a new 3D bioprinting technique termed freeform reversible embedding of suspended hydrogels (FRESH) has been developed [391]. FRESH uses a thermoreversible fugitive support bath, which can be removed afterward, to enable the direct 3D printing of biologically relevant hydrogel inks including alginate, fibrin, collagen type I, and Matrigel in complex, 3D biological structures (Fig. 2.13).

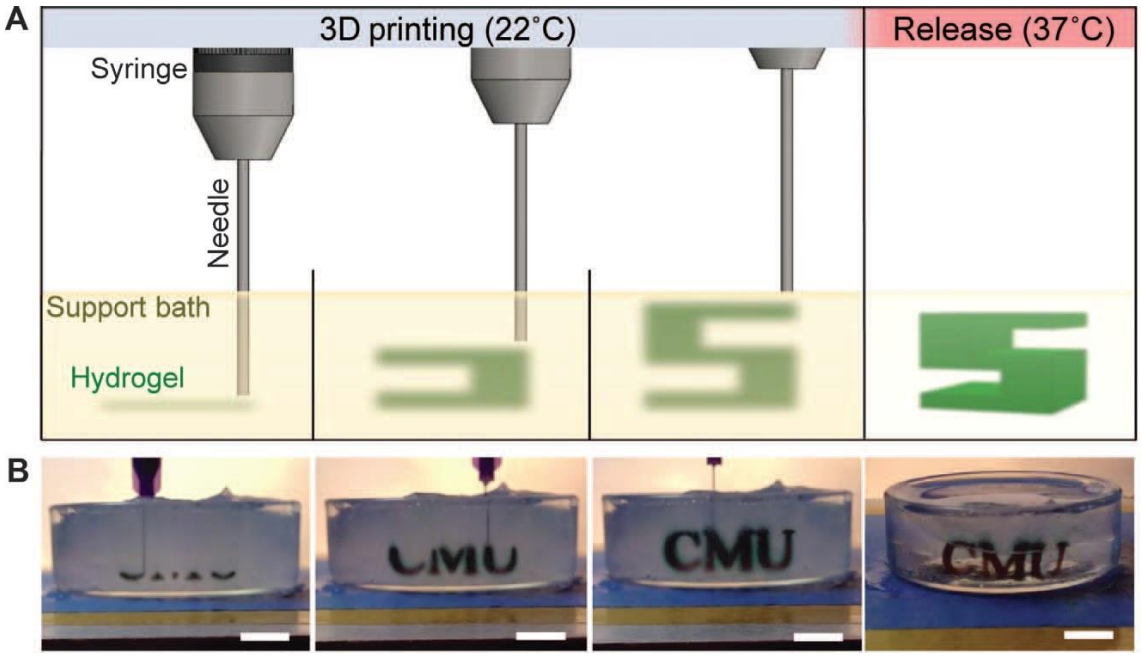

Figure 2.13: FRESH printing. (A) A schematic of the FRESH process showing the hydrogel (green) being extruded and cross-linked within the slurry support bath (yellow). The 3D object is built layer by layer and, when finished, is released by heating to 37°C and melting the bath (gelatin in this case). (B) Images of the letters "CMU" FRESH printed in alginate (black) and released by melting the gelatin support (grey material in the petri dish) [391].

With an improved second generation of FRESH (called FRESH v2.0) the same group showed it is possible to directly 3D bioprint collagen with precise control of composition and microstructure, and to prove it they engineered tissue components of the human heart at

multiple length scales, from capillaries to the full organ [392]. They showed as well that this technique can be directly used with fibrinogen instead of collagen.

Using a similar technique, another group recently 3D bioprinted human MSCs spheroid-laden fibrinogen fibres in a supporting bath composed of an interpenetrating polymer network (IPN) of polyethylene glycol and alginate hydrogel [393]. In this work, after having printed the fibrinogen, which polymerised thanks to the thrombin supplemented to the bath, the pre-polymer bath itself was dual-crosslinked to form the mechanically robust part of the construct. The bath in this case has a double role: to support the printing of a low viscosity bioink (cell-laden fibrinogen) and to become integral part of the construct, forming the load bearing component of the final engineered construct.

2.5 Summary

This literature review has demonstrated that developmentally inspired approaches to bone tissue engineering hold great promise, and could provide a suitable framework for new bone regeneration approaches. It is clear from the literature review that recapitulating EO offers a promising route to bone regeneration, as *in vitro* engineered cartilaginous templates can form new mature bone following *in vivo* implantation. In order to be applied clinically, such developmental precursors need to be scaled up and provided with mechanical reinforcement; scaling such endochondral approaches toward clinical relevance will also require strategies that can support vascularisation *in vivo*. All these issues can be addressed by using 3D printing technologies to fabricate highly ordered, scaled-up engineered cartilage constructs with internal architectures optimised for nutrient transport *in vitro* and vascular invasion *in vivo* and external geometries targeting specific patient anatomies. However, it is also clear from the literature that in order to realize the aforementioned engineered cartilage templates, it will be necessary to identify bioinks that are not only capable of supporting chondrogenesis of MSCs *in vitro*, but which also degrade *in vivo* to enable vascularisation and conversion of the cartilage graft into bone.

This review also highlighted that clinical translation of viable engineered tissues is hampered by practical and logistical considerations, making *off-the-shelf* decellularised constructs clinically preferable. The literature demonstrates that a lot of different methods are available and have been used to decellularised both tissue- and *in vitro* engineered

ECMs, but it remains unclear whether decellularised engineered tissues will retain their capacity to support bone regeneration, which hinders the development and clinical translation of such *off-the-shelf* constructs.

In light of this review, it is hypothesised that bioprinting technology could be employed to spatially pattern MSC-laden fibrin bioinks, which could also be mechanically reinforced, in order to generate cartilage templates of defined size and architecture (chapter 4). It is further hypothesised that such 3D bioprinted constructs could be engineered through a priming culture to produce developmental inspired cartilaginous precursors for the repair of critically sized bone defects; this question will be explored in chapter 5. Finally, it is also hypothesised that by decellularising the 3D bioprinted constructs, *off-the-shelf* engineered cartilaginous templates can be produced which retain their capacity to regenerate such critically sized bone defects; this question will be addressed in chapter 6 of the thesis.

Chapter 3: Biofabrication of Micro-channelled MSC Laden Fibrin Constructs as Templates for Endochondral Bone Repair

3.1 Introduction

Critically sized osseous defects cannot regenerate spontaneously and often require surgical intervention. In 2014, over two millions bone grafting procedures were performed annually worldwide, which is the second most frequent tissue transplantation after blood transfusion [3]. Despite drawbacks such as limited supply and donor-site morbidity [394], autografting still represents the clinical gold standard treatment used in the clinic. This motivates the need for clinically effective tissue engineering and regenerative medicine approaches for bone regeneration.

Traditionally the field of bone tissue engineering has focused on recapitulating the developmental process of intramembranous ossification, trying to directly form bone by driving mesenchymal stem cells (MSCs) or osteoprogenitors cells towards the osteogenic lineage. As documented in the literature review of this thesis, there are a number of limitations with this approach, which has led to increased interest in tissue engineering strategies that attempt to recapitulate the developmental process of endochondral ossification. These approaches aim to create cartilage precursors which *in vivo* can undergo hypertrophy, calcification and finally be replaced by new bone [395]. It has been shown that cartilaginous tissues produced by MSCs can effectively act as templates for endochondral bone formation *in vivo* following subcutaneous implantation in nude mice [18, 19, 396, 397]. Moreover, it has been demonstrated that such TE strategies can be used to repair large bone defects in rodent models [20, 44, 152, 153, 398]. Despite initial encouraging results, there are some requirements that have to be met in order to translate these approaches to the clinical setting, including the scaling-up the engineering of such grafts and ensuring their robust vascularisation *in vivo*. While such endochondral templates are known to become well vascularised *in vivo* [19, 39, 397], this progress typically begins from peripheral regions of the implant, which can lead to the persistence of avascularity in the tissue core [23, 399, 400]. Therefore, in order to scale up these approaches, there is clearly a need for strategies that can stimulate and guide vascularisation within hypertrophic cartilage templates. In a

previous work, we introduced micro-channel networks within gelatin methacrylate (GelMA) hydrogels to engineer channelled cartilaginous templates and implanted them into critically sized femoral bone defects in rats [21]. Compared to solid templates, the micro-channelled constructs supported increased vascularisation and host interaction *in vivo*. However, even after 8 weeks *in vivo* some portions of the hydrogel were still visible, and this was probably limiting complete graft integration and remodelling into functional bone. This motivates the use of alternative biomaterials to GelMA for engineering cartilage templates for endochondral bone regeneration.

Fibrin is a natural biopolymer present in the blood and it is formed in the last step of the clotting process [343], when besides acting as a blood barrier, it provides a temporary scaffold able to support tissue healing and remodelling [401]. Fibrin, formed from fibrinogen and thrombin, is commonly used as a biomaterial in TE applications due to its proven biocompatibility and biodegradability [402], making it a promising candidate biomaterial scaffold for the engineering of our large cartilaginous constructs for endochondral bone TE. The overall aim of this study was to assess MSC chondrogenesis and progression along an endochondral pathway in fibrin hydrogels. To this end, cell-laden fibrin hydrogels were chondrogenically primed for five weeks *in vitro* and the resulting matrix development was assessed using biochemical, histological and immunohistochemical analyses. Furthermore, micro-channels were introduced into these constructs to facilitate nutrient transport *in vitro* and potentially vascularisation *in vivo,* as demonstrated in our previous work [21].

3.2 Materials & Methods

3.2.1 Isolation and expansion of MSCs

Human bone marrow derived MSCs (hBMSCs) were isolated from bone marrow aspirates (Lonza) and expanded in high glucose dulbecco's modified eagle's medium (hgDMEM) GlutaMAX supplemented with 10% v/v FBS, 100 U/ml penicillin, 100 µg/ml streptomycin, 2.5 µg/ml amphotericin B at 5% pO_2 (all Gibco, Biosciences, Dublin, Ireland). Following colony formation, MSCs were trypsinised, counted, seeded at density of 5000 cells/cm^2 in T175 flasks (Thermo Fisher Scientific), supplemented with hgDMEM, 10% v/v FBS, 100 U/ml penicillin, 100 µg/ml streptomycin, 2.5 µg/ml amphotericin B, and 5 ng/ml

human fibroblastic growth factor-2 (FGF-2; Recombinant Human FGF-basic – 154 a.a., Peprotech) and expanded to passage 2 at 5% pO_2.

3.2.2 Construct fabrication

Silicone moulds (Ø = 4.2mm, h = 5 mm) with four vertical pillars (Ø = 1 mm, h = 5 mm) (Fig. 1A) were prepared by casting into negative moulds, and then ETO sterilised. Fibrinogen (F8630, Sigma-Aldrich) (100 mg/ml) was dissolved at 37 °C in Aprotinin (10000 KIU/ml) (Uniphar, Dublin, Ireland) containing 19 mg/ml of sodium chloride (NaCl), and used to resuspend $15x10^6$ cells/ml of hBMSCs. Just before the use, the fibrinogen solution was mixed 1:1 with thrombin (5 IU/ml in DMEM) and pipetted in the silicone moulds. Constructs (with a final concentration of 5% fibrinogen) were crosslinked at 37 °C for 30 minutes, then removed from the silicone moulds and placed in culture.

3.2.3 Chondrogenic priming

The chondrogenic culture conditions applied in this study are defined as culture in a chondrogenic medium (CDM) consisting of hgDMEM GlutaMAX supplemented with 100 U/ml penicillin, 100 mg/ml streptomycin, 100 μg/ml streptomycin, 100 μg/ml sodium pyruvate, 40 μg/ml L-proline, 50 μg/ml L-ascorbic acid-2-phosphate, 4.7 μg/ml linoleic acid, 1.5 mg/ml bovine serum albumine, 1x insulin-transferrin-selenium, 100 nM dexamethasone (all purchased from Sigma-Aldrich), 2.5 mg/ml amphotericin B, 10 ng/ml of human transforming growth factor- β3 (TGF-β3) (Prospec-Tany TechnoGene Ltd., Israel) and 10μl/ml Aprotinin. The constructs were primed for 3 weeks at 5% pO_2 followed by 2 weeks at 20% pO_2.

3.2.4 Biochemical analysis

The biochemical contents of all samples were analysed at day 0, 21 and 35 of culture. Prior to biochemical analysis, constructs were washed in PBS, weighed and frozen for subsequent assessment. Each construct was digested with papain (125 mg/ml) in 0.1M sodium acetate, 5 mM L-cysteine HCl, 0.05 methylenediaminetetraacetic acid (EDTA), pH

6.0 (all from Sigma-Aldrich) at 60 °C and 10 rpm for 18 h. DNA content was quantified using the Hoechst Bisbenzimide 33258 dye assay, with a calf thymus DNA standard. The amount of sulphated glycosaminoglycan (sGAG) was quantified using the dimethyl methylene blue dye-binding assay (Blyscan, Biocolor Ltd., Northern Ireland), with a chondroitin sulphate standard. Total collagen content was determined by measuring the hydroxyproline content using the dimethylaminobenzaldehyde and chloramine T assay and a hydroxyproline to collagen ratio of 1:7.69.

3.2.5 Histological and immunohistochemical analysis

Constructs were fixed in 4% paraformaldehyde, dehydrated in a graded series of ethanol's, embedded in paraffin wax, sectioned at 8 µm and affixed to microscope slides. The sections were stained with alcian blue to assess sGAG content, picrosirius red to assess collagen content and alizarin red to assess calcification. Collagen types I, II and X deposition were evaluated by immunohistochemical analysis. Briefly, sections were treated with chondroitinase ABC (Sigma-Aldrich) in a humidified environment at 37 °C to enhance permeability of the extracellular matrix. Sections were incubated with goat serum to block non-specific sites and collagen type I (ab90395, 1:400), collagen type II (sc-52658, 1:400) or collagen type X (ab49945, 1:200) primary antibodies (mouse monoclonal, from Abcam - Cambridge, UK and Santa Cruz - Texas, United States) were applied over night at 4 °C. Next, the sections were treated with peroxidase to block endo-peroxidise activity. Next, the secondary antibody (Col I, anti-Mouse IgG, B7151, 1.5:200; Col II, anti-Mouse IgG, B7151, 1:300; Col X, anti-IgM, ab49760, 1:200) was added for 1 h at room temperature followed by incubation with ABC reagent (Vectastain PK- 400, Vector Labs, Peterborough, UK) for 45 min. Finally, sections were developed with DAB peroxidase (Vector Labs) until brown staining was observed in the positive controls. Positive and negative controls were included in the immunohistochemistry staining protocol for each batch.

3.2.6 Statistical Analysis

Statistical analysis was performed using GraphPad 8 (GraphPad Software, La Jolla California USA). One-way analysis of variance (ANOVA) with the addition of Turkey's correction was used for multiple comparisons testing. Results are expressed as mean ±

standard deviation. For all comparisons, significance was accepted at a level of $p < 0.05$. Sample size (n) is indicated within the corresponding figure legends.

3.3 Results

3.3.1 Development of micro-channelled fibrin hydrogels

A silicone mould was used to produce fibrin hydrogels containing a network of micro-channels (Figure 3.1A). A plastic master mould was first used to realize silicone moulds with several wells, each of which contained four vertical pillars. These pillars were included to enable the creation of the micro-channels in the final fibrin constructs. Constructs were crosslinked for 30 minutes at 37 °C, removed from the silicone wells and placed in culture. Micro-channels were confirmed to be patent. The experimental setup and timeline are presented in Fig. 3.1B.

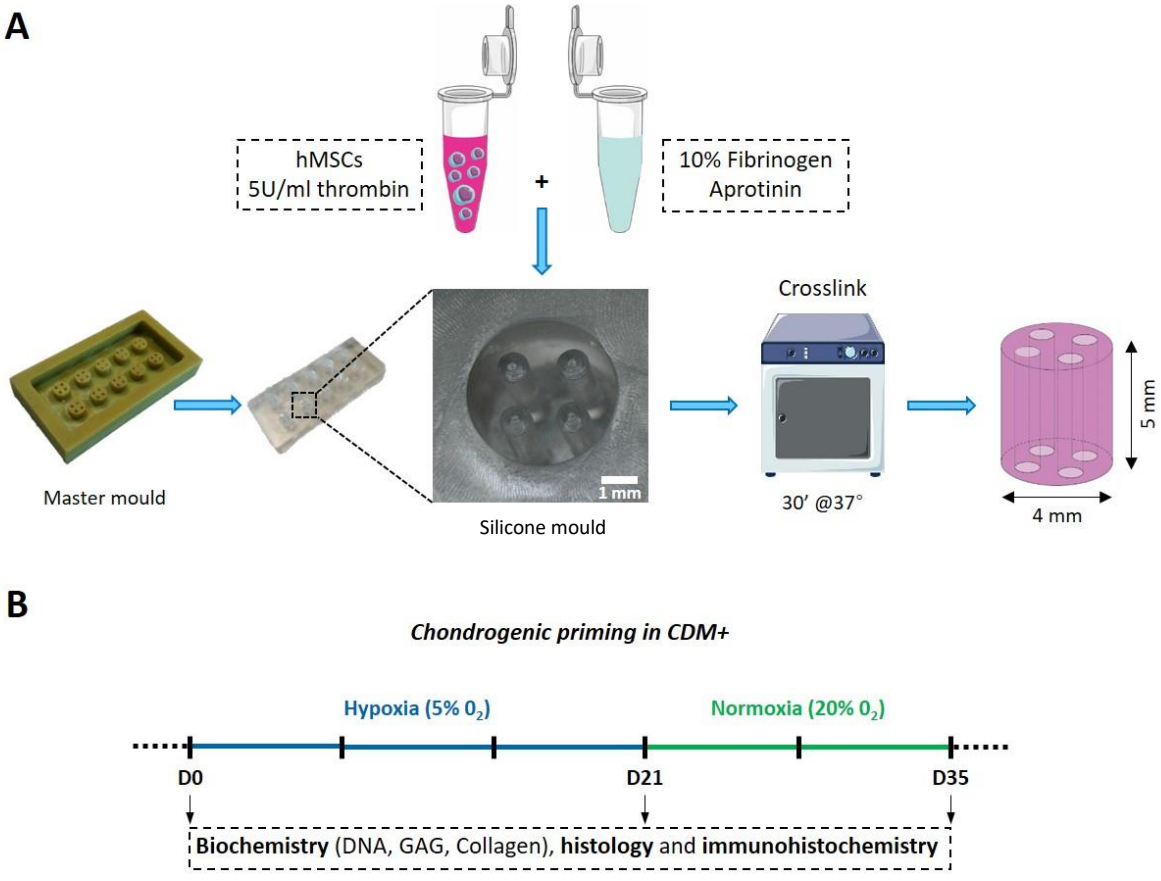

Figure 3.1: Construct realisation process and experimental setup. (A) Steps involved in the realisation of the micro-channelled cell-laden fibrin constructs; (B) experimental setup and time line.

3.3.2 Biochemical analyses

DNA content within the fibrin constructs remained stable over the 35-day culture period (Fig. 3.2A-B). Both sGAG and collagen content significantly increased over time in culture (Fig. 3.2C–F).

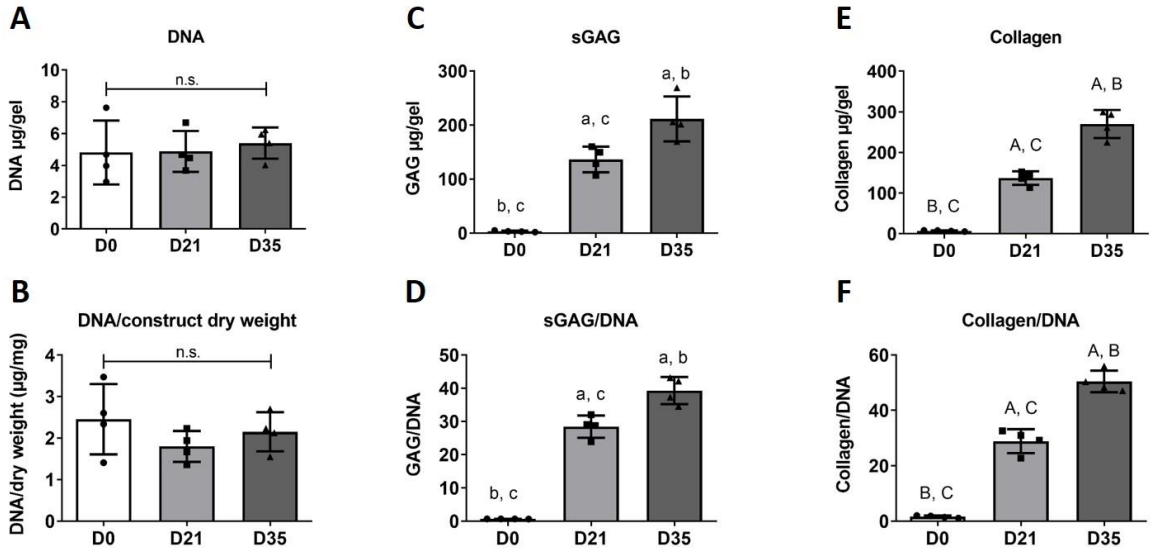

Figure 3.2: Biochemical analyses of micro-channelled constructs chondrogenically primed for 35 days. (A) DNA total content; (B) DNA content normalised to construct dry mass; (C) sGAG total content; (D) sGAG content normalised to DNA content; (E) collagen total content and (F) collagen content normalised to DNA content. n = 4 samples per group per time point, $^{a}p<0.0001$ vs. D0, $^{b}p<0.005$ vs. D21, $^{c}p<0.005$ vs. D35 (for sGAG), $^{A}p<0.0001$ vs. D0, $^{B}p<0.0001$ vs. D21, $^{C}p<0.0001$ vs. D35 (for collagen).

3.3.3 Histological and immunohistochemical analyses

Histological analyses of extracellular matrix deposition was in agreement with the biochemical data (Fig. 3.3). Alcian blue (Fig. 3.3A) and picrosirius red (Fig. 3.3B) staining showed an increase in matrix deposition from day 0 to day 35. Matrix deposition was reasonably homogenous throughout the engineered tissue. Calcification of the engineered tissue was also assessed using alizarin red staining (Fig. 3.3C). Small calcific deposits were observed within the engineered tissues after 35 days of culture.

Moreover, to investigate the nature of the collagen present, we performed immunohistochemical staining for collagen type I, II and X (Fig. 3.4). A clear increase in type II deposition was observed with time in culture (Fig. 3.4B). While staining for collagen type I and X (markers of chondrocyte hypertrophy and endochondral ossification) was less intense, the deposition of these proteins also increased with time in culture (Fig. 3.4A and 3.4C).

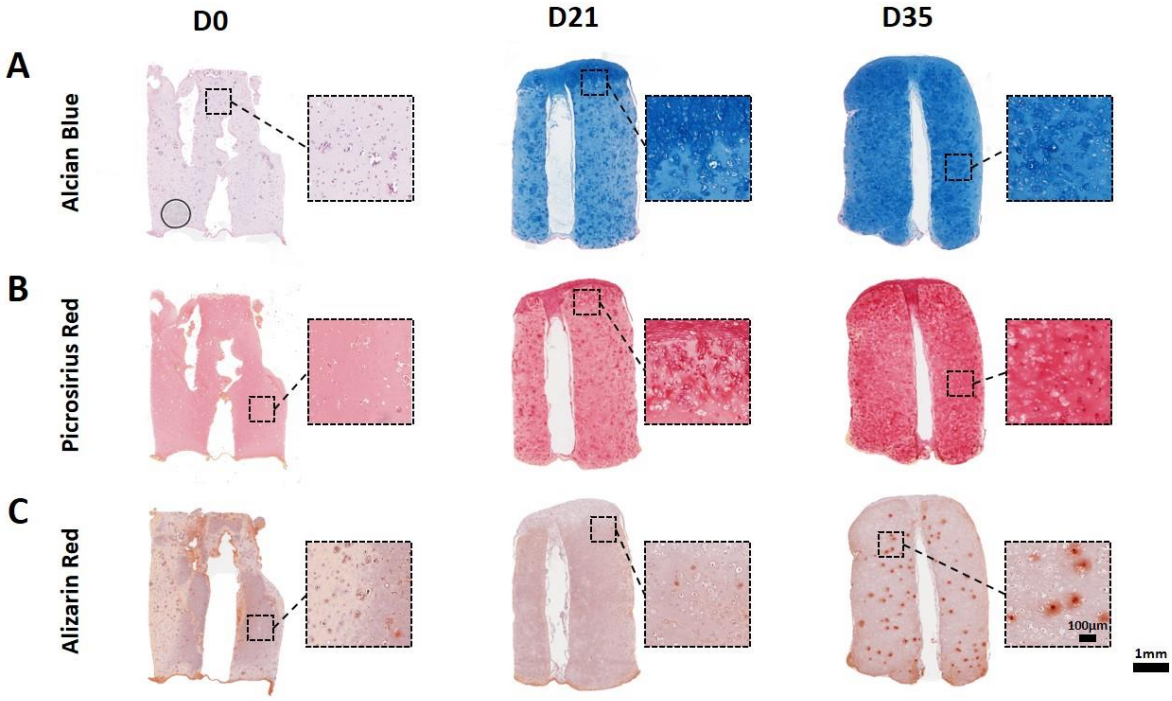

Figure 3.3: Histological analyses of micro-channelled constructs at days 0, 21 and 35. (A) Alcian blue staining for sulphated proteoglycans; (B) picrosirius red staining for collagen; (C) alizarin red staining for calcium.

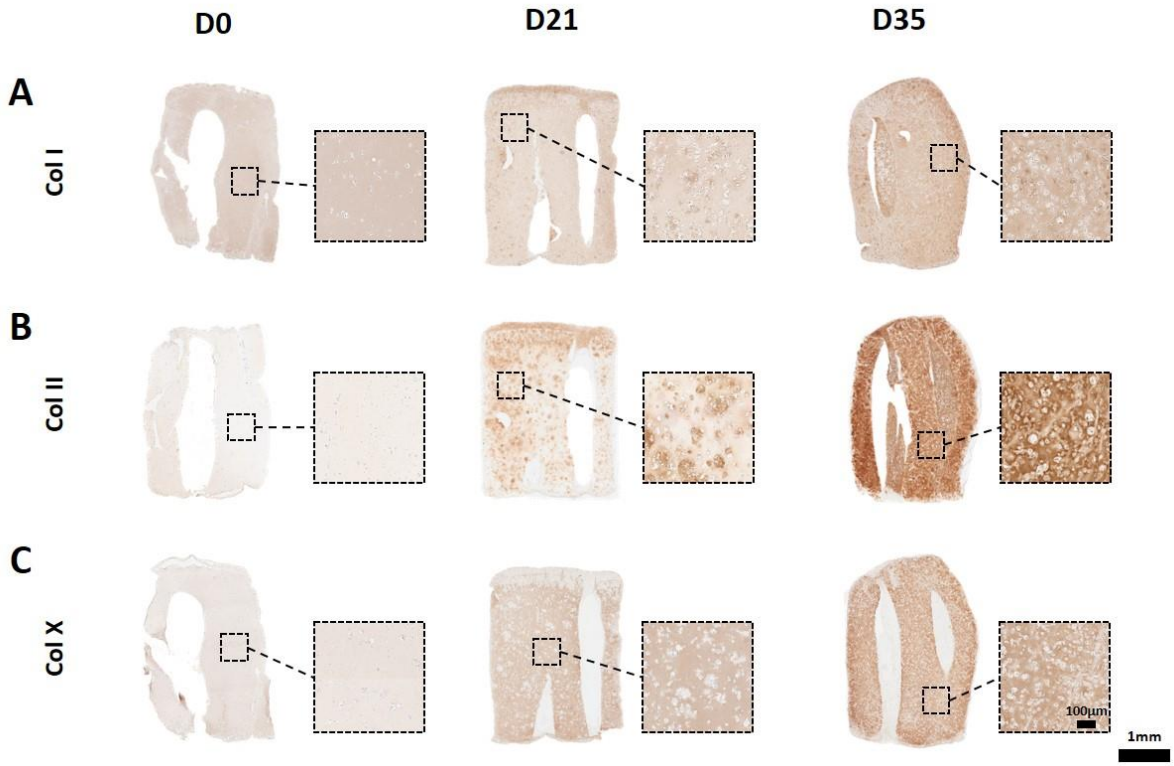

Figure 3.4: Immunohistochemical analyses of micro-channelled constructs at days 0, 21 and 35. (A) Collagen type I; (B) collagen type II; (C) collagen type X.

3.4 Discussion

The overall aim of this chapter was to assess MSC chondrogenesis and progression along an endochondral pathway in fibrin hydrogels. In addition, we sought to introduce micro-channels into these constructs to potentially improve nutrient transport *in vitro* and ultimately vascularisation *in vivo*. With this study, we demonstrated the ability of fibrin to support an endochondral phenotype *in vitro*. Furthermore, we developed a technique to fabricate micro-channelled constructs in a reproducible way.

In recent years there has been increased interest in endochondral bone tissue engineering, aiming to recapitulate this developmental pathway for bone regeneration. Briefly, endochondral ossification is based on the replacement of cartilage intermediaries by new bone [46], which is achieved through tissue invasion by blood vessels [395, 403, 404]. Vessels bring in nutrients and different cell types which start the mineralisation of the cartilaginous matrix and the creation of the bone marrow. The process of vascularisation, mineralisation and creation of bone marrow will continue until the new bone is fully formed.

Although several studies have demonstrated the potential of endochondral bone tissue engineering, when considering the translation of these approaches to the clinical setting, a number of challenges arise, first of which is sufficient implant vascularisation. It has been shown that when constructs are scaled up, avascular regions persist in their core upon implantation *in vivo* [23, 399, 400], therefore there is a clear need of strategies to accelerate and guide vascularisation within large constructs. A number of methods for enhancing vascularisation are currently under investigation. These include modifying the implant architecture, angiogenic factor delivery and *in vitro* pre-vascularisation [405]. For this study, we modified the architecture of the implant as a putative strategy to enhance vascularisation. This was done by introducing a network of internal micro-channels into the body of the engineered tissue. The concept of using micro-channels inside a hydrogel constructs is not new; in fact, in a number of previous studies, both from our and other groups, have used this approach to enhance nutrient diffusion inside large cartilage constructs *in vitro* [406-411].

The micro-channels within the engineered tissues remained patent over 35 days in culture. After 21 days of culture, cells were observed to bridge the endings of the micro-channels, forming a thin layer of new matrix, but the channels remained patent up to day 35. We do not expect this thin bridging layer to represent a problem after implantation *in vivo*. In our previous study that used a similar implant architecture, the micro-channels were infiltrated by host cells along their length following implantation into a rat femoral defect model [21]. In case of unexpected *in vivo* issues with these bridging layers, they could potentially be prevented by the implementation of dynamic culture conditions during the chondrogenic priming. We expect that the agitation of the media and its subsequent flow inside the channels would be sufficient to limit matrix deposition at the micro-channels endings.

In this study, we demonstrated through biochemical and histological analyses that fibrin can support MSC chondrogenesis and, when chondrogenically primed, these hydrogels supported an endochondral phenotype *in vitro*. Over time in culture, embedded MSCs secreted an extracellular matrix rich in sGAG and collagen, which were quite well distributed throughout the construct. At day 21 of culture, a top layer of tissue with a different matrix composition, richer in sGAG and collagen, is observed histologically. It is important to note that this zonal difference is not present at day 35, where samples are characterised by a homogeneous staining. In addition, we performed immunohistochemical staining for collagen type I, II and X, to have an insight on the nature of the deposited

collagen. Abundant collagen type II deposition was observed, which is the main component of hyaline cartilage, and of collagen type I, the collagenous constituent of endochondral osteoid and main component of fully developed bone [412]. Collagen type X deposition was also observed, which is naturally synthesised by hypertrophic chondrocytes during endochondral bone formation and it is localised within the mineralising cartilage and the growth plate [413, 414]. The increase in positive staining for all these three collagen types proves that fibrin was able to drive MSCs towards an endochondral phenotype. For these reasons, the fibrin micro-channelled constructs presented in this chapter have the potential to be effectively used in our endochondral bone tissue engineering applications.

Lastly, it should be noted that along with positive staining for collagen type X, small calcific deposits were also visible, via Alizarin Red staining, within the engineered tissues after 35 days of culture. This demonstrates that although chondrogenic priming was used, the resulting tissue drifted from a cartilaginous to a hypertrophic phenotype (presence of collagen type X and localised mineralisation are clear markers of hypertrophy). We hypothesise that this behaviour is due to a combination of several factors, some connected to the design of the specific priming culture, others to the intrinsic properties of the implants, particularly the intrinsic nature of bone marrow stem cells (BMSCs) to differentiate towards a hypertrophic lineage. It has been widely shown in the literature that chondrogenic induction of BMSCs, which is quite a common strategy used in articular cartilage tissue engineering, is often accompanied by undesired hypertrophy, which can lead to calcification and endochondral ossification after implantation *in vivo* [415-417]. At the moment, it still remains a challenge to support and maintain articular cartilage engineered using BMSCs without subsequent hypertrophy and calcification *in vitro*, and we hypothesise that this intrinsic BMSCs behaviour is also emerging in this study. Here, however, it does not represent an undesired feature; on the contrary it is an aspect of our strategy that can represent an advantage for our final goal of regenerating bones. Another factor that greatly influences MSCs fate is the nutrient environment present during cell culture; in our study, particularly important is the oxygen tension in culture. In the literature, the use of low oxygen tension or physioxia (2–5% oxygen) during cell culture has generated intensive investigation in MSC chondrogenesis. The rationale for it is that the oxygen level within articular cartilage *in vivo* ranges from 2–5% oxygen [418-420]. In addition, *in vitro* results suggest that these conditions are beneficial for MSC expansion and chondrogenesis, particularly in suppressing cartilage hypertrophy [421]. For example, it has been shown that

normoxic conditions (higher level of oxygen) during *in vitro* MSC pellet chondrogenesis promoted the MSC drift towards a hypertrophic phenotype, resulting in the expression of hypertrophic markers (e.g., collagen X, MMP13, alkaline phosphatase) and ectopic bone formation *in vivo*, with pellets mineralisation and vascularisation upon implantation in a nude mouse model [417]. In our study, cell-laden constructs were cultured for the first 3 weeks at 5% pO_2, supporting initial MSCs chondrogenesis, and the last 2 weeks at 20% pO_2. This oxygen tension switch is believed to play an important role in the MSCs drift towards hypertrophy, resulting in localised mineral formation. Finally, the supporting hydrogel bioink properties will also influence MSCs behaviour and fate. For example, it is known that BMSCs morphology and adhesion are highly dependent on the biomaterial mechanical stiffness. Cells become more spread and more adhesive on stiffer matrices [422, 423]. In addition, in a recent study, Engler et al. reported that BMSCs differentiate into tissue specific lineages depending on the stiffness of the supporting substrates when they were cultured on matrices mimicking the stiffness of brain (0.1-1 kPa), muscle (8-17 kPa) and pre-mineralised bone (25-40 kPa) [424]. Notably, a higher proliferation rate and osteogenic commitment on stiff matrices were found to be accompanied by an increase of cell spreading and polygonal morphology. Cell shape has also been shown to be involved in cell proliferation and commitment [425]. McBeath et al. used micro patterning to control MSC shapes and demonstrated that flattened, spread cells prefer to differentiate into osteoblasts, whereas unspread, round cells develop into adipocytes [426]. Thus, matrix stiffness may influence MSCs proliferation and differentiation process through changes in cell shapes. In our study, looking at the histological slides, it can be seen how encapsulated cells look flatten and spread, anchoring themselves to the fibrin gel. This specific cell morphology could be linked to the mineral deposition found *in vitro*. To have a more complete picture of the biomaterial influence, the stiffness of the fibrin used here would needs to be carefully considered.

3.5 Conclusions

In summary, we have realised cell-laden fibrin constructs and assessed MSC chondrogenesis and progression along an endochondral pathway. To facilitate nutrient transport *in vitro* and potentially vascularisation *in vivo*, we introduced micro-channels into these constructs, and we showed that they remained patent for all the culture period. We also proved that fibrin can support an endochondral phenotype *in vitro*. However, complex

moulding techniques were used in this chapter to produce these engineered tissues, which limits the development of grafts with patient-specific geometries. Therefore in the next chapter of this thesis we will look to develop fibrin-based bioinks that can be used for 3D bioprinting of hypertrophic cartilaginous templates.

Chapter 4: Tuning the Composition of Fibrin Bioinks to Enhance Chondrogenesis of Human MSCs in 3D Bioprinted Implants

4.1 Introduction

3D printing is an additive manufacturing based technology for precise 3D construction, which, since its conception, has impacted several fields including engineering, manufacturing and medicine. The term 3D bioprinting is used to describe the precise layering of cells, biomaterials and biologic factors with the goal of recapitulating and mimicking a biologic tissue [300]. Compared to traditional tissue engineering methods, 3D bioprinting enables the accurate deposition of biomaterials and cells in 3D space [301], resulting in greater precision in the spatial relationship between the individual elements of the desired tissue, and in the possibility to realise complex geometries and structures. For these reasons, 3D bioprinting holds great promise for new regenerative medicine applications and its development and utilisation has rapidly increased in recent years [32, 302]. A very important and usually limiting aspect of the 3D bioprinting technologies is the selection of materials to be used in the formulation of bioinks [314]. Although major progress has been made with both natural and synthetic hydrogels in biofabrication [315], current hydrogel bioinks generally do not possess both the mechanical and biological properties to achieve their desired function. The central problem is that the fabrication of complex, tissue-like structures with high resolution requires hydrogels with quite specific ranges of physical and mechanical properties. Moreover, the hydrogel also needs to possess certain biological properties, specifically it should facilitate the migration, proliferation and differentiation of the embedded and endogenous cells [316]. This imposes contrasting requirements on the properties of such materials and the absence of suitable hydrogel inks has been identified as a key factor hindering further progress in this field [317-319]. The *biofabrication window* is a concept that describes the compromises that have traditionally been made to design bioinks [320], working between formulations that support high shape fidelity bioprinting (e.g. appropriate ink viscosity and yield stress) and those that are optimal for supporting cell migration, growth and differentiation.

Fibrin is a natural biopolymer involved in the coagulation cascade and results from the conversion of fibrinogen to cross-linked fibrin catalysed by thrombin. Naturally, fibrin provides a biocompatible structural scaffold and possesses many of the important biological properties needed for successful tissue regeneration. In addition, fibrin matrix is quickly remodelled and resorbed through natural fibrinolysis as cells deposit tissue-specific extracellular matrix components during the regeneration of functional tissues. For all these reasons, fibrin represents an attractive biomaterial for tissue engineering applications [343], and it has been used in many of these, including cardiovascular [345-347], bone [350-352], cartilage [353-355], and nervous [358-360] tissue engineering applications, among many others. However, fibrin lacks the appropriate rheological properties required for many biofabrication applications. Fibrin's low viscosity hinders its use in filament-based deposition techniques, limiting the geometrically complexity of the achievable constructs, which can easily collapse do to fibrin's poor mechanical properties. Several groups have addressed this problem by mixing fibrin with thickening components, like gelatin [380], polyethylene glycol [382], or alginate [384, 385] in order to provide the desired viscosity for 3D printing. By mixing fibrinogen with a gelatin-based carrier gel containing hyaluronic acid and glycerol, it has been possible to 3D bioprint human-scale tissue constructs (e.g. mandible bone, ear-shaped cartilage and skeletal muscle) [30]. It has yet to be established whether such fibrin based bioinks can be used to 3D bioprint cartilage templates capable of supporting endochondral bone formation.

A potential limitation of fibrin-based bioinks for the 3D bioprinting of constructs for bone regeneration are their relatively poor mechanical properties. This limitation will become especially apparent when attempting to print constructs for use in load bearing applications in man. Our group and others have previously incorporated networks of 3D printed polycaprolactone (PCL) into 3D bioprinted constructs to improve their mechanical properties [38-43]. Thermoplastic polymer networks have been largely used in tissue engineering applications to provide the desired shape and strength to the overall construct, while embedded hydrogels can provide a suitable environment and biological cues needed for cell migration, growth and differentiation. By modifying the thermoplastic polymer network, more complex shapes can be achieved [427], and mechanical properties such as Young's modulus, can be tailored to match those of the native target tissues [42].

The main goal of this study was to investigate how the fibrinogen content within fibrin based bioinks influences chondrogenesis of encapsulated hMSCs. Two different

fibrinogen concentrations were used to generate two 3D printable fibrin-based bioinks, which were then used to fabricate cell-laden constructs. These bioprinted constructs were maintained in chondrogenic culture conditions for 5 weeks, and the resulting matrix was assessed using biochemical, histological and immunohistochemical techniques. Furthermore, we sought to introduce 3D printed PCL networks to improve the mechanical properties of these constructs. Compression tests was performed on the PCL reinforcements and PCL-reinforced constructs to investigate the contribution of these PCL networks to the overall mechanical properties of the constructs.

4.2 Materials & Methods

4.2.1 Isolation and expansion of MSCs

Human bone marrow derived MSCs (hBMSCs) were isolated from bone marrow aspirates (Lonza) and expanded in high glucose dulbecco's modified eagle's medium (hgDMEM) GlutaMAX supplemented with 10% v/v FBS, 100 U/ml penicillin, 100 µg/ml streptomycin, 2.5 µg/ml amphotericin B at 5% pO_2 (all Gibco, Biosciences, Dublin, Ireland). Following colony formation, MSCs were trypsinised, counted, seeded at density of 5000 cells/cm^2 in T175 flasks (Thermo Fisher Scientific), supplemented with hgDMEM, 10% v/v FBS, 100 U/ml penicillin, 100 µg/ml streptomycin, 2.5 µg/ml amphotericin B, and 5 ng/ml human fibroblastic growth factor-2 (Recombinant Human FGF-basic – 154 a.a., Peprotech) and expanded to passage 2 at 5% pO_2.

4.2.2 Bioink preparation

The bioink used in this study is a composite hydrogel developed elsewhere [30], and it is a mixture of fibrinogen (F8630), type A gelatin (G6144), hyaluronic acid (HA) (53747) and glycerol (G5516), which were all purchased from Sigma-Aldrich. It was prepared by mixing 1:1 two solutions. Briefly, for the first solution (called from now on gelatin carrier) 6 mg/ml HA were dissolved in DMEM by stirring the solution at 37 °C overnight. Glycerol (20% v/v) was added into the solution and stirred for 1 h at room temperature (RT) and finally gelatin (80 mg/ml) was dissolved by stirring for further 2 hours at 37 °C. The prepared solution was sterilised by filtration through a 0.45-µm syringe filter and was stored

at −20 °C before use. For the second solution, fibrinogen (two different concentrations were used, 70 and 100 mg/ml) was dissolved at 37 °C in Aprotinin (10000 KIU/ml) (Uniphar, Dublin, Ireland) containing 19 mg/ml sodium chloride (NaCl); these solutions were used fresh/immediately. Cells were resuspended in the two fibrinogen solutions, which were then gently mixed in equal parts together with the gelatin carrier, producing two bioinks (with 3.5% and 5% final concentrations of fibrinogen) containing $5x10^6$ cells/ml.

4.2.3 3D bioprinting system

PCL/bioink constructs were fabricated with a two-step print using the 3D Discovery multi-head bioprinting system (Regen Hu, Switzerland). First, molten PCL, with an average molecular weight of approximately 50,000 Da (CAPA 6500D, Perstorp, Sweden), was deposited with the fused deposition modeller to manufacture porous cylindrical (Ø = 4 mm, h = 3.5 mm) scaffolds. They were then treated with 3M sodium hydroxide (NaOH) for 12 hours, to increase their hydrophilicity and improve their bonding with the cell-laden hydrogel, prior to be ETO sterilised. For the second step, the bioink was loaded into the pressure driven piston system, and printed at room temperature (RT). A pressure of 0.08 MPa and a 25 Gauge needle were used to deposit by z-stacking the bioink inside the PCL scaffold. The 3D Discovery was placed in a laminar flow hood to ensure sterility throughout the biofabrication process. Once printed, the constructs were immersed in a 20 U/ml thrombin bath for 20 minutes at RT to crosslink and form fibrin. Finally, constructs were place in culture at 37 °C overnight to wash out all the uncross-linked components (gelatin, HA and glycerol). Constructs were then kept in XPAN for other 24 hours before the start of chondrogenic priming.

4.2.4 PCL frame porosity

The porosity of the 3D printed PCL frame was evaluated experimentally using the following equation:

$$P_e(\%) = \left(1 - \frac{\rho_{frame}}{\rho_{PCL}}\right) * 100 \quad (1)$$

where P_e is the experimental porosity, ρ_{frame} is the apparent density of the frame, and ρ_{PCL} is the PCL density which is 1.145 g/ml. ρ_{frame} was obtained as:

$$\rho_{frame}\left(\frac{g}{ml}\right) = \left(\frac{m_{frame}}{V_{frame}}\right) \quad (2)$$

where m_{frame} and V_{frame} are the weight and the volume of the PCL frame respectively. The weight of the 3D-printed constructs was quantified using an analytical balance (Mettler Toledo Excellence XS205 DualRange).

4.2.5 Chondrogenic priming

The chondrogenic culture conditions applied in this study are defined as culture in a chondrogenic medium (CDM) consisting of hgDMEM GlutaMAX supplemented with 100 U/ml penicillin, 100 µg/ml streptomycin, 100 µg/ml sodium pyruvate, 40 µg/ml L-proline, 50 µg/ml L-ascorbic acid-2-phosphate, 4.7 µg/ml linoleic acid, 1.5 mg/ml bovine serum albumine, 1x insulin-transferrin-selenium, 100 nM dexamethasone (all purchased from Sigma-Aldrich), 2.5 mg/ml amphotericin B, 10 ng/ml of human transforming growth factor-β3 (TGF-β3) (Prospec-Tany TechnoGene Ltd., Israel) and Aprotinin. The constructs were primed for 3 weeks at 5% pO_2 followed by 2 weeks at 20% pO_2.

4.2.6 Mechanical tests

Mechanical tests were carried out in unconfined compression in DMEM at room temperature using a twin column Zwick universal testing machine (Zwick, Roell, Germany). All samples (n = 3) were subjected to a compressive-strain while kept hydrated through immersion in a DMEM (Gibco Biosciences, Ireland) bath maintained at RT. Stress relaxation tests were performed consisting of a ramp displacement up to 20% strain, and a relaxation period of 45 minutes was used. During the ramp phase, specimens were compressed at a cross-head speed of 0.04 %/s (strain controlled) between two impermeable metal platens after applying an initial preload of 0.5 N, to ensure that the construct surface was in direct contact with the platens. A 100 N load cell was used for testing the samples. The load versus displacement data were recorded throughout. The engineering stress and

strain were calculated by dividing the load value with the initial cross-sectional area of each sample and the displacement value with the initial sample height, respectively. The elastic modulus was taken as the slope of the initial linear region of the plotted stress-strain curve.

4.2.7 Biochemical analysis

The biochemical contents of all samples were analysed at day 0, 21 and 35 of culture. Prior to biochemical analysis, constructs were washed in PBS, weighed and frozen for subsequent assessment. Each construct was digested with papain (125 mg/ml) in 0.1M sodium acetate, 5 mM L-cysteine HCl, 0.05 ethylenediaminetetraacetic acid (EDTA), pH 6.0 (all from Sigma-Aldrich) at 60 °C and 10 rpm for 18 h. DNA content was quantified using the Hoechst Bisbenzimide 33258 dye assay, with a calf thymus DNA standard. The amount of sulphated glycosaminoglycan (sGAG) was quantified using the dimethyl methylene blue dye-binding assay (Blyscan, Biocolor Ltd., Northern Ireland), with a chondroitin sulphate standard. Total collagen content was determined by measuring the hydroxyproline content using the dimethylaminobenzaldehyde and chloramine T assay and a hydroxyproline to collagen ratio of 1:7.69.

4.2.8 Histological and immunohistochemical analysis

Constructs were fixed in 4% paraformaldehyde, dehydrated in a graded series of ethanol's, embedded in paraffin wax, sectioned at 8 µm and affixed to microscope slides. The sections were stained with alcian blue to assess sGAG content, picrosirius red to assess collagen content and alizarin red to assess calcification. Collagen types I, II and X deposition were evaluated by immunohistochemical analysis. Briefly, sections were treated with chondroitinase ABC (Sigma-Aldrich) in a humidified environment at 37 °C to enhance permeability of the extracellular matrix. Sections were incubated with goat serum to block non-specific sites and collagen type I (ab90395, 1:400), collagen type II (sc-52658, 1:400) or collagen type X (ab49945, 1:200) primary antibodies (mouse monoclonal, from Abcam - Cambridge, UK and Santa Cruz - Texas, United States) were applied over night at 4 °C. Next, the sections were treated with peroxidase to block endo-peroxidise activity. Next, the secondary antibody (Col I, anti-Mouse IgG, B7151, 1.5:200; Col II, anti-Mouse IgG, B7151, 1:300; Col X, anti-IgM, ab49760, 1:200) was added for 1 h at room temperature followed

by incubation with ABC reagent (Vectastain PK- 400, Vector Labs, Peterborough, UK) for 45 min. Finally, sections were developed with DAB peroxidase (Vector Labs) until brown staining was observed in the positive controls. Positive and negative controls were included in the immunohistochemistry staining protocol for each batch.

4.2.9 Live dead analysis.

Cell viability was assessed using a LIVE/DEAD^{TM} viability/cytotoxicity assay kit (Invitrogen, Bio-science, Ireland). Briefly, constructs were cut in half, washed in phosphate-buffered saline (PBS) followed by incubation for 1 h in PBS containing 2 mM calcein and 4 mM ethidium homodimer-1 (both from Cambridge Bioscience, UK). Sections were again washed in PBS, imaged using a Leica SP8 scanning confocal microscope at 515 and 615 nm channels, and analysed using Leica Application Suite X (LAS X) software. The cell viability was calculated from these images using ImageJ software.

4.2.10 Statistical Analysis

Statistical analysis was performed using GraphPad 8 (GraphPad Software, La Jolla California USA). Pairwise comparisons between means of different groups were performed using a student t-test. One-way analysis of variance (ANOVA) with the addition of Turkey's correction was used for multiple comparisons testing. Results are expressed as mean ± standard deviation. For all comparisons, significance was accepted at a level of $p < 0.05$. Sample size (n) is indicated within the corresponding figure legends.

4.3 Results

4.3.1 3D printing of PCL-reinforced cartilage templates

Reinforcing PCL meshes (h = 3.5 mm; Ø = 4 mm; Figure 4.1A) were produced using fused deposition modelling (FDM) and subsequently treated with 3M NaOH to increase their surface roughness and hydrophilicity. The porosity of the PCL frame was ~70%. After ETO sterilisation, the PCL meshes were filled with the two different bioink formulations using a novel Z-printing strategy [40], and were then cross-linked to form the PCL

reinforced fibrin constructs. This biofabrication process is schematically presented in Fig. 4.1C. A live/dead assay performed at day 1 showed that cells were homogeneously distributed in the constructs and that the majority of them were spread (Fig. 4.1D), with cell viability exceeding 90% in both groups (Fig. 4.1E). After 35 days of culture (Fig. 4.1G) both groups were mechanically tested; the Young's modulus for both PCL reinforced fibrin groups was comparable to the PCL frame only (Fig. 4.1F).

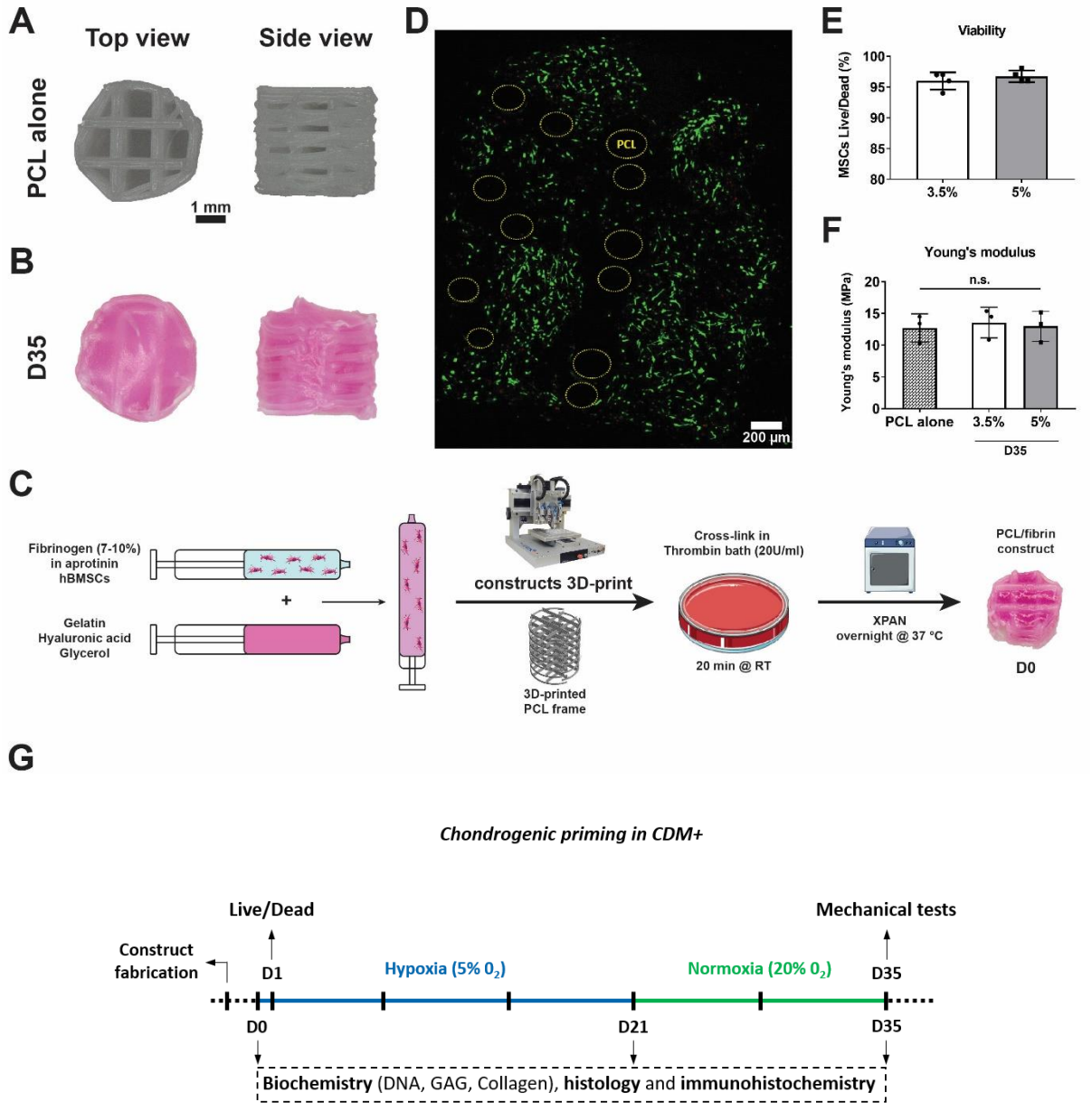

Figure 4.1: PCL/fibrin construct fabrication and characterisation. (A) Top and side view of the 3D printed PCL frame; (B) top and side view of the PCL/fibrin construct after 35 days of culture. (C) Schematic of the biofabrication process, from bioinks formulation to the final composite construct. (D) LIVE/DEAD at day 1

on a longitudinal section; dashed yellow lines represent PCL fibres. (E) hBMSCs viability at day 1 for both groups. (F) Young's modulus of the PCL frame alone, and of the composite constructs with both formulations after 35 days of culture (n=3). (G) Experimental setup and timeline of this study.

4.3.2 Biochemical analyses

The DNA content within both the fibrin concentration groups significantly increased over the 35-day culture period (Fig. 4.2A-B). Both sGAG and collagen content increased over time in culture in both groups (Fig. 4.2C–F). After 35 days of culture, collagen accumulation was significantly higher in the 3.5% fibrin group compared to the 5% fibrin group (Fig. 4.2C-F). sGAG accumulation was comparable in both groups.

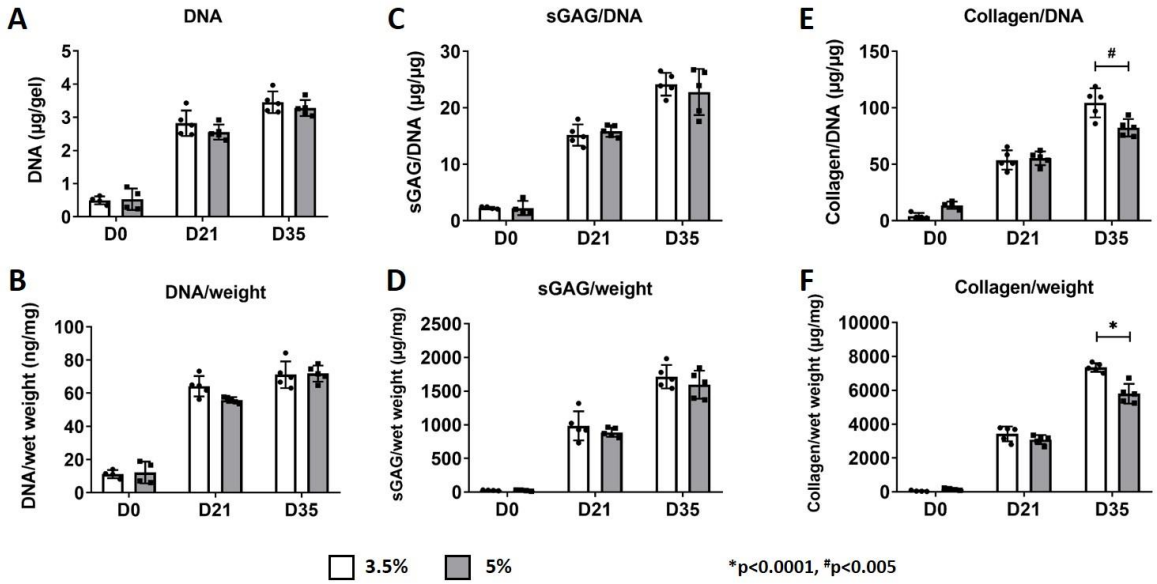

Figure 4.2: Biochemical analyses of PCL-reinforced constructs chondrogenically primed for 35 days. (A) DNA total content; (B) DNA content normalised to construct dry mass; (C) sGAG content normalised to DNA content; (D) sGAG content normalised to construct dry mass; (E) collagen content normalised to DNA content and (F) collagen content normalised to construct dry mass. *n* = 4 samples per group at D0, *n* = 5 samples per group at D21 and D35; #p<0.005, *p<0.0001.

4.3.3 Histological and immunohistochemical analyses

Histological analyses of the bioprinted tissues was in agreement with the results of the biochemical assays (Fig. 4.3). The intensity of alcian blue (Fig. 4.3A) and picrosirius red (Fig. 4.3B) staining increased with time in culture for both groups. Potential calcification of

the grafts was assessed using alizarin red staining (Fig. 4.3C). By day 35 there was some early evidence of calcification at the periphery of the constructs, indicated by red arrows (Fig. 4.3C, which was not observed at day 21.

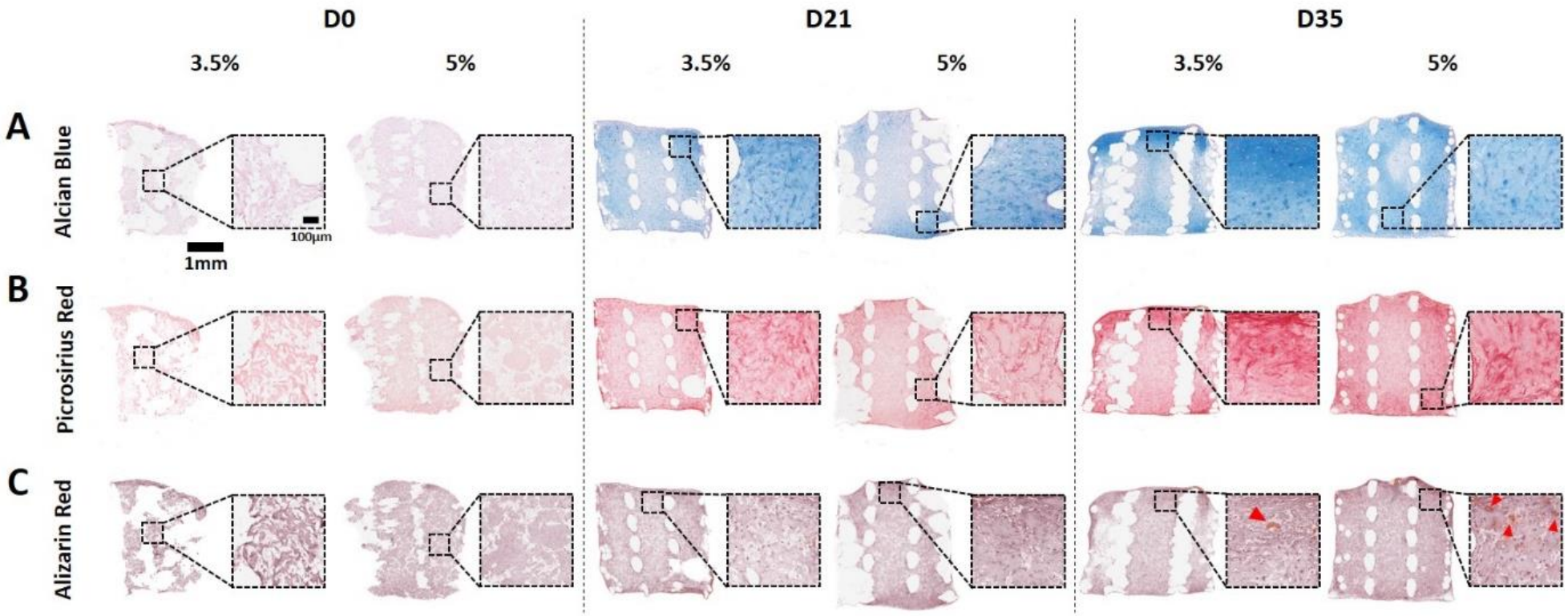

Figure 4.3: Histological analyses of PCL-reinforced constructs at days 0, 21 and 35. (A) Alcian blue staining for sulphated proteoglycans; (B) picrosirius red staining for collagen; (C) alizarin red staining for calcium. Images were taken at 2x, with 10x zoomed in details.

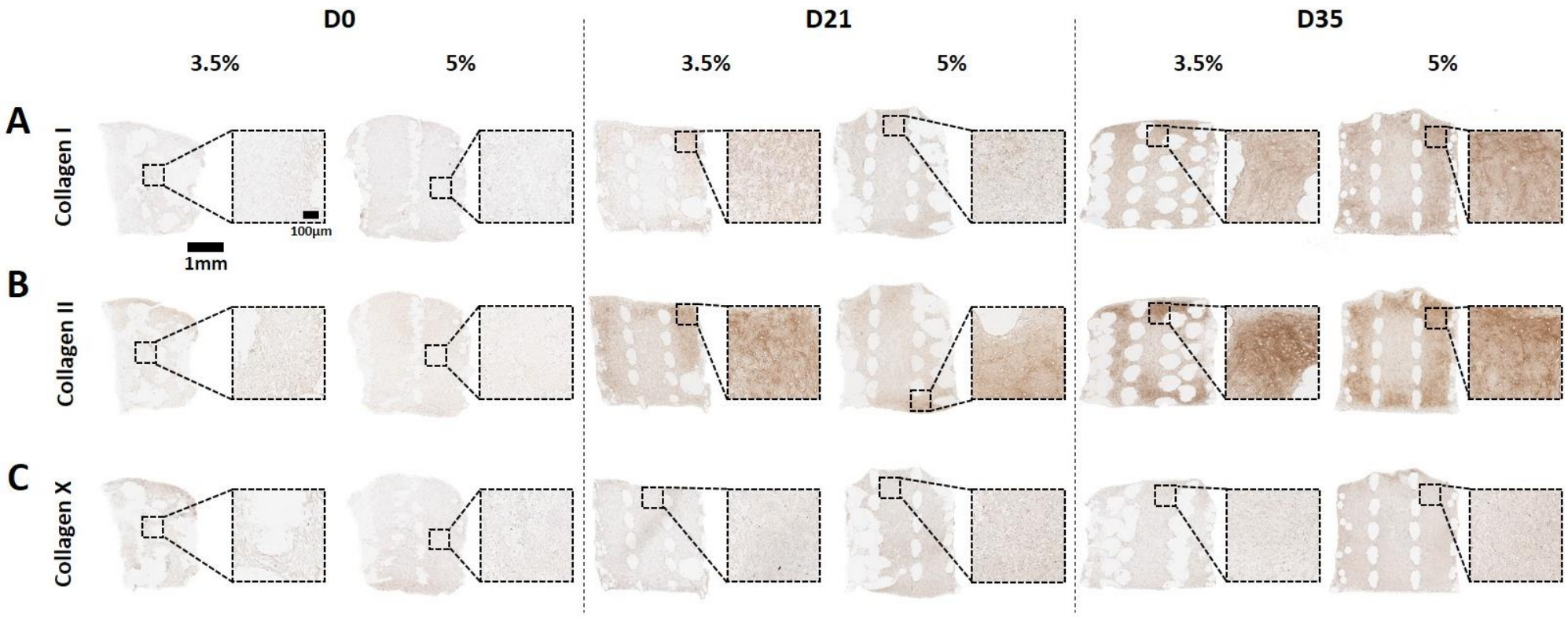

Figure 4.4: Immunohistochemical analyses of PCL-reinforced constructs at days 0, 21 and 35. (A) Collagen type I; (B) collagen type II; (C) collagen type X. Images were taken at 2x, with 10x zoomed in details.

To investigate the nature of the collagen present, immunohistochemical staining for collagen type I, II and X was performed (Fig. 4.4). Collagen type I and II production was found to increase over time in culture (Fig. 4.4A; Fig. 4.4B). There was very little evidence for collagen type X deposition within the bioprinted tissues (Fig. 4.4C).

4.4 Discussion

The main goal of this study was to investigate how tuning fibrin concentration is influencing the *in vitro* chondrogenesis of human MSCs in 3D-bioprinted implants. Using multiple-tool biofabrication, it was possible to produce cell-laden fibrin constructs mechanically reinforced with a network of PCL. MSCs remained viable post-fabrication and were found to be homogenously distributed throughout the construct. The PCL frame was found to be the main determinant of the construct mechanical properties, masking any contribution from the hydrogels or ECM deposited by the cells. Even with the presence of PCL, after chondrogenic priming, these constructs were found to support chondrogenesis of MSCs.

The incorporation of gelatin, HA and glycerol into the bioink formulation to allow fibrinogen printing modified the final hydrogel architecture compared to fibrin constructs obtained exclusively from fibrinogen and thrombin (Fig. 4.5). Gelatin, HA and glycerol are acting only as thickening agents and they are not expected to cross-link during the fabrication process. Therefore it is expected that these components are washed out once the constructs are placed in culture at 37 °C, leaving internal voids within the fibrin structure, as it can be seen in the sample at day 0 (Fig. 4.5), compared to the more compact nature of the constructs from the previous study.

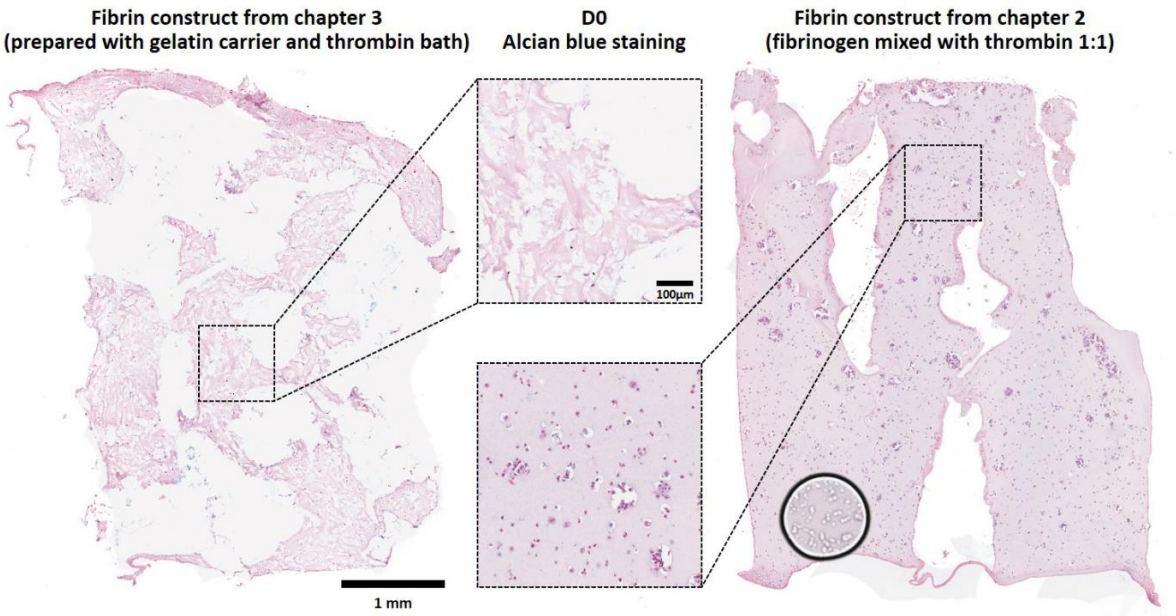

Figure 4.5: Comparison between fibrin construct architectures at D0 from alcian blue staining. (Left) Fibrin construct from chapter 4, obtained from a bioink containing fibrinogen, gelatin, HA and glycerol and using a thrombin bath for the crosslinking. (Right) Fibrin construct from chapter 3, obtained from a mixture of exclusively fibrinogen and thrombin.

These voids can play an important role during both the *in vitro* chondrogenic priming and the following *in vivo* implantation. This increase in construct porosity likely contributes to the increase in cell proliferation, as indicated by the significant increase in the DNA content, from day 0 to day 21 of culture. Moreover, we expect that these empty spaces could accelerate host cell infiltration upon *in vivo* implantation, improving host-construct integration and consequently tissue regeneration.

In this study, despite the fact that a lower cell seeding density was used compared to the previous chapter, it was found that the fibrin based bioinks supported robust cartilage-specific matrix accumulation. We demonstrated that the MSCs embedded in the hydrogels were able to differentiate along a chondrogenic phenotype, and secrete an extracellular matrix rich in sGAG and type II collagen. Both bioink formulations were able to support robust MSCs chondrogenesis, with the softer 3.5% fibrin supporting higher levels of collagen deposition. We have already shown with other biomaterials [21] that *in vivo* degradation is a key parameter for better healing. We expect that the lower material density bioink will degrade faster *in vivo*, allowing better infiltration and integration with host tissue. For this reason, future studies will focus on the use and improvement of the 3.5% fibrin

bioink to produce hypertrophic cartilage templates for *in vivo* endochondral bone tissue regeneration. After the choice of the bioink, future work will look as well how to use 3D printing technology to engineer geometrically complex hypertrophic cartilage templates with controlled architectures to guide endochondral bone repair *in vivo*. The specific geometry of the PCL reinforcements present in this study could be used as a way to physically identify different internal areas for the realisation of a distinctive zonal fabrication. For example, constructs could be realised with a transversal gradient, having a core vertical volume, defined by the central inter-fibre space (as seen from the top view), and an annulus volume around the core, defined by the four main inter-fibre spaces around the central one. Core and annulus could be filled with two bioinks differing in the nature and amount of cells and/or active particles embedded, creating the aforementioned gradient. Alternatively, the core volume could be left empty to create a micro-channel, as schematically shown in Fig. 4.6.

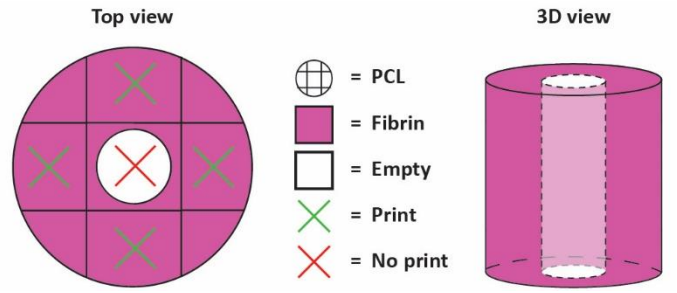

Figure 4.6: Incorporation of a central micro-channel. Schematic top and 3D-view of the construct; green crosses indicate the inter-fibres spaces were the hydrogel would be printed with z-stacking, while the red cross indicates the space that would be left empty to create the channel.

4.5 Conclusions

In summary, we have 3D printed cell-laden PCL-reinforced fibrin constructs with two different fibrin concentrations and assessed how fibrin content influences MSC chondrogenesis and progression along an endochondral pathway. To address the poor mechanical properties of fibrin hydrogels, we decided to incorporate a PCL reinforcement to increase the overall stiffness and strength of our constructs. After having described a biofabrication method to produce 3D-printed reinforced cell-laden hydrogels, we found that

both fibrin concentrations used to prepare the bioinks can support chondrogenesis of MSCs *in vitro*, with the softer 3.5% fibrin supporting higher levels of collagen deposition. The next chapter of this thesis will focus on using this 3.5% fibrinogen bioink to 3D bioprint PCL reinforced cartilage and hypertrophic cartilage templates obtained through specific priming culture, and assess their capacity to support large bone defect healing *in vivo* in a rat femoral defect model.

Chapter 5: Bioprinted Endochondral Templates for Large Bone Defect Healing

5.1 Introduction

Bone defects above a critical size cannot heal on their own and their repair represents a significant clinical challenge. Autografting, which still represents the clinical gold standard, is the transplantation of natural bone tissue from the patient to the injured location; however, there are a number of drawbacks associated with this approach, such as the limited number of sites where bone may be harvested without loss of function [428, 429], the fact that autografts are less effective in irregularly shaped defects and the need for graft resorption/remodelling prior to complete healing [89]. Therefore, there is a clear need for alternative tissue engineering (TE) approaches, which could allow the realisation of large and anatomically precise grafts for bone regeneration, overcoming the aforementioned problems. One possible solution is the use of developmentally inspired TE strategies that seek to mimic the process of endochondral ossification (EO) which occurs during long bone formation and in the natural healing of bone fractures [430]. Unlike the alternative development process of intramembranous ossification, EO requires the initial formation of a cartilage template [19] which becomes hypertrophic and begins to calcify. Complex developmental signals, invasion of blood vessels and the consequent formation of the primary ossification centre, all contribute to the gradually remodelling of the cartilaginous template, which is replaced by a new maturing bone matrix [395]. Bone TE strategies have typically attempted to mimic the developmental process of intramembranous ossification by directing the osteogenic differentiation of MSCs seeded on 3D scaffolds [431, 432]. However, it has been observed that the formation of a calcified matrix during the *in vitro* culture of such grafts can inhibit their vascularisation *in vivo* by acting as a barrier to invading blood vessels, ultimately leading to implant failure [432, 433]. TE strategies inspired by the process of EO may overcome such limitations; indeed a number of studies have already demonstrated the capacity of *in vitro* engineered cartilaginous templates to undergo remodelling into bone tissue by executing an endochondral programme upon implantation *in vivo* [19-21, 148, 149, 286-288, 396, 397, 434-436]. These findings can be linked to the capacity of engineered cartilage templates to not only survive in the initially

hypoxic defect environment, but also to the inherent tendency of chondrogenically primed MSCs to become hypertrophic and secrete factors that support vascularisation and conversion of the engineered tissue into functional bone [23, 288, 432].

Clinical translation of such developmentally inspired TE approaches will require the development of strategies to scale-up the size of such grafts and ensure they mimic specific patient anatomies. However, as TE implants increase in size, the challenges of providing adequate nutrient transport and waste removal during the *in vitro* engineering of the tissue increase. As do the challenges of ensuring rapid vascularisation of the engineered graft once it is implanted into the body. In fact, although it has been shown that cartilage templates can become vascularised *in vivo* [19, 39, 397], vascularisation and subsequent mineralisation occur predominately in the peripheral regions of large tissue engineered constructs, leaving significant avascular cartilage areas at the core [23, 24]. Numerous strategies have been proposed to enhance the vascularisation of bone TE grafts, including optimisation of the scaffold design and architecture, incorporation of pro-angiogenic growth factors and the *in vitro* prevascularisation of the implant using endothelial cells [37, 437-439]. For example, it has been shown that it is possible to accelerate and guide vascularisation by introducing a single or a network of internal micro-channels into the body of the engineered tissue [21, 150, 440, 441]. Such alterations in graft architecture can also potentially enhance nutrient transport during the *in vitro* engineering of such constructs [406, 407, 409, 410, 442, 443]. Indeed, a number of studies have demonstrated that such channels can promote both nutrient transport and extracellular matrix deposition *in vitro* as well as vascular invasion of the graft *in vivo* [444, 445]. To date, the majority of such studies have been undertaken using engineered grafts generated from animal cells; prior to clinical translation in man it will be necessary to confirm that such approaches are also efficacious using human MSCs.

Clinical translation of *in vitro* engineered bone grafts will not only require scaling-up the size of the tissue, but will also require the engineering of grafts that mimic specific patient anatomies. To this end, 3D bioprinting techniques can potentially enable the fabrication of highly ordered, scaled-up engineered constructs with internal architectures optimised for nutrient transport *in vitro* and vascular invasion *in vivo* and external geometries targeting specific patient anatomies. 3D bioprinting is used to describe the precise layering of cells, biomaterials, and biologic factors with the goal of recapitulating and mimicking a biologic tissue [300]. Compared to traditional tissue engineering methods, 3D bioprinting systems allow for accurate deposition of biomaterials and cells in 3D space

[301], resulting in greater precision in the spatial relationship between the individual elements of the construct and the realisation of complex geometries and structures [32, 302]. In order to utilise 3D bioprinting for the engineering of constructs for endochondral bone TE, it will be necessary to identify bioinks that are not only capable of supporting chondrogenesis of MSCs *in vitro*, but which also degrade *in vivo* to enable vascularisation and conversion of the cartilage graft into bone. Previous studies have demonstrated that hydrogel persistence *in vivo* can delay the conversion of engineered cartilage templates into bone [21, 44], challenging the development of hydrogel bioinks for developmentally inspired bioprinting strategies. Another putative advantage of 3D bioprinting is that it can be used to mechanically reinforce engineered tissues to enable them to function during *in vivo* maturation. 3D printed polymeric frames have been extensively used to reinforce soft hydrogels, bioinks and engineered tissues in order to allow them to better withstand challenging physiological loads typically encountered *in vivo* [38-43]. Such 3D bioprinting approaches could also potentially be used to mechanically reinforce engineered cartilage templates designed to support endochondral bone regeneration, however it remains unclear if the presence of such a polymeric network will impede the process of EO within critically sized bone defects. Furthermore, additional work is required to identify the post-bioprinting *in vitro* priming conditions best suited to engineering hypertrophic cartilage grafts capable of regenerating critically sized bone defects.

The objective of this study was to 3D bioprint a PCL reinforced cartilaginous template, containing a central microchannel designed to improve nutrient transport *in vitro* and vascularisation *in vivo*, for large bone defect healing. To this end, this chapter first assessed the capacity of a fibrin-based bioink to support hMSCs chondrogenesis *in vitro*. Fibrin was chosen as it is a natural biomaterial that is easily degraded *in vivo*. This chapter then investigated two different culture priming regimes with the aim of engineering cartilaginous templates primed for endochondral ossification. The capacity of these bioprinted tissues to execute an endochondral programme and mineralise *in vivo* was assessed *via* subcutaneous implantation into nude mice, where levels of bone formation were compared to control MSC laden constructs that were not chondrogenically primed prior to *in vivo* implantation. The capacity of these bioprinted cartilaginous constructs to guide bone regeneration was then assessed in a critically sized rat femoral defect model and compared to a positive control consisting of a collagen type I-nHA sponge soak loaded with BMP-2. To enable an *in vivo* assessment of the capacity of cartilage templates generated using human

MSCs to direct endochondral bone regeneration in this model, rats were administered injections of an immuno-suppressing drug cocktail. A schematic of the whole study, with construct fabrication and *in vivo* implantations, is presented in Fig. 1.

5.2 Materials & Methods

5.2.1 Isolation and expansion of MSCs

Human bone marrow derived MSCs (hBMSCs) were isolated from bone marrow aspirates (Lonza) and expanded in high glucose dulbecco's modified eagle's medium (hgDMEM) GlutaMAX supplemented with 10% v/v FBS, 100 U/ml penicillin and 100 μg/ml streptomycin at 5% pO_2 (all Gibco, Biosciences, Dublin, Ireland). Following colony formation, MSCs were trypsinised, counted, seeded at density of 5000 cells/cm^2 in T175 flasks (Thermo Fisher Scientific), supplemented with hgDMEM, 10% v/v FBS, 100 U/ml penicillin, 100 μg/ml streptomycin, 2.5 μg/ml amphotericin B, and 5 ng/ml human fibroblastic growth factor-2 (Recombinant Human FGF-basic – 154 a.a., Peprotech) and expanded to passage 3 at 5% pO_2.

5.2.2 Bioink preparation

The bioink used in this study is a composite hydrogel developed elsewhere [30], and it is a mixture of fibrinogen (F8630), type A gelatin (G6144), hyaluronic acid (HA) (53747) and glycerol (G5516), which were all purchased from Sigma-Aldrich. It was prepared by mixing 1:1 two solutions. Briefly, for the first solution (called from now on gelatin carrier) 6 mg/ml HA were dissolved in DMEM by stirring the solution at 37 °C overnight. Glycerol (20% v/v) was added into the solution and stirred for 1 h at room temperature (RT) and finally gelatin (80 mg/ml) was dissolved by stirring for further 2 hours at 37 °C. The prepared solution was sterilised by filtration through a 0.45-μm syringe filter and was stored at −20 °C before use. For the second solution, 70 mg/ml fibrinogen was dissolved at 37 °C in Aprotinin (10000 KIU/ml) (Uniphar, Dublin, Ireland) containing 19 mg/ml sodium chloride (NaCl); this solution was used freshly made. Cells were resuspended in the fibrinogen solution, which was then gently mixed in equal parts together with the gelatin

carrier, producing the wanted bioink (with 3.5% final concentrations of fibrinogen) containing $5x10^6$ cells/ml.

5.2.3 3D bioprinting system

PCL/bioink constructs were fabricated with a two-step print using the 3D Discovery multi-head bioprinting system (Regen Hu, Switzerland). First, molten PCL, with an average molecular weight of approximately 50,000 Da (CAPA 6500D, Perstorp, Sweden), was deposited with the fused deposition modeller to manufacture porous cylindrical (Ø = 4 mm, h = 5 mm) scaffolds. They were then treated with 3M sodium hydroxide (NaOH) for 12 hours, to increase their hydrophilicity and improve their bonding with the cell-laden hydrogel, prior to be ETO sterilised. For the second step, the bioink was loaded into the pressure driven piston system, and printed at room temperature (RT). A pressure of 0.08 MPa and a 25 Gauge needle were used to deposit by z-stacking the bioink inside the PCL scaffold, leaving a central micro-channel empty. The 3D Discovery was placed in a laminar flow hood to ensure sterility throughout the biofabrication process. Once printed, the constructs were immersed in a 20 U/ml thrombin (in hgDMEM) bath for 20 minutes at RT to crosslink and form fibrin. Finally, constructs were place in culture at 37 °C overnight to wash out all the uncross-linked components (gelatin, HA and glycerol). Constructs were then kept in XPAN for other 24 hours before the start of priming culture.

5.2.4 Priming cultures

All constructs were primed for 3 weeks at 5% pO_2 followed by 2 weeks at 20% pO_2. Two different priming culture regimes were used in this study, differing only for the media used during the last 2 weeks of culture. For the first 3 weeks, all constructs were cultured in a chondrogenic medium (CDM) consisting of hgDMEM GlutaMAX supplemented with 100 U/ml penicillin, 100 µg/ml streptomycin, 100 µg/ml sodium pyruvate, 40 µg/ml L-proline, 50 µg/ml L-ascorbic acid-2-phosphate, 4.7 µg/ml linoleic acid, 1.5 mg/ml bovine serum albumine, 1x insulin-transferrin-selenium, 100 nM dexamethasone (all purchased from Sigma-Aldrich), 10 ng/ml of human transforming growth factor- β3 (TGF-β3) (Prospec-Tany TechnoGene Ltd., Israel) and Aprotinin. For the last 2 weeks of culture, the first group called *chondrogenic* construct was kept in CDM as before, while the second group, *early*

hypertrophic construct, was cultured in the same CDM formulation but the addition of 50 ng/ml rh-BMP-2 (Peptrotech). At the end of the culture period, constructs were rinsed twice with PBS and stored at -80°C until analyses were performed.

5.2.5 Biochemical analysis

The biochemical contents of all samples were analysed at day 35 of culture. Prior to biochemical analysis, constructs were washed in PBS, weighed and frozen for subsequent assessment. The DNA content was quantified using the Hoechst Bisbenzimide 33258 dye assay, with a calf thymus DNA standard. The amount of sulphated glycosaminoglycan (sGAG) was quantified using the dimethyl methylene blue dye-binding assay (Blyscan, Biocolor Ltd., Northern Ireland), with a chondroitin sulphate standard. Total collagen content was determined by measuring the hydroxyproline content using the dimethylaminobenzaldehyde and chloramine T assay and a hydroxyproline to collagen ratio of 1:7.69. Prior to these biochemical analyses, each construct was digested with papain (125 mg/ml) in 0.1M sodium acetate, 5 mM L-cysteine HCl, 0.05 ethylenediaminetetraacetic acid (EDTA), pH 6.0 (all from Sigma-Aldrich) at 60 °C and 10 rpm for 18 h. Finally the amount of calcium present in the constructs was determined using a Sentinel Calcium kit (Alpha Laboratories Ltd, UK); to run this assay, constructs were digested in 1M HCl at 60 °C and 10 rpm. Four constructs per group were analysed by each biochemical assay.

5.2.6 Histological and immunohistochemical analysis of *in vitro* constructs

Constructs were fixed in 4% paraformaldehyde, dehydrated in a graded series of ethanol's, embedded in paraffin wax, sectioned at 6 µm and affixed to microscope slides. The sections were stained with alcian blue to assess sGAG content, picrosirius red to assess collagen content and alizarin red to assess calcification. Collagen types I, II and X deposition were evaluated by immunohistochemical analysis. Briefly, sections were treated first with hyaluronidase and then with pronase (Sigma-Aldrich) in a humidified environment at 37 °C for 25 minutes each to enhance permeability of the extracellular matrix (antigen retrieval step). Sections were incubated with goat serum to block non-specific sites and collagen type I (ab138492, 1:400), collagen type II (sc52658, 1:400) or collagen type X (ab49945, 1:200) primary antibodies (mouse monoclonal, from Abcam - Cambridge, UK and Santa Cruz - Texas, United States) were applied over night at 4 °C. Next, the sections were treated with

peroxidase to block endo-peroxidise activity. Next, the secondary antibody (Col I, ab6720 Goat anti-Rabbit IgG, 1:200; Col II, Goat anti-Mouse IgG, B7151, 1:300; Col X, Goat anti-Mouse IgM, ab97228, 1:400) was added for 1 h at room temperature followed by incubation with ABC reagent (Vectastain PK- 400, Vector Labs, Peterborough, UK) for 45 min. Finally, sections were developed with DAB peroxidase (Vector Labs) until brown staining was observed in the positive controls. Positive and negative controls were included in the immunohistochemistry staining protocol for each batch.

5.2.7 Subcutaneous implantation

All animal experiments were performed in accordance with the EU Directive 2010/63/EU on the protection of animals used for scientific purposes. Two groups were implanted: primed *chondrogenic* constructs (experimental group) and *Not Primed* constructs (control group). The latter were produced in the same way than the primed constructs (as described in 5.2.3), but implanted immediately before starting the priming culture period. Constructs were implanted subcutaneously into the back of four BALB/cOlaHsd-Foxn1 nu 8-week-old female nude mice (Envigo). Briefly, two subcutaneous pockets were made along the spine, the first one at the shoulders and the second at the hips level. Two constructs were inserted into each pocket (randomised between top and bottom pockets). Eight constructs were implanted per group and constructs were harvested 12 weeks post-implantation. Mice were anaesthetised using 2% - 3% (v/v) isoflurane in balanced oxygen and subcutaneously administered pre-operative analgesia of buprenorphine (0.05 mg/kg). In addition, 1 mg/kg of buprenorphine was added to edible gels (Medigel Hazelnut) for 3 days post-surgery. At the end of the study, mice were sacrificed by CO_2 asphyxiation and the constructs were retrieved. This study and all the protocols involved were approved by the animal welfare committee of Trinity College Dublin and the Health Products Regulatory Agency (HPRA, approval number AE19136/P069).

5.2.8 Rat femoral defect implantation

The male Wistar Han rats used for this study were bred in the Comparative Medicine Unit of the Trinity Biomedical Sciences Institute (TBSI). Three groups were implanted: the two previously described experimental constructs, *chondrogenic* and *early hypertrophic*,

and along them, as positive control a bovine collagen type I – nano hydroxyapatite (Col-nHA) scaffold was used. These Col-nHA sponges were fabricated by O'Brien group as previously described [446, 447], and were soak loaded with 5 µg/scaffold of BMP-2 15 minutes prior to implantation, and incubated at RT. From now on, the positive control construct will be denoted as *Col-nHA+BMP-2*. Critically sized femoral defect surgeries were performed on 24 12-week-old rats as previously described [448]. The rats were anesthetised in an induction box using a mix of isoflurane and oxygen, initially at an initial flow rate of isoflurane of 5 litres/min to induce, followed by 2.5 litres/min to maintain anaesthesia. Once anesthetised, the animal was transferred to a heating plate that was preheated to 37°C and preoperative analgesia was provided by subcutaneous injections of meloxicam (1.5 mg/kg). Surgical access to the femur was achieved via an anterolateral longitudinal skin incision and separation of the hind limb muscles, the vastus lateralis, and biceps femoris. The femoral diaphysis was exposed by circumferential elevation of attached muscles, and the periosteum was removed. Before the creation of the defect, a weight-bearing polyether ether ketone (PEEK) internal plate was fixed to the anterolateral femur. Four holes were created in the femur with a surgical drill using the plate as a template. Screws were then inserted into the drill holes in the femur to maintain the fixation plate in position. A 5 mm defect was created using an oscillating surgical saw under constant irrigation with sterile saline solution. Scaffolds were press-fit into the defect. Soft tissue was accurately readapted with absorbable suture material. Closure of the skin wound was achieved using sutures. All animals were administered post-surgery analgesia with subcutaneous injections of buprenorphine (0.05 mg/kg) during recovery and 1.5 mg/kg of meloxicam for first 3 days post-surgery. In addition, all animals received daily systemic administration of immuno-suppressive drugs FK506 (3.33 mg/ml) and SEW2871 (1.66 mg/ml) for 3 weeks post-operation as previously described [449, 450]. One defect per animal was created, n = 8 animals for each of the three groups. *In vivo* micro-computed tomography (µCT) scans were performed on all the rats at 6 and 12 weeks post-operation (see 5.2.9 section). At 12 weeks rats were sacrificed by CO_2 euthanasia and the left femur, with the intact PEEK plate attached, was harvested for further analysis. One rat from each of the experimental groups had to be culled within a week from the surgery and so excluded from analysis due to complications post-surgery. This animal procedure and study was approved by the ethics commit- tee in Trinity College Dublin and the Health Products Regulatory Authority (HPRA) in Ireland (Approval - AE19136/P087).

5.2.9 Micro-computed tomography (μCT)

To measure the mineralisation of the constructs retrieved after 12 weeks from the subcutaneous implantations, μCT scans analyses were performed using a Scanco Medical 40 μCT system (Scanco Medical, Bassersdorf, Switzerland). Reconstructed 3D images were generated using a Gaussian filter (sigma = 3, support = 5) to suppress noise site and a global threshold of 363, as previously done [37]. For the femoral defect study, *in vivo* μCT scans were performed on constructs using a Scanco Medical vivaCT 80 system (Scanco Medical, Bassersdorf, Switzer- land). Rats were scanned at 6 and 12 weeks post-surgery to assess bone formation within the defect. Animals were anesthetised using 2–4% (v/v) isoflurane in balanced oxygen throughout the scan. Next, a radiographic scan of the whole lower part of the animal was used to identify and isolate the operated rat femur. The animal's femur was aligned parallel to the scanning axis to simplify the following bone volume assessments. Scans were performed using a voltage of 70 kVp, and a current of 114 μA. A Gaussian filter (sigma = 0.8, sup- port = 1) was used to suppress noise and a global threshold of 210 was applied. A voxel resolution of 35 μm was used throughout. 3D evaluation was carried out on the segmented images to determine the bone volume and to reconstruct a 3D image. Bone volume in the defects was quantified by measuring the total quantity of mineral in the central 135 slices of the defect (approximately 4.75mm). To differentiate regional differences in bone formation, three volumes of interest (VOIs) were defined. Concentric circles of Ø2 mm, Ø4 mm, and Ø10 mm were aligned with the defect and used to encompass bone formation. The VOIs were aligned using untreated native bone along the femur. The core bone volume was quantified from the inner Ø2 mm VOI (core region). The annular bone volume was quantified by subtracting the Ø2 mm VOI from the Ø4 mm VOI (annulus region). Ectopic bone volume was quantified by subtracting the Ø4 mm VOI from the Ø10 mm VOI (heterotopic region). The bone volume percentages for each region were then calculated by dividing the corresponding bone volume (i.e. bone volume in the annulus) by the total bone volume in the defect. The bone volume was then quantified using scripts provided by Scanco.

5.2.10 Histological analyses for *in vivo* studies

The samples were fixed in 10% formalin overnight and decalcified using 'Decalcifying Solution-Lite' (Sigma) for approximately 1 week. Samples were frequently checked with X-rays to determine if there was any mineral remaining. When no mineral was visible, the sample was considered decalcified. Samples were then dehydrated in graded series of ethanol solutions (70% - 100%), cleared in xylene, and embedded in paraffin wax (all purchased from Sigma-Aldrich). Sections (8 μm) were rehydrated in graded series of ethanol concentrations and stained with goldner's trichrome (groat's iron haematoxylin, fuchsine, orange G, fast green) for visualising bone and vessels infiltration, and 0.2% (w/v) safranin-O to assess sGAG content post-implantation (all from Sigma). Slides were then imaged using an Aperio ScanScope slide scanner and evaluated for vessel infiltration by counting vessels visible across an entire section using Aperio ImageScope and ImageJ software. In addition, bone formation was semi-quantitatively assessed using ImageJ software. It should be noted that the PCL forming the frame is cleared during the tissue processing and leaves empty spaces in constructs as a result.

5.2.11 Statistical Analysis

Statistical analysis was performed using GraphPad 9 (GraphPad Software, La Jolla California USA). Pairwise comparisons between means of different groups were performed using a student t-test. One-way analysis of variance (ANOVA) with the addition of Turkey's correction was used for multiple comparisons testing. Two-way ANOVA with the addition of Turkey's correction was used for grouped multiple comparisons testing. Results are expressed as mean ± standard deviation. For all comparisons, significance was accepted at a level of $p < 0.05$. Sample size (n) is indicated within the corresponding figure legends.

5.3 Results

5.3.1 Realisation of 3D bioprinted PCL reinforced cartilaginous templates

Meeting the objectives of this study first required the identification of a hydrogel bioink that was both compatible with 3D bioprinting and capable of supporting robust

chondrogenesis *in vitro*, graft vascularisation and endochondral bone formation *in vivo*. To this end we assessed the capacity of a previously developed composite bioink [30], composed of fibrinogen with a gelatin carrier (mixture of gelatin, hyaluronic acid and glycerol) to impart viscosity compatible to 3D bioprinting, to support chondrogenesis of hMSCs. The selected bioink laden with hMSCs was 3D bioprinted into previously 3D printed PCL frames along the z-direction to precisely fill the frames, leaving a central micro-channel empty; fibrinogen was then cross-linked in a thrombin bath. The resulting constructs were then cultured in two different conditions to produce what are defined as *chondrogenic* (5 weeks in chondrogenic media – 3 weeks at 5% pO_2 followed by 2 weeks at 20% pO_2) and *early hypertrophic* (3 weeks at 5% pO_2 in chondrogenic media followed by 2 weeks at 20% pO_2 in chondrogenic media with addition of BMP-2) constructs (Fig. 5.1A). Both constructs contained comparable levels of DNA (Fig. 5.2A), sGAG (Fig. 5.2B) and collagen (Fig. 5.2C), however the calcium content was significantly higher in the *early hypertrophic* group (Fig. 5.2D). Abundant and homogeneous sGAG and collagen deposition was observed histologically, with constructs generally staining negative for calcium deposits (Fig. 5.2E). Both constructs also stained homogenously for collagens type I and II (with some non-specific staining for type I collagen visible in cell free fibrin constructs at day 0; see Fig. 5.3), while only weak staining for collagen type X was observed (Fig. 5.2F).

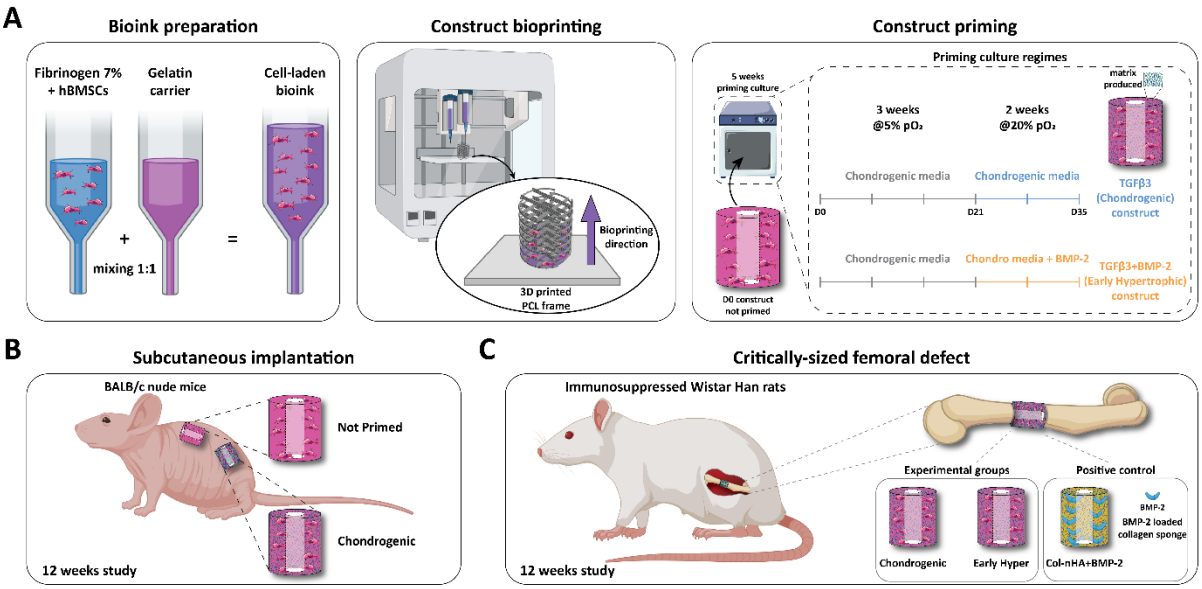

Figure 5.1: Study schematic. (A) 3D bioprinted PCL reinforced cartilaginous templates fabrication; (B) Schematic of the subcutaneous implantation study; (C) Schematic of the critically sized femoral defect implantation study.

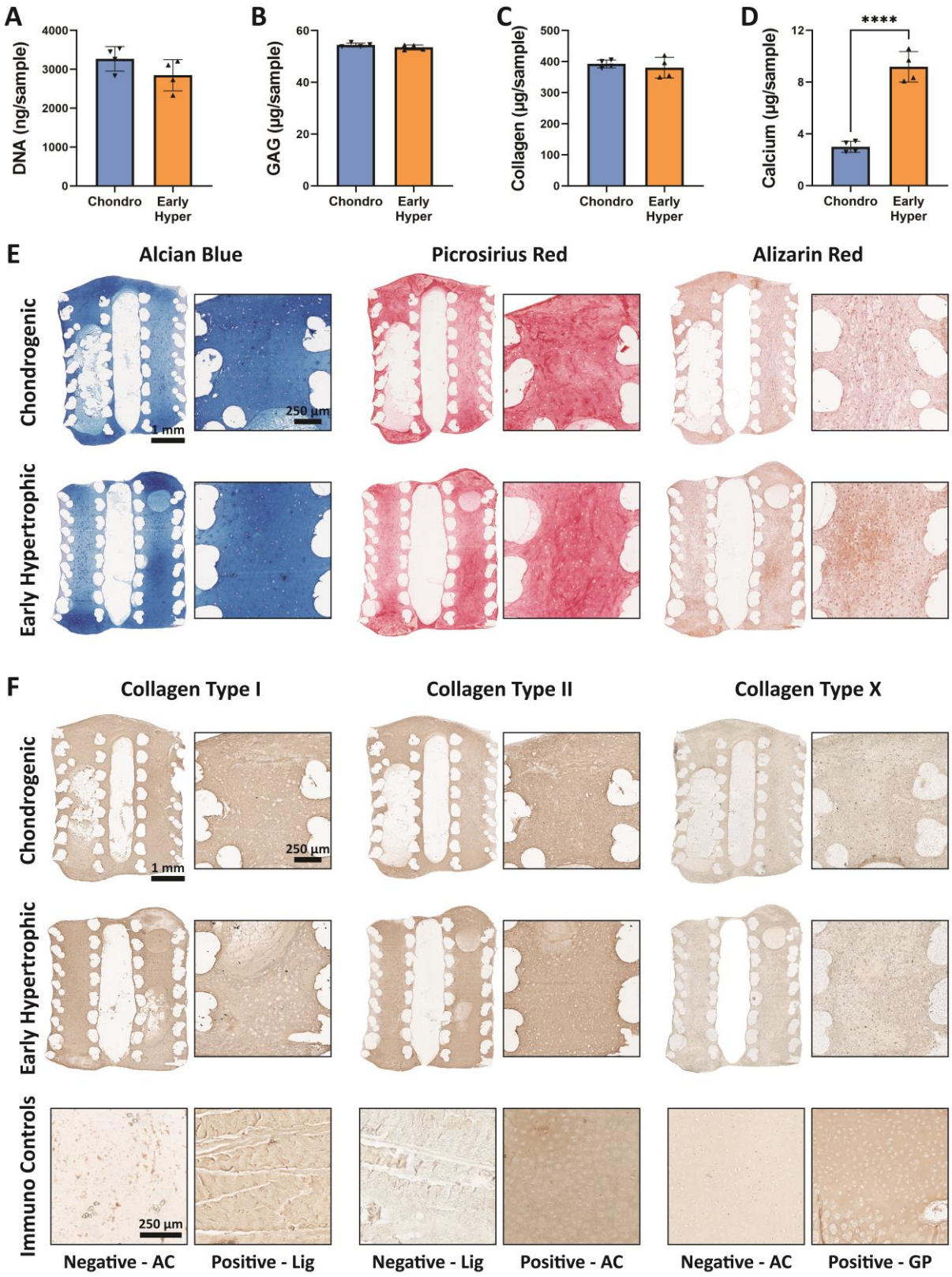

Figure 5.2: Primed 3D bioprinted PCL reinforced cartilaginous templates characterisation. (A) DNA total content for *chondrogenic* and *early hypertrophic* constructs at the end of the priming culture; (B) sGAG content; (C) collagen content; (D) calcium content; $n = 4$ samples per group; ****$p<0.0001$; (E) histological analyses with alcian blue, picrosirius red and alizarin red staining, and (F) immunohistochemical analyses with

collagen type I, II and X staining. Positive and negative controls for immunohistochemical analyses are presented. Acronym legend: articular cartilage (AC), ligament (Lig) and growth plate (GP).

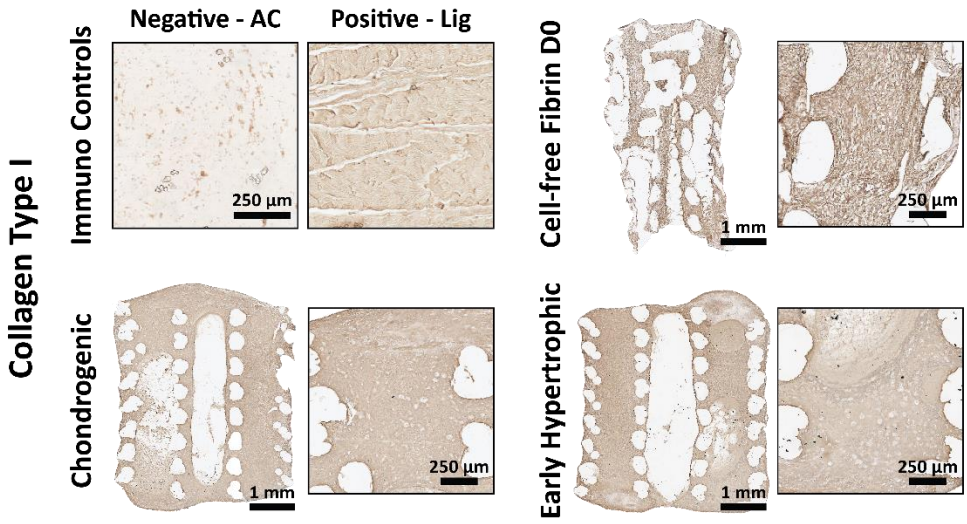

Figure 5.3: Collagen type I non-specific staining in fibrin constructs. Collagen type I immunohistochemical analyses for cell-free fibrin constructs and experimental groups. Positive and negative controls are presented.

5.3.2 Subcutaneous implantation

To confirm the fibrin based bioinks would support vascularisation and endochondral bone formation, and that *in vitro* chondrogenic priming would enhance mineralisation *in vivo*, *chondrogenic* constructs were implanted subcutaneously into nude mice and bone formation after 12 weeks *in vivo* compared to control (*Not Primed*) hMSC-laden constructs that were not cultured prior to implantation (Fig. 5.1B). Micro-CT analyses revealed that chondrogenic priming was necessary to induce construct mineralisation *in vivo*, with little or no mineral deposition observed in the control *Not Primed* constructs (Fig. 5.4A-B). Macroscopically it was clear that the *chondrogenic* constructs were vascularised *in vivo*, with blood vessel infiltration observed in the centre of these implants (Fig. 5.4C). Mineralisation and vascularisation of the primed constructs were confirmed histologically with goldner's trichrome staining (Fig. 5.4D), with positive staining for mineralisation observed in all *chondrogenic* constructs. New vessels could be easily located and counted to characterize vessel infiltration in both groups (Fig. 5.4E), which revealed a significantly higher number of vessels in the *chondrogenic* group compared to the *Not Primed* controls.

As expected, there was no evidence of degradation of the reinforcing PCL network over the 12 week *in vivo* time period. In contrast, it appeared that the fibrin based bioink was completed remodelled *in vivo*, supporting its use as a bioink for endochondral bone TE.

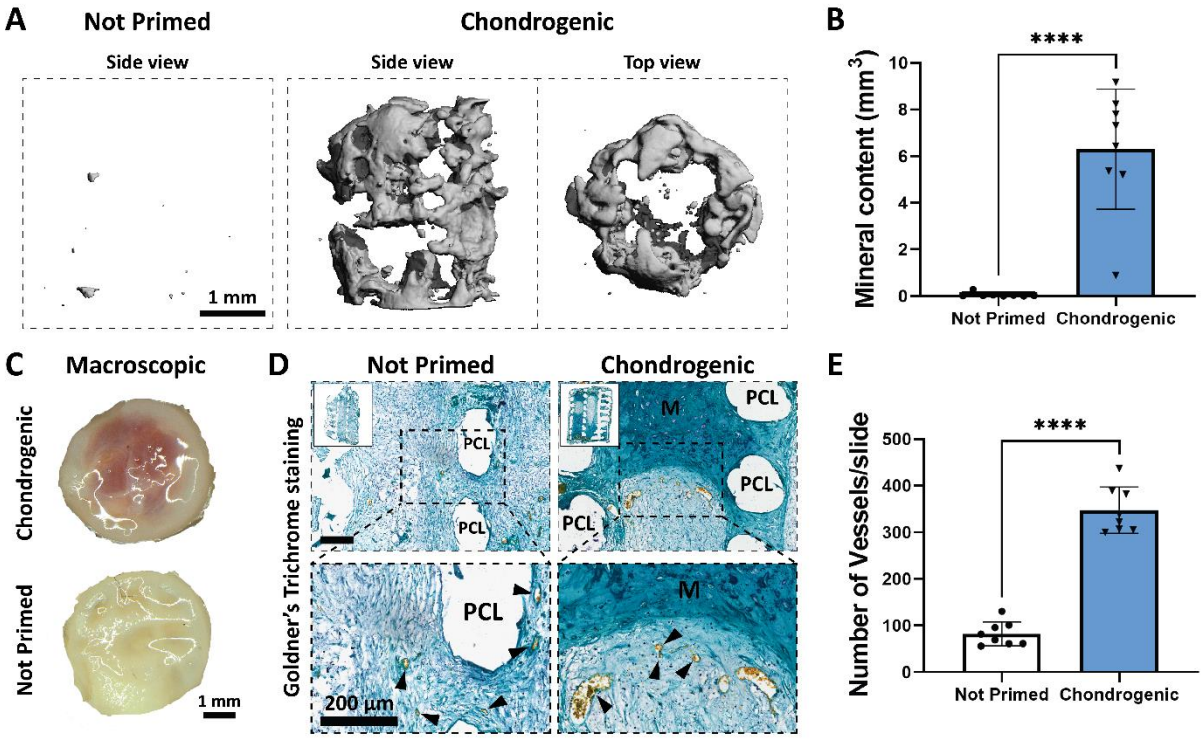

Figure 5.4: Subcutaneous implantation study. (A) Micro-CT 3D reconstruction images for *Not Primed* and *Chondrogenic* constructs; (B) micro-CT analysis on total mineral deposition of both groups after 12 weeks *in vivo*; (C) macroscopic pictures of the resected constructs; (D) goldner's trichrome stained sections for both groups after 12 weeks *in vivo*. Images were taken at 1×, 5.5× and 10×. Arrows denote vessels, M denotes cartilage template that mineralised, PCL denotes areas where the PCL frame was. All scale bars = 200 µm; (E) vessel number per slide. n = 8 constructs per group, n = 4 slices per construct for the histology; ****p<0.0001.

5.3.3 3D bioprinted PCL reinforced cartilaginous templates for large bone defect healing

We next sought to assess whether the 3D bioprinted engineered cartilaginous templates that we developed would support endochondral bone formation within critically sized bone defects. To this end, *chondrogenic* and *early hypertrophic* constructs were prepared and implanted in a 5-mm rat femoral defect (Fig. 5.5A) and compared to a positive control, consisting in a bovine collagen type I – nano hydroxyapatite scaffold, soak loaded

with 5 µg/scaffold of BMP-2 15 minutes prior to implantation (Fig 5.1C). To enable the implantation of human cells, all rats involved in the study were administered daily subcutaneous injections of an immuno- suppressing drug cocktail containing FK506 and SEW2871 for 3 weeks after implantation [449, 450]. Immunosuppression would appear to slightly diminish the animals regenerative potential; in fact, a partially suppression of bone formation is evident by the differences in total new bone formed in untreated or immunosuppressed rats both at 6 and 12 weeks after implantation (Fig. 5.6). Looking at the experimental groups, micro-CT analysis of animals at 12 weeks post-implantation was carried out to visualize and quantify bone formation within the defects (Fig. 5.5B). Compared to the 3D bioprinted groups, there were significantly higher levels of new bone formation in the positive control *Col-nHA+BMP-2* group. To assess the location of new bone formation and the levels of heterotopic bone, region of interest (ROI) bone volume analysis was performed. Within the defect, three regions were defined: core, annulus and heterotopic regions (Fig. 5.5E); the total bone volume for each animal was quantified in these regions (Fig. 5.5C). In both experimental bioprinted groups, bone mainly formed in the annulus of the defect, with significantly higher percentages of new bone deposited there compared to the positive control (Fig. 5.5D). In addition, they were also characterised by little heterotopic bone formation, significantly lower in the *early hypertrophic* group compared to the positive control. Based on an analysis of the micro-CT 3D reconstructions at both 6 weeks (Fig. 5.7) and 12 weeks (Fig. 5.5B), it seems that mineralisation and bone formation occurs first in the central regions of the *early hypertrophic* group, which then progress towards the native bone ends. This pattern of healing is less evident in defects treated with the *chondrogenic* constructs (Fig. 5.5B and 5.7). We next sought to assess the nature of new bone tissue being formed and vessel infiltration based on an analysis of histological staining. Goldner's trichrome staining showed positive staining for new bone, complete with marrow cavities and vessel infiltration, in all three groups 12 weeks after implantation (Fig. 5.8A). Defects treated with the *early hypertrophic* constructs contained significantly more blood vessels compared to both the *chondrogenic* and *Col-nHA+BMP-2* groups (Fig. 5.8B). Quantifying the positive bone area in the available defect area, there was significantly more bone found in the *early hypertrophic* group compared to the other two groups (Fig. 5.8C). (In this analysis, regions of the repair tissue containing PCL were subtracted from the total defect area to determine the available defect area). Finally, safranin-O staining revealed that little cartilage persisted in both experimental groups after

12 weeks, demonstrating that the *in vitro* engineered cartilaginous templates had been remodelled *in vivo* (Fig. 5.9).

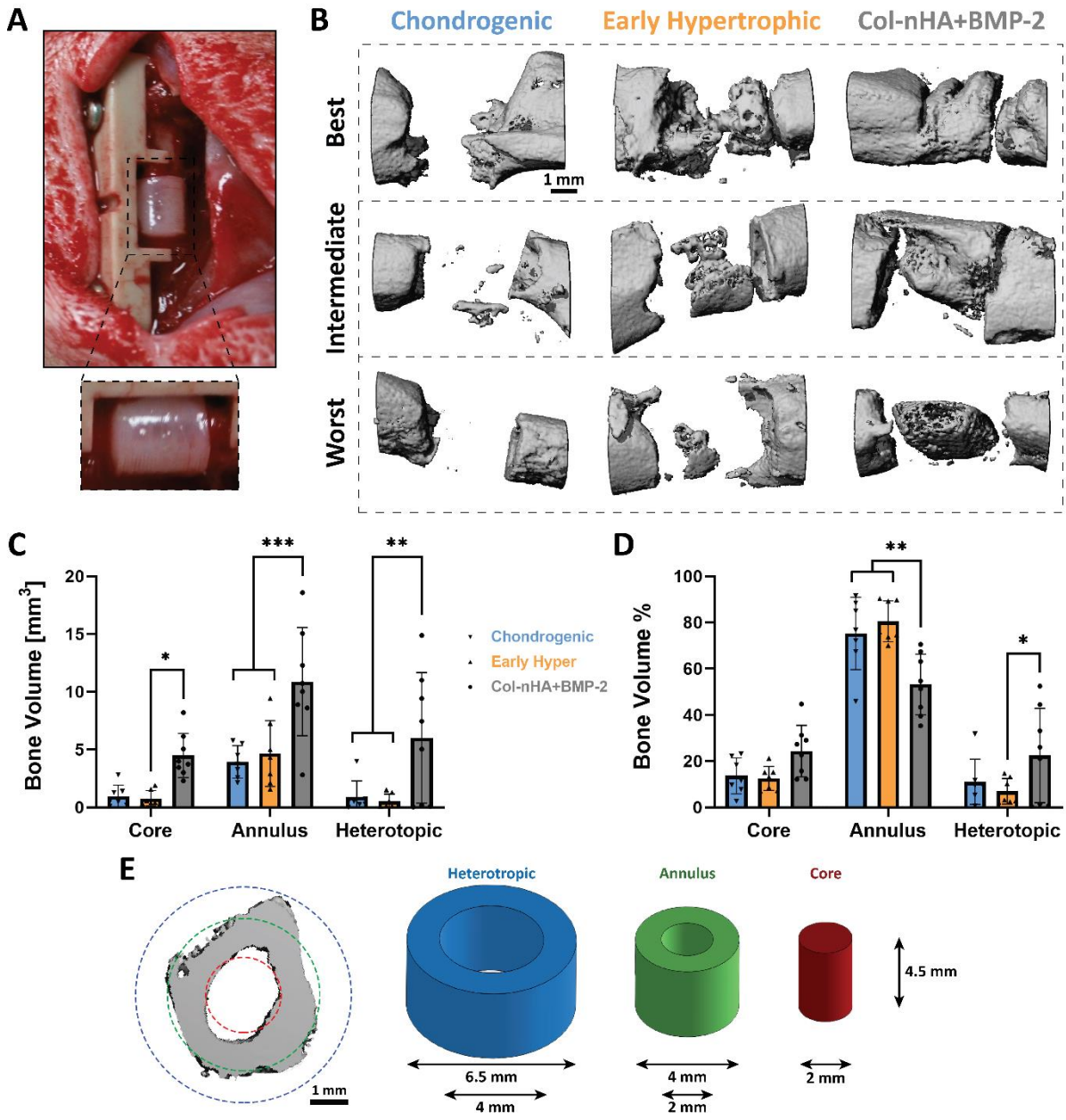

Figure 5.5: Critically sized femoral defect implantation. *In vivo* micro-CT analysis. (A) picture highlighting surgical implantation; (B) reconstructed *in vivo* micro-CT analysis of bone formation in the defects at post-operative week 12; (C) regional quantification of total bone volume (mm^3) in the defects; (D) percentage of new bone in each region related to total new bone; (E) outline of ROI bone volume analysis including definitions of core, annulus, and heterotopic regions. *n* = 7 animals per experimental group (*chondrogenic* and *early hypertrophic*), *n* = 8 animals per positive control group (*Col-nHA+BMP-2*); ****p<0.0001.

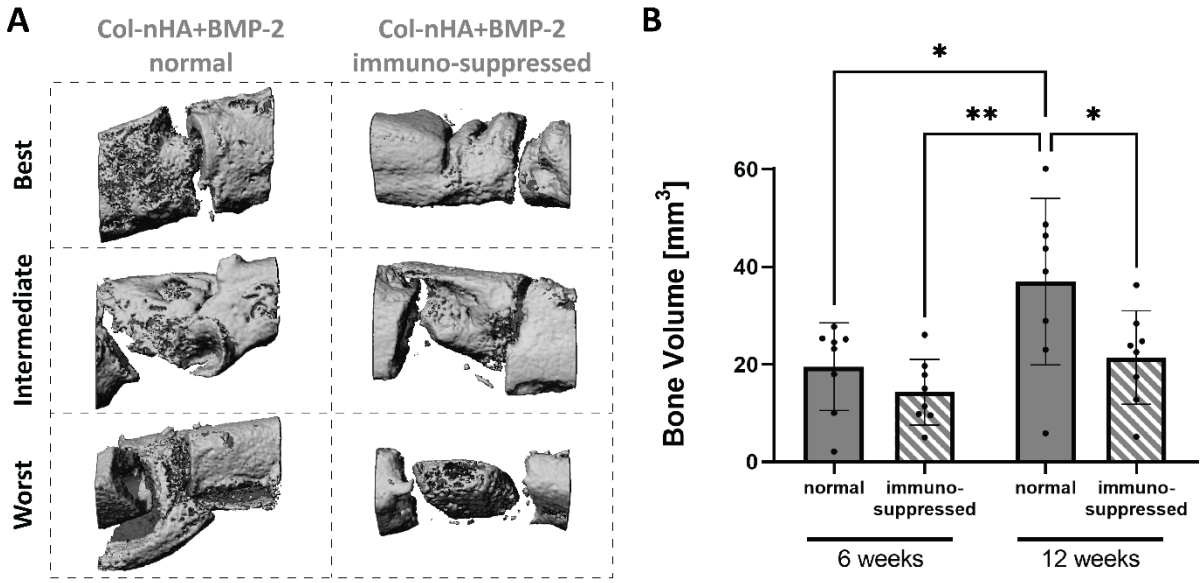

Figure 5.6: Effects of immunosuppression on positive control constructs implanted into critically sized femoral defects. *In vivo* micro-CT analysis. (A) Reconstructed *in vivo* micro-CT images of bone formation at post-operative week 12 for *Col-nHA+BMP-2* constructs in immunocompetent and immunosuppressed rats; (B) total bone quantification (mm^3) in the defects at 6 and 12 weeks post-implantation. n = 8 animals per group; *p<0.05, **p<0.01.

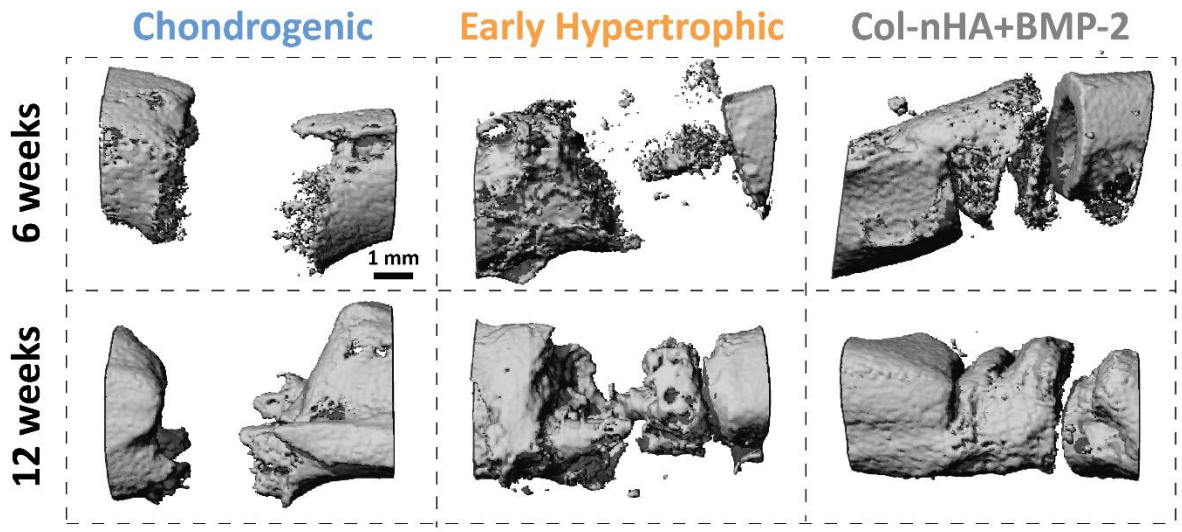

Figure 5.7: Critically sized femoral defect implantation. *In vivo* micro-CT analysis. Reconstructed *in vivo* micro-CT analysis of bone formation in the defects at post-operative week 6 and 12.

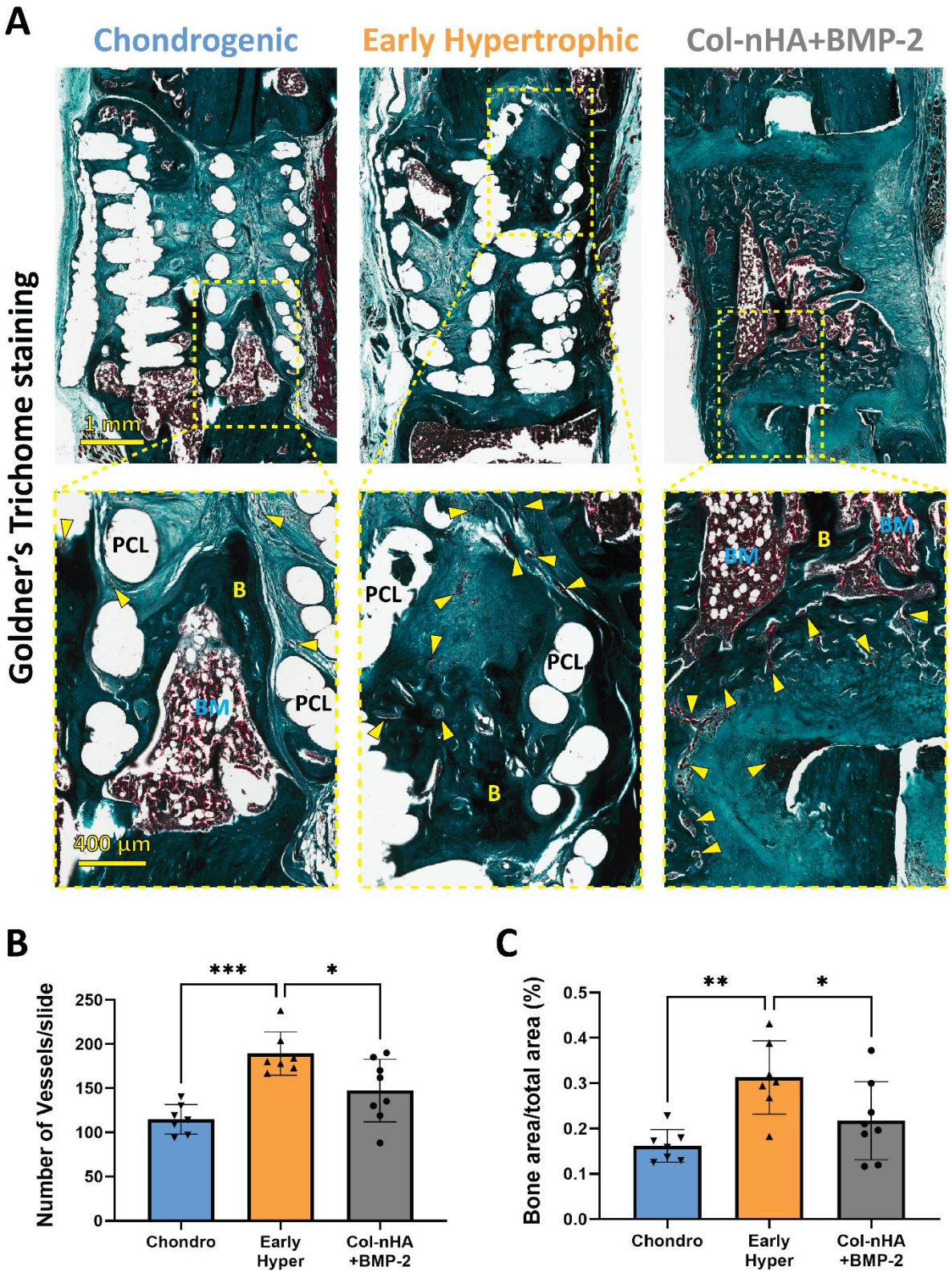

Figure 5.8: Critically sized femoral defect implantation. Histological analysis. (A) Goldner's trichrome stained sections for all groups after 12 weeks *in vivo*. Images were taken at 1× and 3×. Arrows denote vessels, B denotes positive bone tissue, BM denotes bone marrow and PCL denotes areas where the PCL frame was; (B) vessel number per slide; (C) quantification of the amount of bone formation per total area. *n* = 7 animals

per experimental group (*chondrogenic* and *early hypertrophic*), *n* = 8 animals per positive control group (*Col-nHA+BMP-2*), *n* = 4 slices per construct for quantifications; *p<0.05, **p<0.01, ****p<0.0001.

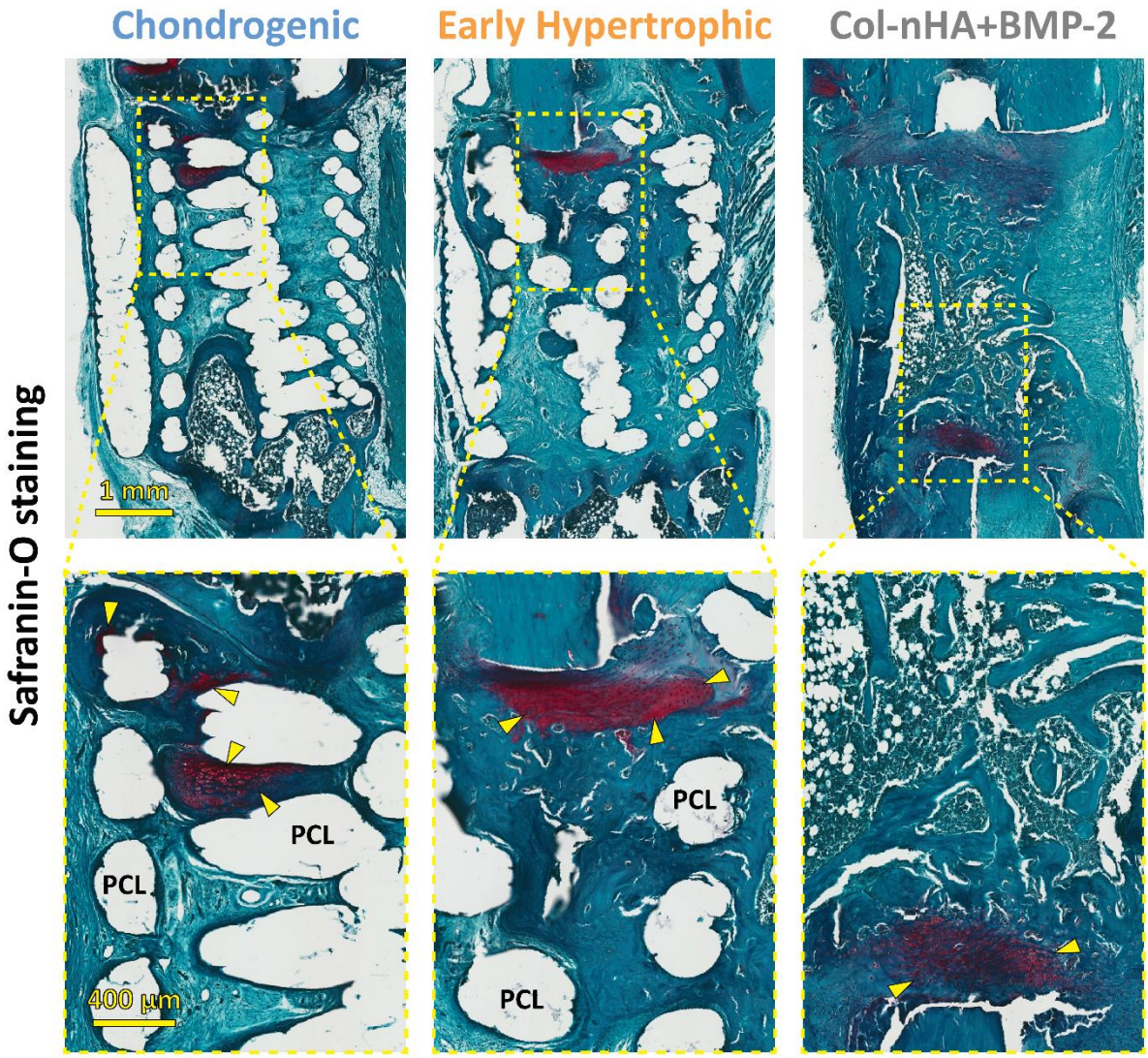

Figure 5.9: Critically sized femoral defect implantation. Histological analysis. Safranin-O stained sections for all groups after 12 weeks *in vivo*. Images were taken at 1× and 3×. Arrows indicates cartilage areas and PCL denotes areas where the PCL frame was.

5.4 Discussion

This study describes the development of 3D bioprinted, PCL reinforced, engineered cartilaginous construct capable of executing an endochondral programme *in vivo* and regenerating critically sized long bone defects. A fibrin-based bioink capable of supporting

chondrogenesis of hMSCs *in vitro* was used to 3D bioprint these constructs, which were then primed using two different culture regimes to produce *chondrogenic* and *early hypertrophic* constructs with unique *in vitro* and *in vivo* phenotypes. Subcutaneous implantation of hMSC laden hydrogels into mice revealed the necessity of chondrogenic priming to trigger construct mineralisation and vascularisation *in vivo*. These studies also confirmed the suitability of a fibrin based bioink for endochondral bone regeneration. After implantation into critically sized rat femoral defects, the bioprinted *early hypertrophic* templates were replaced with new bone. Although higher levels of mineralisation were observed in the control BMP-2 loaded collagen sponges compared the experimental bioprinted groups, the latter supported higher levels of new bone formation in the annular regions of the defect where bone is natively present. The *early hypertrophic* constructs also led to significantly less heterotopic bone formation compared to the control BMP-2 loaded collagen sponges, supported the highest level of vascular invasion and based on the histomorphometric analysis supported the highest levels of new bone formation in the defect region.

In this study, we were able to bioprint hMSC-laden constructs and chondrogenically prime them *in vitro* to adopt unique phenotypes prior to implantation. 5 weeks of priming in chondrogenic media (first 3 weeks at 5% pO_2 and the last 2 weeks at 20% pO_2) produced *chondrogenic* constructs rich in sGAG and collagen (mainly type II) and with very low levels of calcium deposits, while additional stimulation with BMP-2 during the last 2 weeks of culture promoted an "early hypertrophic" phenotype, as evident by the significantly higher amount of calcium deposited *in vitro*. Previous studies have used BMPs to support hMSCs chondrogenesis *in vitro*, demonstrating that BMP-2 enhances the chondrogenic effects of TGF-βs when used in combination [451-453]. After 21 days, hMSCs cultured with both TGF-β3 and BMP-2 expressed higher levels of ACAN, SOX9, COL2A1, COL10A1 and PTHrP compared to cells only stimulated with TGF-β3 [452, 453]. Together, these findings support the combined use of TGF-β3 and BMP-2 to induce an *early hypertrophic* phenotype in hMSCs. Other approaches in the literature have typically followed one or two approaches to generate cartilage templates for endochondral bone TE; either priming cells with chondrogenic media only [22, 152] or generating more hypertrophic cartilage templates by switching to a hypertrophic media (containing thyroxine, β-glycerophosphate, dexamethasone and ascorbic acid) towards the end of the *in vitro* priming protocol [18, 19, 37, 293, 397]. Both approaches have been shown to generate constructs capable of executing

an endochondral program following subcutaneous implantation. Furthermore, hMSCs primed in osteogenic media have been shown lower levels of new bone formation in such *in vivo* models [288]. Our results in an orthotopic defect model also demonstrate that the specifics of the *in vitro* chondrogenic priming regime (*chondrogenic* versus *early hypertrophic*) will also dictate the pattern and quality of bone repair.

It is possible that the differences in bone repair between the chondrogenic and early hypertrophic constructs during bone regeneration (as presented in 5.3.3) might be due to residual or bound BMP-2 from the priming culture, rather than the process of priming itself and the capacity of the resultant engineered tissue to execute an endochondral programme *in vivo*. Some BMP-2 might have failed to be washed away pre-implantation or might have bound to the ECM deposited in culture by the cells. Although a valid hypothesis, it should be noted that the levels of any residual BMP-2 in the constructs is expected to be quite small and may only have a small influence on bone regeneration. As a matter of comparison, considering that the amount of BMP-2 loaded in the control collagen sponges was 5 μg per construct, and in the culture priming regime only 50 ng/ml were used (as a reference the hydrogel volume in the experimental groups is roughly 50 μl), it is clear that the difference in the BMP-2 concentrations is significant. In order to investigate the hypothesis that residual BMP-2 is both present and could influence bone regeneration in vivo, it would be first necessary to measure BMP-2 levels in constructs at the end of the priming culture with an enzyme-linked immunosorbent assay (ELISA), and, if present, immunofluorescence staining for BMP-2 could be used on histological slides to locate its presence within the constructs. In addition, additional second control groups could be included in the in vivo rat orthotopic defect model, specifically an acellular 3D printed reinforced fibrin construct (prepared in the same way as in 5.2.3 but without hMSCs), which would be primed for 5 weeks as the early hypertrophic constructs (including the BMP-2 addition for the last 2 weeks). This setup would allow the influences of trapped/bounded BMP-2 from culture to be assessed in a manner that was decoupled from the effect of culture priming on cells and their ECM.Following the implantation into critically sized femoral bone defects, the *early hypertrophic* constructs supported higher levels of vascularisation and bone formation (based on histomorphometric analysis) compared to the *chondrogenic* constructs. As well, they were characterised by a clear healing pattern, with bone formation occurring firstly in the central regions of the defect, which was less evident in defects treated with the *chondrogenic* constructs. These differences in *in vivo* outcomes are likely due to differences

in cellular phenotype and the specific composition of the ECM arising from the different *in vitro* priming protocols. It is well established that cartilaginous tissues engineered using bone marrow derived MSCs progressively acquire a hypertrophic phenotype and are capable of executing an endochondral programme *in vivo* [403], however the optimal *in vitro* culture conditions to accelerate this process in an orthotopic location remain unclear. Previous studies in a subcutaneous environment have shown that promoting a more hypertrophic phenotype *in vitro* leads to increased bone formation *in vivo* [18]. This chapter demonstrates that the addition of BMP-2 to the *in vitro* priming protocol supported the development of a cartilaginous tissue (demonstrated by the abundant presence of sGAG and collagen type II) that has already started to adopt an early hypertrophic phenotype (as evident by higher levels of calcific deposits) at the time of implantation. This altered phenotype, which has been associated with increased expression of pro-osteogenic factors such as PTHrP [452], would appear to better support endochondral bone formation *in vivo* [454]. Future analyses on our engineered templates gene expression could be helpful to highlight expectable additional differences between the experimental groups.

Overall levels of bone formation *in vivo* following implantation of bioprinted templates into critically sized femoral defects were compared to collagen based scaffolds loaded with BMP-2. Since collagen represents the main organic constituent of natural bone tissue, collagen-based biomaterials have been probably the most commonly used materials for bone TE purposes, and among the different types of collagen, collagen type I has been the most used one, being adopted in orthopaedic surgery and in bone TE research for decades. Collagen-based scaffolds can be produced in multiple different forms, and collagen sponges are, by far, the most widespread and tested form of collagen scaffold [455]. However, collagen type I is not osteoinductive and so is not capable of triggering new bone growth *in vivo*. For this reason numerous researchers have incorporate osteoinductive factors in such collagen scaffolds. Among the most potent of such factors yet discovered are bone morphogenetic proteins (BMPs) [456]. Therefore collagen type I sponges loaded with BMP-2 represent one of the most common approaches in bone TE; for this reason were *Col-nHA+BMP-2* scaffolds were used here as positive controls to compare to the bioprinted cartilage templates.

After 12 weeks post-implantation, the BMP-2 loaded collagen scaffolds produced significantly more total bone than our experimental bioprinted groups. However, only around half of the new bone was deposited in the annular region of the defect (53% of the

total), with significant levels of new bone formation observed heterotopically and in the core of the defect bone where it is not normally present. In contrast, the *early hypertrophic* templates promoted much lower levels of heterotopic bone formation. These results demonstrate that, even if we used a low dose of BMP-2 (5 µg/construct), bone growth in the positive control group is happening in an uncontrolled manner. This adverse outcome associated with the *in vivo* use of BMP-2 is not a new observation and is well established in the literature [145, 457, 458], motivating the development of alterative bone TE strategies that are not limited by the use superphysical levels of exogenous growth factors. During development, stem cells differentiate and progress stepwise through different stages of maturation [213], a process that is accompanied by dynamic changes to the cellular secreteome and the surrounding ECM [214, 215]. By using specific cell types and culture conditions, it is possible to bioprint cartilaginous templates that mimic the dynamic tissues observed during different developmental stages. These engineered tissues will temporally secrete a plethora of different growth factors, at much lower levels than used in traditional TE strategies using exogenous BMP-2, but are still capable of directing bone regeneration. Recapitulating the secretome of the hypertrophic cartilage within a drug eluting scaffold would be extremely complex, which motivates the use of such developmentally inspired templates for long bone defect repair. Furthermore, the composition of the ECM of hypertrophic cartilage is likely optimised over millions of years of evolution to support its conversion into bone, and would be extremely difficult to recapitulate using bottom-up scaffold strategies currently used to develop biomimetic implants for bone TE.

While collagen sponges lack of the variety of bioactive cues naturally present in engineered tissues, they are easier and quicker to obtain, their preparation does not involve complex cell culture and they can be stored for a long time until needed. For all these reasons, they do not have to face the same number of logistical and regulatory challenges associated with live (or viable) engineered tissues, which at the end, simplify their clinical translation and commercialisation. However, there is a way to avoid these challenges with *in vitro* engineered tissues; specifically to generate *off-the-shelf* grafts through the application of decellularisation strategies. By decellularising and hence devitalising the engineered templates, they could be more easily transported and stored and would perhaps face less onerous regulations in order to be translated into the clinic. The next chapter of this thesis will focus on transforming these engineered cartilage templates into *off-the-shelf*

grafts, applying the most appropriate decellularisation method that would allow us to retain their osteoinductive capacity, while minimising DNA and cellular contents.

5.5 Conclusions

The results from this study demonstrate that it is possible to 3D bioprint hypertrophic cartilaginous templates using hMSCs which are capable of directing endochondral bone formation upon *in vivo* implantation. The fibrin based bioink supported hMSCs chondrogenesis and remodelled *in vivo* enabling vascularisation and conversion of the cartilaginous templates into bone, proving its possible use as a bioink for endochondral bone TE. Chondrogenic priming was found to be necessary to trigger both mineralisation and vessel infiltration following subcutaneous implantation of hMSC laden constructs. Once implanted into critically sized rat bone defects, the *early hypertrophic* templates supported higher levels of vascularisation and bone formation (based on histomorphometric analysis) compared to the *chondrogenic* constructs (and the positive controls), proving the superiority of the BMP-2 addition to chondrogenic priming. Although the positive control *Col-nHA+BMP-2* sponges produced significantly more total bone, they were characterised by significantly high levels of abnormal new bone formation (both heterotopic and in the core), indicating how our 3D bioprinted templates supported in many ways more controlled regeneration. This study demonstrates that 3D bioprinting is a viable approach to scale-up the engineering of developmentally inspired templates for bone TE, and that such templates offer key advantages over more commonly used BMP-2 delivery approaches for bone TE applications.

Chapter 6: Decellularised bioprinted grafts for large bone defect healing

6.1 Introduction

The current clinical gold standard for the treatment of large bone defects is the use of an autologous bone graft, where a patient's own bone is harvested and relocated to the defect site. Although clinical outcomes are usually positive, the use of autografts is negatively affected by complications such as the scarcity of harvestable autologous bone, severe donor site morbidity, patient-to-patient variability in clinical outcomes and a decrease in the regenerative capacity of graft material with an increase in donor age [5, 6, 459]. While the use of allograft tissue from another individual can overcome some of these limitations, their use is associated with other significant risks including immune rejection and disease transmission [460]. Finally, xenografting of tissues derived from non-human sources into a human patient is also associated with similar drawbacks, such as infection, rejections and chronic inflammation. All these limitations have motivated the study of developmentally inspired tissue engineering (TE) strategies that recapitulate the process of endochondral ossification (EO) [18, 148, 286, 461, 462]. Such developmentally inspired strategies have been shown to support robust bone regeneration in different preclinical models [21, 22, 153, 397]. We have previously demonstrated that it is possible to 3D bioprint such developmentally inspired grafts, and have leveraged the capabilities of such biofabrication frameworks to both mechanically reinforce the engineered tissues and modify their architecture to support nutrient transport *in vitro* and vascularisation *in vivo*. In the previous chapter of this thesis, such bioprinted grafts were shown to support the regeneration of critically sized bone defects in rats [vital paper]. However, the clinical translation of viable engineered tissues is hampered by practical and logistical considerations such as *off-the-shelf* availability and the preference for single-stage strategies that can be more easily implemented clinically.

O*ff-the-shelf* implants are easier to commercialise and translate into the clinic, as they are available ready-to-use and are less burdened by some of the logistical and regulatory challenges associated with the use live or viable engineered tissues. The challenges associated with the clinical translation of such viable engineered tissues has motivated

increased interest in the decellularisation of *in vitro* engineered tissues as a means of producing extracellular matrix (ECM) derived biomaterials and implants that are available *off-the-shelf* for tissue engineering and single-stage regenerative medicine procedures [27]. *In vitro* engineered tissues offer several potential advantages compared to native animal or human tissue-derived ECM scaffolds (e.g. decellularised small intestine submucosa) currently used clinically as regenerative biomaterials. Engineered tissues are not limited in their availability, their composition can be tightly controlled *in vitro* by using different cell types and culture conditions, and their manufacturing can be standardised. The geometry and porosity of *in vitro* engineered ECM-derived tissue scaffolds can also be controlled, and the engineered ECM deposited by different cell types can be combined to produced more complex, layered biomaterials, especially when combined with emerging biofabrication strategies such as 3D bioprinting. Cell-derived engineered tissues have already been used in the field of bone regeneration [249, 257, 282]; for example, the ECM secreted by MSCs as they undergo direct osteogenic differentiation has previously been shown to be osteoconductive [242, 284]. Decellularisation of hypertrophic cartilaginous templates engineered using MSCs has also been used to generate *off-the-shelf* implants supportive of osteogenesis and large bone defect healing [292-294]. However the optimal composition and architecture of such devitalised engineered cartilaginous templates for supporting bone regeneration has yet to be identified.

The decellularisation process is crucial for disrupting and removing cellular components from the ECM in order to prevent or minimise any negative inflammatory and immunological responses towards the biomaterial and decrease the risk of host rejection after *in vivo* implantation, especially when developing implants from allogeneic and xenogeneic cell or tissue sources [220]. Generally, such decellularised constructs can be easily and cost-effectively shipped and stored to be used when needed. The main aim of decellularisation is to eliminate all cellular and nuclear materials while preserving the molecular composition, bioactivity and structural integrity of the ECM [216]. To improve decellularisation outcomes, a variety of methods have been developed in literature, which can be broadly divided into four categories: physical, chemical, enzymatic, and biological methods. The most effective and robust decellularisation protocols are usually a combination of more than one of these methods. While decellularisation techniques for specific tissues and organs are well established [85, 224-227], additional work is required to

identify appropriate strategies to generate decellularised *off-the-shelf* bone grafting biomaterials from engineered cartilaginous templates.

The objective of this study was to develop decellularised 3D bioprinted cartilaginous templates as *off-the-shelf* grafts for large bone defect healing. 3D printing technology was used to address several aims: (1) to potentially produce implants of a predefined and controlled size and shape, (2) to mechanically reinforce the implants with a biocompatible polymeric frame, and (3) to modify the internal architecture, implementing a central microchannel to support nutrient transport *in vitro* and vascularisation *in vivo*. To this end, we firstly selected an appropriate bioink, which could be both printed and support hMSCs chondrogenesis *in vitro*. Then we investigated three different culture priming regimes with the aim of engineering cartilaginous templates with different phenotypes (chondrogenic, early hypertrophic and late hypertrophic). Four decellularisation protocols were then investigated to produce *off-the-shelf* engineered grafts. Next, the capacity of these decellularised implants to support osteogenesis of hMSCs was assessed *in vitro*. Finally, we assessed how the phenotype of these decellularised grafts influenced their capacity to instruct bone regeneration *in vivo* in a critically sized rat femoral defect. As a positive control, collagen type I-nHA sponges soak loaded with 5 µg BMP-2 per scaffold were also implanted into the defects.

6.2 Materials & Methods

6.2.1 Isolation and expansion of MSCs

Human bone marrow derived MSCs (hBMSCs) were isolated from bone marrow aspirates (Lonza) and expanded in high glucose dulbecco's modified eagle's medium (hgDMEM) GlutaMAX supplemented with 10% v/v FBS, 100 U/ml penicillin and 100 µg/ml streptomycin (expansion media, XPAN) at 5% pO_2 (all Gibco, Biosciences, Dublin, Ireland). Following colony formation, MSCs were trypsinised, counted, seeded at density of 5000 cells/cm^2 in T175 flasks (Thermo Fisher Scientific), supplemented with hgDMEM, 10% v/v FBS, 100 U/ml penicillin, 100 µg/ml streptomycin, 2.5 µg/ml amphotericin B, and 5 ng/ml human fibroblastic growth factor-2 (Recombinant Human FGF-basic – 154 a.a., Peprotech) and expanded to passage 3 at 5% pO_2.

6.2.2 Bioink preparation

The bioink used in this study is a composite hydrogel developed elsewhere [30], and it is a mixture of fibrinogen (F8630), type A gelatin (G6144), hyaluronic acid (HA) (53747) and glycerol (G5516), which were all purchased from Sigma-Aldrich. It was prepared by mixing 1:1 two solutions. Briefly, for the first solution (called from now on gelatin carrier) 6 mg/ml HA were dissolved in DMEM by stirring the solution at 37 °C overnight. Glycerol (20% v/v) was added into the solution and stirred for 1 h at room temperature (RT) and finally gelatin (80 mg/ml) was dissolved by stirring for further 2 hours at 37 °C. The prepared solution was sterilised by filtration through a 0.45-μm syringe filter and was stored at −20 °C before use. For the second solution, 70 mg/ml fibrinogen was dissolved at 37 °C in Aprotinin (10000 KIU/ml) (Uniphar, Dublin, Ireland) containing 19 mg/ml sodium chloride (NaCl); this solution was used freshly made. Cells were resuspended in the fibrinogen solution, which was then gently mixed in equal parts together with the gelatin carrier, producing the wanted bioink (with 3.5% final concentrations of fibrinogen) containing $5x10^6$ cells/ml.

6.2.3 3D bioprinting system

PCL/bioink constructs were fabricated with a two-step print using the 3D Discovery multi-head bioprinting system (Regen Hu, Switzerland). First, molten PCL, with an average molecular weight of approximately 50,000 Da (CAPA 6500D, Perstorp, Sweden), was deposited with the fused deposition modeller to manufacture porous cylindrical (Ø = 4 mm, h = 5 mm) scaffolds. They were then treated with 3M sodium hydroxide (NaOH) for 12 hours, to increase their hydrophilicity and improve their bonding with the cell-laden hydrogel, prior to be ETO sterilised. For the second step, the bioink was loaded into the pressure driven piston system, and printed at room temperature (RT). A pressure of 0.08 MPa and a 25 Gauge needle were used to deposit by z-stacking the bioink inside the PCL scaffold, leaving a central micro-channel empty. The 3D Discovery was placed in a laminar flow hood to ensure sterility throughout the biofabrication process. Once printed, the constructs were immersed in a 20 U/ml thrombin (in hgDMEM) bath for 20 minutes at RT to crosslink and form fibrin. Finally, constructs were place in culture at 37 °C overnight to wash out all the uncross-linked components (gelatin, HA and glycerol). Constructs were then kept in XPAN for other 24 hours before the start of priming culture.

6.2.4 Priming cultures

All constructs were primed for 3 weeks at 5% pO_2 followed by 2 weeks at 20% pO_2. Three different priming culture regimes were used in this study, differing only for the media used during the last 2 weeks of culture. For the first 3 weeks, all constructs were cultured in a chondrogenic medium (CDM) consisting of hgDMEM GlutaMAX supplemented with 100 U/ml penicillin, 100 μg/ml streptomycin, 100 μg/ml sodium pyruvate, 40 μg/ml L-proline, 50 μg/ml L-ascorbic acid-2-phosphate, 4.7 μg/ml linoleic acid, 1.5 mg/ml bovine serum albumine, 1x insulin-transferrin-selenium, 100 nM dexamethasone (all purchased from Sigma-Aldrich), 10 ng/ml of human transforming growth factor- β3 (TGF-β3) (Prospec-Tany TechnoGene Ltd., Israel) and Aprotinin. For the last 2 weeks of culture, the first group called *chondrogenic construct* was kept in CDM as before; the second group, *early hypertrophic construct*, was cultured in the same CDM formulation but the addition of 50 ng/ml rh-BMP-2 (Peptrotech); finally, the third group, *late hypertrophic construct*, was switched to hypertrophic media, consisting of hgDMEM GlutaMAX supplemented with 100 U/ml penicillin, 100 μg/ml streptomycin, 4.7 μg/ml linoleic acid, 1 × insulin–transferrin–selenium, 50 nM L-thyroxine, 100 nM dexamethasone, 250 μM ascorbic acid and 10 mM β-glycerol phosphate (all from Sigma), for a further 2 weeks. At the end of the culture period, constructs were rinsed twice with PBS and snap frozen in liquid nitrogen (LN_2), starting in this way the first cycle of freeze-thawing of the different decellularisation protocols (explained in detail in the following paragraph – 6.2.5).

6.2.5 Construct decellularisation

Following the 5 weeks of culture, the constructs were treated with four different decellularisation protocols, selected and designed from protocols found in literature to be in order of increasing harshness. The first protocol (A), involved three cycles of freezing in LN_2 and thawing in a 37°C water bath, each cycle followed by washes in deionised water (DI H_20) in rotation for 10 min at RT. All the other three protocols started with the same cycles of freeze-thawing and washes, so fully including protocol A, and continued with different solution treatments. In the second protocol (B), constructs were treated with a solution of 0.5% Triton X-100 in PBS for 10 minutes in rotation at 37°C, and then washed

with DI H_20. For the protocol C, a solution of 0.5% Triton X-100 and 20 mM NH_4OH in PBS was used for 10 minutes in rotation at 37°C, and DI H_20 was then used for washing the constructs. In the last protocol (D), after the freeze-thawing cycles, the constructs were treated firstly with a solution of 0.5% Triton X-100 in PBS, in the same way as in the protocol B, and then with a 0.1% sodium dodecyl sulfate (SDS) solution in PBS for 1 hour at RT. All the four protocols included a final treatment with 100 U/ml DNase, in a buffer of 10 mM Tris-HCl, 2.5 mM $MgCl_2$ and 0.5 mM $CaCl_2$ (pH = 7.5), in rotation for 1 hour at 37°C. At the end of the different decellularisation protocols, constructs were washed twice with DI H_20 in rotation, freeze-dried and stored at -80°C until analyses or further studies were performed. For scanning electron microscopy (SEM) imaging of the *off-the-shelf* grafts, samples were prepared by coating with gold/palladium for 40 s at a current of 40 mA. Imaging was conducted in a Zeiss ULTRA plus SEM using InLens and SE2 detectors with an accelerating voltage of 4–5 kV.

6.2.6 Osteogenic potential assessment

The three *off-the-shelf* constructs were sterilised by exposure to ethylene oxide for 12 hours, reseeded with hMSCs ($5x10^5$ cells/construct) and individually placed in the wells of a 24-well plate; cells were allowed to attach to the scaffolds for 2 hours in the incubator at 37 ºC before the addition of the XPAN in the wells. 24 hours after, the media was switched to minimal osteogenic media (mOSM) consisting of hgDMEM GlutaMAX supplemented with 10% v/v FBS, 100 U/ml penicillin, 100 µg/ml streptomycin, 10 nM dexamethasone, 10 mM β-glycerol phosphate and 25µM L-ascorbic acid. Reseeded constructs were cultured in mOSM for 21 days at 20% pO_2. As a control for the experimental grafts, *Fibrin Alone* constructs were prepared using the same bioink as in 6.2.2 and 3D printed in the same way as the experimental grafts (as in 6.2.3) but without the addition of cells. Once printed, constructs were freeze-dried, seeded with hMSCs cultured in mOSM for 21 days at 20% pO_2 along with the reseeded experimental grafts.

6.2.7 Biochemical analysis

The biochemical contents of all samples were analysed at day 0 and 35 of culture, after the decellularisation protocols, and at day 21 of the osteogenic potential assessment.

Prior to biochemical analysis, constructs were washed in PBS, weighed and frozen for subsequent assessment. The DNA content was quantified using the Quant-iT PicoGreen dsDNA Assay (BD Biosciences), with calf thymus DNA as a standard. The amount of sulphated glycosaminoglycan (sGAG) was quantified using the dimethyl methylene blue dye-binding assay (Blyscan, Biocolor Ltd., Northern Ireland), with a chondroitin sulphate standard. Total collagen content was determined by measuring the hydroxyproline content using the dimethylaminobenzaldehyde and chloramine T assay and a hydroxyproline to collagen ratio of 1:7.69. Prior to these biochemical analyses, each construct was digested with 0.5 ml of papain (125 mg/ml) in 0.1M sodium acetate, 5 mM L-cysteine HCl, 0.05 ethylenediaminetetraacetic acid (EDTA), pH 6.0 (all from Sigma-Aldrich) at 60 °C and 10 rpm for 18 h. Finally, the amount of calcium present in the constructs was determined using a Sentinel Calcium kit (Alpha Laboratories Ltd, UK); to run this assay, constructs were digested in 1M HCl at 60 °C and 10 rpm. Four constructs per group were analysed by each biochemical assay.

6.2.8 Histological and immunohistochemical analysis of *in vitro* constructs

Constructs were fixed in 4% paraformaldehyde, dehydrated in a graded series of ethanol's, embedded in paraffin wax, sectioned at 6 µm and affixed to microscope slides. The sections were stained with alcian blue to assess sGAG content, picrosirius red to assess collagen content and alizarin red to assess calcium content. Collagen types I, II and X deposition were evaluated by immunohistochemical analysis. Briefly, sections were treated first with hyaluronidase and then with pronase (Sigma-Aldrich) in a humidified environment at 37 °C for 25 minutes each to enhance permeability of the extracellular matrix (antigen retrieval step). Sections were incubated with goat serum to block non-specific sites and collagen type I (ab138492, 1:400), collagen type II (sc52658, 1:400) or collagen type X (ab49945, 1:200) primary antibodies (mouse monoclonal, from Abcam - Cambridge, UK and Santa Cruz - Texas, United States) were applied over night at 4 °C. Next, the sections were treated with peroxidase to block endo-peroxidise activity. Next, the secondary antibody (Col I, ab6720 Goat anti-Rabbit IgG, 1:200; Col II, Goat anti-Mouse IgG, B7151, 1:300; Col X, Goat anti-Mouse IgM, ab97228, 1:400) was added for 1 h at room temperature followed by incubation with ABC reagent (Vectastain PK- 400, Vector Labs, Peterborough, UK) for 45 min. Finally, sections were developed with DAB peroxidase (Vector Labs) until

brown staining was observed in the positive controls. Positive and negative controls were included in the immunohistochemistry staining protocol for each batch.

6.2.9 Rat femoral defect implantation

The male Wistar Han rats used for this study were bred in the Comparative Medicine Unit of the Trinity Biomedical Sciences Institute (TBSI). Four groups were implanted: the three previously described experimental *off-the-shelf* constructs, *chondrogenic*, *early hypertrophic* and *late hypertrophic*, and along them, as positive control a bovine collagen type I – nano hydroxyapatite (Col-nHA) scaffold was used. These Col-nHA sponges were fabricated by O'Brien group as previously described [446, 447, 463], and were soak loaded with 5 µg/scaffold of BMP-2 15 minutes prior to implantation, and incubated at RT. From now on, the positive control construct will be denoted as *Col-nHA+BMP-2*. Critically sized femoral defect surgeries were performed on 32 12-week-old rats as previously described [448]. The rats were anesthetised in an induction box using a mix of isoflurane and oxygen, initially at an initial flow rate of isoflurane of 5 litres/min to induce, followed by 2.5 litres/min to maintain anaesthesia. Once anesthetised, the animal was transferred to a heating plate that was preheated to 37°C and preoperative analgesia was provided by subcutaneous injections of meloxicam (1.5 mg/kg). Surgical access to the femur was achieved via an anterolateral longitudinal skin incision and separation of the hind limb muscles, the vastus lateralis, and biceps femoris. The femoral diaphysis was exposed by circumferential elevation of attached muscles, and the periosteum was removed. Before the creation of the defect, a weight-bearing polyether ether ketone (PEEK) internal plate was fixed to the anterolateral femur. Four holes were created in the femur with a surgical drill using the plate as a template. Screws were then inserted into the drill holes in the femur to maintain the fixation plate in position. A 5 mm defect was created using an oscillating surgical saw under constant irrigation with sterile saline solution. Scaffolds were press-fit into the defect. Soft tissue was accurately readapted with absorbable suture material. Closure of the skin wound was achieved using sutures. All animals were administered post-surgery analgesia with subcutaneous injections of buprenorphine (0.05 mg/kg) during recovery and 1.5 mg/kg of meloxicam for first 3 days post-surgery. One defect per animal was created, n = 8 animals for each of the four groups. *In vivo* µCT scans were performed on all the rats at 6 and 12 weeks post-operation (see 6.2.10 section). At 12 weeks rats were sacrificed by CO_2

euthanasia and the left femur, with the intact PEEK plate attached, was harvested for further analysis. One rat from the *late hypertrophic* experimental group had to be culled within a week from the surgery and so excluded from analysis due to complications post-surgery. This animal procedure and study was approved by the ethics commit- tee in Trinity College Dublin and the Health Products Regulatory Authority (HPRA) in Ireland (Approval - AE19136/P087).

6.2.10 Micro-computed tomography (μCT)

In vivo μCT scans were performed on constructs using a Scanco Medical vivaCT 80 system (Scanco Medical, Bassersdorf, Switzer- land). Rats were scanned at 6 and 12 weeks post-surgery to assess bone formation within the defect. Animals were anesthetised using 2–4% (v/v) isoflurane in balanced oxygen throughout the scan. Next, a radiographic scan of the whole lower part of the animal was used to identify and isolate the operated rat femur. The animal's femur was aligned parallel to the scanning axis to simplify the following bone volume assessments. Scans were performed using a voltage of 70 kVp, and a current of 114 μA. A Gaussian filter (sigma = 0.8, sup- port = 1) was used to suppress noise and a global threshold of 210 was applied. A voxel resolution of 35 μm was used throughout. 3D evaluation was carried out on the segmented images to determine the bone volume and to reconstruct a 3D image. Bone volume in the defects was quantified by measuring the total quantity of mineral in the central 135 slices of the defect (approximately 4.75mm). To differentiate regional differences in bone formation, three VOIs were defined. Concentric circles of Ø2 mm, Ø4 mm, and Ø10 mm were aligned with the defect and used to encompass bone formation. The VOIs were aligned using untreated native bone along the femur. The core bone volume was quantified from the inner Ø2 mm VOI (core region). The annular bone volume was quantified by subtracting the Ø2 mm VOI from the Ø4 mm VOI (annulus region). Ectopic bone volume was quantified by subtracting the Ø4 mm VOI from the Ø10 mm VOI (heterotopic region). The bone volume percentages for each region were then calculated by dividing the corresponding bone volume (i.e., bone volume in the annulus) by the total bone volume in the defect. The bone volume was then quantified using scripts provided by Scanco.

6.2.11 Histological analyses for *in vivo* studies

The samples were fixed in 10% formalin overnight and decalcified using 'Decalcifying Solution-Lite' (Sigma) for approximately 1 week. Samples were frequently checked with X-rays to determine if there was any mineral remaining. When no mineral was visible, the sample was considered decalcified. Samples were then dehydrated in graded series of ethanol solutions (70% - 100%), cleared in xylene, and embedded in paraffin wax (all purchased from Sigma-Aldrich). Sections (8 μm) were rehydrated in graded series of ethanol concentrations and stained with goldner's trichrome (groat's iron haematoxylin, fuchsine, orange G, fast green) for visualising bone and vessels infiltration, and 0.2% (w/v) safranin-O to assess sGAG content post-implantation (all from Sigma). Slides were then imaged using an Aperio ScanScope slide scanner and evaluated for vessel infiltration by counting vessels visible across an entire section using Aperio ImageScope and ImageJ software. It should be noted that the PCL forming the frame is cleared during the tissue processing and leaves empty spaces in constructs as a result.

6.2.12 Statistical Analysis

Statistical analysis was performed using GraphPad 9 (GraphPad Software, La Jolla California USA). One-way analysis of variance (ANOVA) with the addition of Turkey's correction was used for multiple comparisons testing. Two-way ANOVA with the addition of Turkey's correction was used for grouped multiple comparisons testing. Results are expressed as mean ± standard deviation. For all comparisons, significance was accepted at a level of $p < 0.05$. Sample size (n) is indicated within the corresponding figure legends.

6.3 Results

6.3.1 Realisation of 3D bioprinted PCL reinforced *off-the-shelf* cartilaginous templates

This thesis previously demonstrated how to 3D bioprint developmentally inspired engineered cartilaginous templates that are able to recapitulate the process of endochondral ossification upon implantation *in vivo*. It was possible to both mechanically reinforce the engineered tissues and modify their architecture to support nutrient transport *in vitro* and

vascularisation *in vivo*. These 3D bioprinted grafts were shown to support the regeneration of critically sized bone defects in rats. Here the same biofabrication techniques were used to 3D bioprint such constructs that were then cultured using three different priming regimes to obtain different phenotypes (*chondrogenic*, *early hypertrophic* and *late hypertrophic*; Fig. 6.1A). In order to obtain *off-the-shelf* grafts, these constructs were decellularised and subsequently freeze-dried. Four different decellularisation protocols were investigated in this study, inspired by the most commonly used decellularisation processes for cell-derived ECM found in the literature (Fig. 6.1B). The protocols were selected to be in ascending order of perceived harshness (from "A" to "D"), which all received a final treatment step with DNase. A head-to-head comparison between the two most commonly used DNase concentrations (10 vs 100 U/ml) was carried out on *chondrogenic* and *late hypertrophic* constructs to investigate how they were affecting biochemical properties of the grafts (Fig. 6.2). Using 100 U/ml DNase significantly reduced the remaining DNA value post-decellularisation, while sGAG, collagen and calcium contents were not significantly affected by the higher DNase concentration. For this reason 100 U/ml DNase was chosen for all decellularisation processes. The four protocols were tested on *Chondrogenic* constructs and biochemical analyses were carried out pre-decellularisation (post-printing "D0" and post-priming "D35") and post-decellularisation (protocols "A" to "D") to study how the decellularisation processes were influencing construct properties (Fig. 6.1C). The DNA content post decellularisation significantly dropped for all the protocols compared to the value pre-decellularisation (D35). Moreover, the harsher the protocol, the lower the final DNA content, with protocols C and D resulting in a significantly lower DNA value compared to protocol A. For all the protocols, sGAG and collagen contents diminished, but not significantly compared to pre-decellularisation (D35) values. As the goal was to reduce the DNA content of the grafts whilst simultaneously maintaining both sGAG and collagen levels, protocol C was selected as the preferred decellularisation protocol. The final *off-the-shelf* grafts were imaged both macroscopically (Fig. 6.1E) and with SEM (Fig. 6.1F). From all the images it is possible to see how the central micro-channel remained patent and how the freeze-dried engineered ECM is present throughout the construct and it is well connected to the PCL frame.

Protocol C was next applied to the three different engineered construct phenotypes (Fig. 6.3). The DNA content in all the three groups significantly dropped after decellularisation (Fig. 6.3A), while sGAG (Fig. 6.3B) and collagen (Fig. 6.3C) values for

each group remained comparable between pre- (D35) and post-decellularisation. There was no significant difference between the DNA, sGAG and collagen contents of the three different decellularised grafts. In contrast, calcium content in the *late hypertrophic* groups was significantly higher than the other two groups both pre- and post-decellularisation, with comparable levels observed in the *chondrogenic* and *early hypertrophic* groups (Fig. 6.3D). Finally, the decellularisation protocol significantly lowered the calcium content in the *late hypertrophic* constructs. These results were confirmed by histological analyses, which showed abundant and homogeneous sGAG and collagen deposition in all groups, with strong positive staining for calcium only observed in the *late hypertrophic* group (Fig. 6.3E). In addition, a visible reduction in sGAG (less strong positive alcian Blue staining) and calcium content (significantly less alizarin red positive area) was observed histologically when comparing pre- to post-decellularisation constructs. All groups stained strongly for collagen type II, with positive staining for collagen type I (with some non-specific staining) also observed. Constructs stained weakly for collagen type X (Fig. 6.3F). The intensity of staining for collagen type II diminished after decellularisation (immunohistochemical controls for all staining are shown in Fig 6.6).

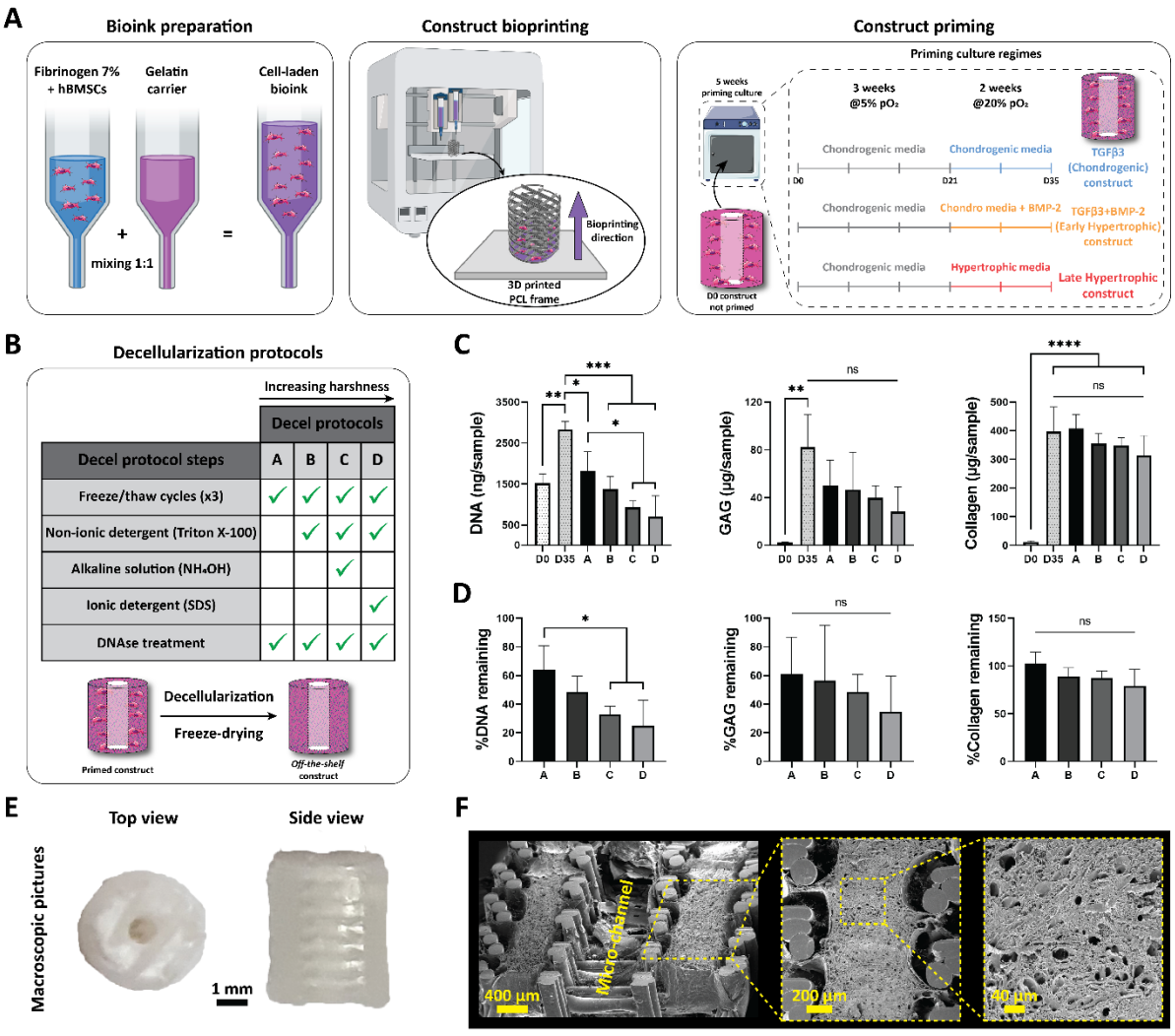

Figure 6.1: *Off-the-shelf* 3D bioprinted PCL reinforced engineered cartilaginous templates fabrication. (A) 3D bioprinted PCL reinforced cartilaginous templates realisation; (B) Schematic of the different decellularisation protocols investigated and their steps; (C) DNA, sGAG and collagen total content for *chondrogenic* constructs pre- and post-decellularisation; (D) percentages of remaining DNA, sGAG and collagen after the decellularisation (referred to D35 mean values), *p<0.05, **p<0.01, ***p<0.001, ****p<0.0001; (E) macroscopic pictures of the *off-the-shelf* grafts after decellularisation and freeze-drying; (F) SEM images of the *off-the-shelf* grafts at 30×, 50× and 200×.

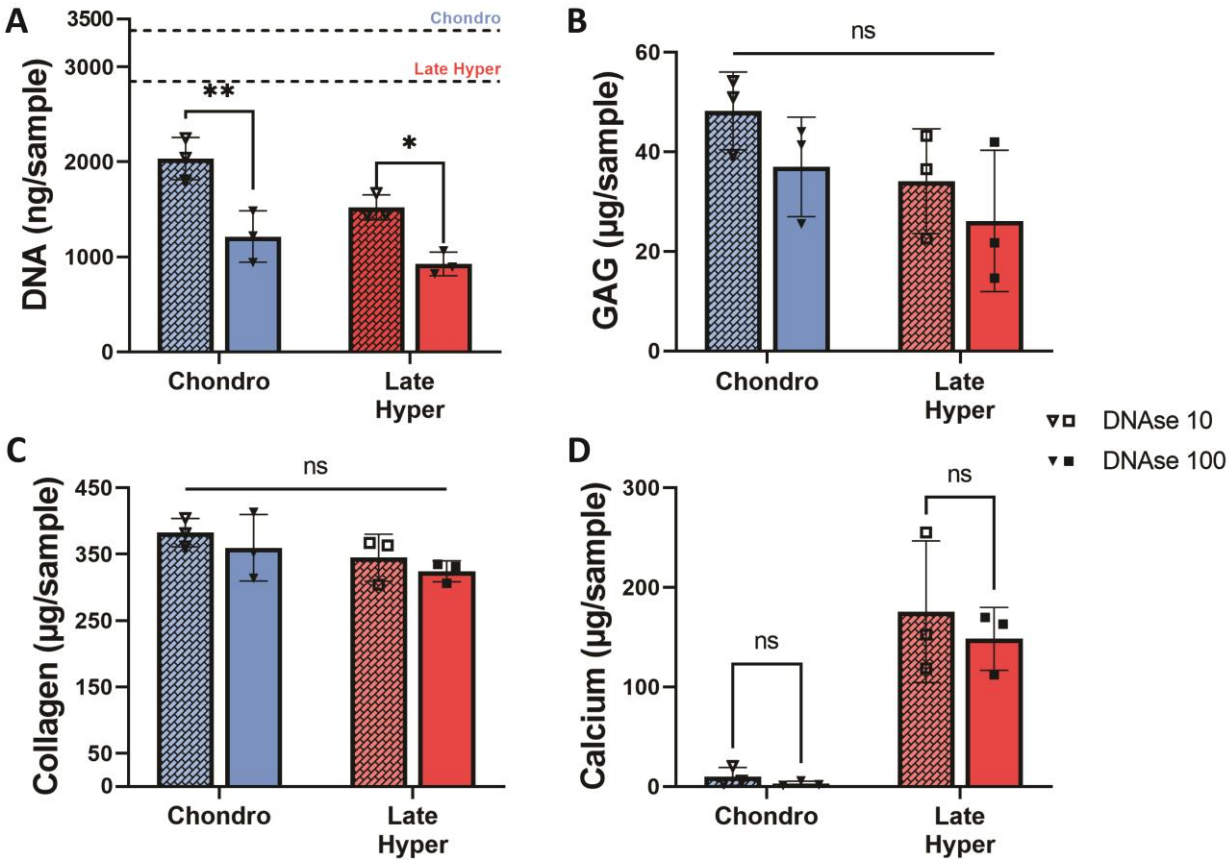

Figure 6.2: DNase concentration comparison for last step of decellularisation protocol. . (A) DNA total content for *chondrogenic* and *late hypertrophic* constructs after decellularisation using DNase 10 or 100 U/ml (dotted lines represent DNA values at D35 pre-decellularisation for *chondrogenic* (3382 ng/sample) and *late hypertrophic* (2848 ng/sample) constructs as indicated); (B) sGAG content; (C) collagen content; (D) calcium content. n = 3 samples per group; *p<0.05, **p<0.01.

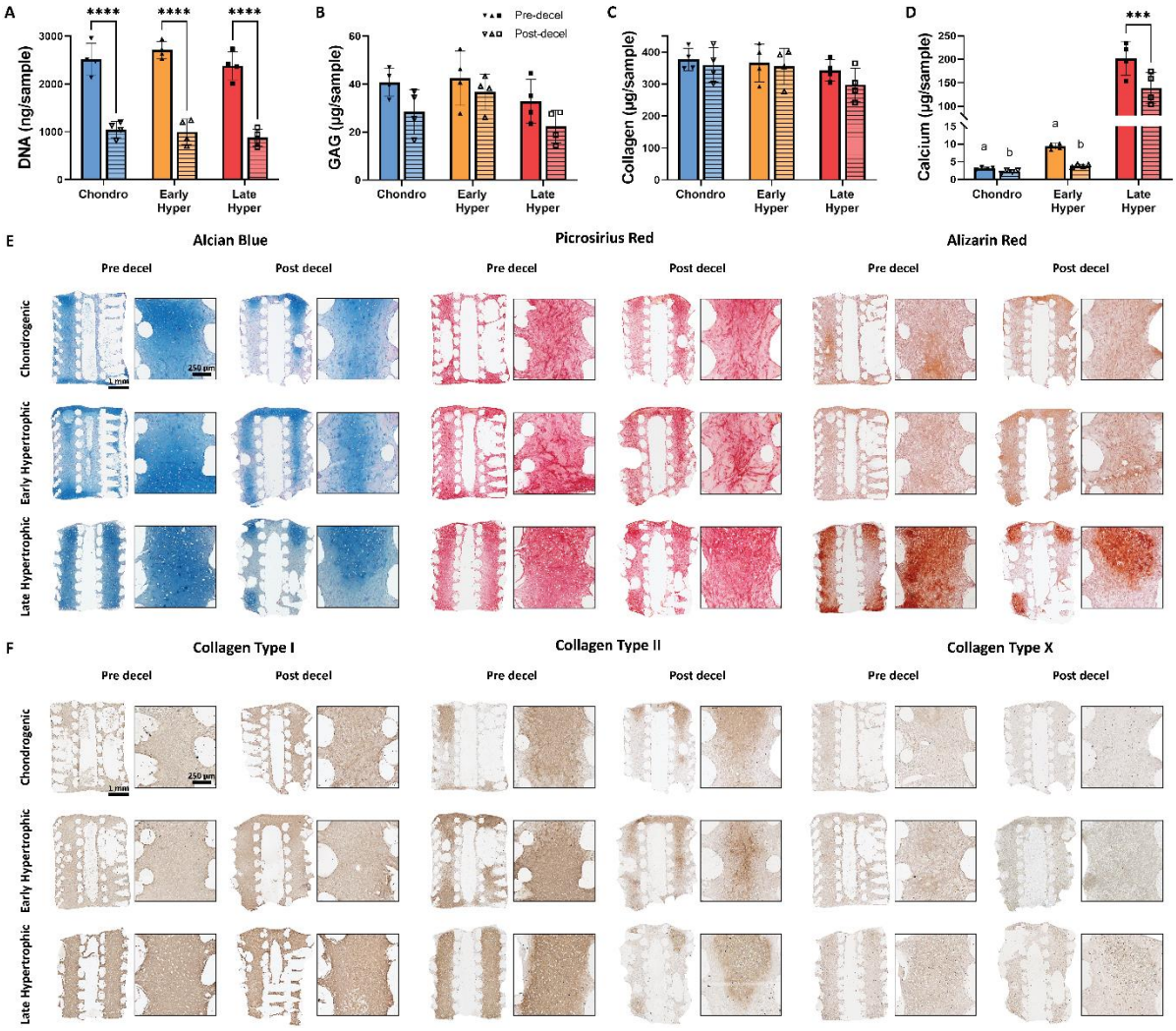

Figure 6.3: 3D bioprinted PCL reinforced engineered cartilaginous templates characterisation pre- and post-decellularisation. (A) DNA, (B) sGAG; (C) collagen and (D) calcium total content for *chondrogenic*, *early hypertrophic* and *late hypertrophic* constructs pre- and post-decellularisation, $n = 4$ samples per group; ***p<0.001, ****p<0.0001, "a" significantly different compared to *late hypertrophic* pre-decel with p<0.0001, "b" significantly different compared to *late hypertrophic* post-decel with p<0.0001; (E) histological analyses with alcian blue, picrosirius red and alizarin red staining, and (F) immunohistochemical analyses with collagen type I, II and X staining. Positive and negative controls for immunohistochemical analyses are presented in Fig. 6.6.

6.3.2 *In vitro* assessment of engineered grafts osteogenic potential

This thesis next sough to assess the *in vitro* osteogenic potential of the three different decellularised grafts. To this end, the decellularised *off-the-shelf* grafts (printed, engineered *in vitro*, decellularised and freeze-dried) were reseeded with hMSCs and cultured for 3 weeks in either expansion media (XPAN) or minimal osteogenic media (mOSM). In a pilot

study, control grafts were first produced by printing and then freeze-drying cell-free bioinks in the same way as the cellular constructs (herein called *Fibrin Alone*). Calcium quantification after the 3 weeks of culture demonstrated the necessity of mOSM to trigger proper mineralisation, and that the *chondrogenic* ECM based grafts supported superior osteogenesis of hMSCs (Fig. 6.4A). Alizarin red staining confirmed that only the decellularised engineered grafts support calcium deposition, while picrosirius red staining demonstrated abundant and homogenous collagen deposition (Fig. 6.4B).

Based on this pilot study, all subsequent assessments of the osteogenic potential of the different decellularised grafts were undertaken using mOSM for 3 weeks at 20% pO_2 (Fig. 6.5A). After 21 days of culture, significantly lower levels of calcium accumulation were observed in the *chondrogenic* grafts, with the higher levels of calcium content observed in the *late hypertrophic* constructs (Fig. 6.3B). Compared to their respective values at Day 0 (D0), both the *early* and *late hypertrophic* constructs supported similar increases in calcium deposition (Fig. 6.5C). The fold increase in calcium content between D0 and D21 was also assessed (Fig. 6.5D). The *early hypertrophic* constructs supported a 20-fold increase in calcium accumulation, with much smaller fold-changes observed in both the *chondrogenic* and *late hypertrophic* constructs (2.3 and 1.7 fold increase respectively) (Fig. 6.5D). Similar results were observed histologically, with little alizarin red positive staining observed in the *chondrogenic* constructs, positive staining observed in the *early hypertrophic* constructs and more intense staining observed in the *late hypertrophic* group. Picrosirius red staining was comparable among the different groups (Fig. 6.5E). Some positive staining for collagen type X was observed in both the *early* and *late hypertrophic* constructs (Fig. 6.6) (immunohistochemical controls for all staining are also shown).

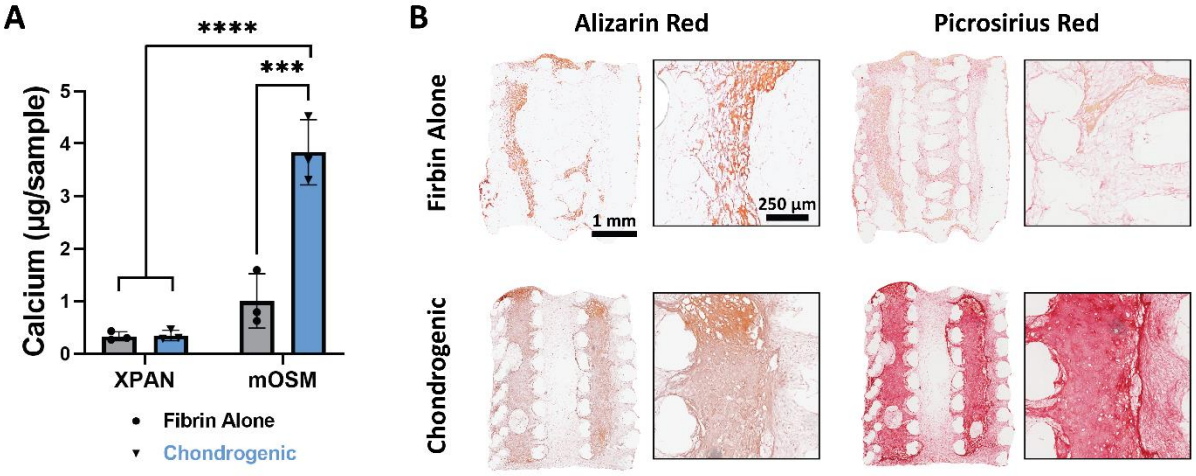

Figure 6.4: *In vitro* pilot on the assessment of engineered grafts osteogenic potential. (A) Calcium content for *chondrogenic* and *Fibrin Alone* control group after 3 weeks of reseeded construct culture in either XPAN or mOSM; ***p<0.001, ****p<0.0001; (B) histological analyses with alizarin red and picrosirius red staining for *chondrogenic* and *Fibrin Alone* group after 3 weeks of reseeded construct culture in mOSM

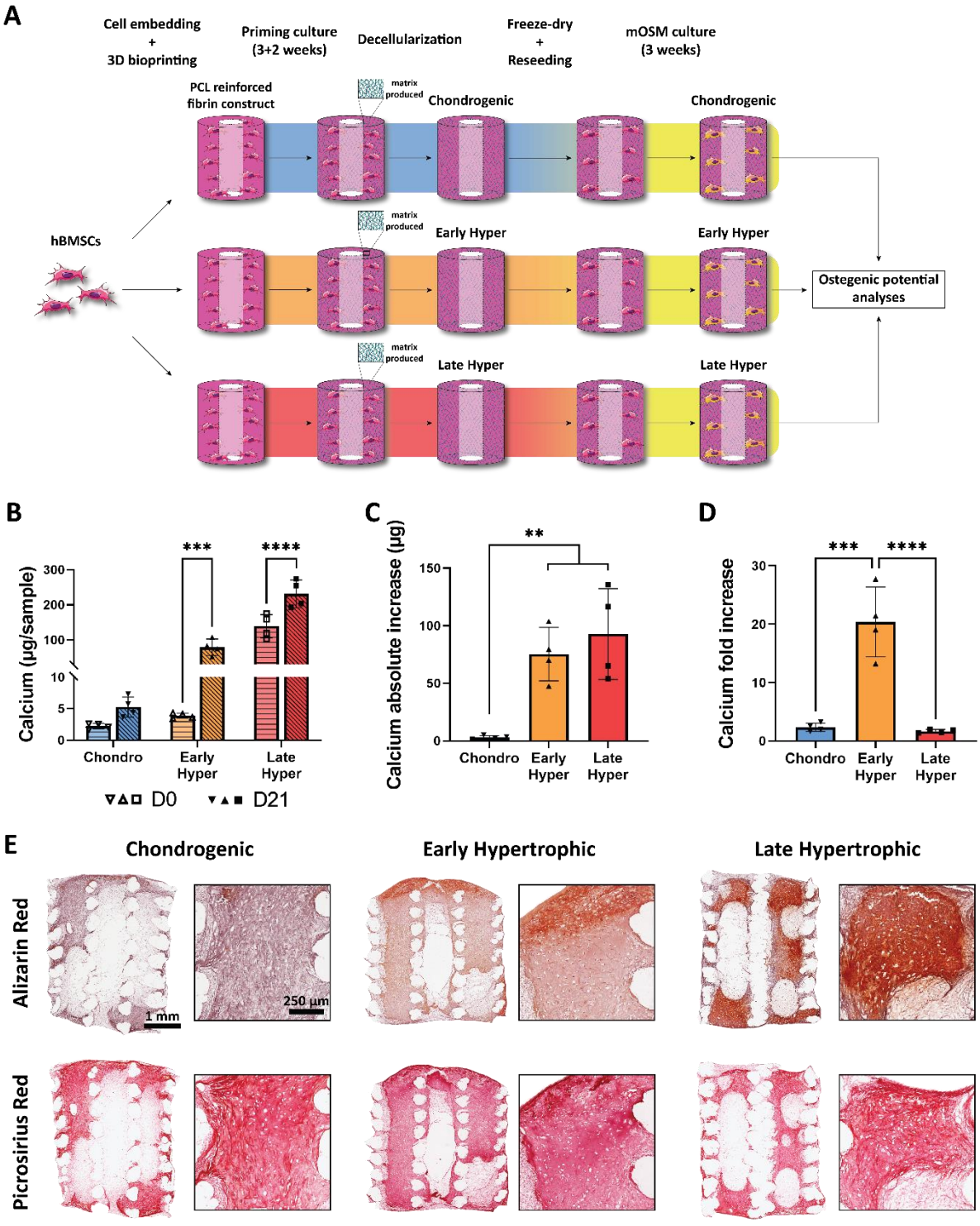

Figure 6.5: *In vitro* assessment of engineered grafts osteogenic potential. (A) Assessment schematic; (B) calcium content for each graft phenotype post-decellularisation (D0) and at the end of the minimal osteogenic culture (D21); (C) calcium absolute increase between D0 and D21; (D) calcium fold increase between D0 and D21; *n* = 4 samples per group; **p<0.01, ***p<0.001, ****p<0.0001; (E) histological analyses with picrosirius red and alizarin red staining.

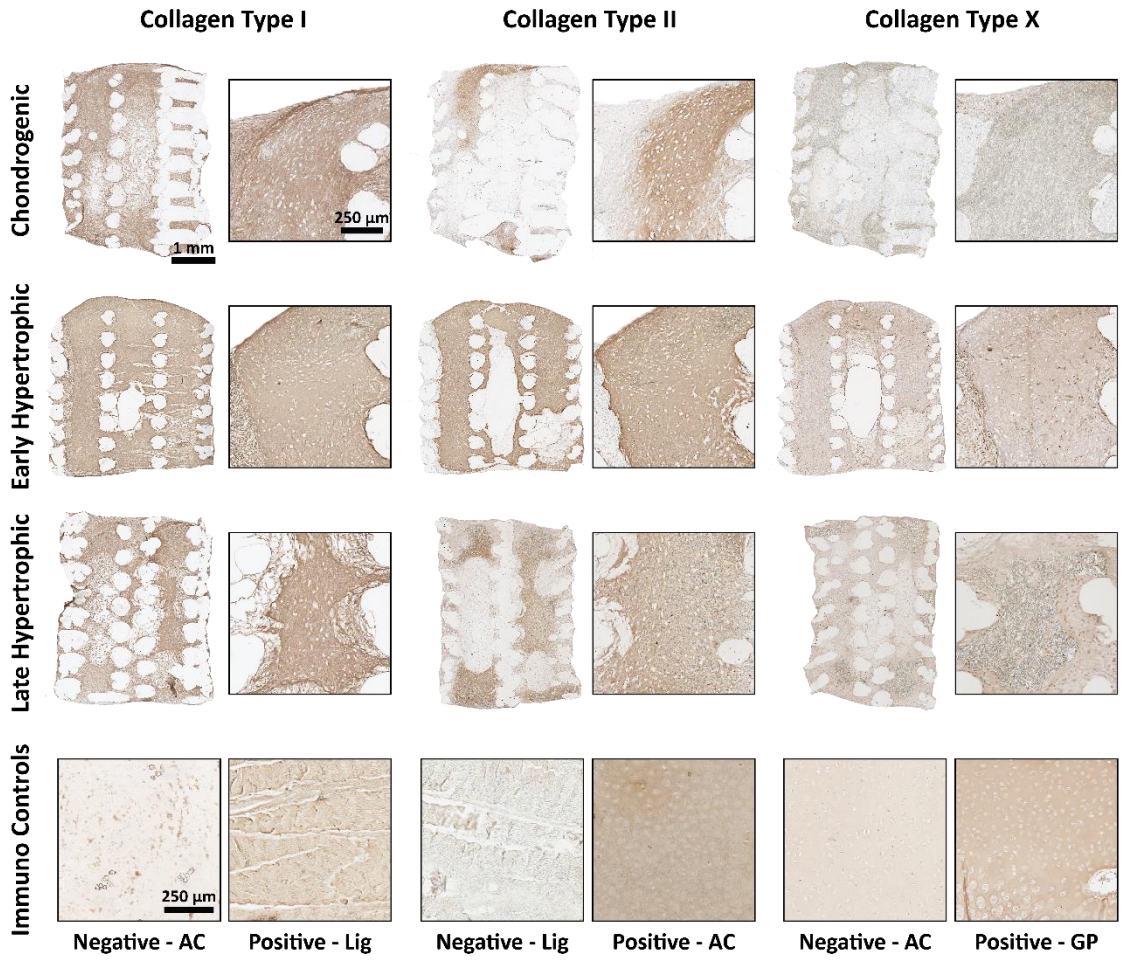

Figure 6.6: *In vitro* assessment of engineered grafts osteogenic potential. Immunohistochemical analyses with collagen type I, II and X staining for all the three experimental grafts. Positive and negative controls for immunohistochemical analyses are presented. Acronym legend: articular cartilage (AC), ligament (Lig) and growth plate (GP).

6.3.3 Decellularised 3D bioprinted cartilaginous constructs as *off-the-shelf* grafts for large bone defect healing

We next sought to assess whether the 3D bioprinted cartilaginous templates, that were decellularised prior to implantation, would accelerate bone regeneration within critically sized femoral defects. To this end, decellularised *chondrogenic*, *early hypertrophic* and *late hypertrophic* grafts were prepared and implanted in a 5-mm rat femoral defect (Fig. 6.7A) and compared to a positive control, which consisted of a bovine collagen type I – nano hydroxyapatite scaffold, soak loaded with 5 µg/scaffold of BMP-2 15 minutes prior to implantation. Micro-CT analysis of animals at 12 weeks post-implantation was carried out

to visualise and quantify bone formation within the defects (Fig. 6.7B). Compared to the experimental groups, significantly higher amounts of new bone formation was observed in the positive control *Col-nHA+BMP-2* group; however visually from the 3D reconstructions, it could be seen how the positive control group was characterised by uncontrolled growth and heterotopic bone formation. To assess the levels of heterotopic bone and the location of new bone formation in all groups, region of interest (ROI) bone volume analysis was performed. The defect volume was divided into three regions: core, annulus, and heterotopic regions (Fig. 6.7E); the total bone volume for each animal was quantified in these regions (Fig. 6.7C). Although the positive control group deposited significantly more new bone than the experimental groups in the annulus region, where natively the bone is present, it was also characterised by very high levels of heterotopic bone. The highest levels of new bone formation were observed in the heterotopic regions (48% of total bone), pointing to uncontrolled growth and abnormal bone formation. In contrast, all of the experimental groups preferentially support new bone formation in the annular region of the defect, with significantly higher percentages of new bone deposited there compared to the positive control (76%, 85.5% and 86% of total bone for *chondrogenic*, *early hypertrophic* and *late hypertrophic* group respectively) (Fig. 6.7D). Among the experimental groups, the *early hypertrophic* constructs supported the highest levels (although not significant) of total new bone and new bone in the annulus region.

We next sought to assess the nature of new bone tissue being formed and vessel infiltration using histological staining (Fig. 6.8A). Goldner's trichrome staining showed positive staining for new bone and vessel infiltration in all four groups 12 weeks after implantation, with extensive bone marrow regions observed in the positive control group. While *Col-nHA+BMP-2* constructs were characterised by new bone formation within the defect area and beyond (heterotopic bone), the experimental groups supported new bone almost exclusively at the bone ends; this is in accordance with what was visualised with the micro-CT 3D reconstructions. Vessel counting demonstrated that all experimental group supported significantly more blood vessel invasion compared to *Col-nHA+BMP-2* group (Fig. 6.8B). Finally, safranin-O staining revealed that the cartilaginous templates were completed remodelled over 12 weeks *in vivo* since there was no trace of residual cartilage within the defect region (Fig. 6.9).

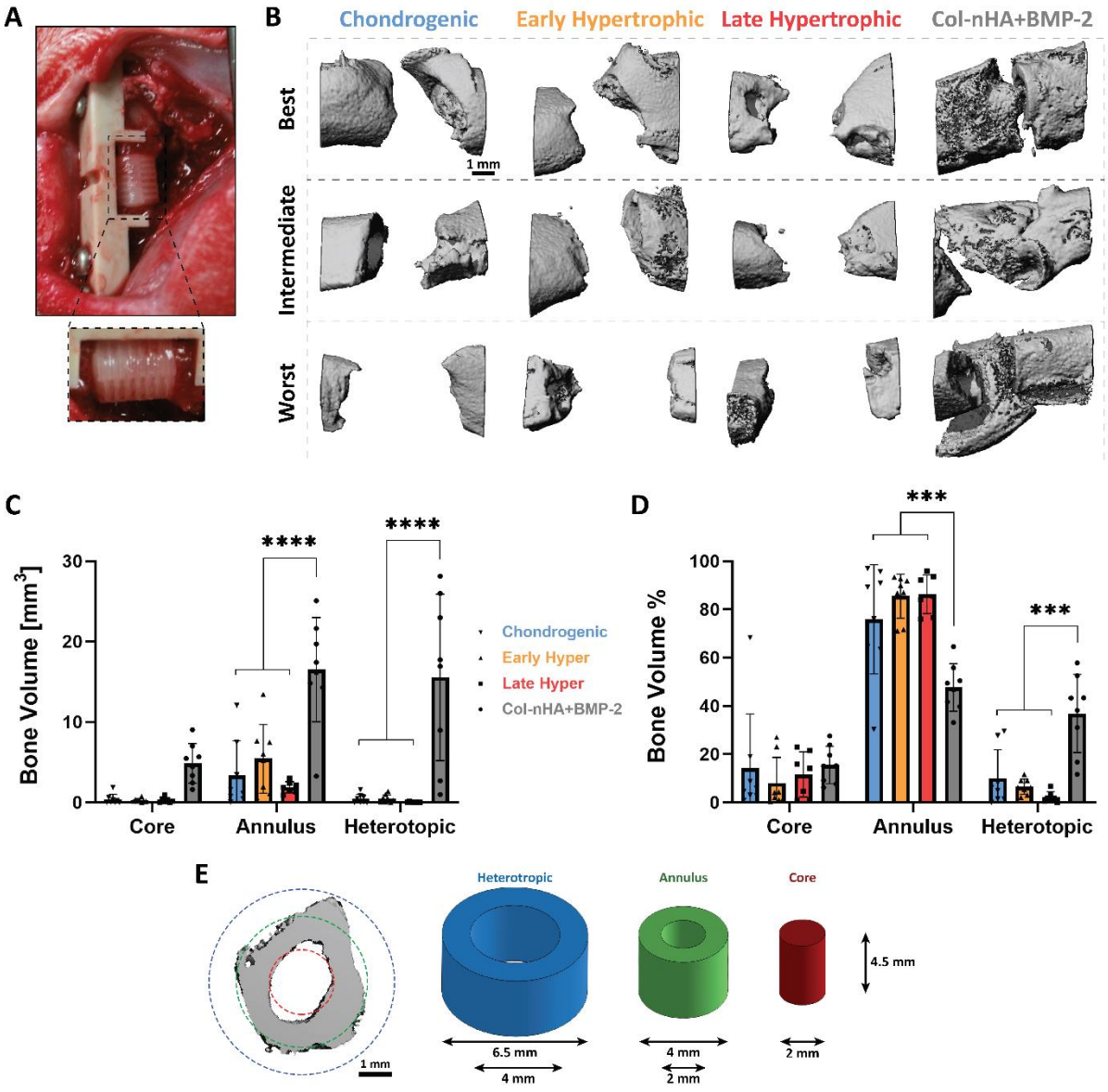

Figure 6.7: Critically sized femoral defect implantation. *In vivo* micro-CT analysis. (A) Picture highlighting surgical implantation; (B) reconstructed *in vivo* micro-CT images of bone formation in the defects at post-operative week 12; (C) regional quantification of total bone volume (mm^3) in the defects; (D) percentage of new bone in each region related to total new bone; (E) outline of ROI bone volume analysis including definitions of core, annulus, and heterotopic regions. n = 8 animals per group except for *late hypertrophic* group having n = 7 animals; ***p<0.001, ****p<0.0001.

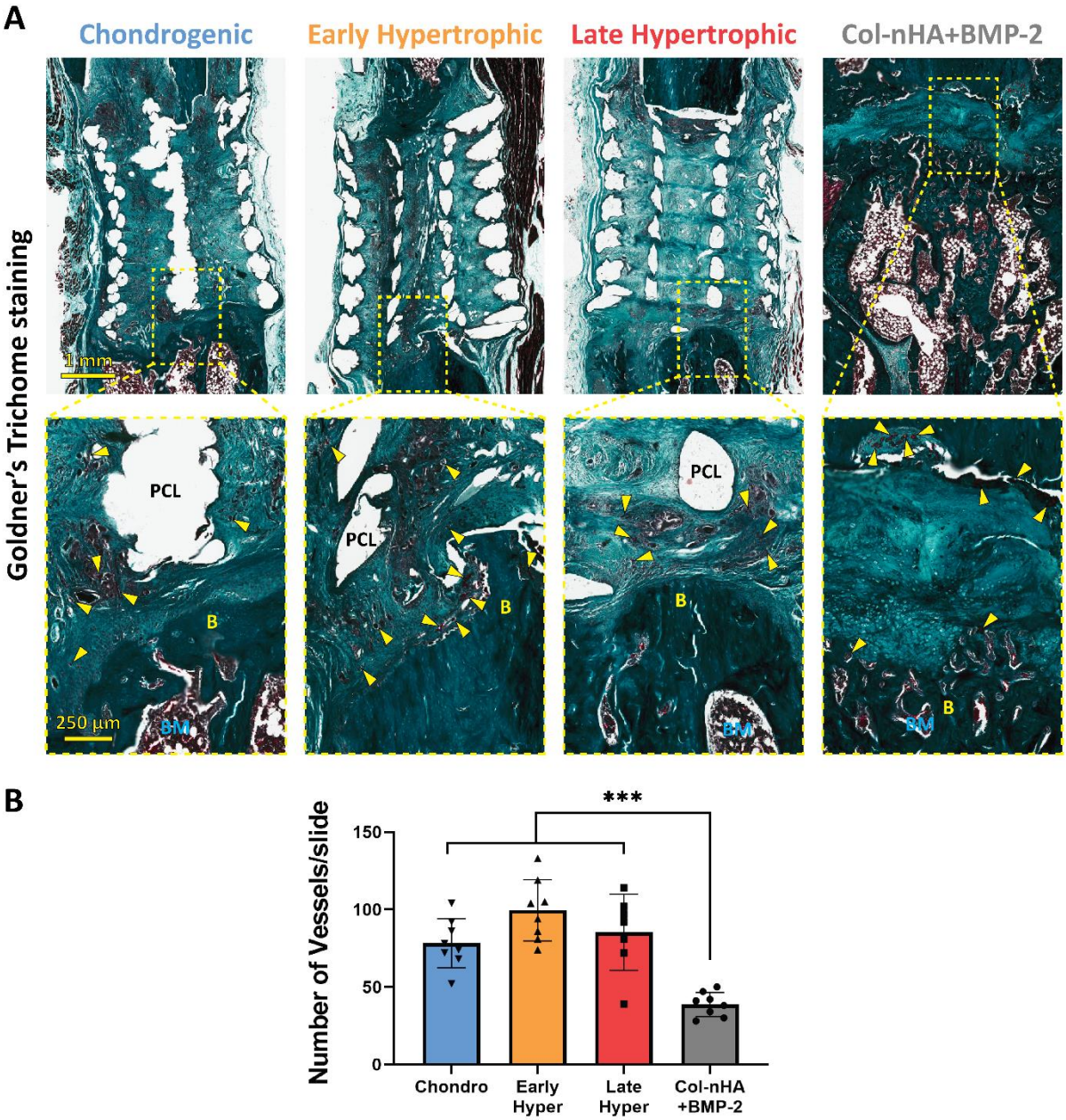

Figure 6.8: Critically sized femoral defect implantation. Histological analysis. (A) Goldner's trichrome stained sections for all groups after 12 weeks *in vivo*. Images were taken at 1× and 4×. Arrows denote vessels, B denotes positive bone tissue, BM denotes bone marrow and PCL denotes areas where the PCL frame was; (B) vessel number per slide. n = 8 animals per group except for *late hypertrophic* group having n = 7 animals, n = 4 slices per construct for quantifications; ***p<0.001.

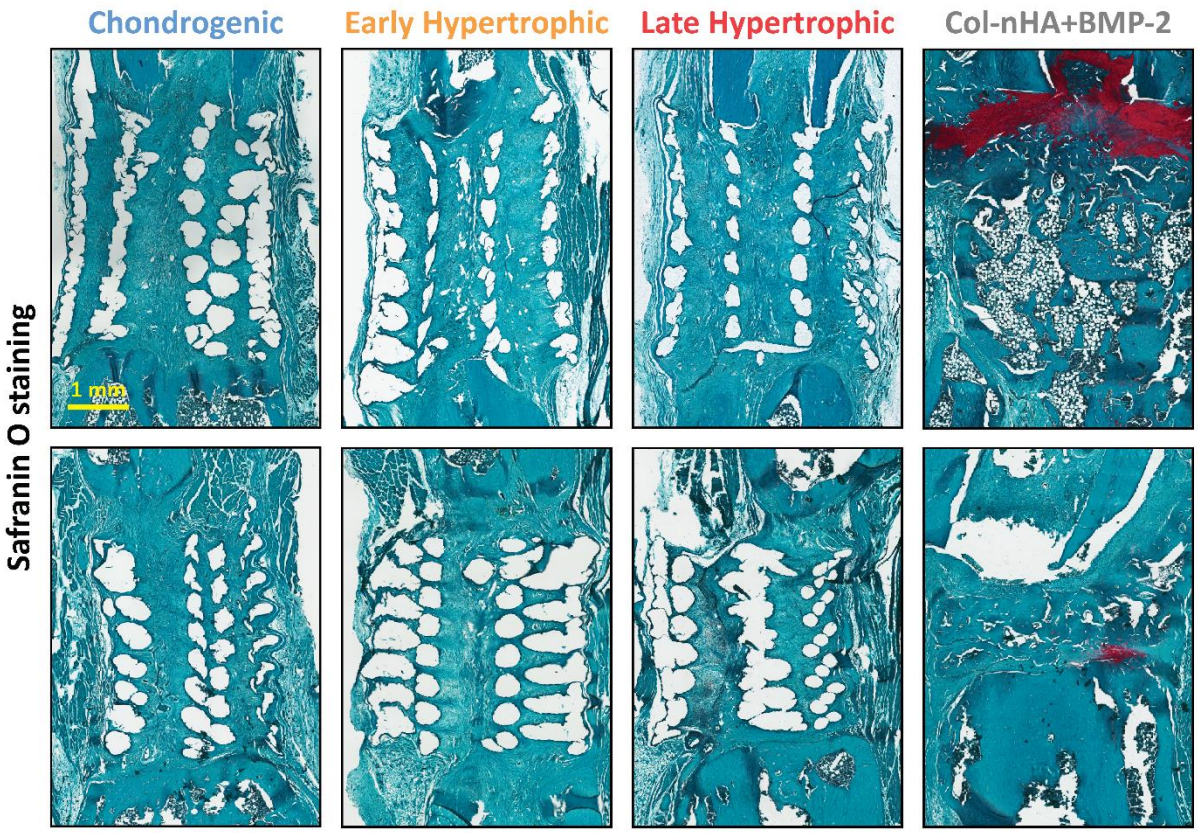

Figure 6.9: Critically sized femoral defect implantation. Histological analysis. Safranin-O stained sections for all groups after 12 weeks *in vivo*. Images were taken at 1×. Two representative animals per group are presented.

6.4 Discussion

This chapter of the thesis sought to develop *off-the-shelf* grafts for large bone defect healing by decellularising PCL reinforced cartilaginous tissues produced by 3D bioprinting. We sought to produce such decellularised *off-the-shelf* implants because they are not hampered by the logistical and regulatory challenges associated with live and viable TE grafts, so they represent a product that can be easier to directly translate into the clinic and to commercialise. A notable example of an *off-the-shelf* product derived from *in vitro* engineered ECM is the Humacyte© vascular graft, which is currently in clinical use [28, 29]. The relative success of this concept suggests that it could be applied to other clinical targets such as large bone defect healing. The *off-the-shelf* grafts developed in this chapter were developed based on the vital engineered constructs in chapter 5 of the thesis. The bioprinted constructs were primed using three different culture regimes to produce different

final phenotypes. Four different decellularisation protocols were investigated in order to produce off-the-shelf grafts from these engineered constructs. It was found that by increasing the harshness of the protocol used, the remaining DNA reduced, but so did the residual sGAG and collagen content. Based on this analysis, a protocol that significantly lowered the DNA content, whilst not significantly affecting other biochemical properties, was selected as the preferred decellularisation protocol. The resulting decellularised and freeze-dried ECMs were then assessed for their osteogenic potential *in vitro*, with the *early hypertrophic* group supporting the highest fold-increase in calcium accumulation (almost 10 times higher than the *chondrogenic* and *late hypertrophic* groups). After implantation into critically sized rat femoral defects, the engineered cartilaginous templates slowly started to be replaced by new bone at the interfaces with native bone ends. Although the overall value of total new bone in the positive control group was significantly higher than the experimental groups, this growth was shown to be uncontrolled, presenting significantly high values of abnormal and heterotopic bone. On the other hand, in all the engineered constructs, at least 75% of the new bone was present in the annulus region, where bone is natively found.

A decellularisation protocol incorporating three cycles of freeze-thawing, a treatment with a solution of 0.5% Triton X-100 and 20 mM NH_4OH, and a final treatment with 100 U/ml DNase was found to significantly drop the DNA content without significantly affecting the sGAG and collagen values post-decellularisation. This protocol was chosen among four different protocols, which we designed based on common decellularisation protocols/steps reported in literature for engineered ECM in bone TE applications. Overall, the biochemical results after each protocol matched our expectations: the harsher the method used, the less DNA was left at the end, but also the higher the loss in sGAG and collagen. For our work, we selected the second harshest protocol (referred as "C"), which combines freeze-thaw cycles, a solution of 0.5% Triton X-100 and 20 mM NH_4OH, and a final treatment with 100 U/ml DNase, because the quantity of DNA remaining after the decellularisation was significantly lower than the one of the blandest protocol (referred as "A"), without significant changes in the sGAG and collagen contents. To the best of our knowledge, it is the first time that this specific combination was used in literature, although there is a number of studies on engineered ECM for bone TE with very similar protocols, with some slight changes in the steps involved and/or in the treatment time and temperature used in each step. For example, the combination 0.5% Triton X-100 and 20 mM NH_4OH was already used as the only decellularisation step [246, 261, 273] or followed by a 100 U/ml

DNase treatment for 1 h at 37°C [240, 252], as we did in our protocol "C". The variety in protocols in the literature point to a very important limitation/problem related to the development of such *off-the-shelf* constructs, which is the lack of standardised decellularisation methods [464]. Such methods would serve as standard controls for comparative purposes [465], which would be useful not only for the assessment of commercially available products, but also to perform more efficient, comparable, and reliable experimental research studies [466]. Focusing again on this study, post-decellularisation the DNA, sGAG and collagen content of all three constructs was comparable, with only the calcium content found to be significantly higher in the *late hypertrophic* group. Furthermore, although decellularisation significantly reduced the DNA content of all groups, the only other statistically significant change after decellularisation was to the calcium content of the *late hypertrophic* constructs. These results suggest that the decellularisation protocol applied was not too detrimental on the main components of the engineered ECM.To assess the osteogenic potential of the *off-the-shelf* grafts *in vitro*, they were reseeded with hMSCs and cultured for 3 weeks at 20% pO_2 in mOSM. Pilot studies demonstrated that XPAN media was not sufficient to support osteogenesis of the reseeded hMSCs. The supplement concentrations used in the mOSM represent minimal levels for the support of osteogenesis [467, 468], and they proved to be adequate in our study. Full OSM was not used because we wanted to trigger hMSCs osteogenesis based on the inherent properties of the engineered matrices and their effects on the reseeded cells. Both *early* and *late hypertrophic* group significantly increased their calcium content between D0 and D21, depositing comparable values of absolute new calcium during the 3 weeks of osteogenic culture. Although at D21 *late hypertrophic* constructs were characterised by significantly higher calcium content, *early hypertrophic* constructs interestingly presented a 20-fold increase in calcium accumulation. These studies demonstrated the high osteogenic potential of the *early hypertrophic* constructs. Although the *chondrogenic* and *early hypertrophic* constructs possessed similar bulk biochemical properties, the *early hypertrophic* constructs supported dramatically higher levels of calcium deposition. It is hypothesised that this could be due to a number of factors. First of all, there may be residual BMP-2 retained from the priming culture in the engineered matrix post-decellularisation; BMP-2 is a well known potent osteoinductive cytokine and is currently the most commonly used protein-based bone graft substitute [458]. Therefore, if some BMP-2 remained trapped in the construct matrix after decellularisation, it could have provided the observed osteoinductive properties. A second potential reason could be more subtle differences in the composition of the different

decellularised ECMs due to the addition of BMP-2 in the *early hypertrophic* priming protocol, which provides a more osteoinductive environment compared to a more cartilaginous template. The addition of BMP-2 to hMSCs undergoing chondrogenesis has been shown to not only increase the expression of chondrogenic markers such as ACAN, SOX9 and COL2A1, but also increases in early hypertrophic phenotype such as COL10A1[452, 453] and PTHrP [452], both factors involved in cartilage hypertrophy and endochondral bone formation [454, 469]. Finally, a fundamental role in the osteogenic capacity of the *early hypertrophic* group could be played by possible specific extracellular vesicles (EVs) retained by the ECM after decellularisation. EVs are small nanoparticles produced by all mammal cells that are released into the microenvironment surrounding the cells and are present in most of the tissue fluids [470]. In the last decade they have been identified as major players in cell-cell communication and recently have been demonstrated to fulfil a role of paramount importance on conveying biological signals, participating in regenerative processes [471]. It has been already shown in an *in vivo* rabbit mandibular bone defect model synergic effects of decellularised bone matrix, hydroxyapatite, and extracellular vesicles on bone regeneration [472]. Future detailed analyses on our engineered templates gene expression and composition could be helpful to better explain the interesting osteoinductive capacity of *early hypertrophic* grafts.

After 12 weeks post-implantation, BMP-2 loaded collagen-nHA sponges supported higher levels of new bone formation that the experimental decellularised grafts, bridging the defect in 3 animals out of 8 (none of the experimental constructs bridged the defect). However, only half of this new bone was deposited in the annulus region (48% of the total) where natively the bone is found, with *Col-nHA+BMP-2* supporting high levels of heterotopic bone formation (37% of total bone, significantly higher than the experimental groups). These results demonstrate that, even if we used a much lower dose of BMP-2 than that used clinically and in some other pre-clinical rat femoral studies (5 µg/construct falls in the low end of the spectrum of the literature dosages), bone growth in the positive control group happened in an uncontrolled way with the formation of significant quantity of abnormal bone. This adverse outcome as a consequence of the use *in vivo* of BMP-2 is a well documented concern with this growth factor clinically [145, 457, 473]. BMP-based therapies have been studied and used for the last five decades in the field of bone tissue engineering, and although BMP-2 showed initial success in pre-clinical studies and in human trials, these strategies have been called for a review on their safety profile and

application in the clinic. In fact, with increasing use of BMP-2 in the clinic, a growing and well-documented side effect profile has emerged, including postoperative inflammation and associated adverse effects, ectopic bone formation, osteoclast-mediated bone resorption, and inappropriate adipogenesis [458]. This brought the FDA to issue a warning of the potential life-threatening complications of BMP-2 [474]. For this reason, there is clearly a need to find alternative approaches in which the presence of such potent growth factors are more controlled, both in their quantities and delivery rates. An example of alternative approaches are the developmentally inspired ones aiming to recapitulate EO. These approaches are usually based on the use of engineered templates and ECMs instead of the delivery of individual growth factors, representing a solution able to mimic closer what is happening naturally, in our case during bone formation and healing. However, a lot of more work is needed to optimize these new strategies to make them comparable in terms of osteoinductive potential of BMP-based strategies; in this study the decellularised grafts osteoinductivity proved to be clearly inferior compared to the *Col-nHA+BMP-2* sponges as it can be seen in the micro-CT analyses at 12 weeks post-implantation.

We suggest that the significant difference in the new bone formation content between the positive control and the experimental groups was strongly influenced by the decellularisation process of the *off-the-shelf* grafts, which we believe diminished their osteoinductive capacity *in vivo*. This hypothesis is visually supported by the comparison of the micro-CT 3D reconstructed images at 12 weeks between the *off-the-shelf* grafts and the vital versions of the *chondrogenic* and *early hypertrophic* groups from the previous chapter (Fig 6.10).

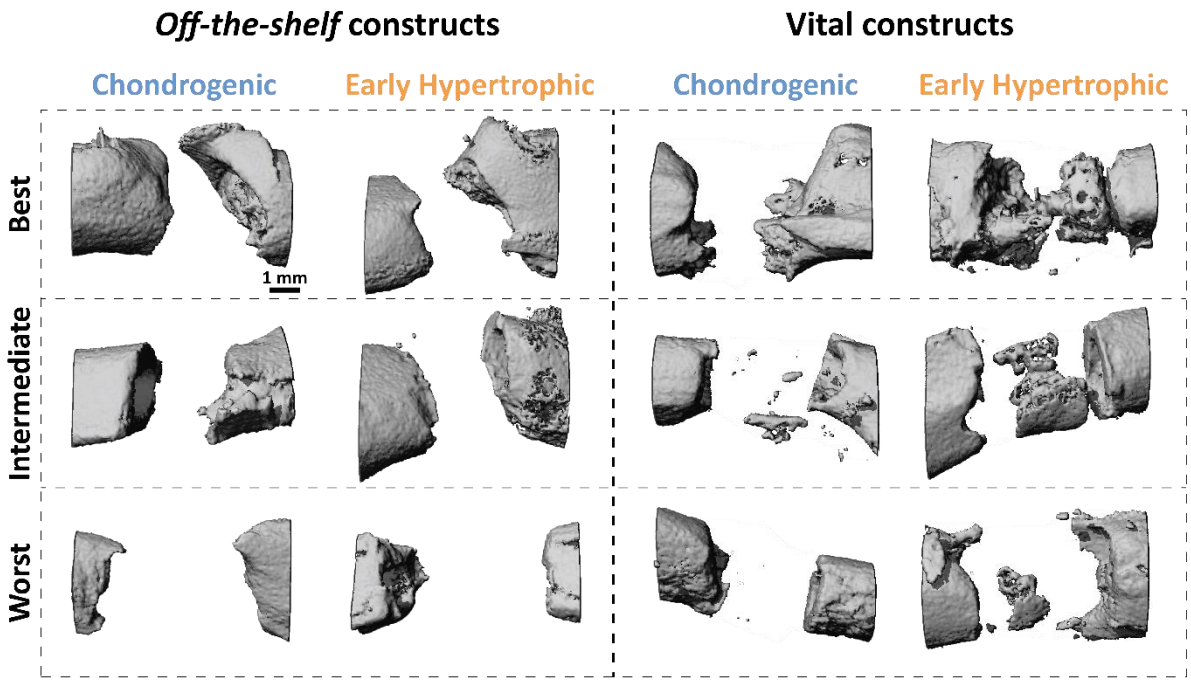

Figure 6.10: Comparison between vital and *off-the-shelf* templates. *In vivo* micro-CT analysis. Reconstructed *in vivo* micro-CT images of bone formation at post-operative week 12 for vital and decellularised *chondrogenic* and *early hypertrophic* constructs.

It is well recognised that cells play a fundamental role during bone formation and regeneration, secreting essential bioactive molecules and exerting paracrine effects, regulating the behaviour of other cells in the host tissues. It has been demonstrated that MSCs are able to stimulate angiogenesis *in vitro* and *in vivo* by releasing in the extracellular space a number of angiogenic factors including basic fibroblast growth factor (bFGF), vascular endothelial growth factor (VEGF), platelet-derived growth factor (PDGF), angiopoietin 1 (ANG-1), placental growth factor (PIGF), IL-6, hepatocyte growth factor (HGF), and monocyte chemoattractant protein 1 (MCP-1) [475-477]. In addition to stimulate angiogenesis, MSCs have been proven to have important immunomodulatory effects exerted by direct cell-to-cell contacts, secretion of cytokines and/or by a combination of both mechanisms [478], significantly suppressing the macrophages production of inflammatory cytokines, including TNF-α, IL-6, IL-12p70, and IFN-γ, while increasing the production of anti- inflammatory cytokines like IL-10 and IL-12p40 [479]. MSCs as well secrete factors (such as transforming growth factor-beta (TGF-β)) that promote recruitment of bone progenitor cells, secrete pro-osteogenic factors (such as Indian Hedgehog), they stimulate progenitor cells differentiation into osteoblasts, and possess anti-apoptotic effects in

osteoblastic lineage cells. Having presented the important MSC role in the bone formation, it is clear that by decellularising vital TE constructs in order to produce a more commercially appealing product with minimised possible immune responses *in vivo*, all the benefits brought by live MSCs are lost. In case of engineered templates, MSCs are primed, conferring them with even higher regenerative potential than naïve MSCs for large bone defect healing. For all these reasons, there is clearly the need to investigate ways to enhance off-the-shelf construct performance *in vivo*, in order to produce grafts with high regenerative potential even after decellularisation. A possible starting point could be measuring pre- and post-decellularisation key growth factors and cytokines, that decellularisation is partially removing, and then trying to increase their retention.

As already reported in this thesis, a number of previous studies that demonstrated the feasibility of using decellularised cartilaginous templates to trigger endochondral bone regeneration ectopically and orthotopically in rodents [292, 480]. Nevertheless, often unsatisfactory results in terms of bone regeneration were observed when the decellularised cartilaginous constructs were compared to the respective living controls [292], suggesting that the applied decellularisation methods lead to suboptimal regeneration, potentially caused by the partial loss of bioactivity of the ECM components. This led to the hypothesis that milder decellularization methods might help to preserve the structural and biochemical integrity of the tissue's ECM. This has led to an increased interest in the use of alternative devitalisation protocols on ECMs to produce bioactive scaffolds for in situ tissue engineering [481]. Both decellularisation and devitalisation processes entail the killing of resident cells while trying to preserve the most bioactive components of the ECM [482]. A key difference between the two methods is that with decellularisation protocols, most or all of the cellular debris is removed, whereas this is not the case for devitalisation strategies [482]. Devitalisation protocols are mainly based on treatments that use physical methods to disrupt cellular functions or lyse cells within a tissue. One example is freezer-milling followed by heat-inactivation to inactivate the cells found in the tissue without removing cells and all cellular components [483]. Freezer-milling pulverises the tissue into particles at low temperatures and the tissue is then heat-inactivated in a gravity oven. Devitalisation can also be achieved through hydrated tissue homogenisation followed by retrieval of tissue particles, freezing, and lyophilisation [484]. However, the most common method to devitalise engineered ECM constructs is the use of freeze thaw cycles followed by washes and/or sonication [485]. Very recently, a number of studies have investigated the use of

devitalised engineered hypertrophic cartilage templates as bone-inducing material [293, 486, 487], showing promising results *in vivo* both ectopically and following orthotopic implantation. Although being really promising, milder devitalisation approaches present a possible downside, due to cellular debris and DNA that is retained within the implanted construct. This has been shown to trigger an immune response that may hamper the regenerative process induced by non-autologous ECM-based scaffolds [488-490]. It is clear that for future studies a comparison between the immune response triggered by the vital, devitalised and decellularised constructs is necessary, especially in the early stages post-implantation; this might lead to the identification of specific immune responses that accelerate or hinder bone regeneration.

6.5 Conclusions

The results from this study demonstrate that it is possible to engineer *in vitro* cartilaginous grafts with different phenotypes, and to then decellularise these constructs to produce *off-the-shelf* hypertrophic cartilage grafts with clear osteogenic potential that can be used in bone repair applications. However, decellularisation was proven to diminish the bone forming capacity of the engineered grafts, and the resulting grafts possessed inferior osteoinductivity compared to Col-nHA sponges soak loaded with BMP-2. Having already stressed the importance of being able to realize *off-the-shelf* implants, it is clear that more work needs to be done to increase the retention of bioactive cues in the decellularised grafts and their subsequent osteoinductivity *in vivo*.

Chapter 7: Discussion and conclusions

7.1 Objective of the thesis

A large number of approaches, involving different regenerative pathways, fabrication techniques, materials, cells and biomolecules are currently being explored for large bone defect regeneration, suggesting that the ideal graft to restore such defects has yet to be identified. The overall goal of this thesis was to 3D bioprint mechanically reinforced cartilaginous templates as developmentally inspired implants for large bone defect regeneration. This required the selection of a biomaterial ink able to support chondrogenesis of hMSCs *in vitro*, the realisation of a reinforcing frame, and the engineering of cartilaginous templates *in vitro*. In chapter 3, fibrin hydrogels were prepared, laden with hMSCs and cultured for 5 weeks in chondrogenic media. In addition, to facilitate nutrient transport *in vitro* and potentially vascularisation *in vivo*, we introduced micro-channels into these constructs, and we showed that they remained patent throughout the culture period. It was demonstrated that fibrin can support encapsulated hMSCs chondrogenesis and progression along an endochondral pathway *in vitro*. In chapter 4, it was shown how the fibrinogen content within fibrin-based bioinks influences chondrogenesis of encapsulated hMSCs and that it was possible to mechanically reinforce 3D bioprinted cartilaginous templates with a 3D printed polymer network. Then in chapter 5, it was demonstrated how, by culture priming 3D bioprinted reinforced constructs, cartilage and hypertrophic cartilage templates were obtained, which were capable of directing endochondral bone formation upon *in vivo* implantation. Finally, in chapter 6, it was demonstrated that it is possible to decellularise the *in vitro* engineered cartilaginous grafts to produce *off-the-shelf* hypertrophic cartilage grafts with osteogenic potential that can be used in bone repair applications.

7.2 Comparing outcomes of viable and decellularised engineered constructs *in vivo*

In the thesis, both viable engineered cartilaginous templates and their decellularised versions were implanted in the same critically sized rat femoral defect model. However, an important difference needs to be pointed out between these two studies: the viable

constructs, along with a positive control, were implanted into immunosuppressed rats (to enable delivery of tissues engineered using human MSCs), while the decellularised constructs, along with the same positive control, were implanted into immune competent animals. Focusing on the outcomes of the positive control BMP-2 loaded scaffolds (which were prepared and treated in the same way for both studies) in both experiments, it appears that immune suppression partially hampered new bone formation. This is evident by the differences in total new bone formed in the two cases, with more new bone formation observed following implantation of BMP-2 loaded collagen scaffolds in the immune-competent animals compared to the immune-suppressed animals. With this in mind, it is plausible to believe that a similar suppression is effecting the vital *chondrogenic* and *early hypertrophic* groups, meaning that in the theoretical case where they were implanted in immune competent animals (i.e. engineered tissue from autologous rat cells), they should produce higher levels of new bone.

Although a direct comparison of *in vivo* outcomes following implantation of the viable and decellularised constructs is not possible, it is worth highlighting some of the differences in the patterns of repair observed following their *in vivo* implantation into critically sized femoral bone defects. First of all, the viable *early hypertrophic* constructs would appear to support higher levels of vascularisation and bone formation (based on histomorphometric analysis), compared to the decellularised version and the viable *chondrogenic* constructs. Furthermore, they were characterised by a clear healing pattern, with bone formation occurring firstly in the central regions of the defect, which was less evident in defects treated with all the other experimental constructs, as it can be seen in the micro-CT reconstructed 3D images. The discrepancy in the *in vivo* outcomes suggest two different points: (i) *in vivo* new bone formation differences between viable constructs are likely due to differences in their cellular phenotype and the specific composition of the ECM arising from the different *in vitro* priming protocols; (ii) although a direct comparison between viable and decellularised constructs cannot be done (due to the aforementioned differences in the rats), *in vivo* new bone formation differences between viable and decellularised constructs (with better regeneration in the viable constructs) are likely due to the decellularisation process. It is plausible to believe that new bone formation was strongly influenced by the decellularisation process of the *off-the-shelf* grafts, which probably diminished their osteoinductive capacity *in vivo*. This drawback in the decellularised constructs represent a clear limitation with respect to their direct application to bone

regeneration, and needs to be addressed. Section 7.4 of this chapter will present future directions, focusing on possible ways to improve these *off-the-shelf* constructs osteoinductive potential.

7.3 3D printing and bioprinting strategies to engineer reinforced cartilage templates for large bone defect healing

It has been shown that the fibrin-based bioink selected for this thesis can successfully be used for endochondral bone TE approaches. In fact, it supported encapsulated hMSCs chondrogenesis and progression along an endochondral pathway, and then remodelled *in vivo* enabling vascularisation and conversion of the cartilaginous templates into bone. Moreover, it was shown that the central micro-channel that was designed and introduced into the engineered constructs with the idea, remained patent for the entire culture period and allowed easy host tissue infiltration *in vivo*. If on one side, the inclusion of this micro-channel seemed to bring some benefits, on the other side no analyses were carried out to investigate its real contribution to nutrient transport *in vitro* and to construct vascularisation *in vivo*. The absence of such analyses could represent a limitation of this thesis and an issue that needs to be addressed in future studies. In chapter 2, the importance of vascularisation in developmentally inspired TE EO approaches was highlighted. Therefore, a solution such a central micro-channel, proven to be able to improve and guide construct vascularisation *in vivo*, would represent a significant advantage for endochondral bone TE.

In the construct realisation, besides the fibrin-based bioink, PCL was used as the reinforcing material throughout the thesis due to its favorable extrusion characteristics and its low melting temperature, and fine print control that can be achieved when using it to generate complex geometries. This made it possible to print perfectly reproducible and reliable polymeric frames which were then used as reinforcement for the bioprinted fibrin-based, cell-laden bioink. These were then engineered *in vitro* into cartilaginous templates that could then mature into new bone *in vivo*. It has been previously demonstrated that 3D printed PCL frameworks are sufficiently mechanically robust to withstand *in vivo*-occurring stresses, for example the ones found in rabbit articulations, following their implantation into the humeral condyles of skeletally mature animals [491]. However, it is important to note that the degradation rate of PCL microfibers is slow, and it typically takes 2-3 years before

the polymer is fully degraded [492, 493]. This was seen as well in all the *in vivo* studies here presented, since there was no evidence of degradation of the reinforcing PCL network over the 12 week *in vivo* time periods. This slow degradation rate may physically impede functional regeneration of the bone. It has been demonstrated in chapter 5 *via* histomorphometric analysis that more bone was found in the e*arly hypertrophic* group compared to the positive control when quantifying the positive bone area in the available defect area (total defect area minus the PCL area). However, if looking at the whole defect area, more bone was present in the control constructs. It is plausible to believe that without or with less PCL, e*arly hypertrophic* constructs could remodel quicker their ECM and produce more bone. Ideally, the rate of PCL degradation would be tailored to match the rate of *in vivo* tissue maturation to enable proper bone regeneration. In addition, minimising the percentage of reinforcing polymer used in the implantable grafts would also help accelerate this regeneration. In this thesis, it was demonstrated that mechanical reinforcements could be 3D printed and incorporated in bioprinted cartilaginous templates, but no further analyses were conducted to understand PCL degradation rate and which frame geometry and volume could bring the best results *in vivo*. Predictive finite element modelling could be used to determine the levels of mechanical reinforcement required pre-implantation; in this way the polymeric frame could be designed in order to match these levels, using the best geometry and the correct material volume to maximize the engineered ECM volume, which represent the fundament of the new bone that can potentially be produced. In addition, degradation studies should be carried out, and in order to meet *in vivo* tissue maturation rate modifications to PCL or selection of different polymeric materials could be taken into account. It is clear that in order to translate such TE approaches to the clinic, the aforementioned issues should be addressed. Since the studies here reported did not focus on this challenge, this could be considered a limitation of this thesis.

7.4 Future directions

In this thesis, it has already been stressed the importance of being able to realize *off-the-shelf* implants, and the advantages they potentially have over living constructs. However, in the study presented in chapter 6, decellularisation was proven to diminish the bone forming capacity of the engineered constructs, and the resulting grafts possessed inferior osteoinductivity compared to the positive control sponges soak loaded with BMP-

2. It is clear that more work needs to be done to increase the retention of bioactive cues in the decellularised grafts and their subsequent osteoinductivity *in vivo*.

Additional studies are warranted to better understand how the decellularization process influences bone regeneration. For example, it would be interesting to better characterise the composition of the engineered ECM pre- and post-decellularisation, in order to have a more detail understanding of which bioactive cues are present and how the decellularization process is influencing their concentration. Once known this, it would be interesting to investigate possible ways to increase key bioactive cues concentrations. This could be done by trying to modify the decellularisation method, in order to retain higher levels of key bioactive cues, or to somehow boost their initial concentrations. One promising way to achieve the former is to use a devitalisation method instead of decellularization, while to achieve the latter gene therapy could be used, which has the potential to enable the engineering of designer decellularised engineered ECMs with specific biochemical compositions that enhance their capacity to support tissue regeneration.

7.4.1 Devitalisation as an alternative to decellularisation

As discussed in chapter 6, one possible way to retain more key bioactive cues after the decellularisation process is to instead use devitalisation methods. Future studies could investigate *off-the-shelf* devitalised *chondrogenic*, *early* and *late hypertrophic* constructs engineered in the same way as presented in both chapter 5 and 6, but using freeze thaw cycles, as found in literature, to devitalise them instead of the decellularisation process that was described and carried out in chapter 6 (Fig 7.1).

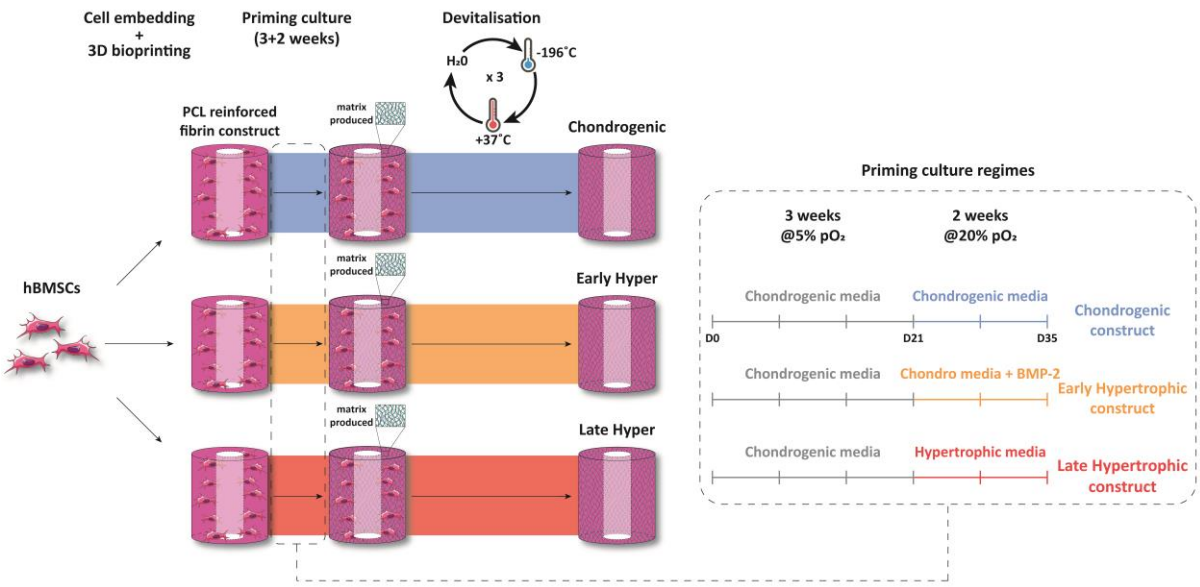

Figure 7.1: Devitalised constructs preparation schematic. Three new experimental groups would be prepared from vital constructs obtained using the same protocol described in 5.2

Once prepared *in vitro*, such devitalised constructs would firstly need be characterised through both biochemical and histological analyses (as described in sections 5.2.5 and 5.2.6). Then a critically sized femoral defect study could be undertaken (as described in section 6.2.9). Together with the microCT and histological analyses carried out in the same way as presented in 6.2.10 and 6.2.11, it would be important to test if residual cellular debris and denatured DNA that could be retained within the implanted devitalised constructs might trigger a negative *in vivo* immune response. This may hamper the regenerative process induced by the engineered constructs, resulting in hindered bone repair. Systemic immune response could be monitored by checking the blood for the presence of an inflammation marker (e.g. α-1-acid glycoprotein) and antibody production (e.g. IgG and IgM) at different time points post-implantation. After euthanasia at 1 and 12 weeks post-implantation (to investigate early and late response), the local immune response could be analysed *via* immunohistological staining. Markers belonging to the innate (macrophages: CD68, CD163, iNOS, and CD206) and adaptive (T lymphocytes: CD3) immune response could be investigated. This new *in vivo* study would allow us to test the effect of culture priming when producing devitalised *off-the-shelf* engineered ECM constructs for bone regeneration.

To these three experimental groups (devitalised *chondrogenic*, *early* and *late hypertrophic* constructs), as mentioned in the discussion of chapter 5, we could add a new control group, which would be an acellular 3D printed reinforced fibrin construct (prepared in the same way as in 5.2.3 but without hMSCs), maintained for 5 weeks as the *early hypertrophic* constructs (including the BMP-2 addition for the last 2 weeks). This new *in vivo* control would allow us to test the possible residual growth factor effects, having the constructs primed but not possessing viable cells and associated ECM.

7.4.2 Gene therapy application to BTE

As previously discussed, engineered ECMs are developed in the laboratory, meaning that their properties can be designed and produced *in vitro*. The idea of genetic manipulating cells has emerged as a possible way to better control the dose and spatiotemporal delivery of key factors into engineered ECMs, mimicking physiological levels, to improve bone regeneration process. The use of genetically engineered cells to induce the overexpression or knockdown of specific target molecules and matrix components would allow to decellularised engineered ECMs to be enriched with specific factors known to enhance tissue regeneration upon *in vivo* implantation. So far, gene therapy research applied to bone tissue regeneration in general, has used the delivery and activation of several factors such as morphogens (Sonic hedgehog (SHH) [494] and mainly BMPs – BMP-2 [101, 495-498], BMP-4 [499, 500], BMP-6 [501], BMP-7 [502], BMP-9 [503, 504]), Wnt proteins [505, 506], angiogenic factors (mainly vascular endothelial growth factor (VEGF) [262, 507, 508]), osteogenic transcription factors (Osterix [509-511] and Runx II [512]), LIM-domain proteins (LMPs) [513, 514], cyclooxygenase-2 [515], and forkhead c2 (Foxc2) (coactivated together with Wnt10b to elicit the noncanonical Wnt pathway [516]). Practical examples from the literature of gene therapy strategies, using different vectors and delivering specific transgenes for bone and musculoskeletal system in general, are reported and discussed in several other review papers [517-519]. Although all these key factors showed promising results, choosing the transgenes for the best performing strategies is still challenging. In fact, the selection is complicated by the choice between the two possible routes to bone formation, the intramembranous or the endochondral route, which requires the initial formation of cartilage [19]. So the specific genes one might want to deliver will depend on whether the graft is being engineered to promote direct or indirect bone formation; if the former then

consideration must be given, for example, to enhancing angiogenesis earlier in the regenerative process. For these reasons, it is clear that the nature and the spatiotemporal manner in which key transgenes are expressed by the genetically modified cells can play a pivotal role in the regeneration outcome, and a lot of work needs to be done to investigate this.

7.4.3 *Off-the-shelf* genetically engineered cell-derived ECMs

It is important to point out that if gene therapy is applied to the generation of engineered ECMs, all genetic manipulations would be moved outside the patient's body (*ex vivo*) and that these engineered biomaterials would be decellularised prior to *in vivo* implantation, eliminating the transgenic cellular components. This would reduce the risks and address safety concerns that are typically associated with the use of gene therapy and transgenic cells, and avoid the possible decrease in vector efficacy due to the immune system, as it happens when the vectors are applied directly *in vivo*. As well, the *ex vivo* use of gene therapy allows for better control over gene expression and a better choice of targeted cells, and it usually offers enhanced regenerative results.

For all the aforementioned reasons, gene technology potentially represents a relevant way to engineer enriched cell-derived ECMs capable of promoting efficient bone repair, enhancing the traditional cell-derived ECMs. However, very little work has been published so far on the realisation of *off-the-shelf* genetically engineered cell-derived ECM grafts. One example is provided by the study of Ma et al., in which murine pre-osteoblast cells (MC3T3-E1) were transduced with the LIM mineralisation protein-1 (LMP-1) [255]. LMP-1 protein as an intracellular factor can upregulate the expression of many different growth factors, and proof of this was found in the overexpression of BMP-2, BMP-4 and BMP-7 by these MC3T3-E1 cells after their modification. ECM–scaffold composites were obtained by seeding the transduced cells into calcined bovine bone scaffolds, culturing them for 7 days in osteogenic media to produce the ECM, and finally decellularising them using a freeze-drying protocol. The obtained composite scaffolds were implanted into critically sized femoral bone defects in rabbits. Twelve weeks after implantation, both microcomputed tomography and histological analyses showed that the cell-modified ECM–scaffold composites induced bone regeneration with significantly larger volume, trabecular thickness and connectivity than the controls (scaffolds without ECM deposition). In another study,

Bourgine et al. aimed to combine suitable cell lines and a bioreactor system in order to create standardised and customised *off-the-shelf* decellularised engineered ECM, enriched with specific molecules to activate endogenous bone formation and tissue vascularisation [262]. Mesenchymal Sword of Damocles (MSOD) cells, an immortalised human stromal cell line carrying an inducible apoptotic genetic device able to trigger cell death, were seeded on 3D porous ceramic scaffolds and cultured within a perfusion bioreactor for four weeks (one week in proliferation medium followed by three weeks in osteogenic medium) to promote cell osteogenic differentiation while stimulating ECM production. The obtained composite scaffolds were decellularised by deliberate cell-apoptosis induction or freeze/thaw method as control. Experimental scaffolds showed superior preservation of ECM and enhanced bone formation in critically sized rat cranial defects. The original MSOD cells were then transduced to overexpress VEGF (MSOD-V), and used to produce with the same technique new selectively enriched ECM scaffolds, which showed increased angiogenic potential and superior vasculature recruitment in a rat ectopic implantation model. Future studies could focus on the use of genetically modified cells engineered to overexpress defined factors and therefore produce enriched ECMs capable of driving one or more of the following: (i) host cell recruitment (through the expression of chemoattractants), (ii) osteoinduction and bone formation (using cells overexpressing specific BMPs or osteogenic transcription factors such as Osterix and RUNX2), (iii) vascularisation (through the expression of angiogenic/vessel stabilising factors such as VEGF or PDGF-BB (Platelet-derived growth factor)), (iv) endochondral ossification of hypertrophic cartilaginous templates (using cells overexpressing factors known to influence endochondral ossification such as BMPs, fibroblast growth factors (FGFs), TGFβs, Wnts, Indian hedgehog IHH [520]).

7.4.4 Gene therapy as a method to modulate immune response to engineered ECMs

Engineered cell-derived ECM could also be enriched to address a positive and useful modulation of the host immune response. In the past years, many studies have shown the existence of a broad crosstalk between the skeletal and immune systems through many shared cytokines, molecular pathways and transcription factors, highlighting how a balanced and coordinated immune system response is essential to critically promote bone healing [521]. A lot of work has been done on studying the mechanisms by which ECM-derived scaffolds promote constructive tissue remodelling, first of which is the release, while

degrading, of important cues such as chemoattractant, antimicrobial, and mitogenic peptides, growth factors, and extracellular vesicles that all contribute to endogenous stem cell recruitment among other bioactive effects [522]. Additionally, these scaffolds have been associated with a robust and favourable immunomodulatory properties that support constructive remodelling outcomes [523]. ECM scaffolds have been proven to modulate the behaviour of responding immune cells, in particular directly influencing macrophages towards a regulatory anti-inflammatory phenotype [524], and mediating macrophage cross-talk with endogenous stem and progenitor cells through paracrine effects [525]. All these findings have contributed to move from the traditionally held view of avoiding the immune response, and to focus on new strategies that aim to engineer ECM-derived biomaterials characterised by osteoimmunomodulatory factors and instruct the inevitable host immune response in favour of bone regeneration [526]. In order to modulate the innate immune response upon implantation, exogenous immunoregulatory factors, such as cytokines, have been added into the ECMs and delivered *in vivo* [527-530]. However, such delivery is subjected to several drawbacks including poor matrix penetration, diffusion, enzymatic degradation and thus uncontrolled doses. To address these problems, many researchers attempted to directly stimulate and modulate, using several biological agents, the natural synthesis and release of immune factors by endogenous MSCs or immune cells, circumventing the problem of exogenous direct delivery, to enhance bone formation [531-534]. In order to have a better control of the dose and the spatiotemporal delivery of osteoimmunomodulatory factors, future studies could focus on genetically modifying MSCs for the realisation of enriched decellularised engineered ECMs. These biomaterials could be designed not only to support osteogenesis, angiogenesis or endochondral ossification as mentioned previously, but as well to possess immunoinstructive properties, which would allow for a better and more efficient bone repair [521].

7.5 Conclusion

To conclude, the results of this thesis demonstrate that:

- Fibrin hydrogels can support encapsulated hMSCs chondrogenesis and progression along an endochondral pathway *in vitro*.

- The fibrinogen content within fibrin-based bioinks influences the *in vitro* properties of the extracellular matrix deposited by the encapsulated hMSCs.
- It is possible to mechanically reinforce 3D bioprinted cartilaginous templates with a 3D printed polymer network.
- It is possible to engineer *in vitro* cartilaginous grafts with different phenotypes (cartilage and hypertrophic cartilage), which are capable of directing endochondral bone formation upon *in vivo* implantation.
- These engineered constructs can be decellularised to produce *off-the-shelf* hypertrophic cartilage grafts with osteogenic potential that can be used in bone repair applications.
- 3D bioprinting is a viable approach to scale-up the engineering of developmentally inspired templates for bone TE.

Bibliography

1. Praemer, A., et al., *Musculoskeletal conditions in the United States.* 1999.
2. Bucholz, R.W., *Nonallograft osteoconductive bone graft substitutes.* Clinical Orthopaedics and Related Research®, 2002. **395**: p. 44-52.
3. Campana, V., et al., *Bone substitutes in orthopaedic surgery: from basic science to clinical practice.* J Mater Sci Mater Med, 2014. **25**(10): p. 2445-61.
4. Fernandez de Grado, G., et al., *Bone substitutes: a review of their characteristics, clinical use, and perspectives for large bone defects management.* Journal of tissue engineering, 2018. **9**: p. 2041731418776819.
5. Younger, E.M. and M.W. Chapman, *Morbidity at bone graft donor sites.* J Orthop Trauma, 1989. **3**(3): p. 192-5.
6. Ong, J.L. and T. Guda, *Translating Biomaterials for Bone Graft: Bench-top to Clinical Applications*. 2017: Crc Press.
7. Laurencin, C.T., et al., *Tissue engineering: orthopedic applications.* Annual review of biomedical engineering, 1999. **1**(1): p. 19-46.
8. Shrivats, A.R., M.C. McDermott, and J.O. Hollinger, *Bone tissue engineering: state of the union.* Drug discovery today, 2014. **19**(6): p. 781-786.
9. Salgado, A.J., O.P. Coutinho, and R.L. Reis, *Bone tissue engineering: state of the art and future trends.* Macromol Biosci, 2004. **4**(8): p. 743-65.
10. Allen, M.R. and D.B. Burr, *Bone modeling and remodeling*, in *Basic and applied bone biology*. 2014, Elsevier. p. 75-90.
11. Yang, Y., . *Skeletal Morphogenesis and Embryonic Development.* ASBMR Primer on the Metabolic Bone Diseases and Disorders of Mineral Metabolism, 2009: p. 2.
12. Vortkamp, A., et al., *Regulation of rate of cartilage differentiation by Indian hedgehog and PTH-related protein.* Science, 1996. **273**(5275): p. 613-622.
13. Mackie, E., *The skeleton: a multi-functional complex organ: the growth plate chondrocyte and Mackie EJ, Ahmed YA, Tatarczuch L, Chen KS & Mirams M 2008 Endochondral ossification: how cartilage is converted into bone in the developing skeleton.* International Journal of Biochemistry & Cell Biology, 2011. **40**: p. 46-62.
14. Provot, S. and E. Schipani, *Molecular mechanisms of endochondral bone development.* Biochemical and biophysical research communications, 2005. **328**(3): p. 658-665.
15. Maes, C., et al., *Osteoblast precursors, but not mature osteoblasts, move into developing and fractured bones along with invading blood vessels.* Developmental cell, 2010. **19**(2): p. 329-344.
16. Kronenberg, H.M., *Developmental regulation of the growth plate.* Nature, 2003. **423**(6937): p. 332.
17. Lenas, P., M. Moos Jr, and F.P. Luyten, *Developmental engineering: a new paradigm for the design and manufacturing of cell-based products. Part I: from three-dimensional cell growth to biomimetics of in vivo development.* Tissue Engineering Part B: Reviews, 2009. **15**(4): p. 381-394.
18. Scotti, C., et al., *Recapitulation of endochondral bone formation using human adult mesenchymal stem cells as a paradigm for developmental engineering.* Proceedings of the National Academy of Sciences, 2010. **107**(16): p. 7251-7256.
19. Scotti, C., et al., *Engineering of a functional bone organ through endochondral ossification.* Proceedings of the National Academy of Sciences, 2013. **110**(10): p. 3997-4002.
20. Harada, N., et al., *Bone regeneration in a massive rat femur defect through endochondral ossification achieved with chondrogenically differentiated MSCs in a degradable scaffold.* Biomaterials, 2014. **35**(27): p. 7800-7810.

21. Daly, A.C., et al., *3D printed microchannel networks to direct vascularisation during endochondral bone repair.* Biomaterials, 2018.
22. Freeman, F.E., et al., *A developmental engineering-based approach to bone repair: endochondral priming enhances vascularization and new bone formation in a critical size defect.* Frontiers in bioengineering and biotechnology, 2020. **8**: p. 230.
23. Sheehy, E.J., et al., *Tissue engineering whole bones through endochondral ossification: regenerating the distal phalanx.* BioResearch open access, 2015. **4**(1): p. 229-241.
24. Mesallati, T., et al., *Tissue engineering scaled-up, anatomically shaped osteochondral constructs for joint resurfacing.* Eur Cell Mater, 2015. **30**: p. 163-85.
25. Turnbull, G., et al., *3D bioactive composite scaffolds for bone tissue engineering.* Bioactive materials, 2018. **3**(3): p. 278-314.
26. Evans, C.H., *Barriers to the clinical translation of orthopedic tissue engineering.* Tissue Eng Part B Rev, 2011. **17**(6): p. 437-41.
27. Lu, H., et al., *Cultured cell-derived extracellular matrix scaffolds for tissue engineering.* Biomaterials, 2011. **32**(36): p. 9658-9666.
28. Lawson, J.H., et al., *Bioengineered human acellular vessels for dialysis access in patients with end-stage renal disease: two phase 2 single-arm trials.* The Lancet, 2016. **387**(10032): p. 2026-2034.
29. Kirkton, R.D., et al., *Bioengineered human acellular vessels recellularize and evolve into living blood vessels after human implantation.* Science translational medicine, 2019. **11**(485).
30. Kang, H.W., et al., *A 3D bioprinting system to produce human-scale tissue constructs with structural integrity.* Nat Biotechnol, 2016. **34**(3): p. 312-9.
31. Mouser, V.H., et al., *Yield stress determines bioprintability of hydrogels based on gelatin-methacryloyl and gellan gum for cartilage bioprinting.* Biofabrication, 2016. **8**(3): p. 035003.
32. Murphy, S.V. and A. Atala, *3D bioprinting of tissues and organs.* Nat Biotechnol, 2014. **32**(8): p. 773-85.
33. Schon, B., G. Hooper, and T. Woodfield, *Modular tissue assembly strategies for biofabrication of engineered cartilage.* Annals of biomedical engineering, 2017. **45**(1): p. 100-114.
34. Hockaday, L., et al., *Rapid 3D printing of anatomically accurate and mechanically heterogeneous aortic valve hydrogel scaffolds.* Biofabrication, 2012. **4**(3): p. 035005.
35. Billiet, T., et al., *The 3D printing of gelatin methacrylamide cell-laden tissue-engineered constructs with high cell viability.* Biomaterials, 2014. **35**(1): p. 49-62.
36. Kolesky, D.B., et al., *3D bioprinting of vascularized, heterogeneous cell-laden tissue constructs.* Advanced materials, 2014. **26**(19): p. 3124-3130.
37. Nulty, J., R. Burdis, and D.J. Kelly, *Biofabrication of Prevascularised Hypertrophic Cartilage Microtissues for Bone Tissue Engineering.* Frontiers in Bioengineering and Biotechnology, 2021. **9**: p. 469.
38. Cunniffe, G.M., et al., *Three-Dimensional Bioprinting of Polycaprolactone Reinforced Gene Activated Bioinks for Bone Tissue Engineering.* Tissue Eng Part A, 2017. **23**(17-18): p. 891-900.
39. Daly, A.C., et al., *3D Bioprinting of Developmentally Inspired Templates for Whole Bone Organ Engineering.* Advanced Healthcare Materials, 2016. **5**(18): p. 2353-2362.
40. Daly, A.C. and D.J. Kelly, *Biofabrication of spatially organised tissues by directing the growth of cellular spheroids within 3D printed polymeric microchambers.* Biomaterials, 2019. **197**: p. 194-206.
41. Pati, F., et al., *Printing three-dimensional tissue analogues with decellularized extracellular matrix bioink.* Nat Commun, 2014. **5**: p. 3935.

42. Schuurman, W., et al., *Bioprinting of hybrid tissue constructs with tailorable mechanical properties.* Biofabrication, 2011. **3**(2): p. 021001.
43. Shim, J.H., et al., *Development of a hybrid scaffold with synthetic biomaterials and hydrogel using solid freeform fabrication technology.* Biofabrication, 2011. **3**(3): p. 034102.
44. Cunniffe, G., et al., *Chondrogenically primed mesenchymal stem cell-seeded alginate hydrogels promote early bone formation in critically-sized defects.* European Polymer Journal, 2015. **72**: p. 464-472.
45. Scott, C.K. and J.A. Hightower, *The matrix of endochondral bone differs from the matrix of intramembranous bone.* Calcified tissue international, 1991. **49**(5): p. 349-354.
46. Gasser, J.A. and M. Kneissel, *Bone Physiology and Biology*, in *Bone Toxicology*. 2017, Springer. p. 27-94.
47. Scott, C.K., S.D. Bain, and J.A. Hightower, *Intramembranous bone matrix is osteoinductive.* The Anatomical Record, 1994. **238**(1): p. 23-30.
48. Chung, U.-i., et al., *Distinct osteogenic mechanisms of bones of distinct origins.* Journal of Orthopaedic Science, 2004. **9**(4): p. 410-414.
49. Lopes, D., et al., *Bone physiology as inspiration for tissue regenerative therapies.* Biomaterials, 2018. **185**: p. 240-275.
50. Hollinger, J.O., et al., *Bone tissue engineering*. 2004: CRC press.
51. Hunziker, E., E. Kapfinger, and C. Saager, *Hypertrophy of growth plate chondrocytes in vivo is accompanied by modulations in the activity state and surface area of their cytoplasmic organelles.* Histochemistry and cell biology, 1999. **112**(2): p. 115-123.
52. Noonan, K.J., et al., *Changes in cell, matrix compartment, and fibrillar collagen volumes between growth-plate zones.* Journal of orthopaedic research, 1998. **16**(4): p. 500-508.
53. Colnot, C., et al., *Altered fracture repair in the absence of MMP9.* Development, 2003. **130**(17): p. 4123-4133.
54. Drake, C.J., *Embryonic and adult vasculogenesis.* Birth Defects Research Part C: Embryo Today: Reviews, 2003. **69**(1): p. 73-82.
55. Ortega, N., et al., *How proteases regulate bone morphogenesis.* Annals of the New York Academy of Sciences, 2003. **995**(1): p. 109-116.
56. Berendsen, A.D. and B.R. Olsen, *Bone development.* Bone, 2015. **80**: p. 14-18.
57. Gerstenfeld, L.C. and F.D. Shapiro, *Expression of bone-specific genes by hypertrophic chondrocytes: implication of the complex functions of the hypertrophic chondrocyte during endochondral bone development.* J Cell Biochem, 1996. **62**(1): p. 1-9.
58. Roach, H.I., J. Erenpreisa, and T. Aigner, *Osteogenic differentiation of hypertrophic chondrocytes involves asymmetric cell divisions and apoptosis.* J Cell Biol, 1995. **131**(2): p. 483-94.
59. Aghajanian, P. and S. Mohan, *The art of building bone: emerging role of chondrocyte-to-osteoblast transdifferentiation in endochondral ossification.* Bone Res, 2018. **6**: p. 19.
60. Thesingh, C.W., C.G. Groot, and A.M. Wassenaar, *Transdifferentiation of hypertrophic chondrocytes into osteoblasts in murine fetal metatarsal bones, induced by co-cultured cerebrum.* Bone Miner, 1991. **12**(1): p. 25-40.
61. Yang, L., et al., *Hypertrophic chondrocytes can become osteoblasts and osteocytes in endochondral bone formation.* Proc Natl Acad Sci U S A, 2014. **111**(33): p. 12097-102.
62. Zhou, X., et al., *Chondrocytes transdifferentiate into osteoblasts in endochondral bone during development, postnatal growth and fracture healing in mice.* PLoS Genet, 2014. **10**(12): p. e1004820.
63. Burr, D.B. and M.R. Allen, *Basic and applied bone biology*. 2013: Academic Press.
64. Boskey, A.L., *Assessment of bone mineral and matrix using backscatter electron imaging and FTIR imaging.* Current osteoporosis reports, 2006. **4**(2): p. 71-75.

65. Liu, Y., D. Luo, and T. Wang, *Hierarchical structures of bone and bioinspired bone tissue engineering.* Small, 2016. **12**(34): p. 4611-4632.
66. Weiner, S. and H.D. Wagner, *The material bone: structure-mechanical function relations.* Annual Review of Materials Science, 1998. **28**(1): p. 271-298.
67. Rossert, J. and B. de Crombrugghe, *Type I collagen: structure, synthesis, and regulation*, in *Principles of Bone Biology (Second Edition)*. 2002, Elsevier. p. 189-XVIII.
68. Burr, D.B. and O. Akkus, *Bone morphology and organization*, in *Basic and applied bone biology*. 2014, Elsevier. p. 3-25.
69. Barbos, M.P., P. Bianco, and A. Ascenzi, *Distribution of osteonic and interstitial components in the human femoral shaft with reference to structure, calcification and mechanical properties.* Cells Tissues Organs, 1983. **115**(2): p. 178-186.
70. Dobnig, H. and R.T. Turner, *Evidence that intermittent treatment with parathyroid hormone increases bone formation in adult rats by activation of bone lining cells.* Endocrinology, 1995. **136**(8): p. 3632-3638.
71. Kim, S.W., et al., *Intermittent parathyroid hormone administration converts quiescent lining cells to active osteoblasts.* Journal of bone and mineral research, 2012. **27**(10): p. 2075-2084.
72. Bonewald, L.F., M. Kneissel, and M. Johnson, *Preface: the osteocyte.* Bone, 2013. **54**(2): p. 181.
73. Tate, M.L.K., et al., *The osteocyte.* The international journal of biochemistry & cell biology, 2004. **36**(1): p. 1-8.
74. Plotkin, L.I. and T. Bellido, *Osteocytic signalling pathways as therapeutic targets for bone fragility.* Nature Reviews Endocrinology, 2016. **12**(10): p. 593.
75. Finkemeier, C.G., *Bone-grafting and bone-graft substitutes.* JBJS, 2002. **84**(3): p. 454-464.
76. Van Heest, A. and M. Swiontkowski, *Bone-graft substitutes.* The Lancet, 1999. **353**: p. S28-S29.
77. Bancroft, G. and A. Mikos, *Bone tissue engineering by cell transplantation*, in *Polymer Based Systems on Tissue Engineering, Replacement and Regeneration*. 2002, Springer. p. 251-263.
78. Lyles, M., et al., *Bone tissue engineering*, in *Regenerative Engineering of Musculoskeletal Tissues and Interfaces*. 2015, Elsevier. p. 97-134.
79. Bruder, S.P. and A.I. Caplan, *Bone regeneration through cellular engineering.* Principles of tissue engineering, 2000. **2**: p. 683-696.
80. Haynesworth, S., et al., *Characterization of cells with osteogenic potential from human marrow.* Bone, 1992. **13**(1): p. 81-88.
81. Bruder, S.P., N. Jaiswal, and S.E. Haynesworth, *Growth kinetics, self-renewal, and the osteogenic potential of purified human mesenchymal stem cells during extensive subcultivation and following cryopreservation.* J Cell Biochem, 1997. **64**(2): p. 278-94.
82. Ren, X., et al., *Growth factor engineering strategies for regenerative medicine applications.* Frontiers in bioengineering and biotechnology, 2020. **7**: p. 469.
83. Mitchell, A.C., et al., *Engineering growth factors for regenerative medicine applications.* Acta biomaterialia, 2016. **30**: p. 1-12.
84. Wang, Z., et al., *Novel biomaterial strategies for controlled growth factor delivery for biomedical applications.* NPG Asia Materials, 2017. **9**(10): p. e435-e435.
85. Badylak, S.F., D.O. Freytes, and T.W. Gilbert, *Extracellular matrix as a biological scaffold material: structure and function.* Acta biomaterialia, 2009. **5**(1): p. 1-13.
86. Mouw, J.K., G. Ou, and V.M. Weaver, *Extracellular matrix assembly: a multiscale deconstruction.* Nature reviews Molecular cell biology, 2014. **15**(12): p. 771-785.
87. Williams, D.F., *The biomaterials conundrum in tissue engineering.* Tissue Engineering Part A, 2014. **20**(7-8): p. 1129-1131.

88. Mansour, A., et al., *Extracellular matrices for bone regeneration: a literature review.* Tissue Engineering Part A, 2017. **23**(23-24): p. 1436-1451.
89. Mistry, A.S. and A.G. Mikos, *Tissue engineering strategies for bone regeneration.* Adv Biochem Eng Biotechnol, 2005. **94**: p. 1-22.
90. Bose, S., M. Roy, and A. Bandyopadhyay, *Recent advances in bone tissue engineering scaffolds.* Trends in biotechnology, 2012. **30**(10): p. 546-554.
91. Caplan, A.I. and D. Correa, *PDGF in bone formation and regeneration: new insights into a novel mechanism involving MSCs.* Journal of Orthopaedic Research, 2011. **29**(12): p. 1795-1803.
92. Caplan, A.I. and D. Correa, *The MSC: an injury drugstore.* Cell stem cell, 2011. **9**(1): p. 11-15.
93. Baksh, D., G.M. Boland, and R.S. Tuan, *Cross-talk between Wnt signaling pathways in human mesenchymal stem cells leads to functional antagonism during osteogenic differentiation.* Journal of cellular biochemistry, 2007. **101**(5): p. 1109-1124.
94. Jones, E.A., P.V. Giannoudis, and D. Kouroupis, *Bone repair with skeletal stem cells: rationale, progress to date and clinical application.* Therapeutic advances in musculoskeletal disease, 2016. **8**(3): p. 57-71.
95. Han, D.S., et al., *Consideration of bone regeneration effect of stem cells: comparison of bone regeneration between bone marrow stem cells and adipose-derived stem cells.* Journal of Craniofacial Surgery, 2014. **25**(1): p. 196-201.
96. Marcacci, M., et al., *Stem cells associated with macroporous bioceramics for long bone repair: 6-to 7-year outcome of a pilot clinical study.* Tissue engineering, 2007. **13**(5): p. 947-955.
97. Kim, S.-J., et al., *A multi-center, randomized, clinical study to compare the effect and safety of autologous cultured osteoblast (Ossron™) injection to treat fractures.* BMC musculoskeletal disorders, 2009. **10**(1): p. 1-9.
98. Zhao, D., et al., *Treatment of early stage osteonecrosis of the femoral head with autologous implantation of bone marrow-derived and cultured mesenchymal stem cells.* Bone, 2012. **50**(1): p. 325-330.
99. Mareschi, K., et al., *Expansion of mesenchymal stem cells isolated from pediatric and adult donor bone marrow.* Journal of cellular biochemistry, 2006. **97**(4): p. 744-754.
100. Both, S.K., et al., *Differential bone-forming capacity of osteogenic cells from either embryonic stem cells or bone marrow-derived mesenchymal stem cells.* Journal of tissue engineering and regenerative medicine, 2011. **5**(3): p. 180-190.
101. Peterson, B., et al., *Healing of critically sized femoral defects, using genetically modified mesenchymal stem cells from human adipose tissue.* Tissue Eng, 2005. **11**(1-2): p. 120-9.
102. Di Bella, C., P. Farlie, and A.J. Penington, *Bone regeneration in a rabbit critical-sized skull defect using autologous adipose-derived cells.* Tissue Engineering Part A, 2008. **14**(4): p. 483-490.
103. Cui, L., et al., *Repair of cranial bone defects with adipose derived stem cells and coral scaffold in a canine model.* Biomaterials, 2007. **28**(36): p. 5477-5486.
104. Mesimäki, K., et al., *Novel maxillary reconstruction with ectopic bone formation by GMP adipose stem cells.* International journal of oral and maxillofacial surgery, 2009. **38**(3): p. 201-209.
105. Lendeckel, S., et al., *Autologous stem cells (adipose) and fibrin glue used to treat widespread traumatic calvarial defects: case report.* Journal of Cranio-Maxillofacial Surgery, 2004. **32**(6): p. 370-373.
106. Thomson, J.A., et al., *Embryonic stem cell lines derived from human blastocysts.* science, 1998. **282**(5391): p. 1145-1147.

107. Tang, M., et al., *Human embryonic stem cell encapsulation in alginate microbeads in macroporous calcium phosphate cement for bone tissue engineering.* Acta biomaterialia, 2012. **8**(9): p. 3436-3445.
108. Taiani, J., et al., *Embryonic stem cell therapy improves bone quality in a model of impaired fracture healing in the mouse; tracked temporally using in vivo micro-CT.* Bone, 2014. **64**: p. 263-272.
109. Woll, N.L., J.D. Heaney, and S.K. Bronson, *Osteogenic nodule formation from single embryonic stem cell-derived progenitors.* Stem cells and development, 2006. **15**(6): p. 865-879.
110. Arpornmaeklong, P., et al., *Expansion and characterization of human embryonic stem cell-derived osteoblast-like cells.* Cellular Reprogramming (Formerly" Cloning and Stem Cells"), 2010. **12**(4): p. 377-389.
111. Cunningham, J.J., et al., *Lessons from human teratomas to guide development of safe stem cell therapies.* Nature biotechnology, 2012. **30**(9): p. 849-857.
112. Richards, M., et al., *Comparative evaluation of various human feeders for prolonged undifferentiated growth of human embryonic stem cells.* Stem cells, 2003. **21**(5): p. 546-556.
113. de Miguel-Beriain, I., *The ethics of stem cells revisited.* Advanced drug delivery reviews, 2015. **82**: p. 176-180.
114. Takahashi, K. and S. Yamanaka, *Induction of pluripotent stem cells from mouse embryonic and adult fibroblast cultures by defined factors.* cell, 2006. **126**(4): p. 663-676.
115. Im, G.I., *Stem cells for reutilization in bone regeneration.* Journal of cellular biochemistry, 2015. **116**(4): p. 487-493.
116. Li, F., S. Bronson, and C. Niyibizi, *Derivation of murine induced pluripotent stem cells (iPS) and assessment of their differentiation toward osteogenic lineage.* Journal of cellular biochemistry, 2010. **109**(4): p. 643-652.
117. Ko, J.-Y., S. Park, and G.-I. Im, *Osteogenesis from human induced pluripotent stem cells: an in vitro and in vivo comparison with mesenchymal stem cells.* Stem cells and development, 2014. **23**(15): p. 1788-1797.
118. Hynes, K., et al., *Generation of functional mesenchymal stem cells from different induced pluripotent stem cell lines.* Stem cells and development, 2014. **23**(10): p. 1084-1096.
119. Kang, H., et al., *Small molecule–driven direct conversion of human pluripotent stem cells into functional osteoblasts.* Science advances, 2016. **2**(8): p. e1600691.
120. Ripamonti, U., *Soluble osteogenic molecular signals and the induction of bone formation.* Biomaterials, 2006. **27**(6): p. 807-822.
121. Komatsu, D.E. and S.J. Warden, *The control of fracture healing and its therapeutic targeting: improving upon nature.* Journal of cellular biochemistry, 2010. **109**(2): p. 302-311.
122. Wozney, J.M., et al., *Novel regulators of bone formation: molecular clones and activities.* Science, 1988. **242**(4885): p. 1528-1534.
123. Chen, D., M. Zhao, and G.R. Mundy, *Bone morphogenetic proteins.* Growth factors, 2004. **22**(4): p. 233-241.
124. Adachi, T., et al., *Influence of LIF and BMP-2 on differentiation and development of glial cells in primary cultures of embryonic rat cerebral hemisphere.* Journal of neuroscience research, 2005. **79**(5): p. 608-615.
125. Hogan, B., *Bone morphogenetic proteins: multifunctional regulators of vertebrate development.* Genes & development, 1996. **10**(13): p. 1580-1594.
126. Reddi, A.H., *Bone morphogenetic proteins: from basic science to clinical applications.* JBJS, 2001. **83**(1_suppl_1): p. S1-S6.
127. Zou, H., et al. *BMP signaling and vertebrate limb development*. in *Cold Spring Harbor symposia on quantitative biology*. 1997. Cold Spring Harbor Laboratory Press.

128. Kang, Q., et al., *Characterization of the distinct orthotopic bone-forming activity of 14 BMPs using recombinant adenovirus-mediated gene delivery.* Gene therapy, 2004. **11**(17): p. 1312-1320.
129. Keskin, D.S., et al., *Collagen–chondroitin sulfate-based PLLA–SAIB-coated rhBMP-2 delivery system for bone repair.* Biomaterials, 2005. **26**(18): p. 4023-4034.
130. Yang, H.S., et al., *Apatite-coated collagen scaffold for bone morphogenetic protein-2 delivery.* Tissue Engineering Part A, 2011. **17**(17-18): p. 2153-2164.
131. Zara, J.N., et al., *High doses of bone morphogenetic protein 2 induce structurally abnormal bone and inflammation in vivo.* Tissue Eng Part A, 2011. **17**(9-10): p. 1389-99.
132. Calori, G., et al., *Application of rhBMP-7 and platelet-rich plasma in the treatment of long bone non-unions: a prospective randomised clinical study on 120 patients.* Injury, 2008. **39**(12): p. 1391-1402.
133. Friedlaender, G.E., et al., *Osteogenic protein-1 (bone morphogenetic protein-7) in the treatment of tibial nonunions: a prospective, randomized clinical trial comparing rhOP-1 with fresh bone autograft.* The Journal of bone and joint surgery. American volume, 2001. **83**(Pt 2): p. S151.
134. Giannoudis, P.V. and C. Tzioupis, *Clinical applications of BMP-7: the UK perspective.* Injury, 2005. **36**(3): p. S47-S50.
135. Govender, S., et al., *Recombinant human bone morphogenetic protein-2 for treatment of open tibial fractures: a prospective, controlled, randomized study of four hundred and fifty patients.* JBJS, 2002. **84**(12): p. 2123-2134.
136. Sun, W., et al., *Recombinant human bone morphogenetic protein-2 in debridement and impacted bone graft for the treatment of femoral head osteonecrosis.* PLoS One, 2014. **9**(6): p. e100424.
137. Swiontkowski, M.F., et al., *Recombinant human bone morphogenetic protein-2 in open tibial fractures: a subgroup analysis of data combined from two prospective randomized studies.* JBJS, 2006. **88**(6): p. 1258-1265.
138. Mont, M.A., et al., *Use of bone morphogenetic proteins for musculoskeletal applications: an overview.* Jbjs, 2004. **86**(suppl_2): p. 41-55.
139. Arrabal, P.M., et al., *Osteogenic molecules for clinical applications: improving the BMP-collagen system.* Biological research, 2013. **46**(4): p. 421-429.
140. Einhorn, T.A., *Clinical applications of recombinant human BMPs: early experience and future development.* Jbjs, 2003. **85**(suppl_3): p. 82-88.
141. Carlisle, E. and J.S. Fischgrund, *Bone morphogenetic proteins for spinal fusion.* The Spine Journal, 2005. **5**(6): p. S240-S249.
142. Gupta, M.C. and S. Maitra, *Bone grafts and bone morphogenetic proteins in spine fusion.* Cell and Tissue Banking, 2002. **3**(4): p. 255-267.
143. Robinson, Y., et al., *Evidence supporting the use of bone morphogenetic proteins for spinal fusion surgery.* Expert review of medical devices, 2008. **5**(1): p. 75-84.
144. Krishnakumar, G.S., et al., *Clinical application of bone morphogenetic proteins for bone healing: a systematic review.* International orthopaedics, 2017. **41**(6): p. 1073-1083.
145. Tannoury, C.A. and H.S. An, *Complications with the use of bone morphogenetic protein 2 (BMP-2) in spine surgery.* The Spine Journal, 2014. **14**(3): p. 552-559.
146. Han, D., et al., *Optimal delivery systems for bone morphogenetic proteins in orthopedic applications should model initial tissue repair structures by using a heparin-incorporated fibrin–fibronectin matrix.* Medical hypotheses, 2008. **71**(3): p. 374-378.
147. Haidar, Z.S., R.C. Hamdy, and M. Tabrizian, *Delivery of recombinant bone morphogenetic proteins for bone regeneration and repair. Part B: Delivery systems for BMPs in orthopaedic and craniofacial tissue engineering.* Biotechnology letters, 2009. **31**(12): p. 1825-1835.

148. Farrell, E., et al., *Chondrogenic priming of human bone marrow stromal cells: a better route to bone repair?* Tissue Eng Part C Methods, 2009. **15**(2): p. 285-95.
149. Scotti, C., et al., *Recapitulation of endochondral bone formation using human adult mesenchymal stem cells as a paradigm for developmental engineering.* Proc Natl Acad Sci U S A, 2010. **107**(16): p. 7251-6.
150. Sheehy, E.J., et al., *Altering the architecture of tissue engineered hypertrophic cartilaginous grafts facilitates vascularisation and accelerates mineralisation.* PLoS One, 2014. **9**(3): p. e90716.
151. Visser, J., et al., *Endochondral bone formation in gelatin methacrylamide hydrogel with embedded cartilage-derived matrix particles.* Biomaterials, 2015. **37**: p. 174-82.
152. van der Stok, J., et al., *Chondrogenically differentiated mesenchymal stromal cell pellets stimulate endochondral bone regeneration in critical-sized bone defects.* Eur Cell Mater, 2014. **27**(137): p. e48.
153. Bernhard, J., et al., *Tissue-engineered hypertrophic chondrocyte grafts enhanced long bone repair.* Biomaterials, 2017. **139**: p. 202-212.
154. De Long, W.G., Jr., et al., *Bone grafts and bone graft substitutes in orthopaedic trauma surgery. A critical analysis.* J Bone Joint Surg Am, 2007. **89**(3): p. 649-58.
155. Ravindran, S., et al., *Biomimetic extracellular matrix-incorporated scaffold induces osteogenic gene expression in human marrow stromal cells.* Tissue Eng Part A, 2012. **18**(3-4): p. 295-309.
156. Barradas, A.M., et al., *Osteoinductive biomaterials: current knowledge of properties, experimental models and biological mechanisms.* Eur Cell Mater, 2011. **21**: p. 407-29; discussion 429.
157. Frantz, C., K.M. Stewart, and V.M. Weaver, *The extracellular matrix at a glance.* Journal of cell science, 2010. **123**(24): p. 4195-4200.
158. Hussey, G.S., J.L. Dziki, and S.F. Badylak, *Extracellular matrix-based materials for regenerative medicine.* Nature Reviews Materials, 2018. **3**(7): p. 159-173.
159. Reilly, G.C. and A.J. Engler, *Intrinsic extracellular matrix properties regulate stem cell differentiation.* Journal of biomechanics, 2010. **43**(1): p. 55-62.
160. Fitzpatrick, L.E. and T.C. McDevitt, *Cell-derived matrices for tissue engineering and regenerative medicine applications.* Biomaterials science, 2015. **3**(1): p. 12-24.
161. Stevens, M.M. and J.H. George, *Exploring and engineering the cell surface interface.* Science, 2005. **310**(5751): p. 1135-1138.
162. Hynes, R.O., *The extracellular matrix: not just pretty fibrils.* Science, 2009. **326**(5957): p. 1216-1219.
163. Tsiridis, E., N. Upadhyay, and P. Giannoudis, *Molecular aspects of fracture healing: which are the important molecules?* Injury, 2007. **38**(1): p. S11-S25.
164. Hayrapetyan, A., J.A. Jansen, and J.J. van den Beucken, *Signaling pathways involved in osteogenesis and their application for bone regenerative medicine.* Tissue Engineering Part B: Reviews, 2015. **21**(1): p. 75-87.
165. Hutmacher, D.W., et al., *State of the art and future directions of scaffold-based bone engineering from a biomaterials perspective.* Journal of tissue engineering and regenerative medicine, 2007. **1**(4): p. 245-260.
166. Jeong, J., et al., *Bioactive calcium phosphate materials and applications in bone regeneration.* Biomaterials research, 2019. **23**(1): p. 1-11.
167. De Witte, T.-M., et al., *Bone tissue engineering via growth factor delivery: from scaffolds to complex matrices.* Regenerative biomaterials, 2018. **5**(4): p. 197-211.
168. Zhang, H., M. Ahmad, and G. Gronowicz, *Effects of transforming growth factor-beta 1 (TGF-β1) on in vitro mineralization of human osteoblasts on implant materials.* Biomaterials, 2003. **24**(12): p. 2013-2020.

169. Yang, S., et al., *In vitro and in vivo synergistic interactions between the Runx2/Cbfa1 transcription factor and bone morphogenetic protein-2 in stimulating osteoblast differentiation.* Journal of Bone and Mineral Research, 2003. **18**(4): p. 705-715.
170. Kaigler, D., et al., *VEGF scaffolds enhance angiogenesis and bone regeneration in irradiated osseous defects.* Journal of bone and mineral research, 2006. **21**(5): p. 735-744.
171. Shekaran, A. and A.J. García, *Extracellular matrix-mimetic adhesive biomaterials for bone repair.* Journal of biomedical materials research Part A, 2011. **96**(1): p. 261-272.
172. Röhlecke, C., et al., *Synergistic effect of titanium alloy and collagen type I on cell adhesion, proliferation and differentiation of osteoblast-like cells.* Cells Tissues Organs, 2001. **168**(3): p. 178-187.
173. Carvalho, M.S., et al., *Biomimetic matrices for rapidly forming mineralized bone tissue based on stem cell-mediated osteogenesis.* Scientific reports, 2018. **8**(1): p. 1-16.
174. Carvalho, M.S., et al., *Cultured cell-derived extracellular matrices to enhance the osteogenic differentiation and angiogenic properties of human mesenchymal stem/stromal cells.* Journal of tissue engineering and regenerative medicine, 2019. **13**(9): p. 1544-1558.
175. Song, J.J. and H.C. Ott, *Organ engineering based on decellularized matrix scaffolds.* Trends in molecular medicine, 2011. **17**(8): p. 424-432.
176. Benders, K.E., et al., *Extracellular matrix scaffolds for cartilage and bone regeneration.* Trends in biotechnology, 2013. **31**(3): p. 169-176.
177. Livesey, S.A., et al., *Transplanted acellular allograft dermal matrix. Potential as a template for the reconstruction of viable dermis.* Transplantation, 1995. **60**(1): p. 1-9.
178. Chen, R.-N., et al., *Process development of an acellular dermal matrix (ADM) for biomedical applications.* Biomaterials, 2004. **25**(13): p. 2679-2686.
179. Badylak, S.F., et al., *The use of xenogeneic small intestinal submucosa as a biomaterial for Achille's tendon repair in a dog model.* Journal of biomedical materials research, 1995. **29**(8): p. 977-985.
180. Mosala Nezhad, Z., et al., *Small intestinal submucosa extracellular matrix (CorMatrix®) in cardiovascular surgery: a systematic review.* Interactive cardiovascular and thoracic surgery, 2016. **22**(6): p. 839-850.
181. Parmaksiz, M., A.E. Elcin, and Y.M. Elcin, *Decellularization of bovine small intestinal submucosa and its use for the healing of a critical-sized full-thickness skin defect, alone and in combination with stem cells, in a small rodent model.* Journal of tissue engineering and regenerative medicine, 2017. **11**(6): p. 1754-1765.
182. Seif-Naraghi, S.B., et al., *Design and characterization of an injectable pericardial matrix gel: a potentially autologous scaffold for cardiac tissue engineering.* Tissue Engineering Part A, 2010. **16**(6): p. 2017-2027.
183. Hülsmann, J., et al., *Transplantation material bovine pericardium: biomechanical and immunogenic characteristics after decellularization vs. glutaraldehyde-fixing.* Xenotransplantation, 2012. **19**(5): p. 286-297.
184. Morticelli, L., et al., *Investigation of the suitability of decellularized porcine pericardium in mitral valve reconstruction.* J Heart Valve Dis, 2013. **22**(3): p. 340-53.
185. Chen, F., J.J. Yoo, and A. Atala, *Acellular collagen matrix as a possible "off the shelf" biomaterial for urethral repair.* Urology, 1999. **54**(3): p. 407-410.
186. Freytes, D.O., et al., *Biaxial strength of multilaminated extracellular matrix scaffolds.* Biomaterials, 2004. **25**(12): p. 2353-2361.
187. Kim, B.-S., A. Atala, and J.J. Yoo, *A collagen matrix derived from bladder can be used to engineer smooth muscle tissue.* World journal of urology, 2008. **26**(4): p. 307-314.
188. Flynn, L., *The use of decellularized adipose tissue to provide an inductive microenvironment for the adipogenic differentiation of human adipose-derived stem cells.* Biomaterials, 2010. **31**(17): p. 4715-4724.

189. Yu, C., et al., *Porous decellularized adipose tissue foams for soft tissue regeneration.* Biomaterials, 2013. **34**(13): p. 3290-3302.
190. Dunne, L.W., et al., *Human decellularized adipose tissue scaffold as a model for breast cancer cell growth and drug treatments.* Biomaterials, 2014. **35**(18): p. 4940-4949.
191. Conklin, B., et al., *Development and evaluation of a novel decellularized vascular xenograft.* Medical engineering & physics, 2002. **24**(3): p. 173-183.
192. Grandi, C., et al., *Decellularized bovine reinforced vessels for small-diameter tissue-engineered vascular grafts.* International journal of molecular medicine, 2011. **28**(3): p. 315-325.
193. Kim, B.S., J.J. Yoo, and A. Atala, *Peripheral nerve regeneration using acellular nerve grafts.* Journal of Biomedical Materials Research Part A: An Official Journal of The Society for Biomaterials, The Japanese Society for Biomaterials, and The Australian Society for Biomaterials and the Korean Society for Biomaterials, 2004. **68**(2): p. 201-209.
194. Karabekmez, F.E., A. Duymaz, and S.L. Moran, *Early clinical outcomes with the use of decellularized nerve allograft for repair of sensory defects within the hand*. 2009, SAGE Publications Sage CA: Los Angeles, CA.
195. Szynkaruk, M., et al., *Experimental and clinical evidence for use of decellularized nerve allografts in peripheral nerve gap reconstruction.* Tissue Engineering Part B: Reviews, 2013. **19**(1): p. 83-96.
196. Macchiarini, P., et al., *Clinical transplantation of a tissue-engineered airway.* The Lancet, 2008. **372**(9655): p. 2023-2030.
197. Wolf, M.T., et al., *Biologic scaffold composed of skeletal muscle extracellular matrix.* Biomaterials, 2012. **33**(10): p. 2916-2925.
198. Fishman, J.M., et al., *Decellularized rabbit cricoarytenoid dorsalis muscle for laryngeal regeneration.* Annals of Otology, Rhinology & Laryngology, 2012. **121**(2): p. 129-138.
199. Lin, C.-H., et al., *Evaluation of decellularized extracellular matrix of skeletal muscle for tissue engineering.* The International journal of artificial organs, 2014. **37**(7): p. 546-555.
200. Cartmell, J.S. and M.G. Dunn, *Effect of chemical treatments on tendon cellularity and mechanical properties.* Journal of Biomedical Materials Research: An Official Journal of The Society for Biomaterials, The Japanese Society for Biomaterials, and The Australian Society for Biomaterials and the Korean Society for Biomaterials, 2000. **49**(1): p. 134-140.
201. Ning, L.J., et al., *Preparation and characterization of decellularized tendon slices for tendon tissue engineering.* Journal of biomedical materials research Part A, 2012. **100**(6): p. 1448-1456.
202. Youngstrom, D.W., et al., *Functional characterization of detergent-decellularized equine tendon extracellular matrix for tissue engineering applications.* PloS one, 2013. **8**(5).
203. Woods, T. and P.F. Gratzer, *Effectiveness of three extraction techniques in the development of a decellularized bone–anterior cruciate ligament–bone graft.* Biomaterials, 2005. **26**(35): p. 7339-7349.
204. Harrison, R.D. and P.F. Gratzer, *Effect of extraction protocols and epidermal growth factor on the cellular repopulation of decellularized anterior cruciate ligament allografts.* Journal of Biomedical Materials Research Part A: An Official Journal of The Society for Biomaterials, The Japanese Society for Biomaterials, and The Australian Society for Biomaterials and the Korean Society for Biomaterials, 2005. **75**(4): p. 841-854.
205. Hashimoto, Y., et al., *The effect of decellularized bone/bone marrow produced by high-hydrostatic pressurization on the osteogenic differentiation of mesenchymal stem cells.* Biomaterials, 2011. **32**(29): p. 7060-7.
206. Gruskin, E., et al., *Demineralized bone matrix in bone repair: history and use.* Adv Drug Deliv Rev, 2012. **64**(12): p. 1063-77.

207. Marcos-Campos, I., et al., *Bone scaffold architecture modulates the development of mineralized bone matrix by human embryonic stem cells.* Biomaterials, 2012. **33**(33): p. 8329-42.
208. Parmaksiz, M., et al., *Clinical applications of decellularized extracellular matrices for tissue engineering and regenerative medicine.* Biomedical materials, 2016. **11**(2): p. 022003.
209. Nakamura, N., T. Kimura, and A. Kishida, *Overview of the development, applications, and future perspectives of decellularized tissues and organs.* ACS Biomaterials Science & Engineering, 2017. **3**(7): p. 1236-1244.
210. Chen, G. and N. Kawazoe, *Biomimetic Extracellular Matrices and Scaffolds Prepared from Cultured Cells.* Adv Exp Med Biol, 2018. **1078**: p. 465-474.
211. Carvalho, M.S., et al., *Co-culture cell-derived extracellular matrix loaded electrospun microfibrous scaffolds for bone tissue engineering.* Mater Sci Eng C Mater Biol Appl, 2019. **99**: p. 479-490.
212. Hoshiba, T., et al., *Development of stepwise osteogenesis-mimicking matrices for the regulation of mesenchymal stem cell functions.* Journal of Biological Chemistry, 2009. **284**(45): p. 31164-31173.
213. Nishimura, R., et al., *Signal transduction and transcriptional regulation during mesenchymal cell differentiation.* Journal of bone and mineral metabolism, 2008. **26**(3): p. 203.
214. Midwood, K.S., L.V. Williams, and J.E. Schwarzbauer, *Tissue repair and the dynamics of the extracellular matrix.* The international journal of biochemistry & cell biology, 2004. **36**(6): p. 1031-1037.
215. Daley, W.P., S.B. Peters, and M. Larsen, *Extracellular matrix dynamics in development and regenerative medicine.* Journal of cell science, 2008. **121**(3): p. 255-264.
216. Hoshiba, T., et al., *Decellularized matrices for tissue engineering.* Expert opinion on biological therapy, 2010. **10**(12): p. 1717-1728.
217. Heath, D.E., *A Review of Decellularized Extracellular Matrix Biomaterials for Regenerative Engineering Applications.* Regenerative Engineering and Translational Medicine, 2019. **5**(2): p. 155-166.
218. Bourgine, P., et al., *Combination of immortalization and inducible death strategies to generate a human mesenchymal stromal cell line with controlled survival.* Stem Cell Res, 2014. **12**(2): p. 584-98.
219. Kusuma, G.D., et al., *Decellularized extracellular matrices produced from immortal cell lines derived from different parts of the placenta support primary mesenchymal stem cell expansion.* PloS one, 2017. **12**(2).
220. Cheng, C.W., L.D. Solorio, and E. Alsberg, *Decellularized tissue and cell-derived extracellular matrices as scaffolds for orthopaedic tissue engineering.* Biotechnol Adv, 2014. **32**(2): p. 462-84.
221. Badylak, S.F., D. Taylor, and K. Uygun, *Whole-organ tissue engineering: decellularization and recellularization of three-dimensional matrix scaffolds.* Annual review of biomedical engineering, 2011. **13**: p. 27-53.
222. Zouhair, S., et al., *Preservation strategies for decellularized pericardial scaffolds for off-the-shelf availability.* Acta biomaterialia, 2019. **84**: p. 208-221.
223. Crapo, P.M., T.W. Gilbert, and S.F. Badylak, *An overview of tissue and whole organ decellularization processes.* Biomaterials, 2011. **32**(12): p. 3233-3243.
224. Gilbert, T.W., T.L. Sellaro, and S.F. Badylak, *Decellularization of tissues and organs.* Biomaterials, 2006. **27**(19): p. 3675-3683.
225. Wong, M.L. and L.G. Griffiths, *Immunogenicity in xenogeneic scaffold generation: antigen removal vs. decellularization.* Acta biomaterialia, 2014. **10**(5): p. 1806-1816.
226. Keane, T.J., I.T. Swinehart, and S.F. Badylak, *Methods of tissue decellularization used for preparation of biologic scaffolds and in vivo relevance.* Methods, 2015. **84**: p. 25-34.

227. Gilpin, A. and Y. Yang, *Decellularization strategies for regenerative medicine: from processing techniques to applications.* BioMed research international, 2017. **2017**.
228. Reing, J.E., et al., *The effects of processing methods upon mechanical and biologic properties of porcine dermal extracellular matrix scaffolds.* Biomaterials, 2010. **31**(33): p. 8626-8633.
229. White, L.J., et al., *The impact of detergents on the tissue decellularization process: a ToF-SIMS study.* Acta biomaterialia, 2017. **50**: p. 207-219.
230. Fitzpatrick, J.C., P.M. Clark, and F.M. Capaldi, *Effect of decellularization protocol on the mechanical behavior of porcine descending aorta.* International journal of biomaterials, 2010. **2010**.
231. Klebe, R.J., *Isolation of a collagen-dependent cell attachment factor.* Nature, 1974. **250**(5463): p. 248-251.
232. Gailit, J. and E. Ruoslahti, *Regulation of the fibronectin receptor affinity by divalent cations.* Journal of Biological Chemistry, 1988. **263**(26): p. 12927-12932.
233. Maurer, P. and E. Hohenester, *Structural and functional aspects of calcium binding in extracellular matrix proteins.* Matrix biology, 1997. **15**(8-9): p. 569-580.
234. Bourgine, P.E., et al., *Tissue decellularization by activation of programmed cell death.* Biomaterials, 2013. **34**(26): p. 6099-108.
235. Tey, S.K., et al., *Inducible caspase 9 suicide gene to improve the safety of allodepleted T cells after haploidentical stem cell transplantation.* Biol Blood Marrow Transplant, 2007. **13**(8): p. 913-24.
236. Van Engeland, M., et al., *Plasma membrane alterations and cytoskeletal changes in apoptosis.* Experimental cell research, 1997. **235**(2): p. 421-430.
237. Raff, M., *Cell suicide for beginners.* Nature, 1998. **396**(6707): p. 119-119.
238. Wei, W., et al., *In vitro osteogenic induction of bone marrow mesenchymal stem cells with a decellularized matrix derived from human adipose stem cells and in vivo implantation for bone regeneration.* Journal of Materials Chemistry B, 2017. **5**(13): p. 2468-2482.
239. Lai, Y., et al., *Reconstitution of marrow-derived extracellular matrix ex vivo: a robust culture system for expanding large-scale highly functional human mesenchymal stem cells.* Stem cells and development, 2010. **19**(7): p. 1095-1107.
240. Zhang, Z., et al., *Bone marrow stromal cell-derived extracellular matrix promotes osteogenesis of adipose-derived stem cells.* Cell biology international, 2015. **39**(3): p. 291-299.
241. Zeitouni, S., et al., *Human mesenchymal stem cell–derived matrices for enhanced osteoregeneration.* Science translational medicine, 2012. **4**(132): p. 132ra55-132ra55.
242. Sadr, N., et al., *Enhancing the biological performance of synthetic polymeric materials by decoration with engineered, decellularized extracellular matrix.* Biomaterials, 2012. **33**(20): p. 5085-5093.
243. Baroncelli, M., et al., *Human osteoblast-derived extracellular matrix with high homology to bone proteome is osteopromotive.* Tissue Engineering Part A, 2018. **24**(17-18): p. 1377-1389.
244. Takeshita, K., et al., *Xenotransplantation of interferon-gamma-pretreated clumps of a human mesenchymal stem cell/extracellular matrix complex induces mouse calvarial bone regeneration.* Stem cell research & therapy, 2017. **8**(1): p. 101.
245. Deutsch, E.R. and R.E. Guldberg, *Stem cell-synthesized extracellular matrix for bone repair.* Journal of Materials Chemistry, 2010. **20**(40): p. 8942-8951.
246. Kang, Y., et al., *The osteogenic differentiation of human bone marrow MSCs on HUVEC-derived ECM and β-TCP scaffold.* Biomaterials, 2012. **33**(29): p. 6998-7007.
247. Tour, G., M. Wendel, and I. Tcacencu, *Human fibroblast-derived extracellular matrix constructs for bone tissue engineering applications.* Journal of Biomedical Materials Research Part A, 2013. **101**(10): p. 2826-2837.

248. Xing, Q., et al., *Osteogenic differentiation evaluation of an engineered extracellular matrix based tissue sheet for potential periosteum replacement.* ACS applied materials & interfaces, 2015. **7**(41): p. 23239-23247.
249. Kim, I.G., et al., *Bioactive cell-derived matrices combined with polymer mesh scaffold for osteogenesis and bone healing.* Biomaterials, 2015. **50**: p. 75-86.
250. Pati, F., et al., *Ornamenting 3D printed scaffolds with cell-laid extracellular matrix for bone tissue regeneration.* Biomaterials, 2015. **37**: p. 230-241.
251. Shtrichman, R., et al., *The generation of hybrid electrospun nanofiber layer with extracellular matrix derived from human pluripotent stem cells, for regenerative medicine applications.* Tissue Engineering Part A, 2014. **20**(19-20): p. 2756-2767.
252. Chen, X.D., et al., *Extracellular matrix made by bone marrow cells facilitates expansion of marrow-derived mesenchymal progenitor cells and prevents their differentiation into osteoblasts.* Journal of bone and mineral research, 2007. **22**(12): p. 1943-1956.
253. Fu, Y., et al., *ECM decorated electrospun nanofiber for improving bone tissue regeneration.* Polymers, 2018. **10**(3): p. 272.
254. Kumar, A., K. Nune, and R. Misra, *Biological functionality of extracellular matrix-ornamented three-dimensional printed hydroxyapatite scaffolds.* Journal of Biomedical Materials Research Part A, 2016. **104**(6): p. 1343-1351.
255. Ma, J., et al., *Biomimetic matrix fabricated by LMP-1 gene-transduced MC3T3-E1 cells for bone regeneration.* Biofabrication, 2017. **9**(4): p. 045010.
256. Narayanan, K., et al., *Three-dimensional reconstituted extracellular matrix scaffolds for tissue engineering.* Biomaterials, 2009. **30**(26): p. 4309-4317.
257. Gao, C.-Y., et al., *Directing osteogenic differentiation of BMSCs by cell-secreted decellularized extracellular matrixes from different cell types.* Journal of Materials Chemistry B, 2018. **6**(45): p. 7471-7485.
258. Datta, N., et al., *Effect of bone extracellular matrix synthesized in vitro on the osteoblastic differentiation of marrow stromal cells.* Biomaterials, 2005. **26**(9): p. 971-977.
259. Pham, Q.P., et al., *The influence of an in vitro generated bone-like extracellular matrix on osteoblastic gene expression of marrow stromal cells.* Biomaterials, 2008. **29**(18): p. 2729-2739.
260. Kwon, S.-H., et al., *Modulation of BMP-2-induced chondrogenic versus osteogenic differentiation of human mesenchymal stem cells by cell-specific extracellular matrices.* Tissue Engineering Part A, 2013. **19**(1-2): p. 49-58.
261. Tour, G., M. Wendel, and I. Tcacencu, *Cell-derived matrix enhances osteogenic properties of hydroxyapatite.* Tissue Eng Part A, 2011. **17**(1-2): p. 127-37.
262. Bourgine, P.E., et al., *Engineered extracellular matrices as biomaterials of tunable composition and function.* Advanced Functional Materials, 2017. **27**(7): p. 1605486.
263. Sun, Y., et al., *Rescuing replication and osteogenesis of aged mesenchymal stem cells by exposure to a young extracellular matrix.* The FASEB Journal, 2011. **25**(5): p. 1474-1485.
264. Rosales, A.M. and K.S. Anseth, *The design of reversible hydrogels to capture extracellular matrix dynamics.* Nature Reviews Materials, 2016. **1**(2): p. 1-15.
265. Chen, Y., et al., *PLGA-collagen-ECM hybrid meshes mimicking stepwise osteogenesis and their influence on the osteogenic differentiation of hMSCs.* Biofabrication, 2020. **12**(2): p. 025027.
266. Dalton, P.D., et al., *Electrospinning and additive manufacturing: converging technologies.* Biomaterials Science, 2013. **1**(2): p. 171-185.
267. Roseti, L., et al., *Scaffolds for bone tissue engineering: state of the art and new perspectives.* Materials Science and Engineering: C, 2017. **78**: p. 1246-1262.
268. Badylak, S.F., *The extracellular matrix as a biologic scaffold material.* Biomaterials, 2007. **28**(25): p. 3587-3593.

269. Bourgine, P.E., *Hard Material Modulation for (Skeletal) Tissue Engineering Purposes*, in *Cell Engineering and Regeneration*, J.M. Gimble, et al., Editors. 2019, Springer International Publishing: Cham. p. 1-18.
270. Thibault, R.A., et al., *Osteogenic differentiation of mesenchymal stem cells on pregenerated extracellular matrix scaffolds in the absence of osteogenic cell culture supplements.* Tissue Eng Part A, 2010. **16**(2): p. 431-40.
271. Thibault, R.A., A.G. Mikos, and F.K. Kasper, *Osteogenic differentiation of mesenchymal stem cells on demineralized and devitalized biodegradable polymer and extracellular matrix hybrid constructs.* Journal of biomedical materials research. Part A, 2013. **101**(5): p. 1225.
272. Jeon, H., et al., *Nanostructured surface of electrospun PCL/dECM fibres treated with oxygen plasma for tissue engineering.* RSC advances, 2016. **6**(39): p. 32887-32896.
273. Silva, J.C., et al., *Extracellular matrix decorated polycaprolactone scaffolds for improved mesenchymal stem/stromal cell osteogenesis towards a patient-tailored bone tissue engineering approach.* Journal of Biomedical Materials Research Part B: Applied Biomaterials, 2020.
274. Kim, B., R. Ventura, and B.T. Lee, *Functionalization of porous BCP scaffold by generating cell-derived extracellular matrix from rat bone marrow stem cells culture for bone tissue engineering.* Journal of tissue engineering and regenerative medicine, 2018. **12**(2): p. e1256-e1267.
275. Kang, Y., et al., *Creation of bony microenvironment with CaP and cell-derived ECM to enhance human bone-marrow MSC behavior and delivery of BMP-2.* Biomaterials, 2011. **32**(26): p. 6119-6130.
276. Antebi, B., et al., *Stromal-cell-derived extracellular matrix promotes the proliferation and retains the osteogenic differentiation capacity of mesenchymal stem cells on three-dimensional scaffolds.* Tissue Engineering Part C: Methods, 2015. **21**(2): p. 171-181.
277. Burgio, F., et al., *Characterization and in ovo vascularization of a 3D-printed hydroxyapatite scaffold with different extracellular matrix coatings under perfusion culture.* Biology open, 2018. **7**(12).
278. Datta, N., et al., *In vitro generated extracellular matrix and fluid shear stress synergistically enhance 3D osteoblastic differentiation.* Proceedings of the National Academy of Sciences, 2006. **103**(8): p. 2488-2493.
279. Pham, Q.P., et al., *Analysis of the osteoinductive capacity and angiogenicity of an in vitro generated extracellular matrix.* Journal of Biomedical Materials Research Part A, 2009. **88**(2): p. 295-303.
280. Kumar, A., K. Nune, and R. Misra, *Biological functionality and mechanistic contribution of extracellular matrix-ornamented three dimensional Ti-6Al-4V mesh scaffolds.* Journal of Biomedical Materials Research Part A, 2016. **104**(11): p. 2751-2763.
281. Chai, Y.C., et al., *Harnessing the osteogenicity of in vitro stem cell-derived mineralized extracellular matrix as 3D biotemplate to guide bone regeneration.* Tissue Engineering Part A, 2017. **23**(17-18): p. 874-890.
282. Junka, R. and X. Yu, *Polymeric nanofibrous scaffolds laden with cell-derived extracellular matrix for bone regeneration.* Materials Science and Engineering: C, 2020: p. 110981.
283. Decaris, M.L., et al., *Cell-derived matrix coatings for polymeric scaffolds.* Tissue engineering Part A, 2012. **18**(19-20): p. 2148-2157.
284. Liu, S., et al., *Off-the-shelf biomimetic graphene oxide–collagen hybrid scaffolds wrapped with osteoinductive extracellular matrix for the repair of cranial defects in rats.* ACS applied materials & interfaces, 2018. **10**(49): p. 42948-42958.
285. Lu, H., et al., *Autologous extracellular matrix scaffolds for tissue engineering.* Biomaterials, 2011. **32**(10): p. 2489-2499.

286. Jukes, J.M., et al., *Endochondral bone tissue engineering using embryonic stem cells.* Proceedings of the National Academy of Sciences, 2008. **105**(19): p. 6840-6845.
287. Janicki, P., et al., *Chondrogenic pre-induction of human mesenchymal stem cells on β-TCP: enhanced bone quality by endochondral heterotopic bone formation.* Acta biomaterialia, 2010. **6**(8): p. 3292-3301.
288. Farrell, E., et al., *In-vivo generation of bone via endochondral ossification by in-vitro chondrogenic priming of adult human and rat mesenchymal stem cells.* BMC musculoskeletal disorders, 2011. **12**(1): p. 31.
289. Sheehy, E.J., et al., *Engineering osteochondral constructs through spatial regulation of endochondral ossification.* Acta biomaterialia, 2013. **9**(3): p. 5484-5492.
290. Bahney, C.S., et al., *Stem cell–derived endochondral cartilage stimulates bone healing by tissue transformation.* Journal of Bone and Mineral Research, 2014. **29**(5): p. 1269-1282.
291. Awad, H.A., et al., *Bone tissue engineering: clinical challenges and emergent advances in orthopedic and craniofacial surgery*, in *Principles of Tissue Engineering*. 2014, Elsevier. p. 1733-1743.
292. Cunniffe, G.M., et al., *Porous decellularized tissue engineered hypertrophic cartilage as a scaffold for large bone defect healing.* Acta Biomaterialia, 2015. **23**: p. 82-90.
293. Todorov, A., et al., *Fat-Derived Stromal Vascular Fraction Cells Enhance the Bone-Forming Capacity of Devitalized Engineered Hypertrophic Cartilage Matrix.* Stem cells translational medicine, 2016. **5**(12): p. 1684-1694.
294. Bourgine, P.E., et al., *Osteoinductivity of engineered cartilaginous templates devitalized by inducible apoptosis.* Proc Natl Acad Sci U S A, 2014. **111**(49): p. 17426-31.
295. Quang Le, B., C. Van Blitterswijk, and J. De Boer, *An approach to in vitro manufacturing of hypertrophic cartilage matrix for bone repair.* Bioengineering, 2017. **4**(2): p. 35.
296. Bracaglia, L.G., et al., *3D printing for the design and fabrication of polymer-based gradient scaffolds.* Acta Biomater, 2017. **56**: p. 3-13.
297. Guillemot, F., V. Mironov, and M. Nakamura, *Bioprinting is coming of age: Report from the International Conference on Bioprinting and Biofabrication in Bordeaux (3B'09).* Biofabrication, 2010. **2**(1): p. 010201.
298. Gopinathan, J. and I. Noh, *Recent trends in bioinks for 3D printing.* Biomater Res, 2018. **22**: p. 11.
299. Ozbolat, I.T., W. Peng, and V. Ozbolat, *Application areas of 3D bioprinting.* Drug Discov Today, 2016. **21**(8): p. 1257-71.
300. Bishop, E.S., et al., *3-D bioprinting technologies in tissue engineering and regenerative medicine: Current and future trends.* Genes Dis, 2017. **4**(4): p. 185-195.
301. Derakhshanfar, S., et al., *3D bioprinting for biomedical devices and tissue engineering: A review of recent trends and advances.* Bioact Mater, 2018. **3**(2): p. 144-156.
302. Melchels, F.P., et al., *Additive manufacturing of tissues and organs.* Progress in Polymer Science, 2012. **37**(8): p. 1079-1104.
303. Lee, W., et al., *Multi-layered culture of human skin fibroblasts and keratinocytes through three-dimensional freeform fabrication.* Biomaterials, 2009. **30**(8): p. 1587-95.
304. Cohen, D.L., et al., *Increased mixing improves hydrogel homogeneity and quality of three-dimensional printed constructs.* Tissue Eng Part C Methods, 2011. **17**(2): p. 239-48.
305. Duan, B., et al., *3D bioprinting of heterogeneous aortic valve conduits with alginate/gelatin hydrogels.* J Biomed Mater Res A, 2013. **101**(5): p. 1255-64.
306. Duan, B., et al., *Three-dimensional printed trileaflet valve conduits using biological hydrogels and human valve interstitial cells.* Acta biomaterialia, 2014. **10**(5): p. 1836-1846.
307. Cui, X., et al., *Direct human cartilage repair using three-dimensional bioprinting technology.* Tissue Eng Part A, 2012. **18**(11-12): p. 1304-12.

308. Fedorovich, N.E., et al., *Hydrogels as extracellular matrices for skeletal tissue engineering: state-of-the-art and novel application in organ printing.* Tissue Eng, 2007. **13**(8): p. 1905-25.
309. Jia, W., et al., *Direct 3D bioprinting of perfusable vascular constructs using a blend bioink.* Biomaterials, 2016. **106**: p. 58-68.
310. Vanaei, S., et al., *An overview on materials and techniques in 3d bioprinting toward biomedical application.* Engineered Regeneration, 2021. **2**: p. 1-18.
311. Bose, S., S. Vahabzadeh, and A. Bandyopadhyay, *Bone tissue engineering using 3D printing.* Materials today, 2013. **16**(12): p. 496-504.
312. Fedorovich, N.E., et al., *Distinct tissue formation by heterogeneous printing of osteo- and endothelial progenitor cells.* Tissue Eng Part A, 2011. **17**(15-16): p. 2113-21.
313. Ahlfeld, T., et al., *Bioprinting of mineralized constructs utilizing multichannel plotting of a self-setting calcium phosphate cement and a cell-laden bioink.* Biofabrication, 2018. **10**(4): p. 045002.
314. Malda, J. and J. Groll, *A Step Towards Clinical Translation of Biofabrication.* Trends Biotechnol, 2016. **34**(5): p. 356-357.
315. Billiet, T., et al., *A review of trends and limitations in hydrogel-rapid prototyping for tissue engineering.* Biomaterials, 2012. **33**(26): p. 6020-41.
316. Malda, J., et al., *25th anniversary article: Engineering hydrogels for biofabrication.* Adv Mater, 2013. **25**(36): p. 5011-28.
317. Mironov, V., et al., *Organ printing: promises and challenges.* Regen Med, 2008. **3**(1): p. 93-103.
318. Derby, B., *Printing and prototyping of tissues and scaffolds.* Science, 2012. **338**(6109): p. 921-6.
319. Ferris, C.J., et al., *Biofabrication: an overview of the approaches used for printing of living cells.* Appl Microbiol Biotechnol, 2013. **97**(10): p. 4243-58.
320. Chimene, D., et al., *Advanced Bioinks for 3D Printing: A Materials Science Perspective.* Ann Biomed Eng, 2016. **44**(6): p. 2090-102.
321. Kyle, S., et al., *'Printability' of Candidate Biomaterials for Extrusion Based 3D Printing: State-of-the-Art.* Adv Healthc Mater, 2017. **6**(16).
322. Christensen, K., et al., *Freeform inkjet printing of cellular structures with bifurcations.* Biotechnol Bioeng, 2015. **112**(5): p. 1047-55.
323. Gao, Q., et al., *Coaxial nozzle-assisted 3D bioprinting with built-in microchannels for nutrients delivery.* Biomaterials, 2015. **61**: p. 203-15.
324. Kundu, J., et al., *An additive manufacturing-based PCL-alginate-chondrocyte bioprinted scaffold for cartilage tissue engineering.* J Tissue Eng Regen Med, 2015. **9**(11): p. 1286-97.
325. Shim, J.-H., et al., *Bioprinting of a mechanically enhanced three-dimensional dual cell-laden construct for osteochondral tissue engineering using a multi-head tissue/organ building system.* Journal of Micromechanics and Microengineering, 2012. **22**(8): p. 085014.
326. Levato, R., et al., *The bio in the ink: cartilage regeneration with bioprintable hydrogels and articular cartilage-derived progenitor cells.* Acta Biomater, 2017. **61**: p. 41-53.
327. Blaeser, A., et al., *Biofabrication under fluorocarbon: a novel freeform fabrication technique to generate high aspect ratio tissue-engineered constructs.* Biores Open Access, 2013. **2**(5): p. 374-84.
328. Fedorovich, N.E., et al., *Three-dimensional fiber deposition of cell-laden, viable, patterned constructs for bone tissue printing.* Tissue Engineering Part A, 2008. **14**(1): p. 127-133.
329. Kreimendahl, F., et al., *Three-Dimensional Printing and Angiogenesis: Tailored Agarose-Type I Collagen Blends Comprise Three-Dimensional Printability and Angiogenesis Potential for Tissue-Engineered Substitutes.* Tissue Eng Part C Methods, 2017. **23**(10): p. 604-615.

330. Mori, H., K. Shimizu, and M. Hara, *Dynamic viscoelastic properties of collagen gels with high mechanical strength.* Mater Sci Eng C Mater Biol Appl, 2013. **33**(6): p. 3230-6.
331. Rhee, S., et al., *3D bioprinting of spatially heterogeneous collagen constructs for cartilage tissue engineering.* ACS Biomaterials Science & Engineering, 2016. **2**(10): p. 1800-1805.
332. Yeo, M., et al., *An innovative collagen-based cell-printing method for obtaining human adipose stem cell-laden structures consisting of core–sheath structures for tissue engineering.* Biomacromolecules, 2016. **17**(4): p. 1365-1375.
333. Yeo, M.G. and G.H. Kim, *A cell-printing approach for obtaining hASC-laden scaffolds by using a collagen/polyphenol bioink.* Biofabrication, 2017. **9**(2): p. 025004.
334. Das, S., et al., *Bioprintable, cell-laden silk fibroin-gelatin hydrogel supporting multilineage differentiation of stem cells for fabrication of three-dimensional tissue constructs.* Acta Biomater, 2015. **11**: p. 233-46.
335. Rodriguez, M.J., et al., *Silk based bioinks for soft tissue reconstruction using 3-dimensional (3D) printing with in vitro and in vivo assessments.* Biomaterials, 2017. **117**: p. 105-115.
336. Highley, C.B., C.B. Rodell, and J.A. Burdick, *Direct 3D Printing of Shear-Thinning Hydrogels into Self-Healing Hydrogels.* Adv Mater, 2015. **27**(34): p. 5075-9.
337. Ouyang, L., et al., *3D printing of shear-thinning hyaluronic acid hydrogels with secondary cross-linking.* ACS Biomaterials Science & Engineering, 2016. **2**(10): p. 1743-1751.
338. Poldervaart, M.T., et al., *3D bioprinting of methacrylated hyaluronic acid (MeHA) hydrogel with intrinsic osteogenicity.* PLoS One, 2017. **12**(6): p. e0177628.
339. Mosesson, M.W., K.R. Siebenlist, and D.A. Meh, *The structure and biological features of fibrinogen and fibrin.* Ann N Y Acad Sci, 2001. **936**: p. 11-30.
340. Spotnitz, W.D. and R. Prabhu, *Fibrin sealant tissue adhesive--review and update.* J Long Term Eff Med Implants, 2005. **15**(3): p. 245-70.
341. Ahmed, T.A., E.V. Dare, and M. Hincke, *Fibrin: a versatile scaffold for tissue engineering applications.* Tissue Eng Part B Rev, 2008. **14**(2): p. 199-215.
342. Jockenhoevel, S., et al., *Fibrin gel -- advantages of a new scaffold in cardiovascular tissue engineering.* Eur J Cardiothorac Surg, 2001. **19**(4): p. 424-30.
343. Catelas, I., *Fibrin*, in *Comprehensive Biomaterials Vol 2*. 2011, Oxford: Elsevier. p. 303-328.
344. Cho, S.W., et al., *Enhancement of adipose tissue formation by implantation of adipogenic-differentiated preadipocytes.* Biochem Biophys Res Commun, 2006. **345**(2): p. 588-94.
345. Cummings, C.L., et al., *Properties of engineered vascular constructs made from collagen, fibrin, and collagen–fibrin mixtures.* Biomaterials, 2004. **25**(17): p. 3699-3706.
346. Divya, P. and L.K. Krishnan, *Glycosaminoglycans restrained in a fibrin matrix improve ECM remodelling by endothelial cells grown for vascular tissue engineering.* Journal of tissue engineering and regenerative medicine, 2009. **3**(5): p. 377-388.
347. Kneser, U., et al., *Engineering of vascularized transplantable bone tissues: induction of axial vascularization in an osteoconductive matrix using an arteriovenous loop.* Tissue engineering, 2006. **12**(7): p. 1721-1731.
348. Long, J.L. and R.T. Tranquillo, *Elastic fiber production in cardiovascular tissue-equivalents.* Matrix Biol, 2003. **22**(4): p. 339-50.
349. Mol, A., et al., *Fibrin as a cell carrier in cardiovascular tissue engineering applications.* Biomaterials, 2005. **26**(16): p. 3113-21.
350. Arnaud, E., *Advances in cranioplasty with osteoinductive biomaterials: summary of experimental studies and clinical prospects.* Child's Nervous System, 2000. **16**(10-11): p. 659-668.
351. Yamada, Y., et al., *Bone regeneration following injection of mesenchymal stem cells and fibrin glue with a biodegradable scaffold.* Journal of Cranio-Maxillofacial Surgery, 2003. **31**(1): p. 27-33.

352. Schmoekel, H.G., et al., *Bone repair with a form of BMP-2 engineered for incorporation into fibrin cell ingrowth matrices.* Biotechnology and bioengineering, 2005. **89**(3): p. 253-262.
353. Hendrickson, D.A., et al., *Chondrocyte-fibrin matrix transplants for resurfacing extensive articular cartilage defects.* Journal of orthopaedic research, 1994. **12**(4): p. 485-497.
354. Peretti, G.M., et al., *Review of injectable cartilage engineering using fibrin gel in mice and swine models.* Tissue Engineering, 2006. **12**(5): p. 1151-1168.
355. Park, S.-H., et al., *Chondrogenesis of rabbit mesenchymal stem cells in fibrin/hyaluronan composite scaffold in vitro.* Tissue Engineering Part A, 2011. **17**(9-10): p. 1277-1286.
356. Balestrini, J.L. and K.L. Billiar, *Equibiaxial cyclic stretch stimulates fibroblasts to rapidly remodel fibrin.* J Biomech, 2006. **39**(16): p. 2983-90.
357. Hojo, M., et al., *Induction of vascular endothelial growth factor by fibrin as a dermal substrate for cultured skin substitute.* Plast Reconstr Surg, 2003. **111**(5): p. 1638-45.
358. Gao, C., et al., *Siatic nerve regeneration in rats stimulated by fibrin glue containing nerve growth factor: an experimental study.* Injury, 2008. **39**(12): p. 1414-20.
359. Wood, M.D., et al., *Heparin-binding-affinity-based delivery systems releasing nerve growth factor enhance sciatic nerve regeneration.* Journal of Biomaterials Science, Polymer Edition, 2010. **21**(6-7): p. 771-787.
360. Wood, M.D., et al., *Fibrin matrices with affinity-based delivery systems and neurotrophic factors promote functional nerve regeneration.* Biotechnology and bioengineering, 2010. **106**(6): p. 970-979.
361. Dietrich, F. and P.I. Lelkes, *Fine-tuning of a three-dimensional microcarrier-based angiogenesis assay for the analysis of endothelial-mesenchymal cell co-cultures in fibrin and collagen gels.* Angiogenesis, 2006. **9**(3): p. 111-25.
362. Liu, J.Y., et al., *Functional tissue-engineered blood vessels from bone marrow progenitor cells.* Cardiovasc Res, 2007. **75**(3): p. 618-28.
363. Urech, L., et al., *Mechanical properties, proteolytic degradability and biological modifications affect angiogenic process extension into native and modified fibrin matrices in vitro.* Biomaterials, 2005. **26**(12): p. 1369-79.
364. Van Lieshout, M., et al., *A knitted, fibrin-covered polycaprolactone scaffold for tissue engineering of the aortic valve.* Tissue Eng, 2006. **12**(3): p. 481-7.
365. Venkatesan, J.K., et al., *Chondrogenic Differentiation Processes in Human Bone-Marrow Aspirates Seeded in Three-Dimensional-Woven Poly(varepsilon-Caprolactone) Scaffolds Enhanced by Recombinant Adeno-Associated Virus-Mediated SOX9 Gene Transfer.* Hum Gene Ther, 2018. **29**(11): p. 1277-1286.
366. Eyrich, D., et al., *Long-term stable fibrin gels for cartilage engineering.* Biomaterials, 2007. **28**(1): p. 55-65.
367. Dikovsky, D., H. Bianco-Peled, and D. Seliktar, *The effect of structural alterations of PEG-fibrinogen hydrogel scaffolds on 3-D cellular morphology and cellular migration.* Biomaterials, 2006. **27**(8): p. 1496-506.
368. Ahmed, T.A., M. Griffith, and M. Hincke, *Characterization and inhibition of fibrin hydrogel-degrading enzymes during development of tissue engineering scaffolds.* Tissue Eng, 2007. **13**(7): p. 1469-77.
369. Smith, J.D., et al., *Immobilization of aprotinin to fibrinogen as a novel method for controlling degradation of fibrin gels.* Bioconjug Chem, 2007. **18**(3): p. 695-701.
370. Briquez, P.S., et al., *Human Kunitz-type protease inhibitor engineered for enhanced matrix retention extends longevity of fibrin biomaterials.* Biomaterials, 2017. **135**: p. 1-9.
371. Fergusson, D.A., et al., *A comparison of aprotinin and lysine analogues in high-risk cardiac surgery.* N Engl J Med, 2008. **358**(22): p. 2319-31.
372. McEvoy, M.D., et al., *Aprotinin in cardiac surgery: a review of conventional and novel mechanisms of action.* Anesth Analg, 2007. **105**(4): p. 949-62.

373. Saupe, S.M. and T. Steinmetzer, *A new strategy for the development of highly potent and selective plasmin inhibitors.* J Med Chem, 2012. **55**(3): p. 1171-80.
374. Saupe, S.M., et al., *Development of new cyclic plasmin inhibitors with excellent potency and selectivity.* J Med Chem, 2013. **56**(3): p. 820-31.
375. Lorentz, K.M., et al., *Engineered aprotinin for improved stability of fibrin biomaterials.* Biomaterials, 2011. **32**(2): p. 430-8.
376. Kaiser, N.J., et al., *Optimizing Blended Collagen-Fibrin Hydrogels for Cardiac Tissue Engineering with Human iPSC-derived Cardiomyocytes.* ACS Biomater Sci Eng, 2019. **5**(2): p. 887-899.
377. Coffin, S.T. and G.R. Gaudette, *Aprotinin extends mechanical integrity time of cell-seeded fibrin sutures.* J Biomed Mater Res A, 2016. **104**(9): p. 2271-9.
378. Paul, M., et al., *Use of Clotted Human Plasma and Aprotinin in Skin Tissue Engineering: A Novel Approach to Engineering Composite Skin on a Porous Scaffold.* Tissue Eng Part C Methods, 2015. **21**(10): p. 1098-104.
379. Colosi, C., et al., *Microfluidic bioprinting of heterogeneous 3D tissue constructs using low-viscosity bioink.* Advanced materials, 2016. **28**(4): p. 677-684.
380. Xu, W., et al., *Rapid prototyping three-dimensional cell/gelatin/fibrinogen constructs for medical regeneration.* Journal of bioactive and compatible polymers, 2007. **22**(4): p. 363-377.
381. Zhang, K., et al., *3D bioprinting of urethra with PCL/PLCL blend and dual autologous cells in fibrin hydrogel: An in vitro evaluation of biomimetic mechanical property and cell growth environment.* Acta Biomater, 2017. **50**: p. 154-164.
382. Rutz, A.L., et al., *A multimaterial bioink method for 3D printing tunable, cell-compatible hydrogels.* Adv Mater, 2015. **27**(9): p. 1607-14.
383. England, S., et al., *Bioprinted fibrin-factor XIII-hyaluronate hydrogel scaffolds with encapsulated Schwann cells and their in vitro characterization for use in nerve regeneration.* Bioprinting, 2017. **5**: p. 1-9.
384. Li, S., et al., *Direct fabrication of a hybrid cell/hydrogel construct by a double-nozzle assembling technology.* Journal of Bioactive and Compatible Polymers, 2009. **24**(3): p. 249-265.
385. Li, S., et al., *Gradient hydrogel construct based on an improved cell assembling system.* Journal of Bioactive and Compatible Polymers, 2009. **24**(1_suppl): p. 84-99.
386. Xu, M., et al., *An cell-assembly derived physiological 3D model of the metabolic syndrome, based on adipose-derived stromal cells and a gelatin/alginate/fibrinogen matrix.* Biomaterials, 2010. **31**(14): p. 3868-3877.
387. Zhao, Y., et al., *Three-dimensional printing of Hela cells for cervical tumor model in vitro.* Biofabrication, 2014. **6**(3): p. 035001.
388. Zhou, X., C. Liu, and X. Wang, *A 3D bioprinting liver tumor model for drug screening.* World J. Pharm. Pharm. Sci, 2016. **5**: p. 196-213.
389. Lee, Y.B., et al., *Bio-printing of collagen and VEGF-releasing fibrin gel scaffolds for neural stem cell culture.* Exp Neurol, 2010. **223**(2): p. 645-52.
390. Xu, Y. and X. Wang, *Fluid and cell behaviors along a 3D printed alginate/gelatin/fibrin channel.* Biotechnol Bioeng, 2015. **112**(8): p. 1683-95.
391. Hinton, T.J., et al., *Three-dimensional printing of complex biological structures by freeform reversible embedding of suspended hydrogels.* Science advances, 2015. **1**(9): p. e1500758.
392. Lee, A., et al., *3D bioprinting of collagen to rebuild components of the human heart.* Science, 2019. **365**(6452): p. 482-487.
393. de Melo, B.A., et al., *3D Printed Cartilage-Like Tissue Constructs with Spatially Controlled Mechanical Properties.* Advanced functional materials, 2019: p. 1906330.
394. Betz, R.R., *Limitations of autograft and allograft: new synthetic solutions.* Orthopedics, 2002. **25**(5 Suppl): p. s561-70.

395. Thompson, E.M., et al., *Recapitulating endochondral ossification: a promising route to in vivo bone regeneration.* J Tissue Eng Regen Med, 2015. **9**(8): p. 889-902.
396. Visser, J., et al., *Endochondral bone formation in gelatin methacrylamide hydrogel with embedded cartilage-derived matrix particles.* Biomaterials, 2015. **37**: p. 174-182.
397. Thompson, E.M., et al., *An endochondral ossification-based approach to bone repair: chondrogenically primed mesenchymal stem cell-laden scaffolds support greater repair of critical-sized cranial defects than osteogenically stimulated constructs in vivo.* Tissue Engineering Part A, 2016. **22**(5-6): p. 556-567.
398. Matsiko, A., et al., *An endochondral ossification approach to early stage bone repair: Use of tissue-engineered hypertrophic cartilage constructs as primordial templates for weight-bearing bone repair.* J Tissue Eng Regen Med, 2018. **12**(4): p. e2147-e2150.
399. Lyons, F.G., et al., *The healing of bony defects by cell-free collagen-based scaffolds compared to stem cell-seeded tissue engineered constructs.* Biomaterials, 2010. **31**(35): p. 9232-43.
400. Mesallati, T., et al., *Tissue engineering scaled-up, anatomically shaped osteochondral constructs for joint resurfacing.* European Cells and Materials, 2015. **30**: p. 163-186.
401. Helgerson, s.S., et al., *Fibrin*, in *Encyclopedia of Biomaterials and Biomedical Engineering Vol 2*. 2007, CRC Press. p. 1072-1079.
402. Noori, A., et al., *A review of fibrin and fibrin composites for bone tissue engineering.* Int J Nanomedicine, 2017. **12**: p. 4937-4961.
403. Gerstenfeld, L.C., et al., *Fracture healing as a post-natal developmental process: molecular, spatial, and temporal aspects of its regulation.* J Cell Biochem, 2003. **88**(5): p. 873-84.
404. Shapiro, F., *Bone development and its relation to fracture repair. The role of mesenchymal osteoblasts and surface osteoblasts.* Eur Cell Mater, 2008. **15**: p. 53-76.
405. Rouwkema, J., N.C. Rivron, and C.A. van Blitterswijk, *Vascularization in tissue engineering.* Trends Biotechnol, 2008. **26**(8): p. 434-41.
406. Sheehy, E.J., C.T. Buckley, and D.J. Kelly, *Chondrocytes and bone marrow-derived mesenchymal stem cells undergoing chondrogenesis in agarose hydrogels of solid and channelled architectures respond differentially to dynamic culture conditions.* J Tissue Eng Regen Med, 2011. **5**(9): p. 747-58.
407. Mesallati, T., et al., *Scaffold architecture determines chondrocyte response to externally applied dynamic compression.* Biomech Model Mechanobiol, 2013. **12**(5): p. 889-99.
408. Daly, A.C., B.N. Sathy, and D.J. Kelly, *Engineering large cartilage tissues using dynamic bioreactor culture at defined oxygen conditions.* J Tissue Eng, 2018. **9**: p. 2041731417753718.
409. Cigan, A.D., et al., *Nutrient channels and stirring enhanced the composition and stiffness of large cartilage constructs.* J Biomech, 2014. **47**(16): p. 3847-54.
410. Cigan, A.D., et al., *Nutrient Channels Aid the Growth of Articular Surface-Sized Engineered Cartilage Constructs.* Tissue Eng Part A, 2016. **22**(17-18): p. 1063-74.
411. Cigan, A.D., et al., *Optimizing nutrient channel spacing and revisiting TGF-beta in large engineered cartilage constructs.* J Biomech, 2016. **49**(10): p. 2089-2094.
412. von der Mark, K. and H. von der Mark, *The role of three genetically distinct collagen types in endochondral ossification and calcification of cartilage.* J Bone Joint Surg Br, 1977. **59-B**(4): p. 458-64.
413. Knupp, C. and J.M. Squire, *Molecular packing in network-forming collagens.* Adv Protein Chem, 2005. **70**: p. 375-403.
414. Bächinger, H.P., et al., *Collagen formation and structure*, in *Comprehensive Natural Products II: Chemistry and Biology*. 2010, Elsevier Ltd.
415. Huey, D.J., J.C. Hu, and K.A. Athanasiou, *Unlike bone, cartilage regeneration remains elusive.* Science, 2012. **338**(6109): p. 917-921.

416. Mueller, M.B. and R.S. Tuan, *Functional characterization of hypertrophy in chondrogenesis of human mesenchymal stem cells.* Arthritis & Rheumatism, 2008. **58**(5): p. 1377-1388.
417. Pelttari, K., et al., *Premature induction of hypertrophy during in vitro chondrogenesis of human mesenchymal stem cells correlates with calcification and vascular invasion after ectopic transplantation in SCID mice.* Arthritis & Rheumatism: Official Journal of the American College of Rheumatology, 2006. **54**(10): p. 3254-3266.
418. BRIGHTON, C.T. and R.B. HEPPENSTALL, *Oxygen Tension in Zones of the Epiphyseal Plate, the Metaphysis and Diaphysis: AN: in Vitro: AND: in Viro: STUDY IN RATS AND RABBITS.* JBJS, 1971. **53**(4): p. 719-728.
419. Lafont, J.E., *Lack of oxygen in articular cartilage: consequences for chondrocyte biology.* International journal of experimental pathology, 2010. **91**(2): p. 99-106.
420. Zhou, S., Z. Cui, and J.P. Urban, *Factors influencing the oxygen concentration gradient from the synovial surface of articular cartilage to the cartilage–bone interface: a modeling study.* Arthritis & Rheumatism, 2004. **50**(12): p. 3915-3924.
421. Pattappa, G., et al., *The importance of physioxia in mesenchymal stem cell chondrogenesis and the mechanisms controlling its response.* International journal of molecular sciences, 2019. **20**(3): p. 484.
422. Lo, C.-M., et al., *Cell movement is guided by the rigidity of the substrate.* Biophysical journal, 2000. **79**(1): p. 144-152.
423. Yeung, T., et al., *Effects of substrate stiffness on cell morphology, cytoskeletal structure, and adhesion.* Cell motility and the cytoskeleton, 2005. **60**(1): p. 24-34.
424. Engler, A.J., et al., *Matrix elasticity directs stem cell lineage specification.* Cell, 2006. **126**(4): p. 677-689.
425. Kumar, G., et al., *Freeform fabricated scaffolds with roughened struts that enhance both stem cell proliferation and differentiation by controlling cell shape.* Biomaterials, 2012. **33**(16): p. 4022-4030.
426. McBeath, R., et al., *Cell shape, cytoskeletal tension, and RhoA regulate stem cell lineage commitment.* Developmental cell, 2004. **6**(4): p. 483-495.
427. Visser, J., et al., *Biofabrication of multi-material anatomically shaped tissue constructs.* Biofabrication, 2013. **5**(3): p. 035007.
428. Brown, K.L. and R.L. Cruess, *Bone and cartilage transplantation in orthopaedic surgery. A review.* J Bone Joint Surg Am, 1982. **64**(2): p. 270-9.
429. Enneking, W.F., J.L. Eady, and H. Burchardt, *Autogenous cortical bone grafts in the reconstruction of segmental skeletal defects.* J Bone Joint Surg Am, 1980. **62**(7): p. 1039-58.
430. Marsell, R. and T.A. Einhorn, *The biology of fracture healing.* Injury, 2011. **42**(6): p. 551-555.
431. Meijer, G.J., et al., *Cell-based bone tissue engineering.* PLoS medicine, 2007. **4**(2): p. e9.
432. Sheehy, E.J., D.J. Kelly, and F.J. O'Brien, *Biomaterial-based endochondral bone regeneration: a shift from traditional tissue engineering paradigms to developmentally inspired strategies.* Materials Today Bio, 2019. **3**: p. 100009.
433. Lyons, F.G., et al., *The healing of bony defects by cell-free collagen-based scaffolds compared to stem cell-seeded tissue engineered constructs.* Biomaterials, 2010. **31**(35): p. 9232-9243.
434. Miot, S., et al., *Influence of in vitro maturation of engineered cartilage on the outcome of osteochondral repair in a goat model.* Eur Cell Mater, 2012. **23**: p. 222-236.
435. Freeman, F.E., et al., *Effects of in vitro endochondral priming and pre-vascularisation of human MSC cellular aggregates in vivo.* Stem cell research & therapy, 2015. **6**(1): p. 1-18.
436. Gawlitta, D., et al., *Decellularized cartilage-derived matrix as substrate for endochondral bone regeneration.* Tissue Engineering Part A, 2015. **21**(3-4): p. 694-703.

437. Santos, M.I. and R.L. Reis, *Vascularization in bone tissue engineering: physiology, current strategies, major hurdles and future challenges.* Macromolecular bioscience, 2010. **10**(1): p. 12-27.
438. Mercado-Pagán, Á.E., et al., *Vascularization in bone tissue engineering constructs.* Annals of biomedical engineering, 2015. **43**(3): p. 718-729.
439. Shahabipour, F., et al., *Key components of engineering vascularized 3-dimensional bioprinted bone constructs.* Translational Research, 2020. **216**: p. 57-76.
440. Yu, T., et al., *Vascularization of plastic calcium phosphate cement in vivo induced by in-situ-generated hollow channels.* Materials Science and Engineering: C, 2016. **68**: p. 153-162.
441. Won, J.-E., et al., *Hierarchical microchanneled scaffolds modulate multiple tissue-regenerative processes of immune-responses, angiogenesis, and stem cell homing.* Biomaterials, 2020. **227**: p. 119548.
442. Buckley, C.T., S.D. Thorpe, and D.J. Kelly, *Engineering of large cartilaginous tissues through the use of microchanneled hydrogels and rotational culture.* Tissue Engineering Part A, 2009. **15**(11): p. 3213-3220.
443. Holmes, B., et al., *A synergistic approach to the design, fabrication and evaluation of 3D printed micro and nano featured scaffolds for vascularized bone tissue repair.* Nanotechnology, 2016. **27**(6): p. 064001.
444. Rnjak-Kovacina, J., et al., *Arrayed hollow channels in silk-based scaffolds provide functional outcomes for engineering critically sized tissue constructs.* Advanced functional materials, 2014. **24**(15): p. 2188-2196.
445. Yu, T., et al., *Channeled β-TCP scaffolds promoted vascularization and bone augmentation in mandible of beagle dogs.* Advanced Functional Materials, 2016. **26**(37): p. 6719-6727.
446. Cunniffe, G.M., et al., *Development and characterisation of a collagen nano-hydroxyapatite composite scaffold for bone tissue engineering.* Journal of Materials Science: Materials in Medicine, 2010. **21**(8): p. 2293-2298.
447. Curtin, C.M., et al., *Innovative collagen nano-hydroxyapatite scaffolds offer a highly efficient non-viral gene delivery platform for stem cell-mediated bone formation.* Advanced materials, 2012. **24**(6): p. 749-754.
448. Freeman, F.E., et al., *3D bioprinting spatiotemporally defined patterns of growth factors to tightly control tissue regeneration.* Science advances, 2020. **6**(33): p. eabb5093.
449. Liu, F., et al., *Rapid and reliable healing of critical size bone defects with genetically modified sheep muscle.* European cells & materials, 2015. **30**: p. 118.
450. Rodolfo, E., et al., *Contribution of implanted, genetically modified muscle progenitor cells expressing BMP-2 to new bone formation in a rat osseous defect.* Molecular Therapy, 2018. **26**(1): p. 208-218.
451. Schmitt, B., et al., *BMP2 initiates chondrogenic lineage development of adult human mesenchymal stem cells in high-density culture.* Differentiation, 2003. **71**(9-10): p. 567-577.
452. Sekiya, I., et al., *Comparison of effect of BMP-2,-4, and-6 on in vitro cartilage formation of human adult stem cells from bone marrow stroma.* Cell and tissue research, 2005. **320**(2): p. 269-276.
453. Shen, B., et al., *BMP-2 enhances TGF-β3–mediated chondrogenic differentiation of human bone marrow multipotent mesenchymal stromal cells in alginate bead culture.* Tissue Engineering Part A, 2009. **15**(6): p. 1311-1320.
454. Martin, T.J., *Parathyroid hormone-related protein, its regulation of cartilage and bone development, and role in treating bone diseases.* Physiological reviews, 2016. **96**(3): p. 831-871.
455. Rico-Llanos, G.A., et al., *Collagen type I Biomaterials as scaffolds for bone tissue engineering.* Polymers, 2021. **13**(4): p. 599.

456. Geiger, M., R. Li, and W. Friess, *Collagen sponges for bone regeneration with rhBMP-2.* Advanced drug delivery reviews, 2003. **55**(12): p. 1613-1629.
457. Shields, L.B., et al., *Adverse effects associated with high-dose recombinant human bone morphogenetic protein-2 use in anterior cervical spine fusion.* Spine, 2006. **31**(5): p. 542-547.
458. James, A.W., et al., *A review of the clinical side effects of bone morphogenetic protein-2.* Tissue Engineering Part B: Reviews, 2016. **22**(4): p. 284-297.
459. Fischer, C.R., et al., *A systematic review of comparative studies on bone graft alternatives for common spine fusion procedures.* European Spine Journal, 2013. **22**(6): p. 1423-1435.
460. Bostrom, M.P. and D.A. Seigerman, *The clinical use of allografts, demineralized bone matrices, synthetic bone graft substitutes and osteoinductive growth factors: a survey study.* HSS Journal®, 2005. **1**(1): p. 9-18.
461. Thompson, E.M., et al., *Recapitulating endochondral ossification: a promising route to in vivo bone regeneration.* Journal of tissue engineering and regenerative medicine, 2015. **9**(8): p. 889-902.
462. Fu, R., et al., *Bone defect reconstruction via endochondral ossification: A developmental engineering strategy.* Journal of Tissue Engineering, 2021. **12**: p. 20417314211004211.
463. Lackington, W.A., et al., *Incorporation of hydroxyapatite into collagen scaffolds enhances the therapeutic efficacy of rhBMP-2 in a weight-bearing femoral defect model.* Materials Today Communications, 2021: p. 102933.
464. Mendibil, U., et al., *Tissue-specific decellularization methods: Rationale and strategies to achieve regenerative compounds.* International Journal of Molecular Sciences, 2020. **21**(15): p. 5447.
465. Bruyneel, A.A. and C.A. Carr, *Ambiguity in the presentation of decellularized tissue composition: the need for standardized approaches.* Artificial organs, 2017. **41**(8): p. 778-784.
466. Hoshiba, T. and T. Yamaoka, *Decellularized Extracellular Matrix: Characterization, Fabrication and Applications*. Vol. 6. 2019: Royal Society of Chemistry.
467. Stavenschi, E., M.-N. Labour, and D.A. Hoey, *Oscillatory fluid flow induces the osteogenic lineage commitment of mesenchymal stem cells: The effect of shear stress magnitude, frequency, and duration.* Journal of biomechanics, 2017. **55**: p. 99-106.
468. Eichholz, K.F., et al., *Human bone marrow stem/stromal cell osteogenesis is regulated via mechanically activated osteocyte-derived extracellular vesicles.* Stem cells translational medicine, 2020. **9**(11): p. 1431-1447.
469. Knuth, C., et al., *Collagen type X is essential for successful mesenchymal stem cell-mediated cartilage formation and subsequent endochondral ossification.* European cells & materials, 2019. **38**: p. 106-122.
470. Pethő, A., Y. Chen, and A. George, *Exosomes in extracellular matrix bone biology.* Current osteoporosis reports, 2018. **16**(1): p. 58-64.
471. Riazifar, M., et al., *Stem cell extracellular vesicles: extended messages of regeneration.* Annual review of pharmacology and toxicology, 2017. **57**: p. 125-154.
472. Emami, A., et al., *Synergic effects of decellularized bone matrix, hydroxyapatite, and extracellular vesicles on repairing of the rabbit mandibular bone defect model.* Journal of Translational Medicine, 2020. **18**(1): p. 1-18.
473. Carragee, E.J., E.L. Hurwitz, and B.K. Weiner, *A critical review of recombinant human bone morphogenetic protein-2 trials in spinal surgery: emerging safety concerns and lessons learned.* Spine J, 2011. **11**(6): p. 471-91.
474. Rocque, B.G., et al., *Bone morphogenetic protein–associated complications in pediatric spinal fusion in the early postoperative period: an analysis of 4658 patients and review of the literature.* Journal of Neurosurgery: Pediatrics, 2014. **14**(6): p. 635-643.

475. Kwon, H.M., et al., *Multiple paracrine factors secreted by mesenchymal stem cells contribute to angiogenesis.* Vascular pharmacology, 2014. **63**(1): p. 19-28.
476. Kehl, D., et al., *Proteomic analysis of human mesenchymal stromal cell secretomes: a systematic comparison of the angiogenic potential.* NPJ Regenerative medicine, 2019. **4**(1): p. 1-13.
477. Maacha, S., et al., *Paracrine mechanisms of mesenchymal stromal cells in angiogenesis.* Stem cells international, 2020. **2020**.
478. Pittet, M.J., M. Nahrendorf, and F.K. Swirski, *The journey from stem cell to macrophage.* Annals of the New York Academy of Sciences, 2014. **1319**(1): p. 1.
479. Oryan, A., et al., *Role of mesenchymal stem cells in bone regenerative medicine: what is the evidence?* Cells Tissues Organs, 2017. **204**(2): p. 59-83.
480. Cunniffe, G.M., et al., *Growth plate extracellular matrix-derived scaffolds for large bone defect healing.* European Cells and Materials, 2017. **33**: p. 130-142.
481. Ho-Shui-Ling, A., et al., *Bone regeneration strategies: Engineered scaffolds, bioactive molecules and stem cells current stage and future perspectives.* Biomaterials, 2018. **180**: p. 143-162.
482. Sutherland, A.J., et al., *The bioactivity of cartilage extracellular matrix in articular cartilage regeneration.* Advanced healthcare materials, 2015. **4**(1): p. 29-39.
483. Wang, Y., et al., *Endogenous regeneration of critical-size chondral defects in immunocompromised rat xiphoid cartilage using decellularized human bone matrix scaffolds.* Tissue Engineering Part A, 2012. **18**(21-22): p. 2332-2342.
484. Yang, Q., et al., *In vitro cartilage tissue engineering with cartilage extracellular matrix-derived porous scaffolds and bone marrow mesenchymal stem cells.* Zhonghua yi xue za zhi, 2011. **91**(17): p. 1161-1166.
485. Levorson, E.J., et al., *Cell-derived polymer/extracellular matrix composite scaffolds for cartilage regeneration, Part 2: construct devitalization and determination of chondroinductive capacity.* Tissue Engineering Part C: Methods, 2014. **20**(4): p. 358-372.
486. Epple, C., et al., *Prefabrication of a large pedicled bone graft by engineering the germ for de novo vascularization and osteoinduction.* Biomaterials, 2019. **192**: p. 118-127.
487. Longoni, A., et al., *Acceleration of Bone Regeneration Induced by a Soft-Callus Mimetic Material.* Advanced Science, 2022. **9**(6): p. 2103284.
488. Keane, T.J. and S.F. Badylak, *The host response to allogeneic and xenogeneic biological scaffold materials.* Journal of tissue engineering and regenerative medicine, 2015. **9**(5): p. 504-511.
489. Londono, R., et al., *The effect of cell debris within biologic scaffolds upon the macrophage response.* Journal of biomedical materials research Part A, 2017. **105**(8): p. 2109-2118.
490. Longoni, A., et al., *Endochondral bone regeneration by non-autologous mesenchymal stem cells.* Frontiers in bioengineering and biotechnology, 2020: p. 651.
491. Lee, C.H., et al., *Regeneration of the articular surface of the rabbit synovial joint by cell homing: a proof of concept study.* The Lancet, 2010. **376**(9739): p. 440-448.
492. Sun, H., et al., *The in vivo degradation, absorption and excretion of PCL-based implant.* Biomaterials, 2006. **27**(9): p. 1735-1740.
493. Woodruff, M.A. and D.W. Hutmacher, *The return of a forgotten polymer—Polycaprolactone in the 21st century.* Progress in polymer science, 2010. **35**(10): p. 1217-1256.
494. Huang, C., et al., *Overexpressing sonic hedgehog peptide restores periosteal bone formation in a murine bone allograft transplantation model.* Molecular therapy, 2014. **22**(2): p. 430-439.
495. Lieberman, J.R., et al., *Regional gene therapy with a BMP-2-producing murine stromal cell line induces heterotopic and orthotopic bone formation in rodents.* Journal of Orthopaedic Research, 1998. **16**(3): p. 330-339.

496. Lieberman, J.R., et al., *The effect of regional gene therapy with bone morphogenetic protein-2-producing bone-marrow cells on the repair of segmental femoral defects in rats.* J Bone Joint Surg Am, 1999. **81**(7): p. 905-17.
497. Blum, J.S., et al., *In vivo evaluation of gene therapy vectors in ex vivo-derived marrow stromal cells for bone regeneration in a rat critical-size calvarial defect model.* Human gene therapy, 2003. **14**(18): p. 1689-1701.
498. Ishihara, A., et al., *Dermal fibroblast-mediated BMP2 therapy to accelerate bone healing in an equine osteotomy model.* Journal of orthopaedic research, 2010. **28**(3): p. 403-411.
499. Wright, V.J., et al., *BMP4-expressing muscle-derived stem cells differentiate into osteogenic lineage and improve bone healing in immunocompetent mice.* Molecular Therapy, 2002. **6**(2): p. 169-178.
500. Shen, H.C., et al., *Structural and functional healing of critical-size segmental bone defects by transduced muscle-derived cells expressing BMP4.* The Journal of Gene Medicine: A cross-disciplinary journal for research on the science of gene transfer and its clinical applications, 2004. **6**(9): p. 984-991.
501. Sheyn, D., et al., *Gene-modified adult stem cells regenerate vertebral bone defect in a rat model.* Molecular pharmaceutics, 2011. **8**(5): p. 1592-1601.
502. Breitbart, A.S., et al., *Gene-enhanced tissue engineering: applications for bone healing using cultured periosteal cells transduced retrovirally with the BMP-7 gene.* Annals of plastic surgery, 1999. **42**(5): p. 488-495.
503. Xiang, L., et al., *BMP9-induced osteogenetic differentiation and bone formation of muscle-derived stem cells.* BioMed Research International, 2012. **2012**.
504. Dumanian, Z.P., et al., *Repair of critical sized cranial defects with BMP9-transduced calvarial cells delivered in a thermoresponsive scaffold.* PloS one, 2017. **12**(3).
505. Gao, F., et al., *Lentivirus-mediated Wnt10b overexpression enhances fracture healing in a rat atrophic non-union model.* Biotechnology letters, 2015. **37**(3): p. 733-739.
506. Liu, H., et al., *Effect of Human Wnt10b Transgene Overexpression on Peri-Implant Osteogenesis in Ovariectomized Rats.* Human gene therapy, 2018. **29**(12): p. 1416-1427.
507. Jabbarzadeh, E., et al., *Induction of angiogenesis in tissue-engineered scaffolds designed for bone repair: a combined gene therapy–cell transplantation approach.* Proceedings of the National Academy of Sciences, 2008. **105**(32): p. 11099-11104.
508. Li, R., et al., *Effect of cell-based VEGF gene therapy on healing of a segmental bone defect.* Journal of Orthopaedic Research, 2009. **27**(1): p. 8-14.
509. Tu, Q., P. Valverde, and J. Chen, *Osterix enhances proliferation and osteogenic potential of bone marrow stromal cells.* Biochemical and biophysical research communications, 2006. **341**(4): p. 1257-1265.
510. Tu, Q., et al., *Osterix overexpression in mesenchymal stem cells stimulates healing of critical-sized defects in murine calvarial bone.* Tissue Eng, 2007. **13**(10): p. 2431-40.
511. Wu, L., et al., *Osteogenic differentiation of adipose derived stem cells promoted by overexpression of osterix.* Molecular and cellular biochemistry, 2007. **301**(1-2): p. 83-92.
512. Han, D. and J. Li, *Repair of bone defect by using vascular bundle implantation combined with Runx II gene-transfected adipose-derived stem cells and a biodegradable matrix.* Cell and tissue research, 2013. **352**(3): p. 561-571.
513. Boden, S., et al., *Lumbar spine fusion by local gene therapy with a cDNA encoding a novel osteoinductive protein (LMP-1).* Spine, 1998. **23**(23): p. 2486-2492.
514. Lattanzi, W., et al., *Ex vivo-transduced autologous skin fibroblasts expressing human Lim mineralization protein-3 efficiently form new bone in animal models.* Gene Therapy, 2008. **15**(19): p. 1330-1343.
515. Rundle, C.H., et al., *Retroviral-based gene therapy with cyclooxygenase-2 promotes the union of bony callus tissues and accelerates fracture healing in the rat.* The journal of gene medicine, 2008. **10**(3): p. 229-241.

516. Hsu, M.-N., et al., *Coactivation of Endogenous Wnt10b and Foxc2 by CRISPR Activation Enhances BMSC Osteogenesis and Promotes Calvarial Bone Regeneration.* Molecular Therapy, 2020. **28**(2): p. 441-451.
517. Evans, C.H., *Gene delivery to bone.* Adv Drug Deliv Rev, 2012. **64**(12): p. 1331-40.
518. Kimelman Bleich, N., et al., *Gene therapy approaches to regenerating bone.* Adv Drug Deliv Rev, 2012. **64**(12): p. 1320-30.
519. Shapiro, G., et al., *Recent advances and future of gene therapy for bone regeneration.* Current osteoporosis reports, 2018. **16**(4): p. 504-511.
520. Dreier, R., *Hypertrophic differentiation of chondrocytes in osteoarthritis: the developmental aspect of degenerative joint disorders.* Arthritis research & therapy, 2010. **12**(5): p. 216.
521. García-García, A. and I. Martin, *Extracellular matrices to modulate the innate immune response and enhance bone healing.* Frontiers in Immunology, 2019. **10**: p. 2256.
522. Dziki, J.L., et al., *Extracellular matrix bioscaffolds as immunomodulatory biomaterials.* Tissue Engineering Part A, 2017. **23**(19-20): p. 1152-1159.
523. Brown, B.N., et al., *Macrophage phenotype as a predictor of constructive remodeling following the implantation of biologically derived surgical mesh materials.* Acta biomaterialia, 2012. **8**(3): p. 978-987.
524. Slivka, P., et al., *Fractionation of an ECM hydrogel into structural and soluble components reveals distinctive roles in regulating macrophage behavior.* Biomaterials science, 2014. **2**(10): p. 1521-1534.
525. Sicari, B.M., et al., *The promotion of a constructive macrophage phenotype by solubilized extracellular matrix.* Biomaterials, 2014. **35**(30): p. 8605-8612.
526. Franz, S., et al., *Immune responses to implants–a review of the implications for the design of immunomodulatory biomaterials.* Biomaterials, 2011. **32**(28): p. 6692-6709.
527. Spiller, K.L., et al., *Sequential delivery of immunomodulatory cytokines to facilitate the M1-to-M2 transition of macrophages and enhance vascularization of bone scaffolds.* Biomaterials, 2015. **37**: p. 194-207.
528. Martino, M.M., et al., *Inhibition of IL-1R1/MyD88 signalling promotes mesenchymal stem cell-driven tissue regeneration.* Nature communications, 2016. **7**: p. 11051.
529. Hachim, D., et al., *Shifts in macrophage phenotype at the biomaterial interface via IL-4 eluting coatings are associated with improved implant integration.* Biomaterials, 2017. **112**: p. 95-107.
530. Schlundt, C., et al., *Macrophages in bone fracture healing: Their essential role in endochondral ossification.* Bone, 2018. **106**: p. 78-89.
531. Kajahn, J., et al., *Artificial extracellular matrices composed of collagen I and high sulfated hyaluronan modulate monocyte to macrophage differentiation under conditions of sterile inflammation.* Biomatter, 2012. **2**(4): p. 226-273.
532. Kim, Y.-H., H. Furuya, and Y. Tabata, *Enhancement of bone regeneration by dual release of a macrophage recruitment agent and platelet-rich plasma from gelatin hydrogels.* Biomaterials, 2014. **35**(1): p. 214-224.
533. Wang, M., et al., *Improved osteogenesis and angiogenesis of magnesium-doped calcium phosphate cement via macrophage immunomodulation.* Biomaterials science, 2016. **4**(11): p. 1574-1583.
534. Lo, C.S. and R. Tasso, *Harnessing Endogenous Cellular Mechanisms for Bone Repair.* Frontiers in Bioengineering and Biotechnology, 2017. **5**: p. 52-52.